STRUCTURAL ANALYSIS OF THE MIT MICRO ROCKET COMBUSTION CHAMBER

by

Erin E. Noonan

S.B. Aeronautics and Astronautics
Massachusetts Institute of Technology, 2000

Submitted to the Department of Aeronautics and Astronautics
in partial fulfillment of the requirements for the degree of

Master of Science in Aeronautics and Astronautics

at the

Massachusetts Institute of Technology
June 2002

Author:______________________________
Erin E. Noonan
Department of Aeronautics and Astronautics
May 17, 2002

Certified by:______________________________
Professor S. Mark Spearing
Associate Professor of Aeronautics and Astronautics
Thesis Supervisor

Accepted by:______________________________
Professor Wallace E. Vander Velde
Professor of Aeronautics and Astronautics
Chairman, Departmental Graduate Committee

STRUCTURAL ANALYSIS OF THE
MIT MICROROCKET COMBUSTION CHAMBER

by
Erin E. Noonan

Submitted to the Department of Aeronautics and Astronautics
on May 17, 2002 in partial fulfillment of the requirements for the
Degree of Master of Science in Aeronautics and Astronautics

Abstract

The micro rocket is one of several power microelectromechanical systems (MEMS) under development at MIT. The micro rocket is experiencing structural failures at operating parameters far below the designed performance level. The deterministic strength of brittle materials, such as silicon, is critically dependent on the local strength and flaw population. Experiments and correlating modeling were used to pursue the root cause of the micro rocket structural failure. This thesis presents the results of these experiments and analysis to characterize the strength of deep reactive ion etched single crystal silicon structures and to clarify the influence of geometry on a structure's characteristic strength.

The test specimens used for this work were pressurized cavities with the same geometry as the micro rocket combustion chamber and radiused hub flexure specimens. These geometries were correlated with numerical models and finite element models for determination of failure stress levels. Applying Weibull statistics, the strength of the material and the effect of the specimen geometry were quantified. Scanning electron microscope inspection of the etched surfaces provided visual evidence of surface roughness conditions, supporting the experimental results.

Pressure tests were used to identify failure modes of the micro rocket geometry without the complex subsystem geometries required for the operational device. A slight variation in geometric configuration of the chamber pressure ports yielded significant differences in device strength. Radiused hub flexure specimens were used to compare the strength of the micro rocket etch recipe, ADAM06, to a baseline etch, MIT69. Additionally, the radiused hub flexure specimens were used to characterize the role of a secondary isotropic smoothing etch in improving the effective material strength of deep etched surfaces. It was determined that the micro rocket etch was not optimized sufficiently to achieve baseline surface roughness. The role of the secondary isotropic etch was determined to be key in achieving high strengths in etched single crystal silicon.

The experimental data was used to establish a scaling correlation for strength values from the two different specimen geometries. Using the effective areas of the two structures, characteristic strength for chambers was predicted based on the characteristic strength of radiused hub flexure specimens. The predicted scaling did not correlate particularly well with the data. However, the limited number of samples and a modeling inaccuracy are suspected to have significant influence on the quality of the prediction. Improvement of these conditions could yet yield a useful predictive tool.

The results of this thesis are demonstration of the influence of specimen geometry and surface roughness on the characteristic strength of deep etched single crystal silicon structures. Additionally, the predictive scaling between different specimen geometries was attempted with marginal results that might be improved with further testing. Recommendations for future work include further investigation of the effects of slight variations in specimen geometry in fabrication and material strength, characterization of the smoothing effects of isotropic etching with time, reevaluation of the optimization of the micro rocket etch recipe, and further study of the nature of flaws introduced by primary deep etches and their behavior as surface or volume flaws.

Thesis Supervisor: Professor S. Mark Spearing
Title: Associate Professor of Aeronautics and Astronautics

Acknowledgements

There are many individuals whose assistance, advice, and encouragement have been invaluable to the work that has culminated in this thesis. I would like to thank Professor Mark Spearing for his guidance, insight and enthusiasm on this project. I have learned a lot and got to break a bunch of things, what fun! I also owe great thanks to Yoav Peles for his ever expedient production in the clean room; without him there would have been nothing to break. Thank you to Noel Nemeth for his help with the CARES/LIFE software. Thanks also to Dennis Ward and Linhvu Ho for their assistance in the Microsystems Technology Laboratories, and particularly for the use of very valuable STS time. Kevin Turner and Seth Kessler provided much help and advice concerning testing instrumentation and equipment. Thanks to Shaun Berry at MIT Lincoln Labs for all of his help with finite element modeling. Thank you to Viktor Dubrowski for always finding a few minutes to take care of the little fixes on my test rig. Thank you to Professor Epstein and Professor Kerrebrock and everyone on the micro rocket project, particularly Chris Protz for his assistance with the micro rocket test stand and Carole Joppin for making it so easy to share a common testing space.

Then there are also those who have been helpful on the less technical side of things, Chris Gouldstone and Mark Kepets for the mental health break that is lunch each day and Lori Martinez for a little bit of non-technical conversation and great snack food. Thanks to my family for all of their support and their interest in my work even though sometimes it's a little complicated to explain. And finally, thank you to Brian, for always being there, making me laugh, and making life more interesting.

This work was supported by ARO Grant #DAAG55-98-1-0179, Technical Monitor Dr. Richard Paur, DARPA Grants #DABT63-98-C-0004 and #DABT63-00-1-0001, Technical Monitor Dr. Robert L. Rosenfeld, and the ARL Collaborative Technology Alliance Power and Energy Consortium: Honeywell GPA #A00041587 under ARL prime award DAAD19-01-2-0010, Technical Monitors Dr. Mukund Acharya (Honeywell) and Mr. John Hopkins (ARL).

Table of Contents

Table of Figures

Table of Tables

Chapter 1 Introduction

1.1 The MIT Micro Rocket Program

The micro rocket is one of several microelectromechanical systems (MEMS) devices currently under development at MIT [1,2]. Many of these devices are power generation systems, including a micro gas turbine generator, a micro heat engine, and a micro rocket. These devices are fabricated using microfabrication technologies of etching and bonding silicon wafers to create three-dimensional structures.

The goal of the project is to build a microfabricated silicon liquid bipropellant rocket that is regeneratively cooled and turbopump pressurized. These devices offer several advantages not available with traditional rocket engine technology. A rocket engine fabricated on a silicon wafer, using microchip technology, changes the concept of mass production from producing several rocket engines in parallel to producing a batch of rocket engines that might consist of tens of devices on one wafer stack. In addition, the amount of space to fabricate a batch of rocket engines is significantly less than that required to fabricate and assemble a full size rocket engine.

A silicon rocket has the potential to offer thrust to weight ratios of 1000:1; by contrast, the space shuttle thrust to weight ratio is 56:1 at sea level and 68:1 in a vacuum. [3] In addition, the small rocket engine produces a small amount of thrust and takes up a small amount of space, allowing for tailored arrays of engines to meet specific thrust requirements. The microrocket will enable a new class of small launch vehicles. These small launch vehicles could put payloads of the order of 2 kg into low earth orbit and reduce the cost of putting an object into orbit from millions of dollars to thousands of dollars. A study of small-scale launch vehicles was conducted to identify an ideal launch vehicle configuration. [4] This study elected to focus on a two stage launch vehicle with a gross lift off weight of 80 kg and the ability to carry a one to four kilogram payload, depending on desired altitude. Such a vehicle would require 102 engines for stage one and 10 engines for stage two.

1.2 Performance of the Microrocket

The micro rocket currently operates with gaseous propellants and liquid coolant. The propellants are methane and oxygen and the coolant is either liquid water or ethanol. The rocket is designed to produce 1 N of thrust with a chamber pressure of 125 atmospheres. The rocket has not yet successfully reached these operating conditions. The device's combustion chamber structure has failed catastrophically at pressures below the design chamber pressure (Figure 1-1). At the beginning of this inquiry into the chamber failures, the maximum pressure achieved in a cold test was 40 atmospheres. Hot tests yielded a maximum pressure of 12.3 atmospheres [5]. The difference in failure pressures between hot and cold indicate that heat transfer and insufficient cooling are likely contributing to the strength problems. However, cold test failures suggest that even with improvements to the combustion chamber cooling, the device will continue to fail unless changes are made to the structure itself.

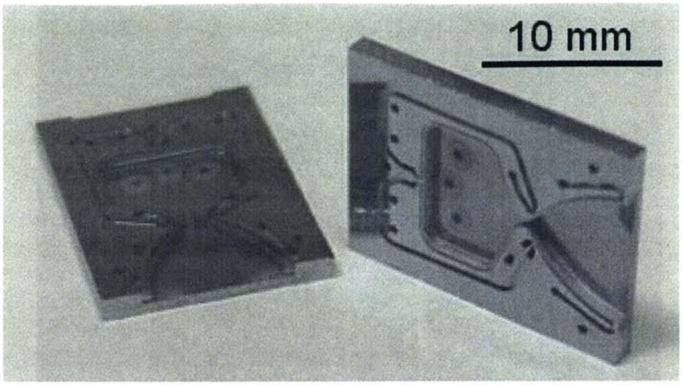

Figure 1-2: MIT Microrocket [7]

1.3.2 Deep Reactive Ion Etching

Deep reactive ion etching is a microfabrication process to create deep features in silicon substrates. For most MEMS devices the geometry is critical to the operation of the device therefore it is imperative that a fabrication process yield features as close to the intended design as possible. It is for this reason that DRIE has become a staple of MEMS fabrication. In order to achieve these features, time-multiplexed deep etching has been characterized and studied to understand how to maintain high selectivity to masking material, good profile control, and low non-uniformity across a wafer. [8]

DRIE is a dry processing of silicon using fluorinated chemistry. The etch rate is a function of spontaneous reactions of silicon and fluorine, ion bombardment, and some physical sputtering. This etch process consists of two alternating cycles, etching and passivation. In the etch step a shallow trench is formed in the substrate by the bombarding ions. In the passivation step a protective fluorocarbon film is deposited on all surfaces. In the following etch step the ion bombardment enables preferential removal of material from horizontal surfaces. This preferential removal facilitates the creation of highly anisotropic

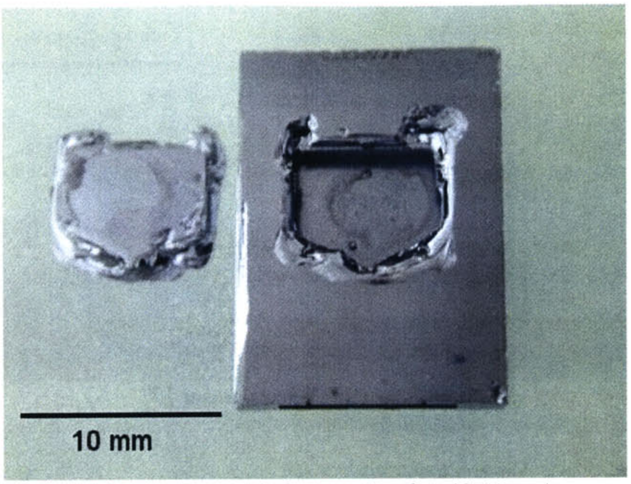

Figure 1-1: Failed Micro Rocket (C. Protz)

1.3 Structure of the Micro Rocket

1.3.1 Micro Rocket Fabrication

The MIT micro-rocket is fabricated using semi-conductor grade n-type <100> silicon wafers. The device features are deep reactive ion etched (DRIE) using a Surface Technology Systems™ (STS) inductively coupled plasma etcher. [6] The wafers are diffusion bonded to form a stack of six 500 μm (+/-25 μm) wafers. The device is symmetric (Figure 1-2); therefore only three different patterned wafers must be fabricated. Each of these wafers requires three masks for a total of nine. The details of these masks and the overall fabrication process is documented elsewhere [6].

features with many etch cycles. The characteristics of deep reactive ion etching presented in this section have been established through work conducted at MIT to characterize the etch processes, the resulting structures, and the equipment used for these processes [8,9,10].

An etch recipe is defined by coil power, gas flow (SF_6 for the etch cycle and C_4F_8 for the passivation cycle), platen power, and Automatic Pressure Controller (APC) angle. Each of these elements affect etch rates of silicon and photo resist as well as contributing to the characteristics of the fully etched wafer. Increasing coil power raises the ion flux density. Greater SF6 flow boosts the concentration of the etchant species (F) and decreases the amount of etchant product (SiF4) that is redeposited on the wafer. Platen power affects ion bombardment energy. The etch rate of silicon increases with increases in the values of each of the aforementioned conditions. Pressure is controlled by APC angle and gas flow rate. Increased pressure will initially raise the etch rate of silicon as it increases the concentration of etchant (F), however, if it gets too high, it will begin to reduce the ion energy/flux which will decrease the etch rate. Photo resist etch rate increases with increased platen power (higher ion bombardment energy) and lower pressure. Photo resist etch rate is also influenced by the length of each cycle; a longer etch cycle increases the amount of photo resist removed while a longer passivation cycle decreases the amount of photo resist removed because a thicker protective film is deposited and has to be removed in order to etch more photo resist.

Ion bombardment energy is proportional to anisotropy and inversely proportional to selectivity. The APC angle influences sputtering effects and the redeposition of masking materials. Increased APC angle promotes the formation of micro columns or grass as well as increasing damage to structures and excessive polymer deposition. For these reasons, the APC angle is not typically set above 75 degrees. Residence time is proportional to the pressure and inversely proportional to the flow rate. This influences the reactant concentration as well as the removal rate of etch products from the chamber.

Ideal features of an etched wafer are minimal surface roughness, minimum nonuniformity, and the desired profile, achieved with the etch anisotropy. Each of these characteristics are significantly influenced by the etch conditions. There are typically two types of surface roughness, both on the sidewalls of an etched trench, scallops and striations. The scallops are a byproduct of the alternation between etch and passivation cycles. They cannot be avoided, but can be minimized for a given process by varying the operating conditions. It has been documented that the scallop depth on a sidewall is primarily due to spontaneous etching of the silicon by fluorine [8]. The vertical striations that may be present on etched sidewalls are caused by uneven recession of masking materials. Uniformity across an etched wafer is predominately affected by local plasma density, which is in turn a product of the location of the power coil and heating source. For this reason, the outer edges of a wafer are subject to a higher etch rate that the center of the wafer. Uniformity is also influenced by the APC angle and the etchant flow rates. A lower APC angle improves uniformity because diffusivity is inversely proportional to pressure. Lower pressure can also be achieved with lower SF_6 flow rates. Anisotropy, which ultimately controls the profile of the etched trench, is influenced by the difference between the etch and passivation cycle durations. If the etch time is too short, the passivation film will not be completely removed and will ultimately cause significant surface roughness as well as micro masking and grass formation. Anisotropy increases with lower pressure because the average ion energy decreases which increases the ion angle of incidence. Anisotropy can also be increased with decreased etchant flow, which will also decrease pressure for a fixed APC angle. The roughness of these surfaces, particularly near and in the fillet radius at the base of a trench, has significant implications for the strength of a device. The characteristic surface flaws of DRIE surfaces are effectively cracks and as such, they create stress concentrations which increase the likelihood of failure at a flaw location, rather than at a flaw free region subject to higher stresses.

1.3.3 Original Micro Rocket Design

Wafers 1 and 6 have inlet holes for propellants and coolant on the front side. The back side is etched with the upper half of the top/bottom cooling passages and propellant manifolds, passages to feed and collect coolant from the cooling passages, passages to feed propellant to the manifolds, and injector holes. Wafers 2 and 4 have the lower half of the top/bottom cooling passages and propellant manifolds on their fronts. On the back is the first section of the combustion chamber and nozzle, side cooling passages, and coolant transport passages. Wafers 3 and 4 are etched through in the region of the combustion chamber and the nozzle, adding depth to the cavities. On the front side, these wafers have side cooling passages etched and on the back there are coolant transport passages. [6]

The combustion chamber is principally comprised of wafers 2 through 5. On the top and bottom walls, wafers two and five, there are numerous small features. These elements contain and comprise a large number of possible failure origins. The presence of such detailed features inhibits identification of large-scale structural issues that may be present. For this reason, an experiment investigating the basic structure of the device is being conducted.

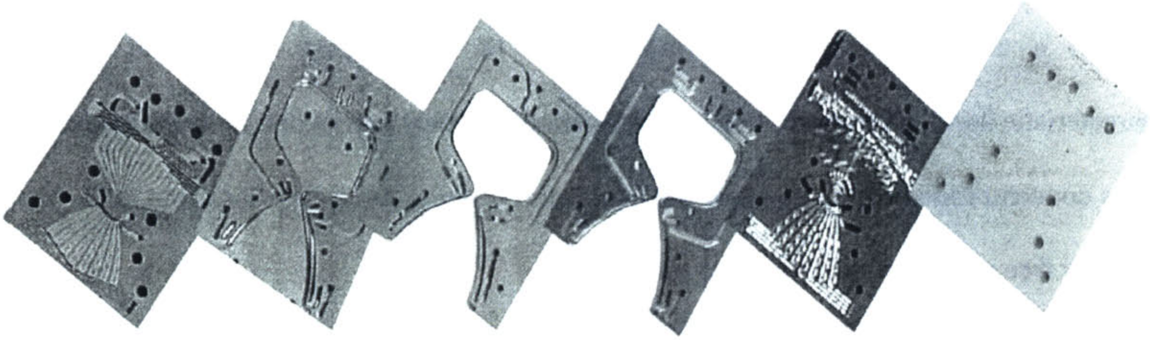

Figure 1-3: Micro Rocket Device Layers [7]

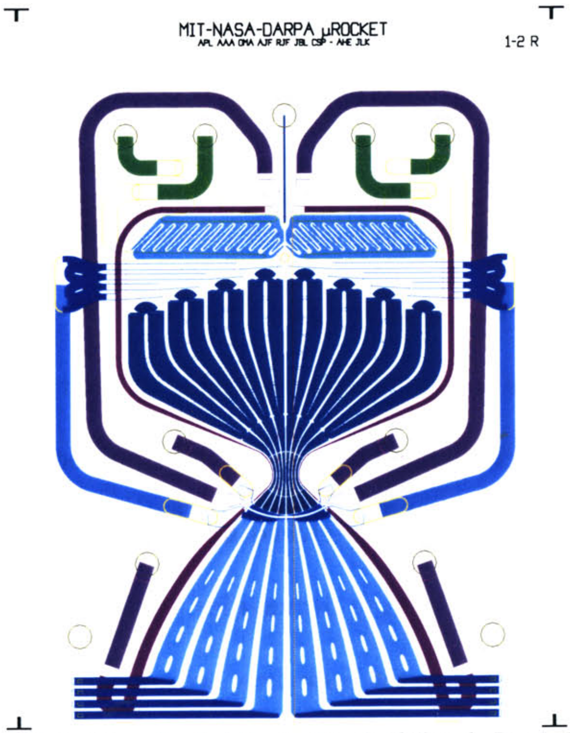

Figure 1-4: Micro Rocket Masks Overlaid (Single Device)[11]

1.3.4 Micro Rocket Modifications

Modifications have been made to the rocket to improve its performance. These changes were identified from a detailed finite element analysis of the structure [5]. The modifications included changes to the cooling passages and wafers 1 and 6.

Figure 1-5 presents the overlaid masks for the modifications made to the micro rocket. Coolant channels above and below the combustion chamber have been extended 300 μm to reduce stress concentrations (1). The coolant area at the throat has been increased with a 20 μm etch on wafers 1 and 6 (2). This will increase coolant flow and improve cold side heat transfer capabilities. In addition, wafers 1 and 6 have increased in thickness by 475 μm to lower the stress in the walls of the chamber. In these outer wafers, recesses have been etched to control the placement of the glass beads (or o-rings) for the device packaging (3). [11]

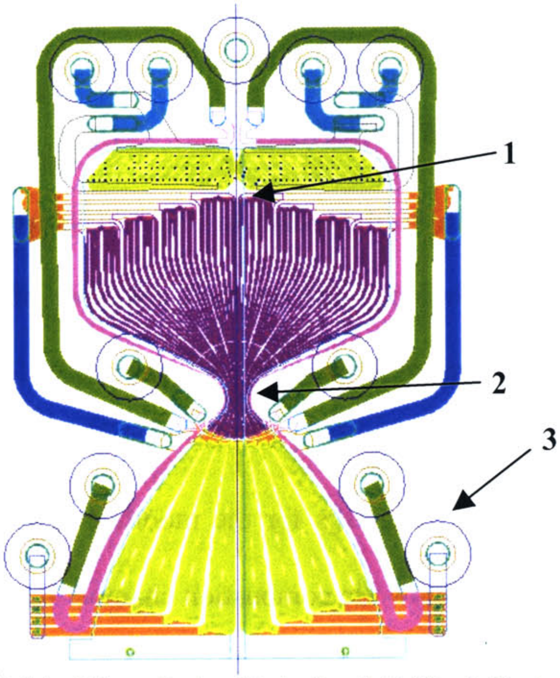

Figure 1-5: Modified Micro Rocket Masks Overlaid (Single Device) [11]

These modifications have improved hot test performance from a maximum achieved chamber pressure of 12 atm to 19.5 atm with thrust of approximately 1.6 N. Though these changes have allowed the rocket to reach greater pressures, the increase in thickness of the cap plates increases the mass of the device and therefore, reduces the thrust to weight ratio that might be achieved. Thus, it is desirable to identify the factors contributing to the failure of the device as originally designed.

1.3.5 Fracture Strength of Silicon

The strength of silicon structures is critically dependent on the flaw population of the material and the local stress levels due to stress concentrations. Strength-controlling flaws are most commonly introduced during processing and handling. This dependence has been investigated in many variations and is well documented [12,13,14]. In particular, surface roughness introduced during etching can have a severe detrimental effect. To identify the most significant weakness in the structure, strength data must be collected from a statistically significant sampling of devices [12]. In micro-fabricated devices common structural issues include poor wafer bonds, bonded wafer misalignment, and various stress concentrations. Stress concentrations can develop from processed surface roughness, fillet radii, inadequate load distribution, or geometric features. The micro-rocket could be experiencing increased stress levels and/or reduced strengths from any one or combination of these conditions. The failure occurs consistently about the circumference of the combustion chamber. This provides some indication of the most likely failure causes. In order to address the structural failure of the device, the contributing factors must be identified.

Material strength of brittle materials, like silicon, is a stochastic variable. This variation means that the failure of the material is determined by both stress level and local strength in a structure. In accounting for local strength, the failure of a structure becomes less easily predicted because it does not necessarily occur at the location of highest stress. Instead, it is possible to determine the probability that a given material will have a certain strength, and therefore be able to withstand a particular load. For this reason, the probabilistic nature of the material strength must be incorporated into the structural design.

The Weibull probability density function is commonly applied in structural design. This function calculates the probability of failure of a structure of volume, V, and subject to a load, σ:

$$P_{\mathrm{fv}} = 1 - \exp\left(- \int_{vol} \left(\frac{\sigma}{\sigma_o} \right)^m dV \right) \qquad (1\text{-}1)$$

where m and σ_o are constants determined from experimental data. σ_o is the reference strength, the stress at which 37% of a sample of test specimens survive and m is the Weibull modulus, which describes the variability in the strength—as m decreases, the variation in material strength increases.[15] This equation applies only to uniaxial loading of a specimen.

Weibull statistics are effectively 'weakest-link' statistics; the lowest strength region is the limiting factor for the entire structure. In addition, the consequences of multiaxial loading must be accounted for. For a volume, V, under a constant stress the probability of failure of that volume is assumed to be:

$$P_{\mathrm{fV}} = 1 - \exp\left(\frac{V}{V_0 \sigma_0^m} \left(\sigma_1^m + \sigma_2^m + \sigma_3^m \right) \right) \qquad (1\text{-}2)$$

where σ_i is the principal stress on the volume in the ith principal direction, σ_o is the reference strength, V_o is the reference volume, and m is the Weibull modulus. This formulation assumes that there is no interaction between the principal stresses and their influence on the strength controlling defects. The probability can also be calculated for surface flaws by substituting surface area for volume in Equation (1-2). This latter case is more relevant to single crystal silicon as the material is free of bulk mechanical defects.

The probability of failure also scales with the effective volume or area under stress (Figure 1-6). The three elements are of equivalent total volume (or surface area) and all have the same maximum stress levels. However the volume (or surface area) actually subject to that maximum stress varies with the manner in which the load is applied. Uniaxial tensile loading creates a uniform stress state in the loaded volume, so the entire volume is experiencing the maximum stress level. Under a rotational load the stress varies with radial position and is constant through the thickness, therefore only a fraction of the volume experiences the maximum stress. In a biaxial loading condition the stress state varies radially and through the thickness, subjecting an even smaller volume to the maximum stress state. The probability of failure scales with the volume under maximum stress, therefore the uniaxially loaded specimen has a higher failure of probability than the rotating specimen and the biaxial specimen. In order for the three configurations to have the same probability of failure, the rotating specimen and the bending specimen would have to have larger volumes and subject to greater stresses. This concept will be revisited in Chapter 5.

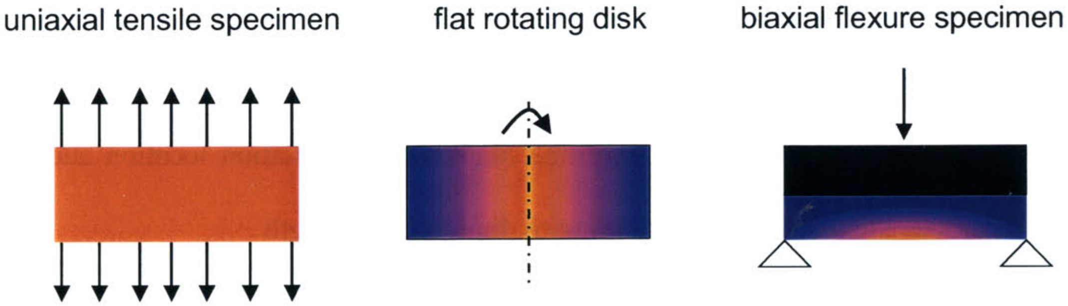

Figure 1-6: Variation in Stress State with Loading Condition

Chen's work to characterize the strength of etched silicon [12] offers a substantial foundation on which to build a more extensive understanding of the strength of etched silicon. Using biaxial flexure specimens and radiused hub flexure specimens, the room temperature strength of processed single crystal silicon was characterized. The effects of secondary isotropic etches were observed and quantified with respect to material strength, data scatter, and surface roughness. The application of a secondary etch could improve the characteristic strength of the material by a factor upwards of two, depending on the nature of the etch. The application of the isotropic etch increased the scatter in the data. Ultimately Chen demonstrated that it is possible to obtain high strength properties from etched silicon.

1.4 Motivation and Outline of Thesis

The goal of this research is to conduct a structural analysis of the micro rocket using analytical modeling and experimental data collection. This analysis is intended to enhance the current understanding of the micro rocket structural failure mechanisms. Specific objectives for this analysis include:

- Identify repeatable failure modes in the device geometry
- Determine the effective strength of silicon processed using the microrocket etch recipes and its statistical distribution
- Examine failed devices to determine likely failure initiation location and surface characteristics or flaws contributing to diminished strength
- Identify and evaluate modifications that may be made to the device design or fabrication process to improve effective material strength
- Evaluate ability to predict strength of MEMS structures (ie complex) based on test data from test specimens (ie simple)

The progression of this analysis, and the layout of this thesis, is represented in Figure 1-7. Chapter 1 details the micro rocket device and its performance history. Chapter 2 addresses the initial experimental characterization of the rocket geometry and material, the pressurized chamber tests. The characterization of the strength of the processed material is presented in Chapter 3. In Chapter 4, a second round of pressurized chamber tests, with modifications dictated by the radiused hub flexure tests, is discussed. The Weibull statistics of the material strength of silicon and its effect on the micro rocket design are presented in Chapter 5. Chapter 6 contains discussion of the results and Chapter 7 provides conclusions and suggestions for further work.

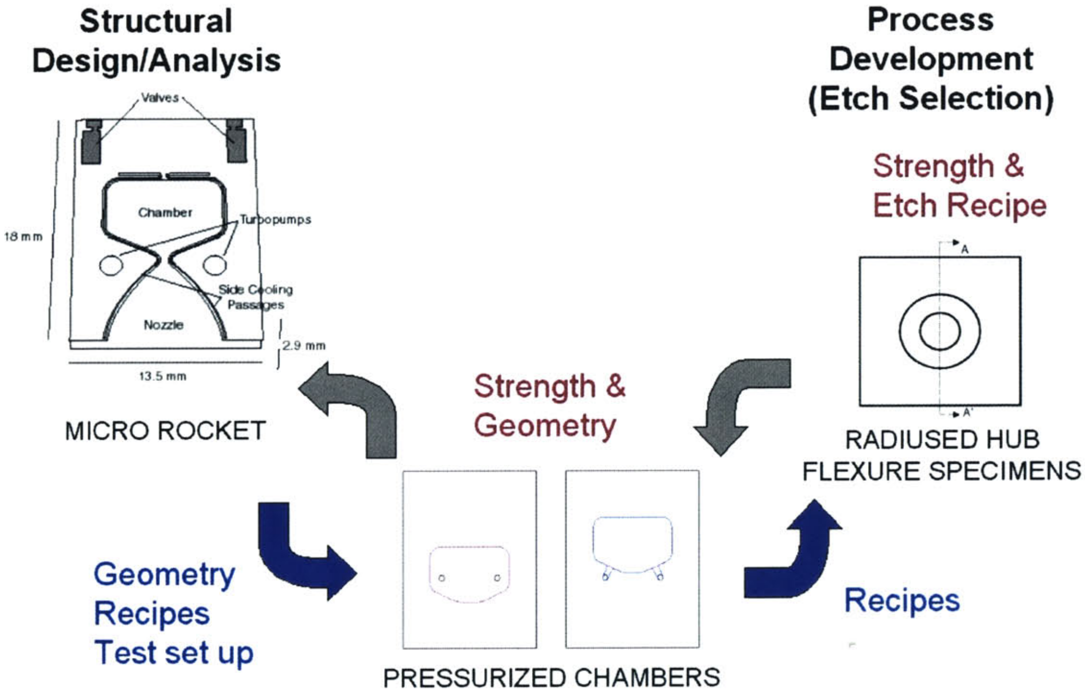

Figure 1-7: Experimental Approach

Chapter 2 Pressure Testing of the Micro Rocket Combustion Chamber

2.1 Pressurized Chamber Tests

The goal of the pressurized chamber experiment is to characterize the in situ material strength of the micro-rocket combustion chamber. The device used in these tests is a 'simplified chamber.' As the name implies, the simplified chamber lacks any of the coolant and propellant supply channels present in the micro-rocket, thereby avoiding the structural elements that complicate the process of distinguishing highly stressed areas intrinsic to the geometry from stress concentrations induced by the complex structures. The chamber does not have a throat opening, allowing it to be internally pressurized. There are two pressure ports on the upper wall. One is for pressurizing the chamber. The other is connected to a pressure transducer used to measure the static pressure inside the chamber. Figure 2-1 shows the two pressure port configurations. In Configuration A, the ports are located on the chamber wall and in Configuration B the ports are located off the wall and are connected to the chamber through a small channel. The two configurations make it possible to determine if there are effects from geometric stress concentrations on the chamber wall. The similar geometry and same planar size of the chamber enables the use of a similar packaging configuration, allowing the devices to be tested on the same test stand.

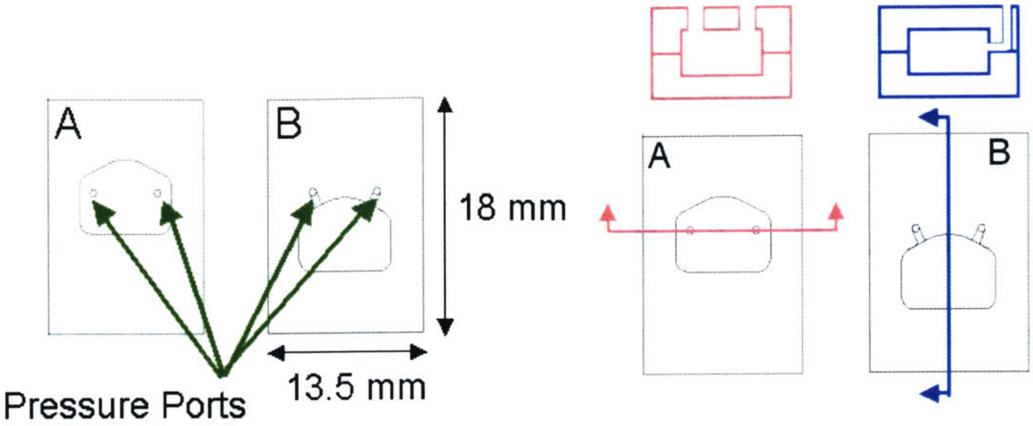

Figure 2-1: Pressure Chamber Configurations

2.2 Fabrication

The chamber device is fabricated using the same basic steps and recipes as the micro-rocket chamber. A summary of the fabrication process will be presented. Additional details of the processes can be found in Appendix A. The chamber is a two-wafer device with the same geometry as the micro-rocket combustion chamber. Each wafer is 400 μm (+/-25 μm) thick with an etched chamber 250 μm deep. There are sixteen devices on each wafer stack.

2.2.1 Etch Recipes

The primary recipe used to fabricate the micro rocket is ADAM06. This recipe was developed specifically to etch the rocket chamber and nozzle during the preliminary design and fabrication of the device. The recipe is a derivative of recipe MIT37, which was developed during the characterization of the Surface Technology Systems etcher used at MIT [6]. Recipe MIT37 provided an etch rate that was nearly independent of feature size.

Such a trait is crucial for the micro rocket because it was critical to the design to etch the chamber and nozzle (large features) and the same time and to the same depth as the cooling passages surrounding the chamber and nozzle (small features) (Figure 2-2). Through iterations varying passivation cycle time, etch platen power, and Automatic Pressure Controller (APC) angle, a recipe was achieved that provided satisfactory surface roughness, bottom surface profile, and etch rate dependence on feature size. This recipe, ADAM06, has lower APC angle and passivation cycle time than MIT37 (Table 2-1). Further discussion of deep reactive ion etching and the etched profiles and surface roughness for the micro rocket chamber can be found in London's PhD dissertation. [6]

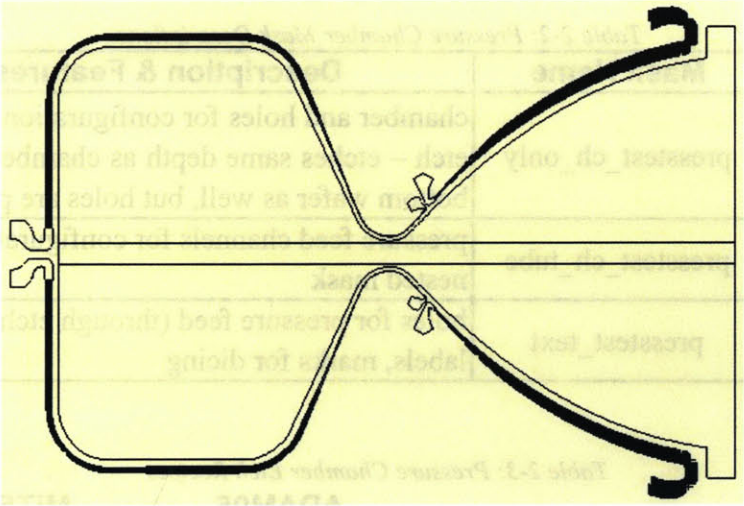

Figure 2-2: Micro Rocket Chamber, Nozzle & Side Cooling Passages

Table 2-1: Micro Rocket Etch Recipe Development

	MIT37		ADAM06	
	Etch	Passivate	Etch	Passivate
Time (s)	15	11	15	9.5
Platen Generator Power (W)	120	0	120	0
Coil Generator Power (W)	600	600	600	600
SF6 Flow (sccm)	140	0	140	0
C4F8 Flow (sccm)	0	95	0	95
APC Angle	65	65	62.5	62.5
Overrun	0.5	0	0.5	0

2.2.2 Process Steps

Both wafers are RCA cleaned and 0.5 μm of thermal oxide is grown. The bottom wafer goes through the photolithography steps (Appendix A) with thick photo resist and is exposed with Mask 1 (Table 2-2and Figure 2-3). For the first exposure on each side of the wafer, there is an alignment mark etch which is very shallow (~2 μm). The wafer is then removed and the alignment marks are patched with photo resist to protect them from the deep etch. Then the lower half of the chamber is etched with the recipe ADAM06 (see Table 2-3) for 250 μm in the Surface Technologies System etcher (STS1).

Table 2-2: Pressure Chamber Mask Descriptions

Mask #	Mask Name	Description & Features
1	presstest_ch_only	chamber and holes for configuration B through etch – etches same depth as chamber (used for bottom wafer as well, but holes are patched)
2	presstest_ch_tube	pressure feed channels for configuration B in nested mask
3	presstest_text	holes for pressure feed (through etch), die labels, marks for dicing

Table 2-3: Pressure Chamber Etch Recipes

	ADAM06		MIT59	
	Etch	Passivate	Etch	Passivate
Time (s)	15	9.5	15	11
Platen Generator Power (W)	120	0	120	60
Coil Generator Power (W)	600	600	750	600
First Step	X		X	
SF6 Flow (sccm)	140	0	105	0
C4F8 Flow (sccm)	0	95	0	40
APC Angle	62.5	62.5	65	65
Overrun	0.5	0	0.5	0

See Section 3.3.1 for discussion of the development of etch recipe MIT59.

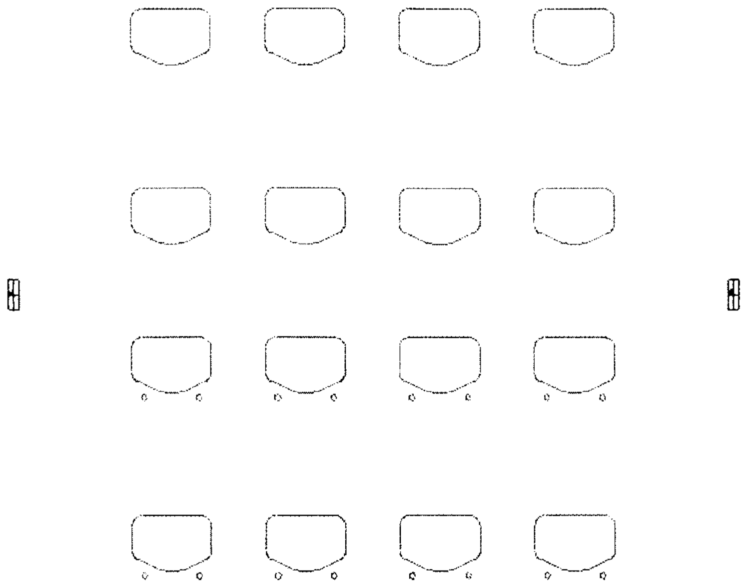

Figure 2-3: Pressure Chamber Mask 1

The top wafer is etched using a nested mask. It is coated with thin photo resist and exposed with Mask 2 (Table 2-2 and Figure 2-4). Then the photo resist is stripped with a piranha etch. The wafer is coated with thick photo resist and exposed to Mask 1. The top half of the chamber is etched with recipe ADAM06 for 240 μm in STS1. The photo resist is then stripped with piranha and the last 10 μm of the chamber, as well as the feed channels for chamber Configuration B, are etched.

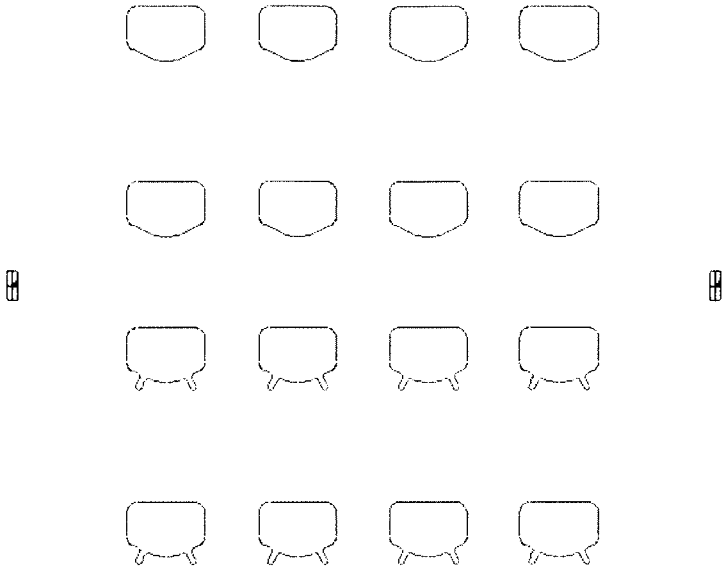

Figure 2-4: Pressure Chamber Mask 2

The back of the top wafer is coated with thick photo resist and exposed with the mask Mask 3 (Table 2-2 and Figure 2-5). The top wafer is mounted on a handle wafer to process the backside. The wafer is etched with MIT59 (Table 2-3) until the holes are etched through. Then the wafer is unmounted from the handle wafer.

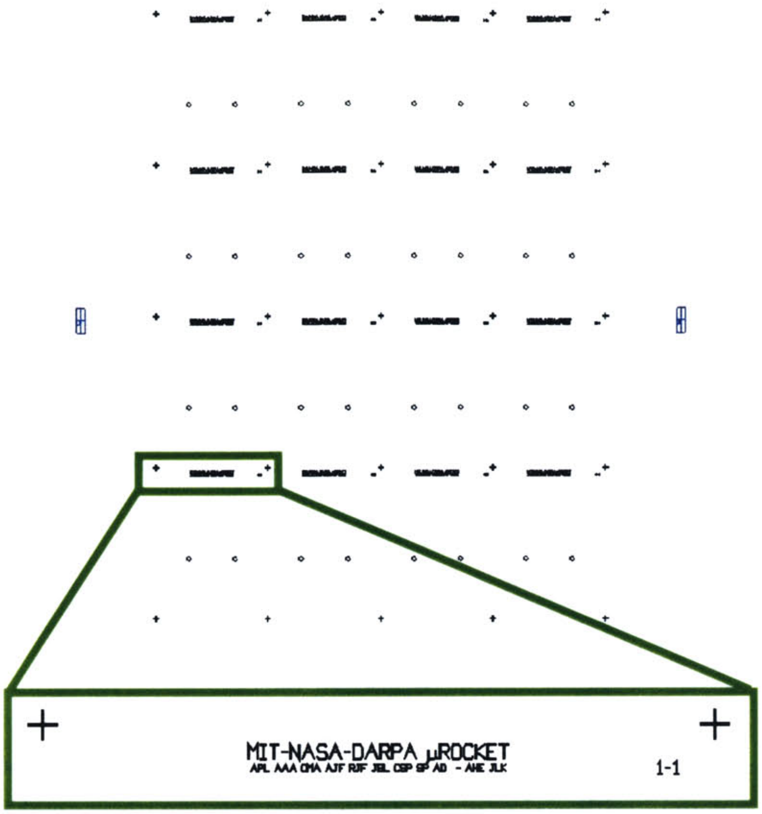

Figure 2-5: Pressure Chamber Mask 3

When all of the etches are complete, the photo resist is stripped with piranha. The wafers are RCA cleaned. The top and bottom wafers are bonded and annealed. After the wafers are annealed, the devices are cut with the die saw and are ready to be tested.

2.3 Experimental Setup

2.3.1 Packaging

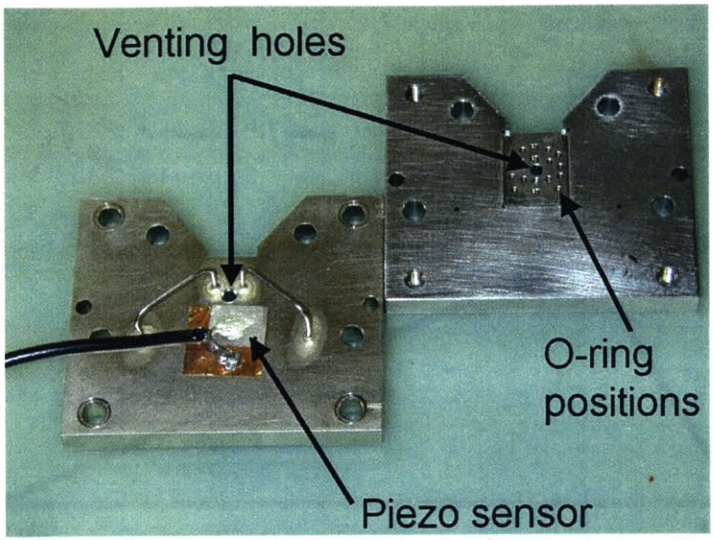

Figure 2-6: Pressure Test Packaging

The chamber is packaged with o-ring contacts between two stainless steel plates that serve as an interface between the macro connections of the test stand and the micro connections of the device (Figure 2-6). The O-rings encircle the chamber and create a fixed boundary condition around the of the chamber walls (Figure 2-7). They also surround the pressure connections to create a seal at the interfaces. The transition between macro and micro pressure feeds occurs through Kovar tubes brazed into the top packaging plate. Helium is fed from a pressurized bottle through piping on the test stand and the mounted packaging into the device. On both packaging plates there is a hole aligned with the center of the chamber. This hole allows the helium to escape the packaging when the chamber fails. Below the venting hole on the front plate there is a piezo sensor mounted. The piezo responds to the vibration of the packaging plates initiated by gas escaping the pressurized chamber as it fails. Because the test stand is remotely located from the controls for the experiment, the response signal of the piezo is an indication of the chamber failure, which may be only a partial fracture of the chamber wall and does not consistently cause an audible explosion.

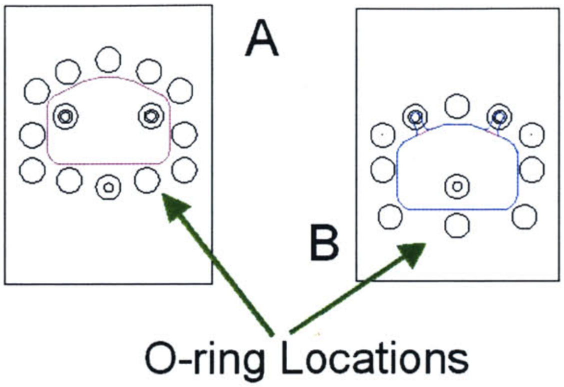

Figure 2-7: O-ring Packaging Placement for Both Device Configurations

2.3.2 Test Set Up

The pressurized chamber tests make use of the test stand designed and built to run the micro rocket. The chambers are pressurized through the coolant system. A detailed description of the test stand and of the original micro rocket packaging, from which the pressure chamber packaging is derived, are available elsewhere [6]. The helium is fed through a gauge controlled outside the test cell chamber and through a series of mass flow meters and filters inside the test cell. When it reaches the plate to which the packaging is mounted, it is fed through the plates, sealed with O-rings, into a kovar tube which feeds back into the plate and into the chamber pressure port. The pressure in the chamber is measured through the second port in the chamber, which leads to another kovar tube, through the packaging plates and to a pressure transducer. The output signals collected are from the pressure transducer and the piezo mounted on the packaging, as well as from an additional pressure transducer located downstream of the device, at a tank used to feed coolant, pressurized by the helium used for these tests. These signals are run through a panel of signal conditioners, into a computer data acquisition card and processed, displayed, and recorded through a LabVIEW vi file (Appendix B).

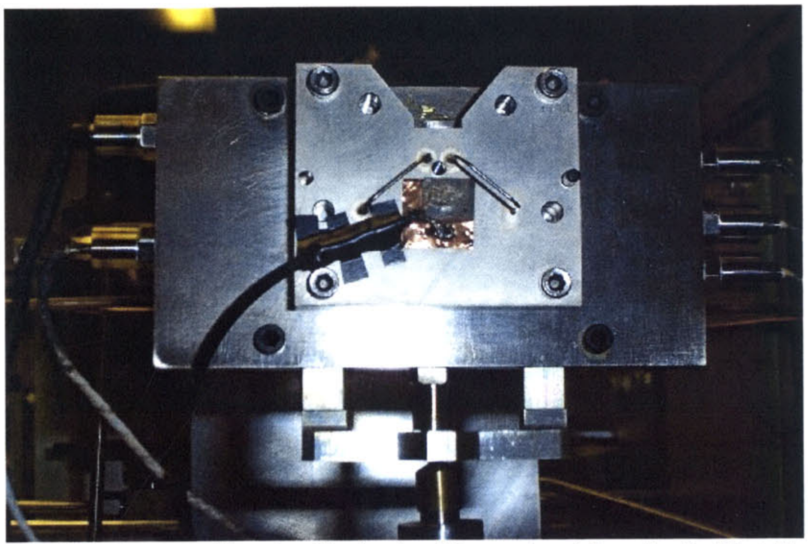

Figure 2-8: Pressure Chamber Packaging Mounted on Micro Rocket Test Stand

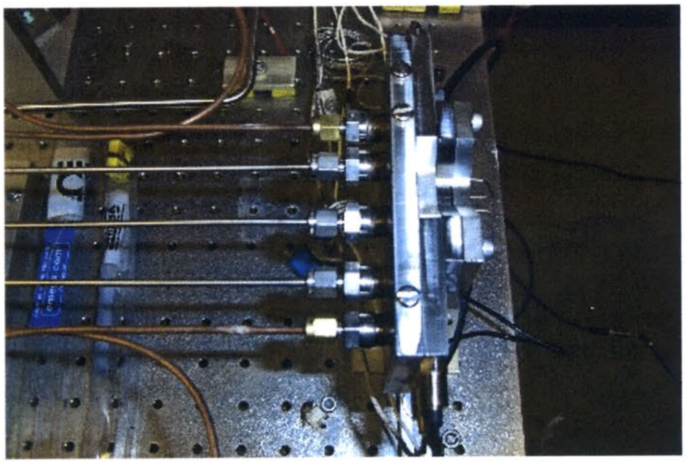

Figure 2-9: Micro Rocket Test Stand

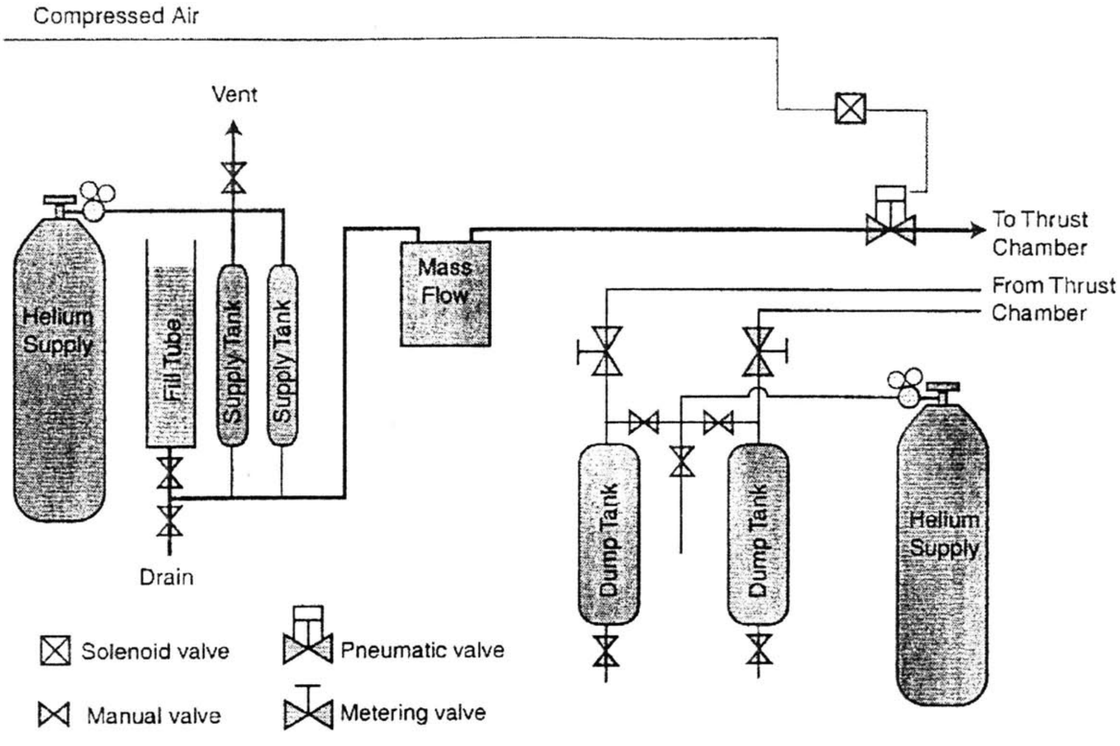

Figure 2-10: Micro Rocket Test Stand Cooling System Configuration [6]

2.4 Modeling

2.4.1 Analytical Modeling

The device wall is modeled as a rectangular plate fixed on all sides and is loaded with a uniform pressure across its surface. In a rectangular plate subject to these conditions, the maximum tensile stress is at the midpoint of the longer side on the top or bottom. This maximum stress location corresponds to the maximum stressed point in a three-dimensional finite element analysis of the chamber geometry (Figure 2-11 and Figure 2-12). Since all of the test chambers are of nominally identical size and geometry, an approximate plate analysis is used here for data reduction. Due to variations in etch rates, slight variations in chamber depth and wall thickness were found. These were accounted for using the failure pressure recorded from the experiment and the measured thickness of the failed wall. The stress in the chamber is calculated as:

$$\sigma_{\max} = -\frac{\beta_1 q b^2}{t^2} \tag{2-1}$$

where b is the in plane dimension of the plate, t is the chamber wall thickness, q is the applied pressure, and β_1 is a fit factor from the analysis and is a function of the chamber geometry [16].

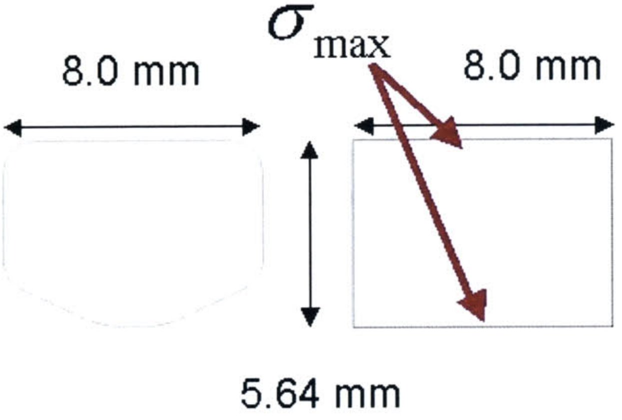

Figure 2-11: Comparison of Chamber Geometry to Rectangle

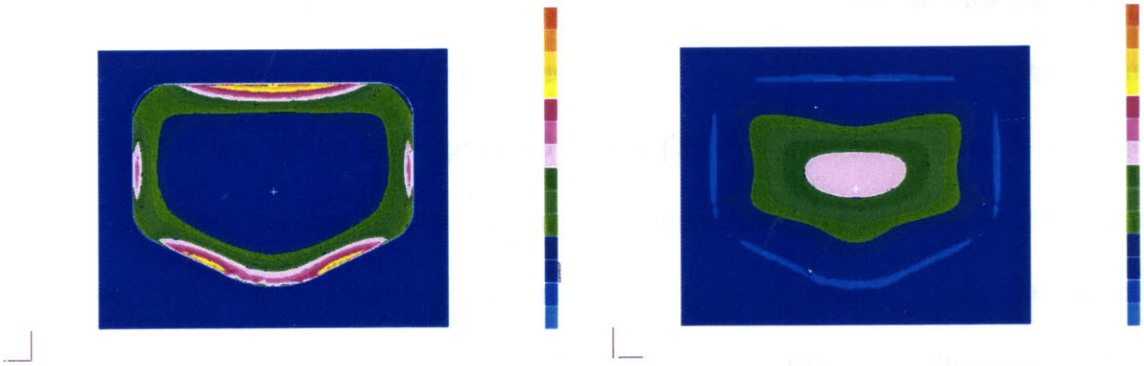

Figure 2-12: Maximum Principal Stress Distribution in Chamber Under Uniform Pressure (Outside & Inside of Chamber)

2.4.2 Stress Concentration Factor

The effect of the fillets at the top and bottom of the chamber is also incorporated into the stress calculation as a stress concentration factor, K_t. Using curves generated from photoelastic testing for a specific test configuration (loading and geometry), a stress concentration factor is estimated. [17] The geometry selected resembles that of the chamber with a comparable loading condition. The fillet radius of a device is measured by fitting a circle to the scanning electron microscope (SEM) image of a cross section. Assuming ideal device geometry (wafer thickness = 400 μm, etch depth = 250 μm, and fillet radius = 30 μm), the stress concentration factor, Kt, is approximately 1.5.

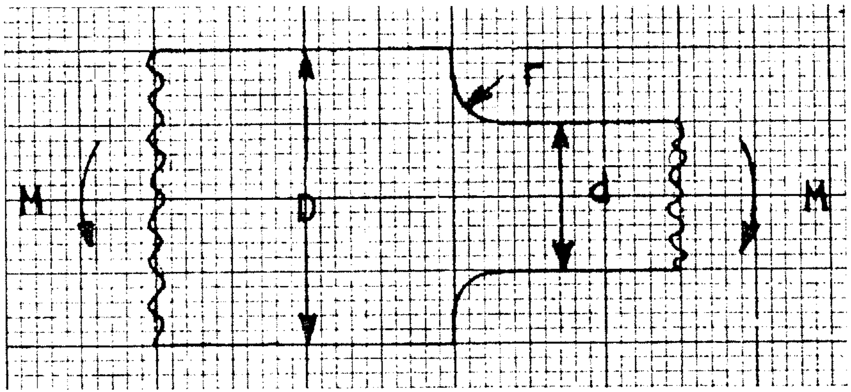

Figure 2-13: Assumed Stress Concentration Geometry [17]

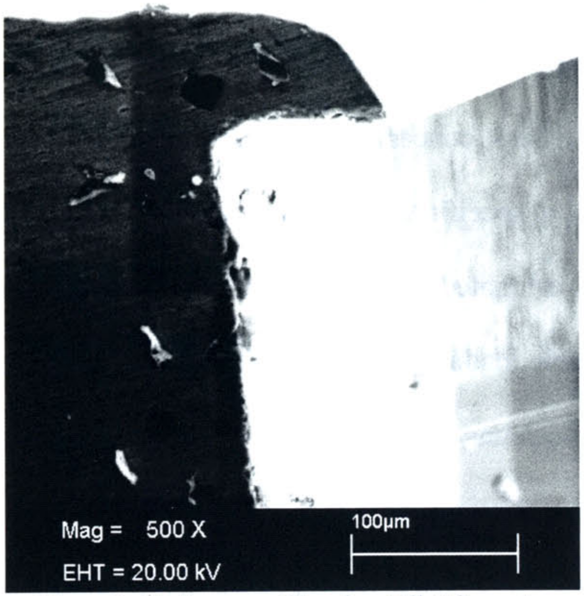

Figure 2-14: Pressure Chamber Fillet Geometry

2.4.3 Finite Element Analysis

A three-dimensional solid finite element model of a half chamber was created. There are two versions, one with holes in the chamber wall (to represent Configuration A) and one without (to represent Configuration B's top plate and both bottom plates). The path to the pressure taps from the chamber in Configuration B was not modeled.

The purpose of the model was to obtain the primary stress distribution in the geometry for a uniform stress applied on all inner surfaces. Therefore, there is no fillet geometry modeled at the corners. This analysis demonstrates that the highest stresses occur at the upper and lower edges of the chamber. A comparison of the two configurations indicates that the introduction of holes on the chamber wall does not create stress states higher than those achieved at the edges of the walls. This appears to be consistent with results obtained in testing, chambers with holes on the walls had at least one hole intact following failure for 85% of the specimens tested.

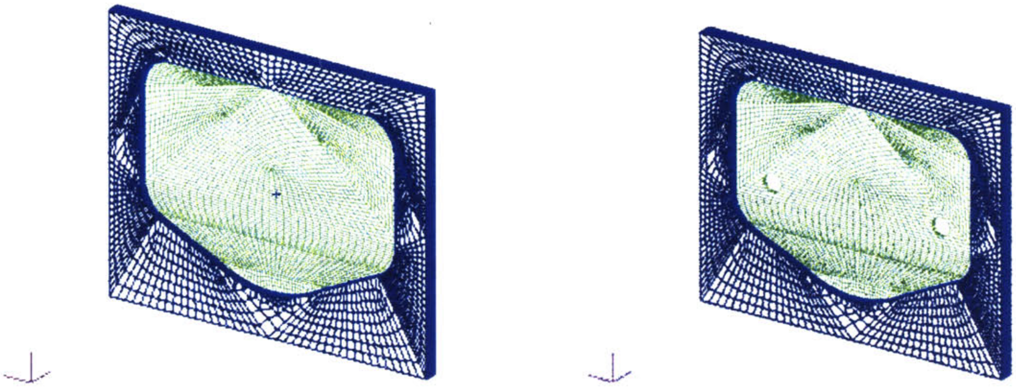

Figure 2-15: Chamber Finite Element Meshes

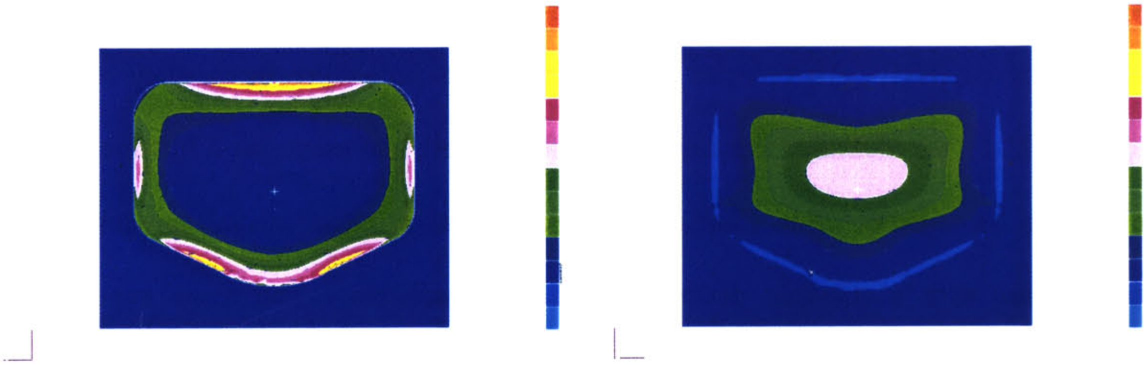

Figure 2-16: Chamber Maximum Principal Stress Distribution (Outside & Inside of Chamber)

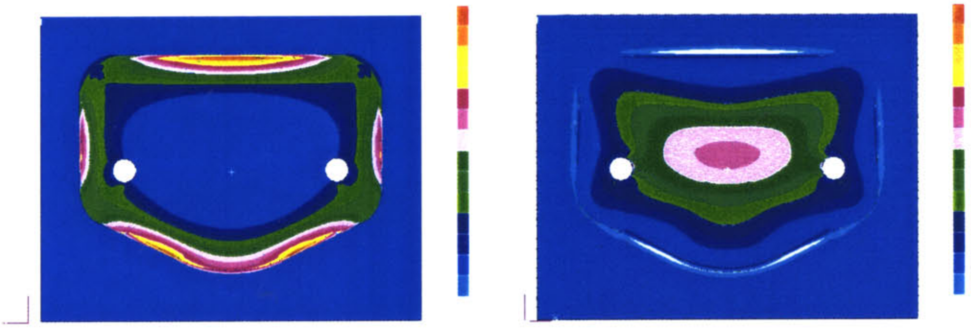

Figure 2-17: Chamber with Holes Maximum Principal Stress Distribution (Outside & Inside of Chamber)

2.5 Experimental Results

The tests were conducted using devices from two fabrication batches. Of the 32 possible devices, only 19 were useable. The unusable devices were due to a fabrication error on the Configuration B devices on one wafer (8 devices) and a broken wafer and incomplete bonding on the second wafer (5 devices). Of these 19 devices, 12 were successfully tested with data recorded and analyzed, 3 did not have recoverable test data, 2 failed in handling, and two were diced for examination in the scanning electron microscope (SEM).

2.5.1 Failure Pressure

Figure 2-18 and Figure 2-19 present the experimental failure pressure for Configurations A and B, respectively. Also plotted is the theoretical expected pressures, calculated using Equation (2-1), the measured thickness of the failed wall, and assuming a fracture strength of 1 GPa for silicon. For Configuration A, the mean experimental pressure is 5.6 atmospheres with a standard deviation of 1.4 atmospheres. The mean experimental pressure for Configuration B is 5.0 atmospheres with a standard deviation of 0.7 atmospheres.

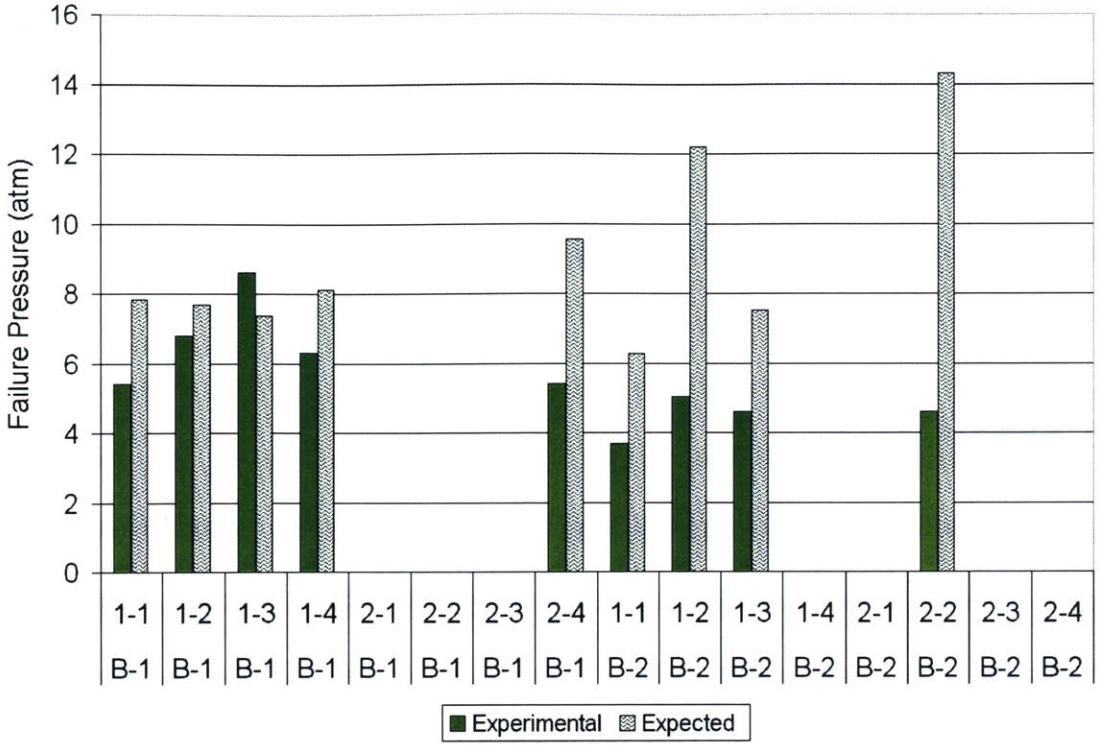

Figure 2-18: Configuration A: Experimental & Theoretical Failure Pressure

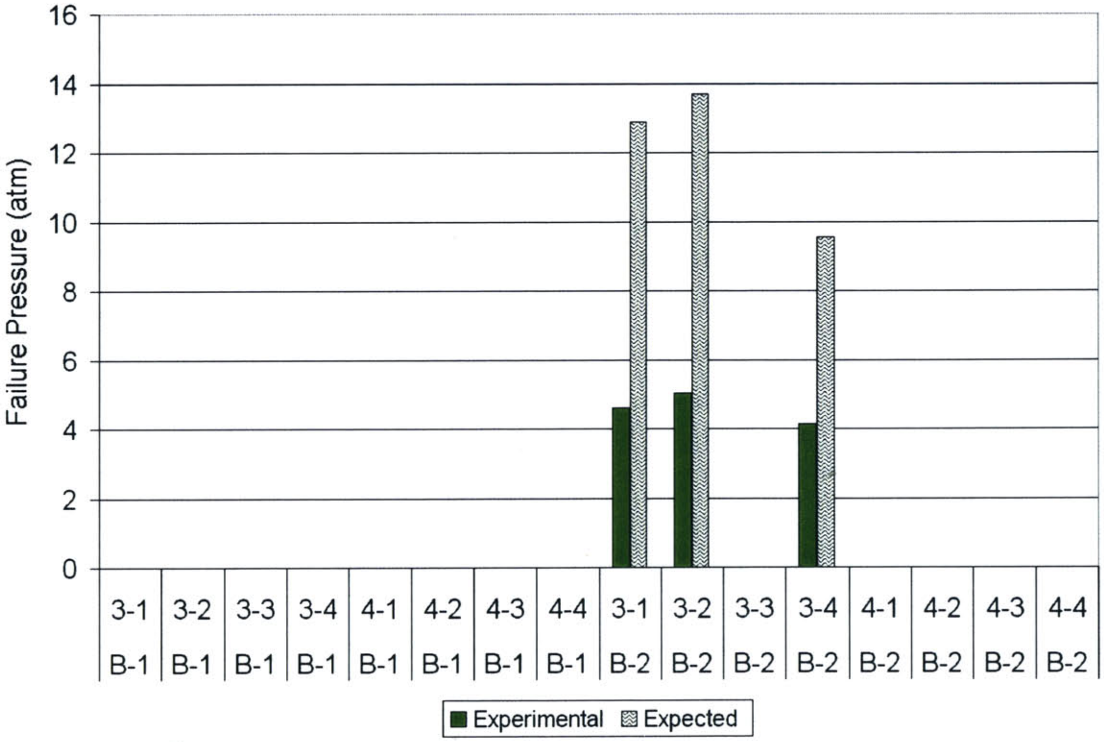

Figure 2-19: Configuration B: Experimental & Theoretical Failure Pressure

In general, the devices from batch two were much closer to the target values for the device geometry, having a wall thickness of 150 μm. However, these devices failed at much lower pressures than the devices from batch one. This is evidence of either local stress concentrations or increased surface roughness present in these devices.

2.5.2 Failure Stress

Figure 2-20 and Figure 2-21 present the nominal stress levels in each failed device, calculated using Equation (2-1). Also plotted is the failure stress multiplied by an approximate stress concentration factor. The stress concentration factor is estimated from photoelastic experimental curves [17] and is a function of device geometry. The average stress concentration factor for Configuration A was 1.41 and 1.47 for Configuration B. Incorporating the stress concentration factor, only three of twelve devices failed at stresses above 1 GPa, the expected allowable stress for the silicon, which was used for the original micro rocket design.

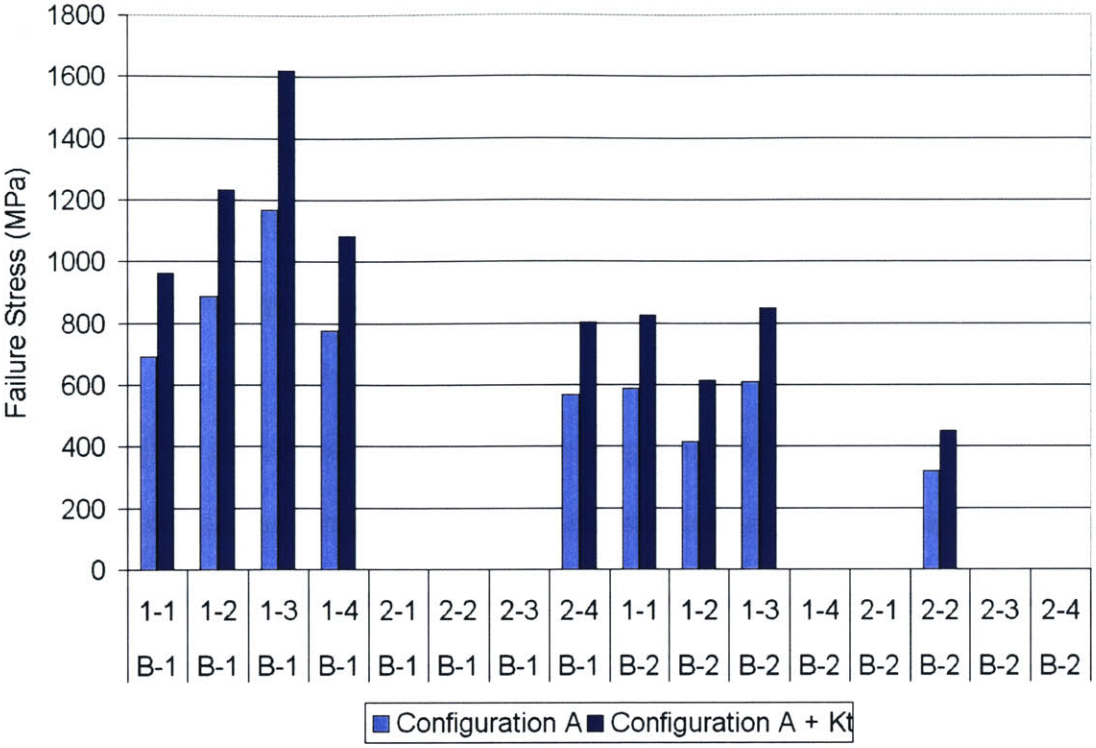

Figure 2-20: Configuration A: Pressure Test Failure Stress

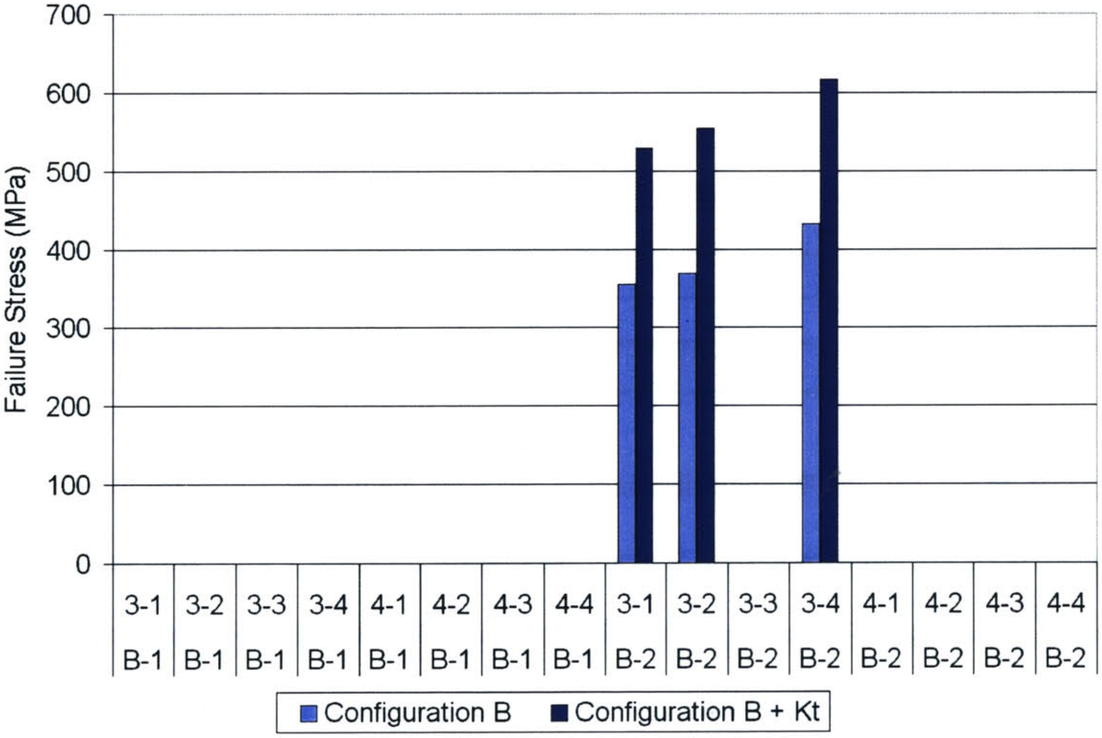

Figure 2-21: Configuration B: Pressure Test Failure Stress

2.5.3 Weibull Distribution

A 2-parameter Weibull curve fit (see Section 1.3.5) was performed for both configurations with the calculated failure stresses (Figure 2-22). Also present in Figure 2-22 are curves representing the Weibull parameters of radiused hub flexure specimen (RHFS) tests conducted by Chen [12] to characterize the strength of etched silicon. The distance between these curves may be due to any of several factors. Variation in surface roughness might be attributed not only to a difference in etch recipe used, but also to the lack of a smoothing isotropic etch in the chambers. There may also be a disparity due to the effective volume/surface area of the two specimen geometries. This issue will be further examined in Chapter 5. The Weibull parameters are listed in Table 2-4. The analysis can only be considered preliminary because the Weibull modulus (m) is low and to ensure an accurate calculation, a larger number of devices per data set, around 30 or more, is recommended [18].

Table 2-4: Weibull Parameters for Configurations A & B

	Configuration			
	A	**B**	**A + Kt**	**B + Kt**
m	2.5	6.86	2.57	9.67
σ_o (MPa)	762	409	1067	591

Figure 2-22 presents the Weibull distribution curve for the two pressure chamber data sets as well as curves representing the Weibull parameters for Chen's work with radiused hub flexure specimens. There appears to be a significant difference between the values, however they cannot be directly compared. The specimen geometries and loading conditions are very different and therefore the effectively loaded areas (or volumes) would be required for accurate comparison. This will be discussed further in Chapter 5.

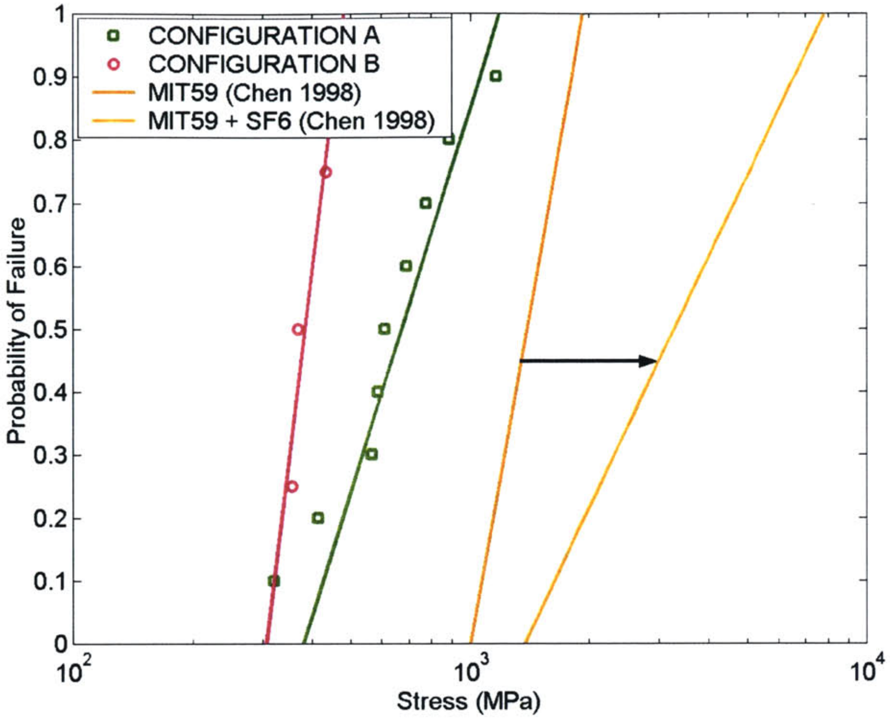

Figure 2-22: Pressure Test Weibull Distribution

Figure 2-23 displays the effect of the stress concentration factor on the Weibull statistics. The slope of the shifted curves is not perfectly parallel because the stress concentration factor was calculated for each individual specimen's geometry. Thus, as the wall thickness of the chambers vary due to etching nonuniformity, the stress concentration factor will vary as well.

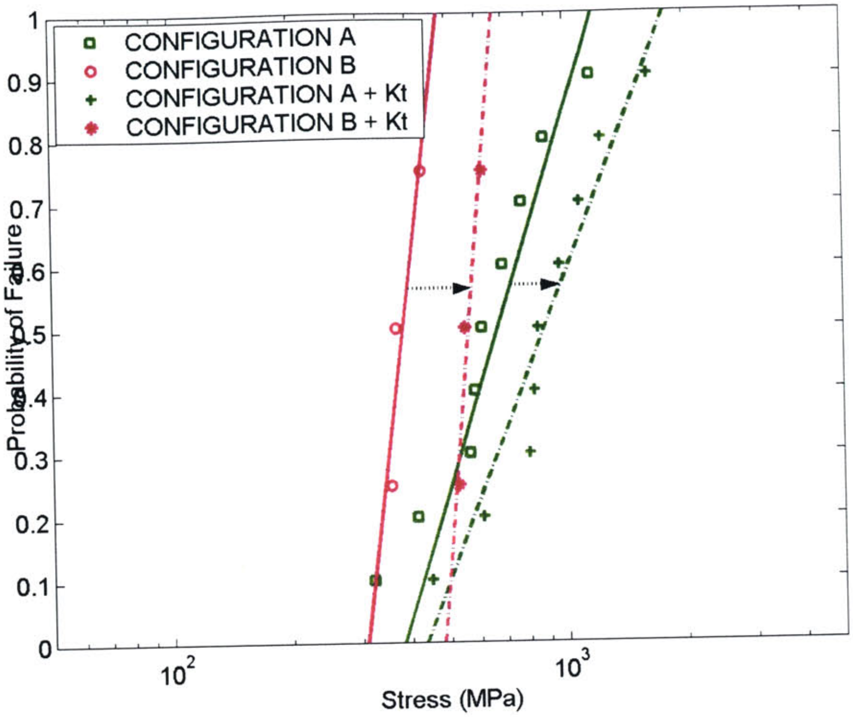

Figure 2-23: Pressure Test Weibull Distribution Stress Concentration Effect

2.5.4 Surface Roughness

Examination of several failed devices with a scanning electron microscope (SEM) revealed surface features like those in Figure 2-24. The fracture appears to initiate on the sidewall of the chamber and to propagate to the chamber wall. The surfaces appear similar to those studied and documented by Rice [19] and are characteristic of fractures in single crystals. The fracture begins with a smooth mirror region that shows no crystallographic dependence. As it expands, the surface becomes striated in a mist/hackle region. Finally, the fracture propagates in arcs that are stepped because the mechanism favors particular crystallographic planes (usually <111> in silicon). In none of the devices examined was there any evidence of failure initiating at or near the bond line. Additionally, there was no clear evidence of failure inducing stress concentrations at the pressure ports on the chamber wall.

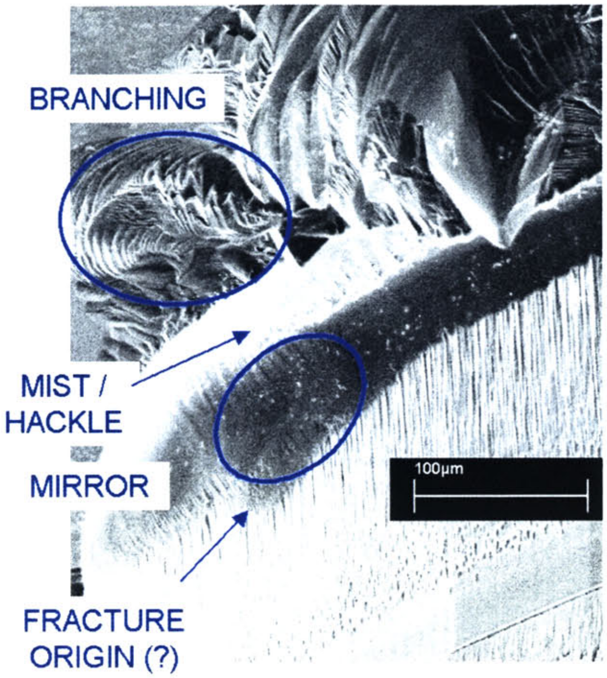

Figure 2-24: Typical Fracture Surface from Pressurized Chamber

The chamber sidewalls are extremely rough surfaces with features on the order of 5 µm (Figure 2-25). Chen established that to achieve a strength of 1 GPa, the maximum allowable flaw size in a device is approximately 0.3 µm [12]. Therefore, it is highly probable that the leading failure mechanism in the chamber devices is the surface roughness of the sidewalls.

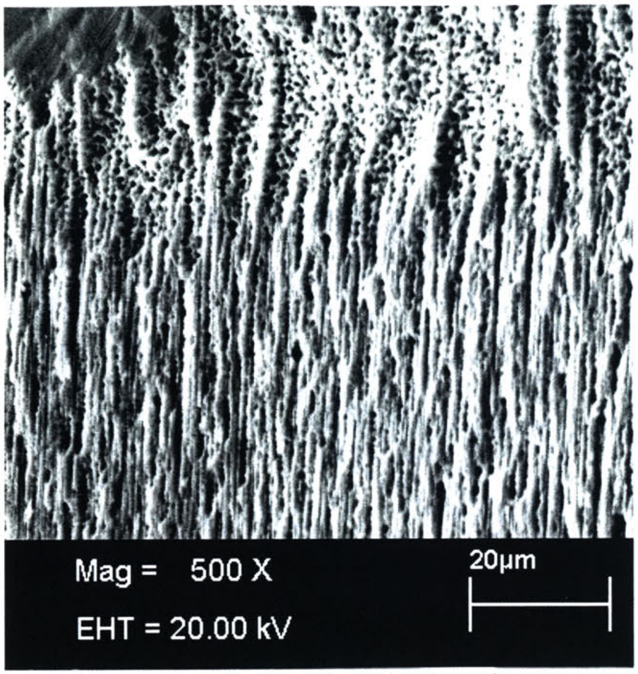

Figure 2-25: Side Wall Surface Roughness

2.6 Summary

The pressurized chamber experiments presented thus far provided insight as to which factors were the most likely contributors to chamber failure. These tests offered no evidence of problems with or stress concentrations from the bond interface of the device. Additionally, misalignment did not appear to be an issue. The analysis conducted corresponded well with the observed behavior of consistent failure at the top of the chamber, away from the throat.

Close examination of the internal surfaces of the devices indicated that surface roughness was a contributing factor to the observed diminished strength. This roughness suggested that the rocket fabrication process is not optimized to retain material strength. The etch recipe used was optimized to achieve equivalent etch rates in small and large features, the cooling channels and the combustion chamber, respectively [6]. In order to relieve this low strength surface concentration condition, the etch process will have to be modified and re-optimized to achieve a balance between feature definition and uniformity, etch rate, and residual surface characteristics contributing to achievable device strength.

Prior to fabricating and testing additional chamber devices, a better understanding of the characteristic strength of the micro rocket etch recipe was desired. This was achieved with a series of radiused hub flexure specimen tests [12] (see Chapter 3). The results from these flexure tests were used to modify fabrication steps for the chamber experiments to follow (Chapter 4).

Chapter 3 Strength Testing of Etched Silicon

3.1 Background

Chen's work with radiused hub flexure specimens demonstrated the effect of the smoothing etch on deep reactive ion etched features to improve effective material strength. Isotropic etching rounds sharp edges, creating blunt notches rather than sharp cracks [12], which decreases the effective stress concentration. Chen demonstrated improvements of effective silicon strength of more than a factor of two [12].

In order to understand better the effect of the micro rocket fabrication process on the effective material strength of processed silicon, radiused hub flexure specimens were fabricated with ADAM06, the micro rocket etch recipe. Devices were also fabricated using ADAM06 followed by an SF6 isotropic smoothing etch. In order to obtain a baseline measure of strength, two additional sets of devices were fabricated using etch MIT69, a standard etch which had been optimized to achieve acceptable strength. One of these two sets was also etched with the isotropic etch to quantify the effect of the smoothing on the baseline. The data that these experiments will be compared to (from Chen's work) tested specimens etched with MIT59 and a 20 second SF6 etch. These etch recipes are further described in Section 3.3.1.

3.2 Radiused Hub Flexure Specimens

The radiused hub flexure specimen is represented in Figure 3-1, where the dimensions are $h_1 = 0.40$ mm, $h_2 = 0.15$ mm, $r = 1$ mm, $R = 2.5$ mm, and $L = 10$ mm.

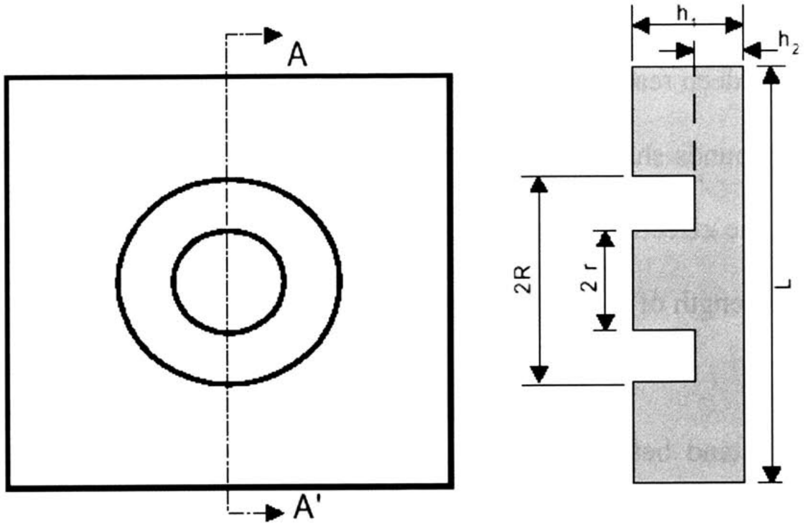

Figure 3-1: Radiused Hub Flexure Specimen [12]

3.3 Fabrication

Fabrication of the radiused hub flexure specimen is a straightforward process. The devices are made on one wafer with two masks, one for each side. The masks used to fabricate these devices are the same ones used in the original study. They are shown in Figure 3-2. Mask 1 creates alignment marks on the back of the wafer, providing a guide for load application on the center of the die. Mask 2 creates the features of the specimen. The dimensions are defined in Figure 3-1. Each 4-inch wafer has 32 specimens.

3.3.1 Etch Recipes

Table 3-1: Radiused Hub Flexure Specimen Recipes

	MIT69a		ADAM06		MIT59		SF6-4
	Etch	Passivate	Etch	Passivate	Etch	Passivate	Etch
Time (s)	14	11	15	9.5	15	11	
Platen Generator Power (W)	100	60	120	0	120	60	120
Coil Generator Power (W)	750	600	600	600	750	600	950
First Step	X		X		X		X
SF6 Flow (sccm)	105	0	140	0	105	0	30
C4F8 Flow (sccm)	0	40	0	95	0	40	0
APC Angle	75	75	62.5	62.5	65	65	75
Overrun	0.5	0	0.5	0	0.5	0	

The etch recipes used for this study are documented in Table 3-1. Also included in Table 3-1 is the recipe used in Chen's work (MIT59). The development of the recipe ADAM06 is presented in Section 2.2.1. Etch recipes MIT59 and MIT69 have origins with recipe MIT47 (Table 3-2). MIT47 was developed for its production of smooth trench walls. However, this recipe did not successfully etch multiple high aspect ratio trenches in close vicinity. In order to remedy this situation, the ion flux during the etch cycle was increased by changing the applied coil power. The optimization of this modification to MIT47 became MIT59, which is documented as optimized for etching narrow trenches (~4 μm) in the vicinity of wide trenches (~40 μm) where trench width is observed to increase approximately 1μm for every 100 μm of etched depth. Recipe MIT69 was derived from MIT59 for etching through wafers thicker than 525 μm. By lowering the etch step electrode power, the selectivity is increased by accepting slight decreases in etch rate and anisotropy. [20] Detailed discussion of the effects of etch parameters is available in Section 1.3.2.

Table 3-2: MITxx Etch Recipes

	MIT47		MIT59		MIT69a	
	Etch	Passivate	Etch	Passivate	Etch	Passivate
Time (s)	15	11	15	11	14	11
Platen Generator Power (W)	120	60	120	60	100	60
Coil Generator Power (W)	600	600	750	600	750	600
First Step	X		X		X	
SF6 Flow (sccm)	105	0	105	0	105	0
C4F8 Flow (sccm)	0	20	0	40	0	40
APC Angle	65	65	65	65	75	75
Overrun (s)	1	0	0.5	0	0.5	0

3.3.2 Process Steps

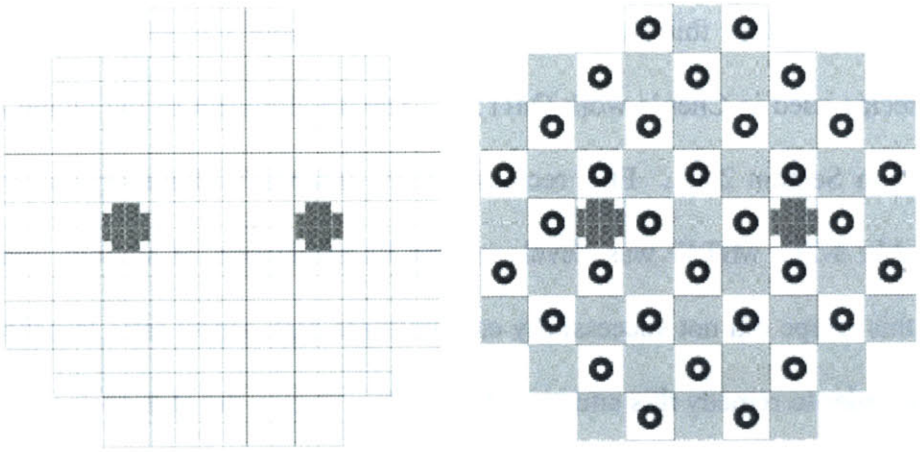

Mask 1 Mask 2

Figure 3-2: Radiused Hub Flexure Specimen Masks [21]

Each wafer is cleaned with an RCA clean and a thin thermal oxide layer is grown. The wafer is coated with thin photo resist and exposed through Mask 1. The oxide is removed with BOE and the wafer is etched with the ALIGN recipe (Appendix A). The photo resist is removed with piranha (3:1 H_2SO_4:H_2O_2). The other side of the wafer is then coated with thick photo resist (10 μm) and exposed to Mask 2. The wafer is mounted on a handle wafer for the deep etch. This is done because a large amount of material is removed, creating a checkerboard pattern about the devices, and this removal of material makes the wafer very fragile. The hub feature is etched for 250 μm, using one of the etch recipe combinations discussed above. The photo resist is removed. The etch depth is measured for each device using a Nomarski interference contrast microscope. The wafer thickness is measured with a digital micrometer. The devices are then die sawed and tested.

3.4 Test Set Up

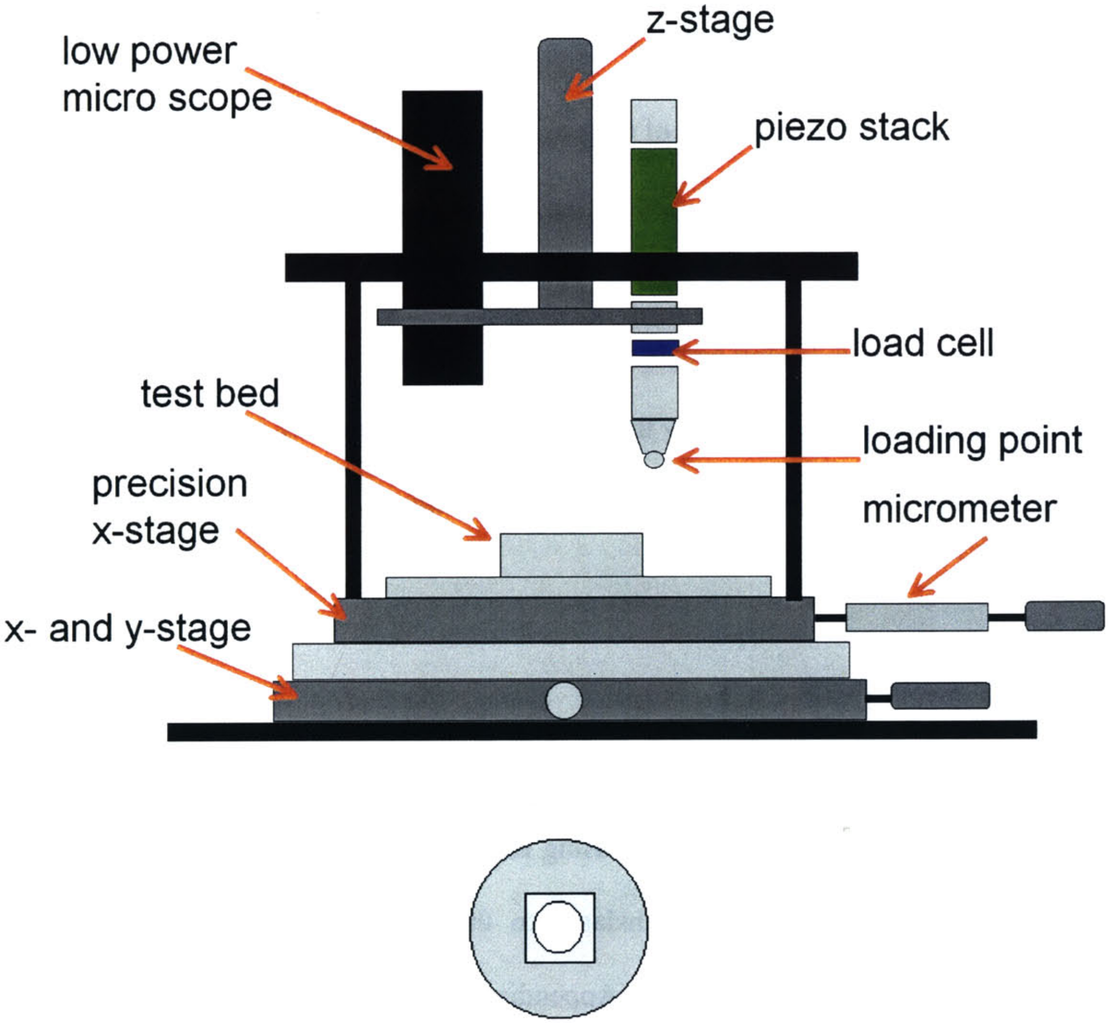

Figure 3-3: RHFS Test Fixture

The test fixture (Figure 3-3) used for the radiused hub flexure specimens is comprised of several translation stages , a low-power microscope, an actuator, a load cell, and a test bed for the specimen. The base is an x-y stage with an optical precision single axis translation stage mounted on it. The precision stage controls movement in the x-direction, between the microscope and the loading point, and has a digital micrometer attached. There is also a z-direction stage that translates to bring the load application point into contact with the specimen as well as to achieve the correct focal length to view the specimen through the microscope for alignment. The load cell is commercially available and is strain gauge based with a full-scale range of 500 N. The load cell is actuated with a commercially available piezo actuator with a range of 60 μm. The load was applied to the specimen with a 1.5 mm steel ball, which is attached to the load cell. The specimen was placed in a machined aluminum base that fits into an interface plate attached to the precision stage. This base has a 10 mm x 10 mm square to hold the specimen in place and a 7 mm diameter hole in the center of the base to allow the specimen to deflect under load. The calibrations performed for this test fixture are documented in Appendix C. [22]

3.5 Test Procedure

The specimen is placed into the test fixture with the hub feature facing down. The device is aligned with cross hairs in the viewer using an x-y stage (Figure 3-4). Using a second (precision) x-stage, the device is translated to the loading position. This distance is determined by a positioning calibration (Appendix C) conducted each time the load cell is mounted.

A compliance curve can be generated using the piezo stack inline with the load cell. This allows for a very smooth load-displacement curve. However, the stack does not have a large enough displacement to allow its use for the test to failure of these specimens. The piezo was initialized to zero and brought into contact with the device. The loading was then controlled through incremented voltage increases to extend the piezo stack. This was done through a LabVIEW .vi file (Appendix B). The .vi file also recorded the values output from the piezo and the load cell.

For the tests to failure, the device was loaded by hand. The load was applied by translating the load cell and its application point vertically using a z-stage. The same LabVIEW file recorded the load cell output, which was then post-processed into failure load data.

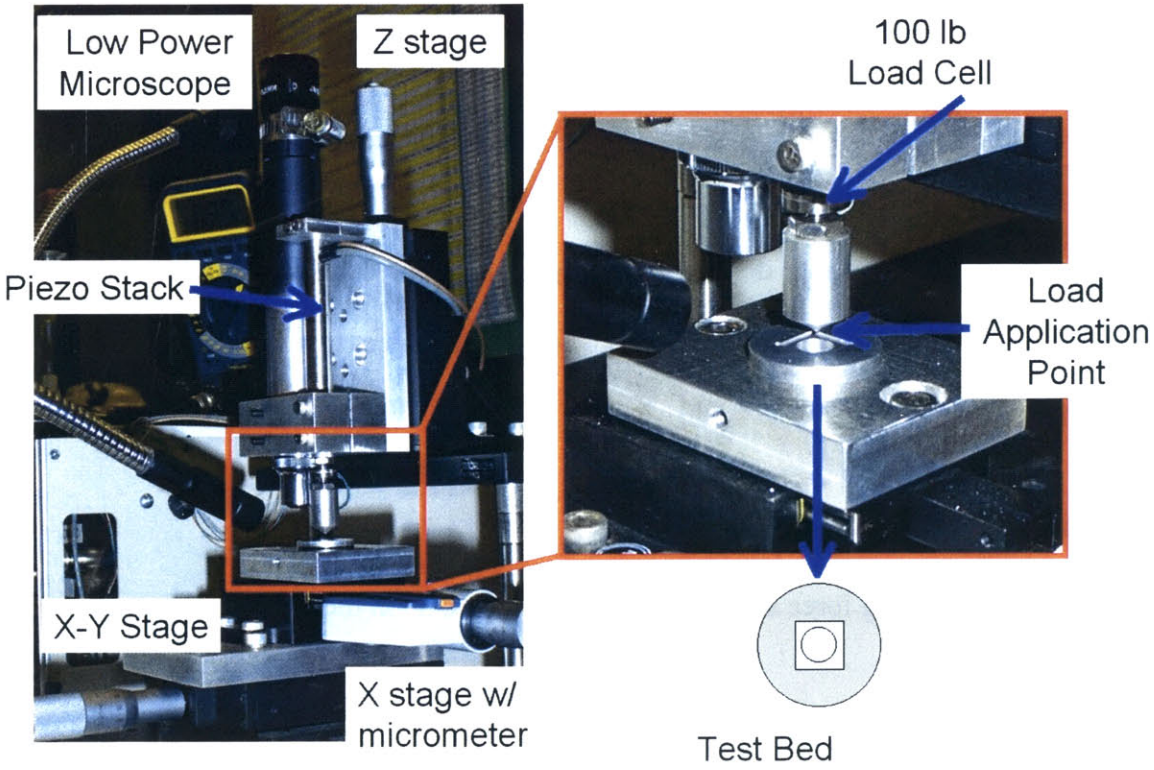

Figure 3-4: RHFS Test Set Up

3.6 Modeling Correlation

3.6.1 Analytical Model

The deflection of this specimen can be calculated by superimposing the deflection from two simple loading cases for a circular plate with a circular hole at the center from annular plate theory [23]. Case one is a plate subject to a bending moment, M_1, and case two is a plate subject to bending by shearing forces, Q (Figure 3-5). The deflection equations are

$$w_1 = -\frac{1}{4}C_1 r^2 - C_2 \ln(r) + C_3 \tag{3-1}$$

$$w_2 = \frac{1}{8}\frac{Fr^2 \ln(r)}{\pi D} - \frac{1}{8}\frac{Fr^2}{\pi D} - \frac{1}{4}C_1 r^2 - C_2 \ln(r) + C_3 \tag{3-2}$$

where r is the radial location, and D is the plate modulus:

$$D = \frac{Eh^3}{12(1-\nu^2)} \tag{3-3}$$

C_1, C_2, and C_3 are constants derived by applying boundary conditions to the equations (assumed pinned at the edges for this configuration and subject to a load at the hole). F is the applied load:

$$F = 2\pi bQ \tag{3-4}$$

where Q is the shearing force and b is the radius of the hole in the plate.

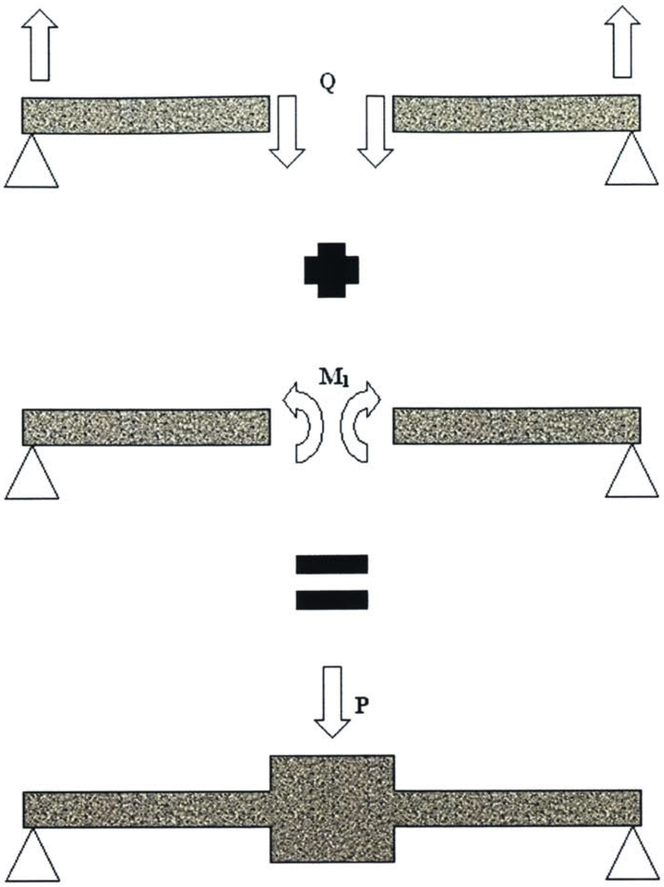

Figure 3-5: Superposition of Annular Plate Loading Conditions

From the equation for deflection, the moment in the radial and tangential directions can be calculated:

$$M_r = -D\left[\frac{d^2w}{dr^2} + \frac{\nu}{r}\frac{dw}{dr}\right] \qquad (3\text{-}5)$$

$$M_t = -D\left[\frac{1}{r}\frac{dw}{dr} + \nu\frac{d^2w}{dr^2}\right] \qquad (3\text{-}6)$$

And the corresponding stresses can be calculated:

$$\sigma = \frac{6M}{h^2} \qquad (3\text{-}7)$$

where h is the plate thickness.

The plots of deflection and stress generated by the model for a load of 1 N are in Figure 3-6 and Figure 3-7, respectively. The Matlab code for this model is available in Appendix D.

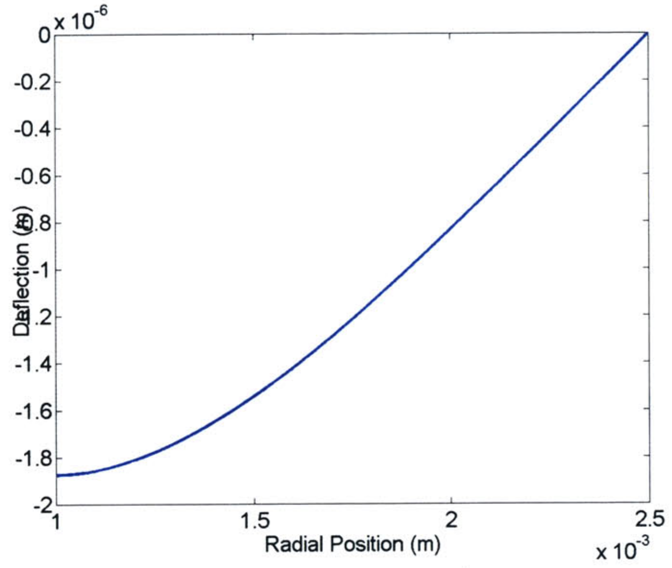

Figure 3-6: RHFS Model Deflection

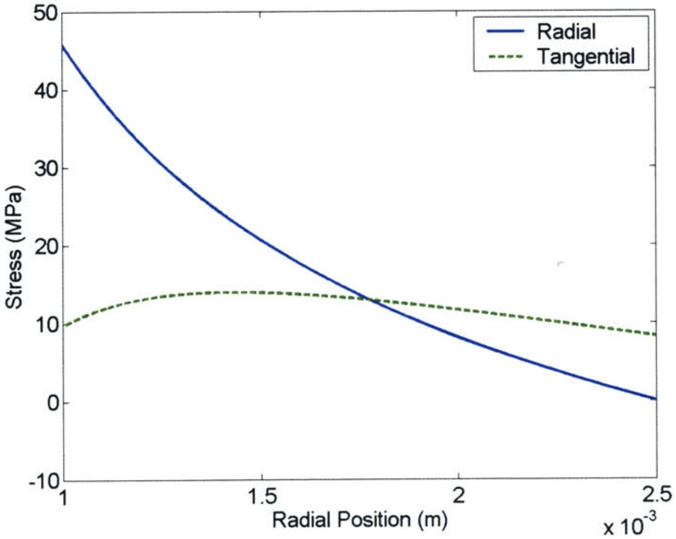

Figure 3-7: RHFS Model Stress States

3.6.2 Stress Concentration Factor

The stress concentration factor of a device is determined by the fillet radius of the etched geometry. The model used to estimate this value is discussed in Section 2.4.2. Fillet measurements were approximated using a scanning electron microscope (see figures below). Though there is variation in fillet size with variation in etch recipe, the fillets on the radiused hub flexure specimens are all approximately of the same order of magnitude. For the calculation of a stress concentration factor, it is estimated that the fillet radius is 8 μm. The stress concentration factor applied is estimated from a curve fit and the ratio of the fillet radius to the wall thickness. The average stress concentration factor for each specimen set is listed in Table 3-3. The effect of the stress concentration factor can be seen in the failure stress plots presented in Section 3.7.2.

Table 3-3: Average Stress Concentration Factor for RHFS Recipes

Recipe	MIT69	MIT69 + SF6	ADAM06	ADAM06 + SF6
Kt avg	2.41	2.52	2.30	2.36
Std Dev	0.013	0.009	0.025	0.025

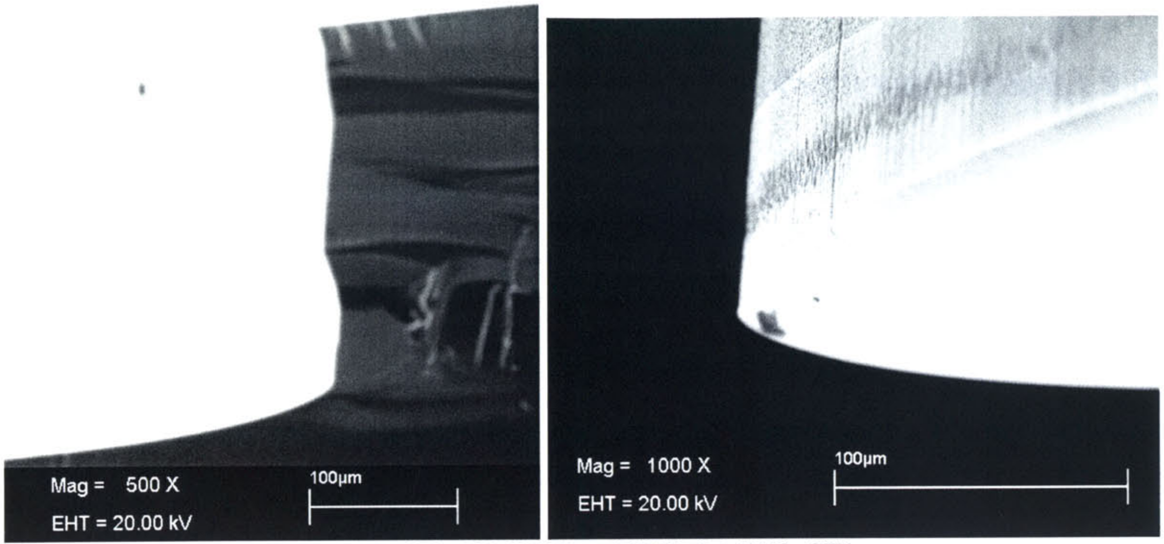

Figure 3-8: RHFS Fillets: MIT69 & MIT69+SF6

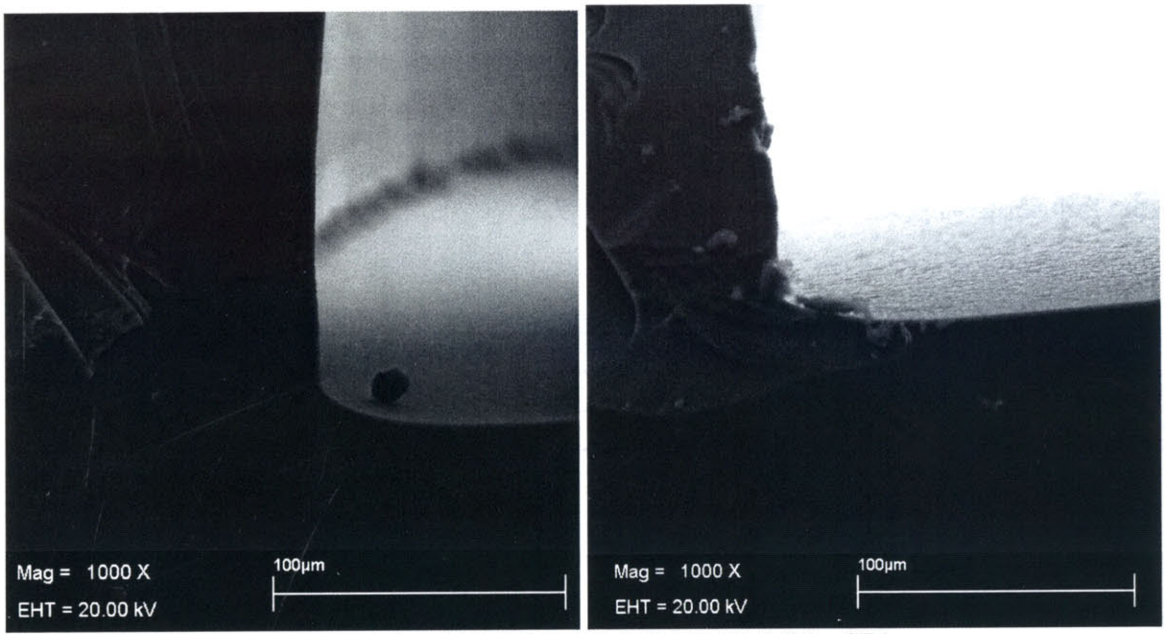

Figure 3-9: RHFS Fillets: ADAM06 & ADAM06 + SF6

3.7 Experimental Results

Four etch conditions were tested, each with thirty specimens for each condition. Failure loads ranged from 6 N to 130 N. This variation was due to process dependent material strength as well as variation in wall thickness, also due to processing. The non-uniformity in etch depth across the wafer is represented in Figure 3-10, where each shaded square represents a die on the wafer (see Figure 3-2). The failure load statistics are summarized in Table 3-4.

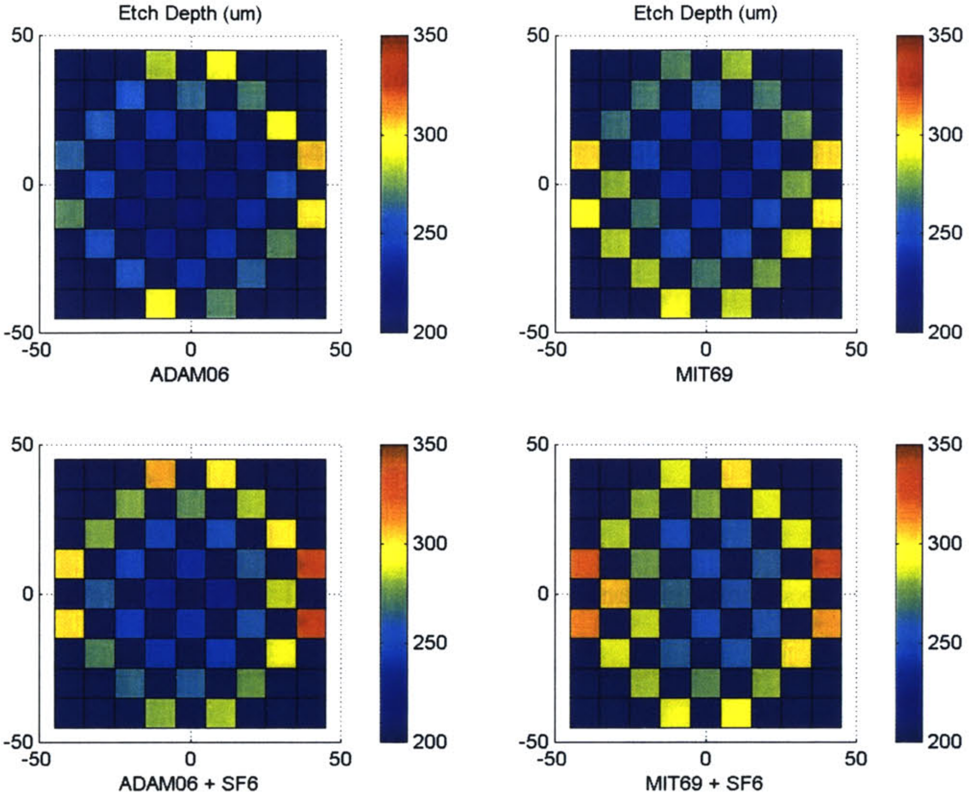

Figure 3-10: Etch Variation Across RHFS Wafers

3.7.1 Failure Load

Table 3-4: RHFS Failure Load Statistics

	Failure Load (N)	
Etch Recipe	**Mean**	**Std Dev**
MIT69	36.9	11.1
MIT69 + SF6	80.2	27.5
ADAM06	22.6	8.5
ADAM06 + SF6	65.3	24.0

There was considerable variation in failure stresses across the data sets as well as within each data set.

3.7.2 Failure Stress

The failure stress of each specimen was estimated using the measured failure load, measured dimensions of the specimen (wall thickness and wafer thickness), and the model presented in Section 3.6.1. A stress concentration factor was then calculated for each specimen's geometry and applied to the calculated failure stress. The effect of these stress concentration factors is quite significant and can be seen in the following figures. The Matlab code used to calculate these values is available in Appendix D.

The majority of specimens in each set failed above the 1 GPa stress level prior to the application of the stress concentration factor. 13% of the specimens without isotropic etch and 3% of devices with isotropic etch failed at a stress below 1 GPa. With the stress concentration factor applied, 3% or less of devices failed at a stress lower than 2 GPa.

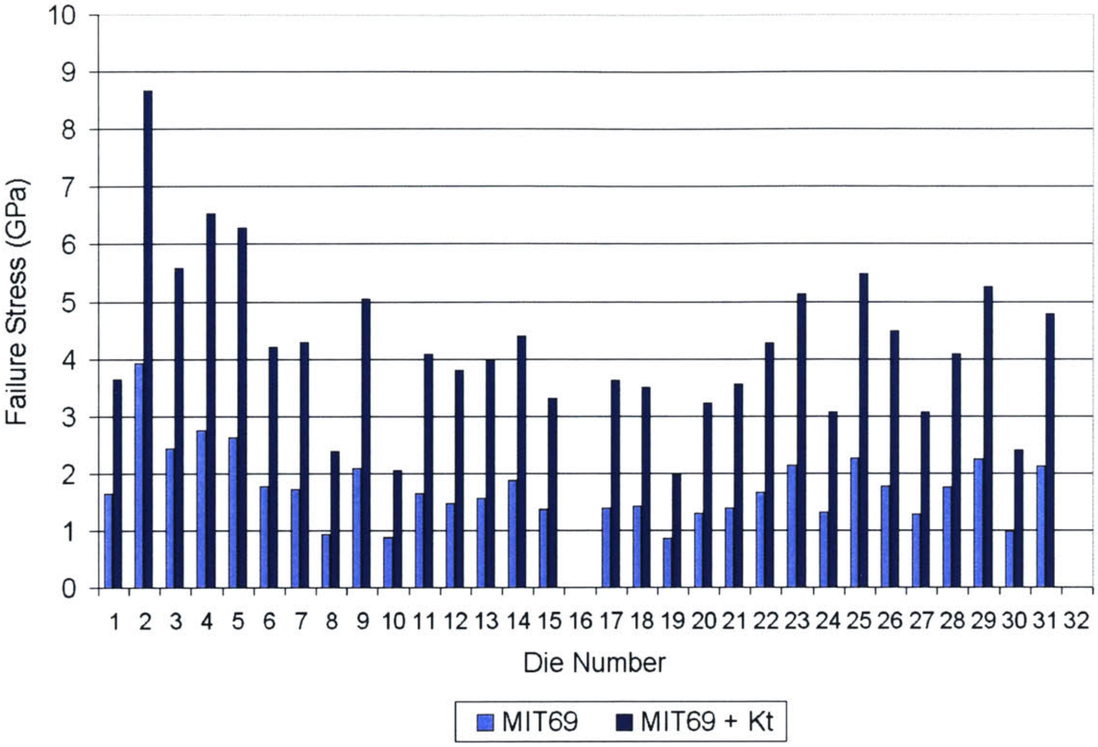

Figure 3-11: MIT69 Failure Stress

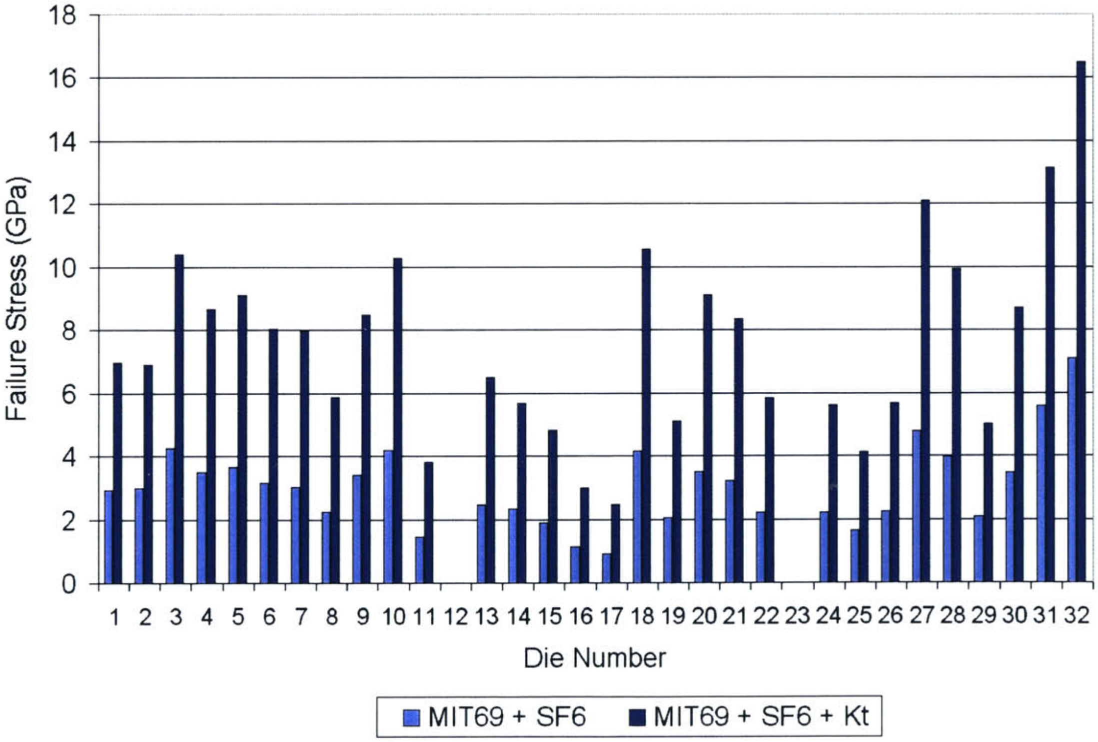

Figure 3-12: MIT69 + SF6 Failure Stress

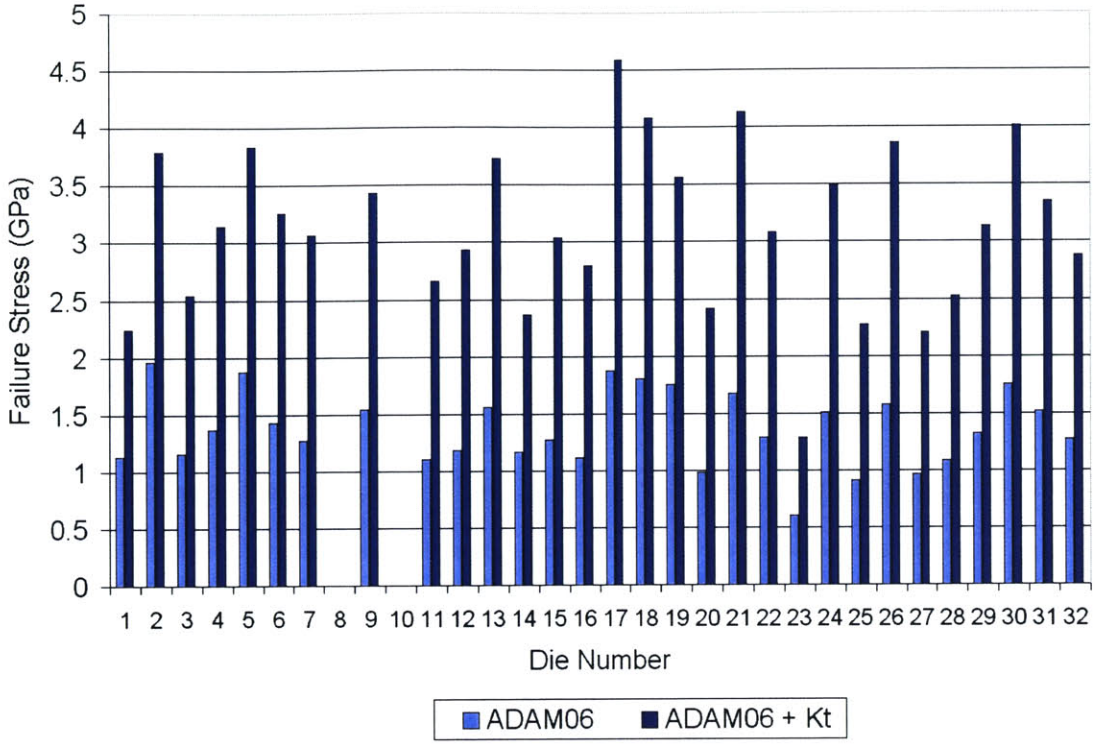

Figure 3-13: ADAM06 Failure Stress

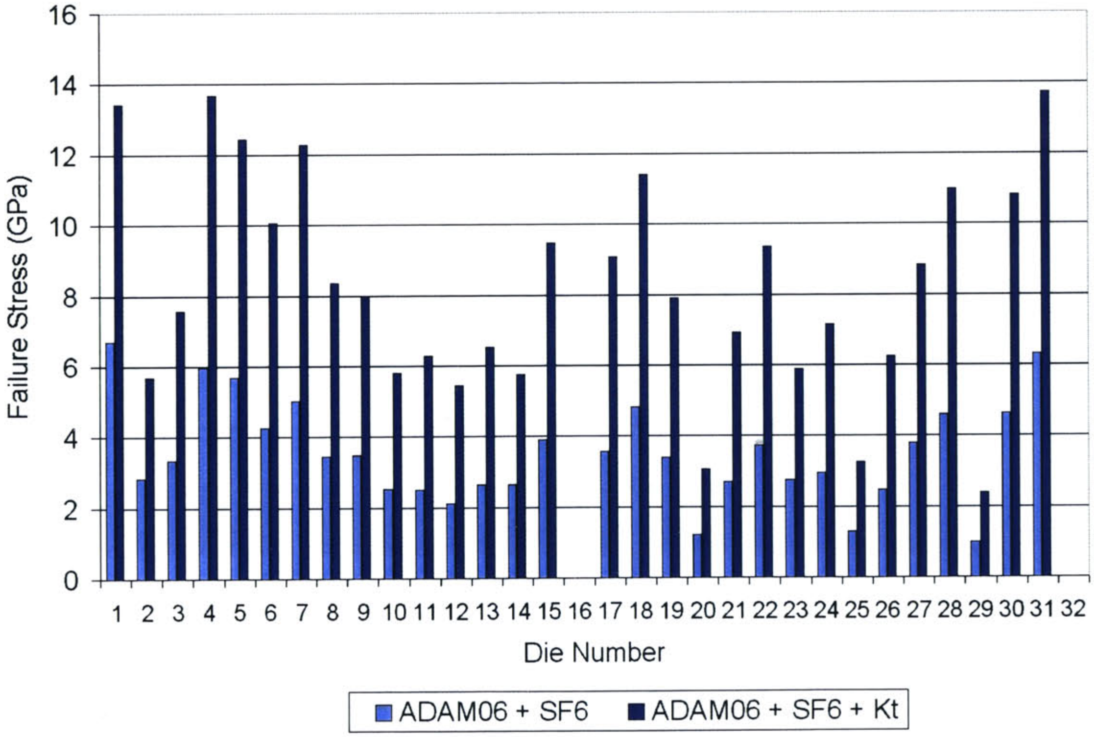

Figure 3-14: ADAM06 + SF6 Failure Stress

3.7.3 Weibull Distribution of Strength

In order to compare the relative strengths of the etch recipes tested, a 2-parameter Weibull analysis (see Section 1.3.5) was conducted. This analysis does not consider the volumetric or surface area effects (see Chapter 5); however, the data sets can be compared because they are for the same tests and the specimens are of nominally identical geometries. Figure 3-15 presents the data from all four etch conditions tested and compares those sets to curves representing the results of Chen's work with radiused hub flexure specimens fabricated by similar processes. The arrows indicate the shift in strength due to the introduction of an isotropic (SF_6) etch (2 minutes long for this study, 20 seconds for Chen's data). The calculated Weibull parameters for the data in Figure 3-15 are summarized in Table 3-5.

Table 3-5: Weibull Data for RHFS Etches

			Kt	
Etch Recipe	**m**	**sigma**	**m**	**sigma**
ADAM06	4.3	1500	4.3	3440
ADAM06 + SF6	2.4	4030	2.6	9380
MIT69	3.1	1960	3.3	4690
MIT69 +SF6	2.5	3460	2.6	8600
MIT59	9.1	1510	--	--
MIT59 + SF6	3.3	4000	--	--

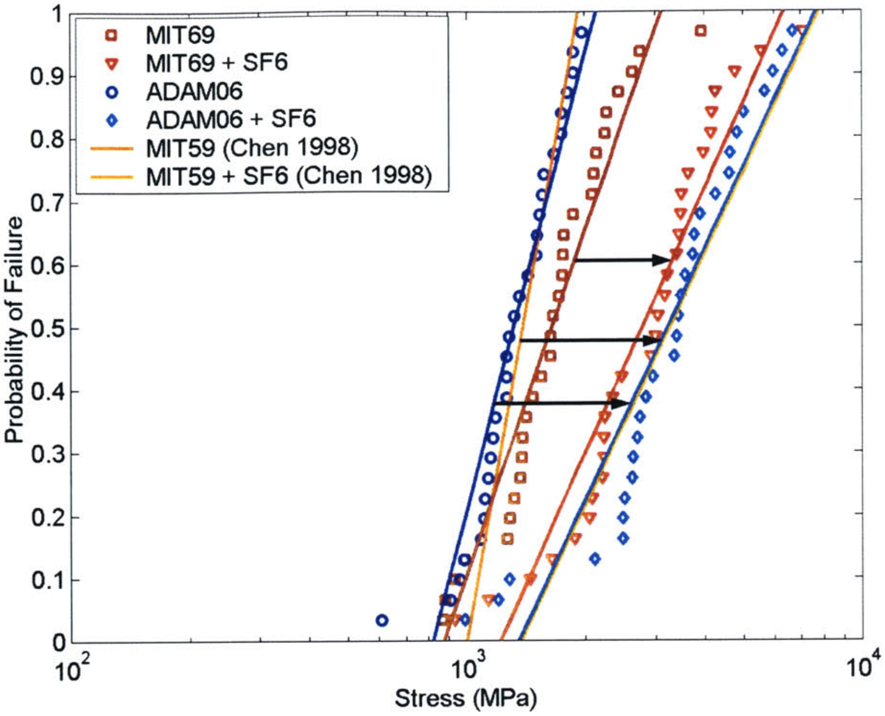

Figure 3-15: Weibull Data for Radiused Hub Flexure Specimens Fabricated with Six Etch Recipes (No Kt)

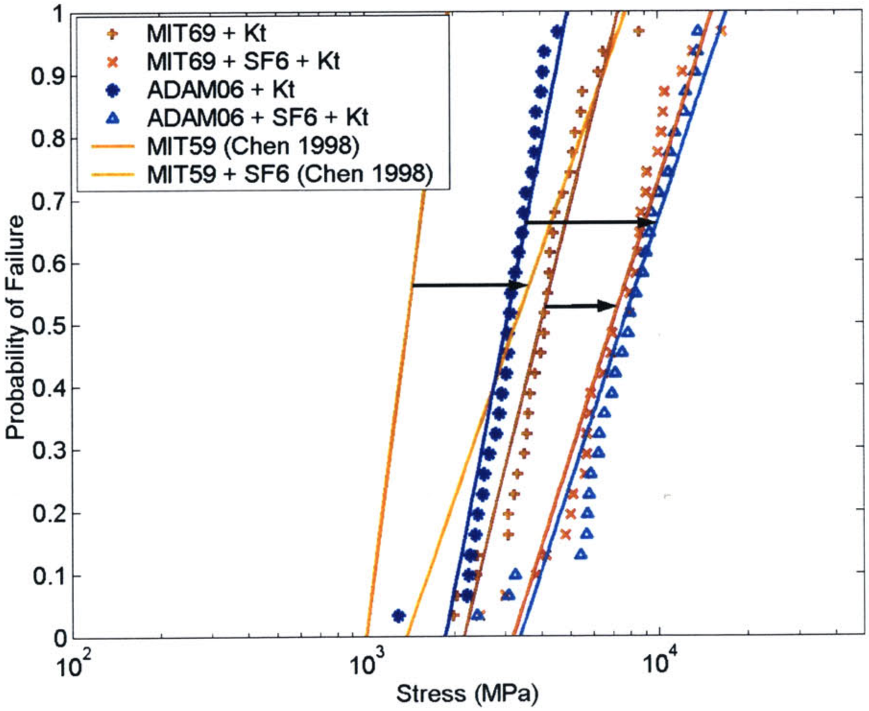

Figure 3-16: Weibull Data for Radiused Hub Flexure Specimens Fabricated with Six Etch Recipes (With Applied Stress Concentration Factor)

From both the plot and the Weibull parameters it is clear that the introduction of the isotropic etch is beneficial to the strength of the devices. Unmodified the ADAM06 etch creates weaker specimens than MIT69 (the baseline) but with the SF6 etch, ADAM06 leads to a greater strength than MIT69. The curves for these recipes correlate rather well with the MIT59 curves prior to the incorporation of the stress concentration factor.

The effect of the stress concentration can also be seen in the Weibull plots for this data. The arrows in Figure 3-17 and Figure 3-18 show the shift in the fitted curve when the stress concentration is applied to the Weibull data. This offers significant increase in the characteristic strength of the material (Table 3-5).

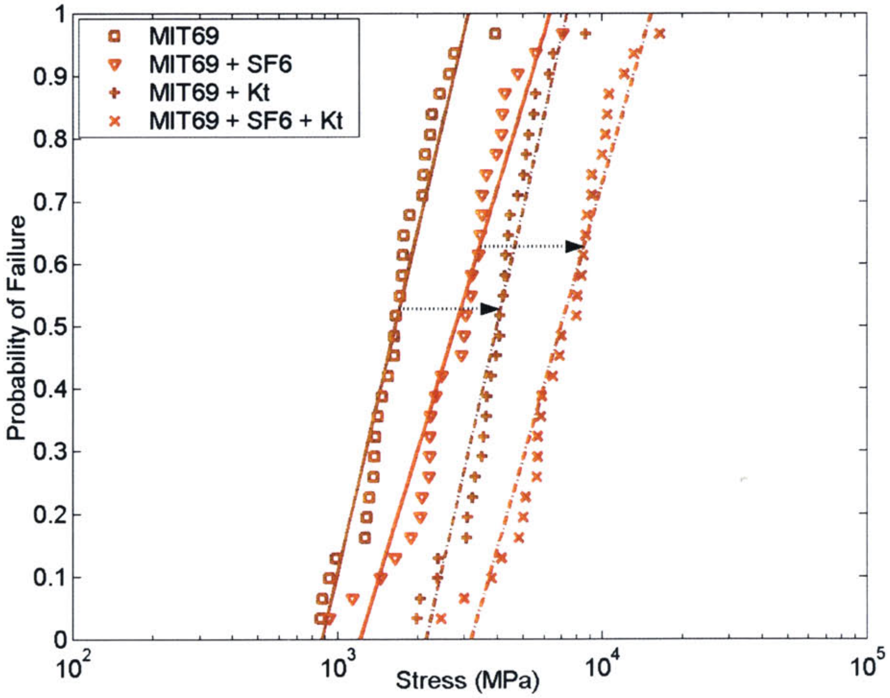

Figure 3-17: RHFS MIT69: Shift in Weibull Plot with Stress Concentration Factor

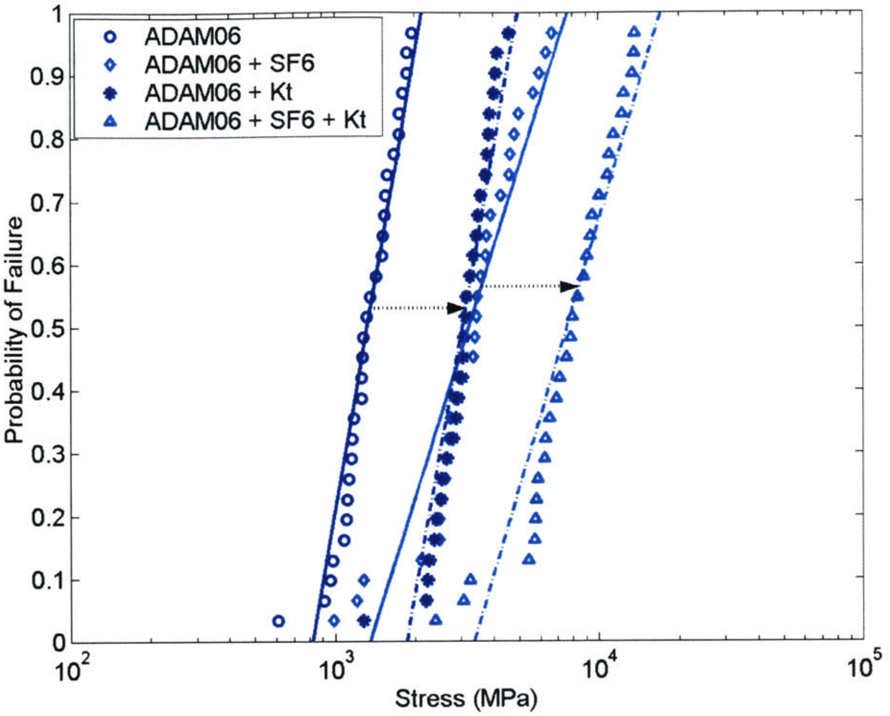

Figure 3-18: RHFS ADAM06: Shift in Weibull Plot with Stress Concentration Factor

3.7.4 Surface Roughness

The scanning electron microscope allows examination of the etched surfaces of the RHFS devices. What is learned from this examination is that the surfaces vary significantly across the etch recipes. The figures below contain images of RHFS devices under various high level magnifications. These images allow a qualitative comparison of the surfaces. Additional images are available in Appendix D.

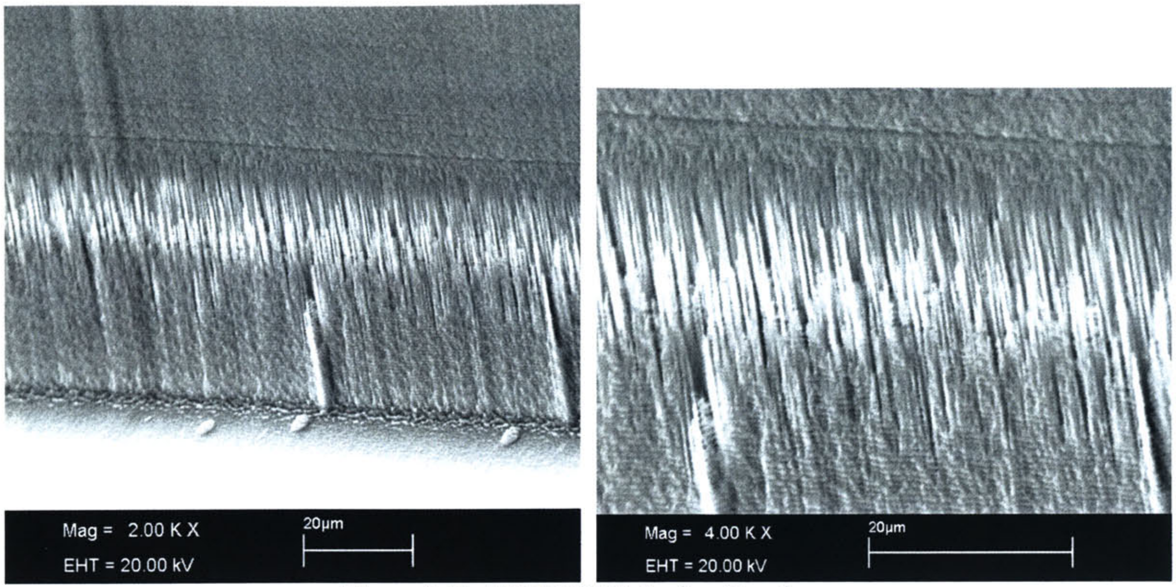

Figure 3-19: MIT69 RHFS Surface Roughness

The MIT69 surface appears quite smooth, as part of its optimization process was to achieve good surfaces. Figure 3-19 shows the primary source of roughness, and therefore stress concentrations from this etch. These jagged protrusions behave effectively as cracks when the specimen is loaded. The scalloped texture of the surface from the alternating etch cycles is also visible in the image on the right.

The application of the isotropic etch, SF6-4, changes the appearance of the surface dramatically. Figure 3-20 shows images of approximately the same scale as Figure 3-19. The isotropically etched surface appears almost porous. The jagged features visible in Figure 3-19 have been reduced if not removed and it is assumed that the uniform etching has rounded out the sharp crack-like features, reducing the local stress concentrations.

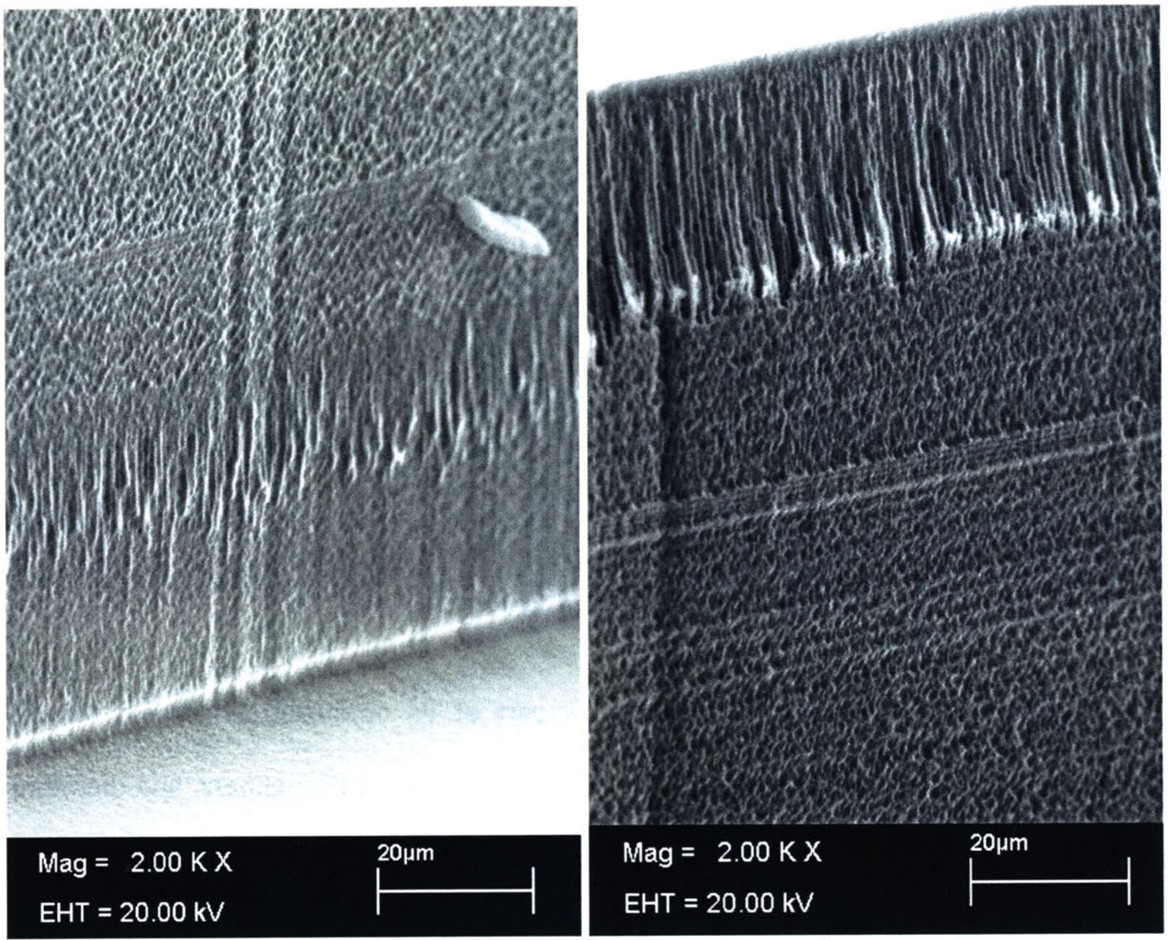

Figure 3-20: MIT69 + SF6 RHFS Surface Roughness

The ADAM06 surface has very subtle crack-like features, except at the top of the trench, where they better resemble the features on the MIT69 surfaces. Again, at the bottom of the trench, scalloping is visible on the etched surface. The cracks appear to extend further up the wall than the MIT69 ones, which have a more uniform end point.

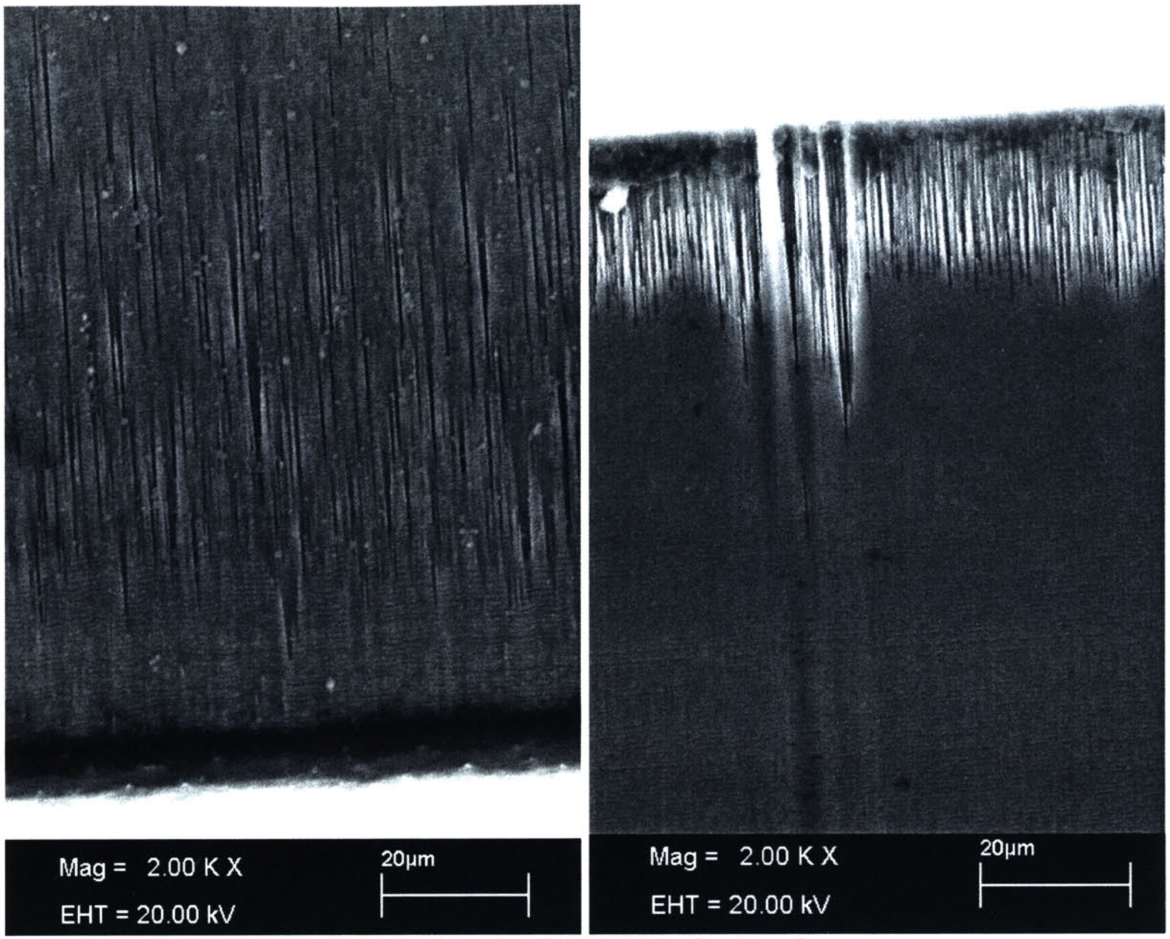

Figure 3-21: ADAM06 RHFS Surface Roughness

The isotropic removal of material on the ADAM06 surfaces was extensive. The rough appearance of the surface reveals how extensive the hidden surface cracks are. The depth of these features raises the question of whether these etch introduced flaws can be considered as small compared to the length scale of the stress distribution. This issue will be further addressed in Chapter 5.

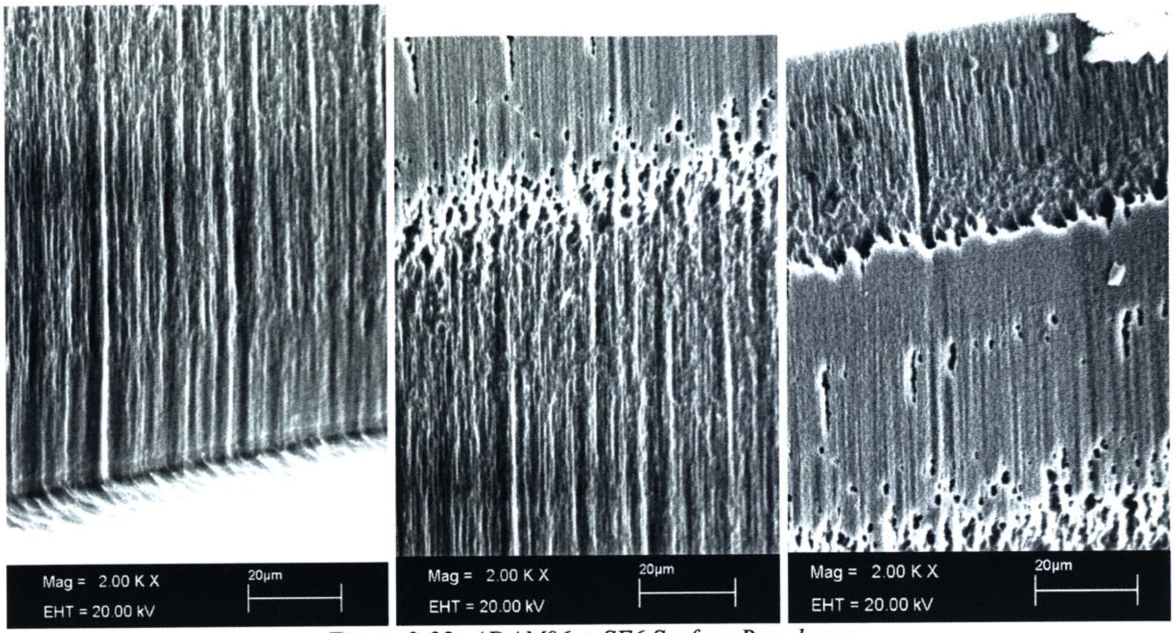

Figure 3-22: ADAM06 + SF6 Surface Roughness

3.8 Effects of Isotropic Etch

The Weibull statistics presented in Section 3.7.3 demonstrate the effect that an isotropic etch can have on the strength of etched silicon. While improving the reference strength, significantly in the case of ADAM06, there is a notable increase in the scatter of the data, corresponding to a decrease in the Weibull modulus. The dramatic shift in the ADAM06 data indicates that the optimization of this etch recipe should be reevaluated, perhaps with more emphasis on the nature of the surface roughness. It should be determined whether the compromise between surface roughness, bottom surface profile, and etch rate dependence on feature size is still acceptable given the current performance of the device.

3.9 Summary

The objective of the radiused hub flexure tests was twofold: to characterize the strength of silicon etched with the micro rocket recipe ADAM06 and to investigate and characterize the effect of an isotropic smoothing etch on anisotropic etches. The strength of the ADAM06 recipe has been demonstrated to be well below that of two different baseline etches (MIT59 and MIT69). The strength recovery ability of an isotropic etched device has been demonstrated for both recipes tested. In addition, the isotropic etch improved the strength of the silicon etched with ADAM06 above the strength of the isotropic etched MIT69 devices. The application of these results to the pressure chamber devices was believed to be a first step in improving the strength of the chambers. The results of this investigation are presented in Chapter 4. In addition to improving the strength of the chamber devices, the correlation of the radiused hub flexure data and the isotropic etched chambers may offer insight into the effect of geometry and loading on the material strength.

Chapter 4 Chamber Pressure Tests (Revisited)

4.1 Test Device Modifications

4.1.1 Fabrication

The fabrication steps for these additional chamber devices vary only in the etch steps. The devices are etched for 240 mm with ADAM06. Then the last 10 mm (approximately) to achieve a 250 mm deep chamber is etched with a two minute isotropic etch with SF6-4 (see Table 4-1). This isotropic etch is designed to smooth the roughness created in the deep etch process. Prior to bonding, the depth of each etched chamber is measured using a diffractive microscope and the thickness of each wafer is measured with a micrometer. These measurements allow calculation of the chamber wall thickness and thus, calculated predictions for chamber pressure at failure (assuming a failure stress of 1 GPa). Additionally, the measurements allow wafers with similar wall thickness to be paired in an attempt to make the likelihood of failure equivalent for either wall.

Table 4-1: Pressure Chamber Etch Recipes

	ADAM06		**SF6-4**
	Etch	Passivate	Etch
Time (s)	15	9.5	
Platen Generator Power (W)	120	0	120
Coil Generator Power (W)	600	600	950
First Step	X		X
SF6 Flow (sccm)	140	0	30
C4F8 Flow (sccm)	0	95	0
APC Angle	62.5	62.5	75
Overrun	0.5	0	--

4.2 Experimental Results

From the two wafer stacks fabricated (32 possible devices), 25 devices were successfully tested. From stack 1, 6 Configuration A devices were tested and 8 Configuration B devices were tested. The two remaining devices were unusable because the top wafer broke during bonding and the devices were not bonded. Seven Configuration A devices were tested from stack 2. The eighth device had a visible nick on the chamber wall, and it was not tested because of the likelihood of that flaw inducing failure. All 8 devices from Configuration B were tested, however, the piezo sensor stopped responding and no signal was provided to indicate the point of failure. This prevented conclusive identification of a failure point for 4 of 8 devices.

4.2.1 Failure Pressure

The failure pressures for Configuration A and B devices are plotted in Figure 4-1 and Figure 4-2, respectively. Also shown are theoretical predictions for failure pressure calculated using Equation (2-1), the measured thickness of the failed wall and assuming a failure stress of silicon of 1 GPa. The mean failure pressure of Configuration A devices is 57.2 atmospheres with a standard deviation of 31.7 atmospheres. For Configuration B the mean failure pressure is 15.4 atmospheres with a standard deviation of 10.6 atmospheres. The failure pressures for these devices are significantly higher than those of the original devices.

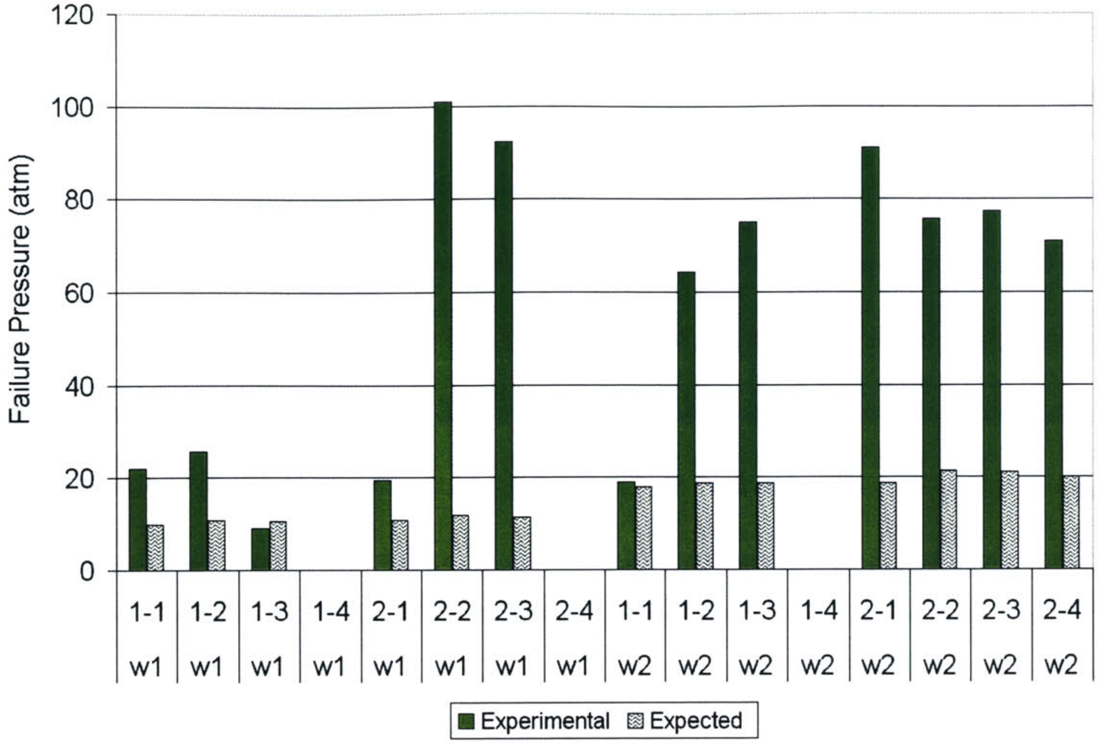

Figure 4-1: Configuration A: Experimental & Theoretical Failure Pressure

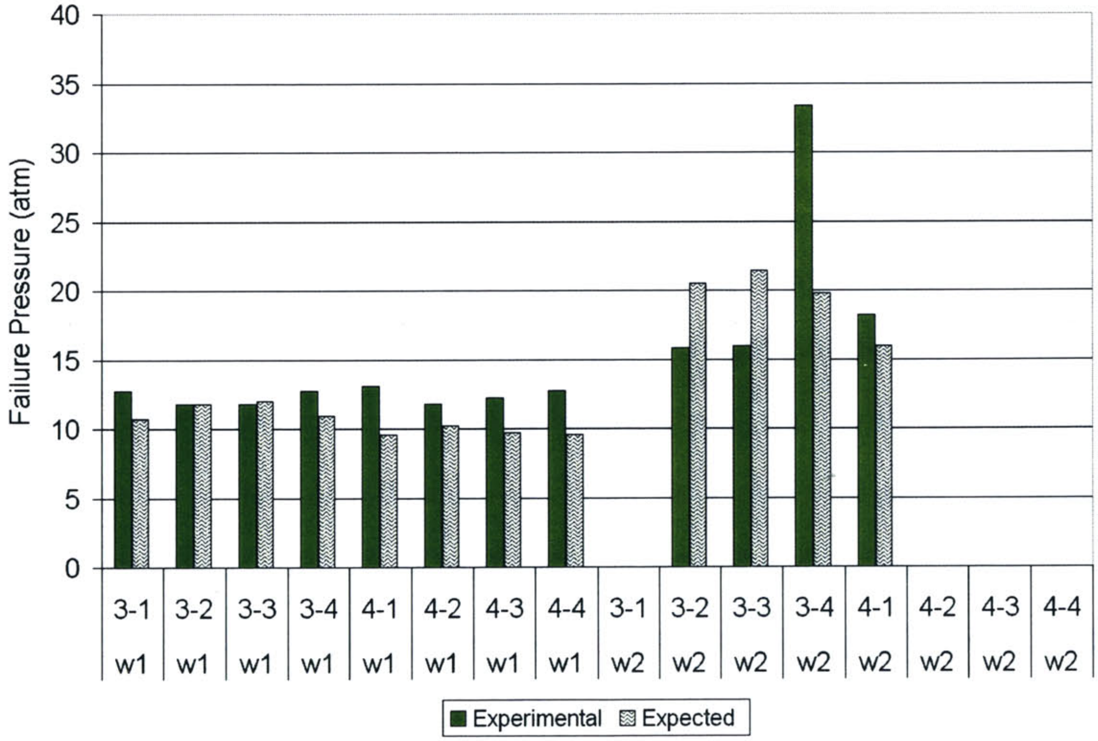

Figure 4-2: Configuration B: Experimental & Theoretical Failure Pressure

4.2.2 Failure Stress

In these devices the failure stresses are considerably greater, and therefore improved. When comparing these stresses, Figure 4-3 and Figure 4-4, it becomes apparent that there is a distinction between the inherent strength of the two configurations. Previously there were not enough data points in the Configuration B set to identify this difference. The data suggests that there is a feature of Configuration B, whether strictly geometric or a fabrication effect due to the nature of the geometry, which is reducing the strength of the device.

The effect of the introduction of a stress concentration factor is quite significant. The fillet radius is assumed to be approximately 30 μm, as in the previous pressure chamber builds and in the micro rocket chamber. Again the measured dimensions of each device were used to estimate a stress concentration factor for that device. The average stress concentration factor was 1.51 for both configurations. Plots of failure stress without the stress concentration factor applied are available in Appendix D. Without the stress concentration applied, only 8% of Configuration A devices failed below 1 GPa and 23% failed below 2 GPa. For Configuration B those numbers were 54% and 100%, respectively. When the effect of the fillet is accounted for, none of the Configuration A devices failed at stresses below 1 GPa and 23% failed below 2 GPa. Configuration B also had no devices failing below 1 GPa with the stress concentration and only 9% failure below 2 GPa.

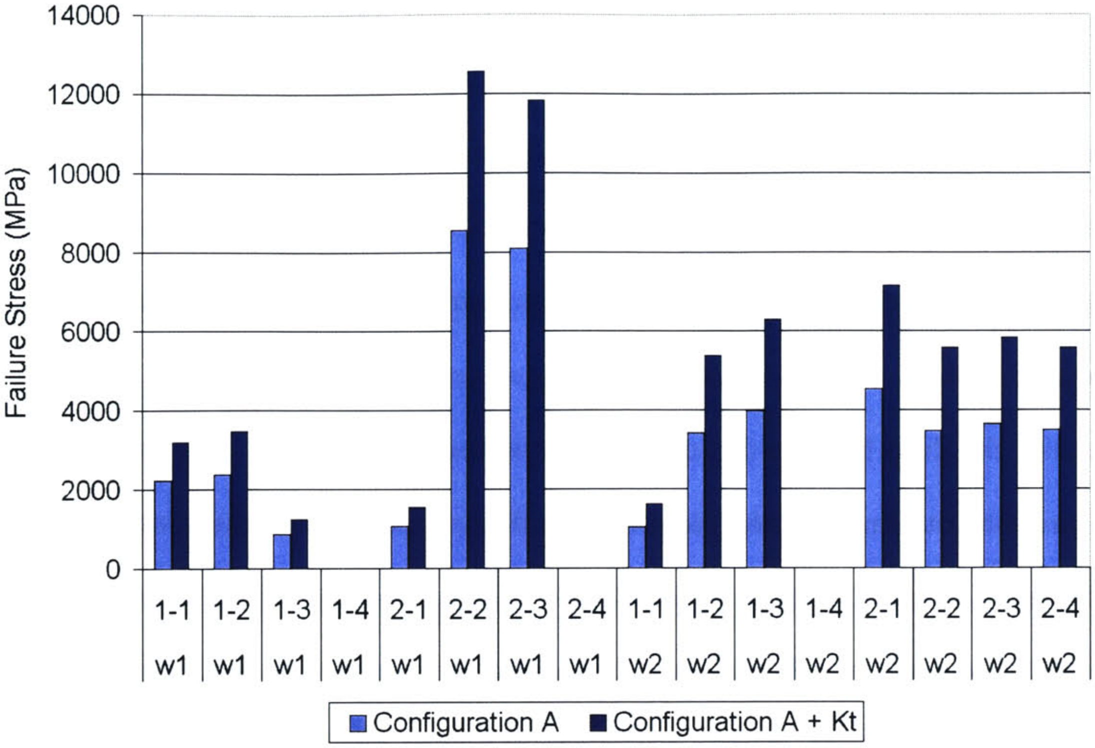

Figure 4-3: Configuration B: Pressure Test (Revisited) Failure Stress

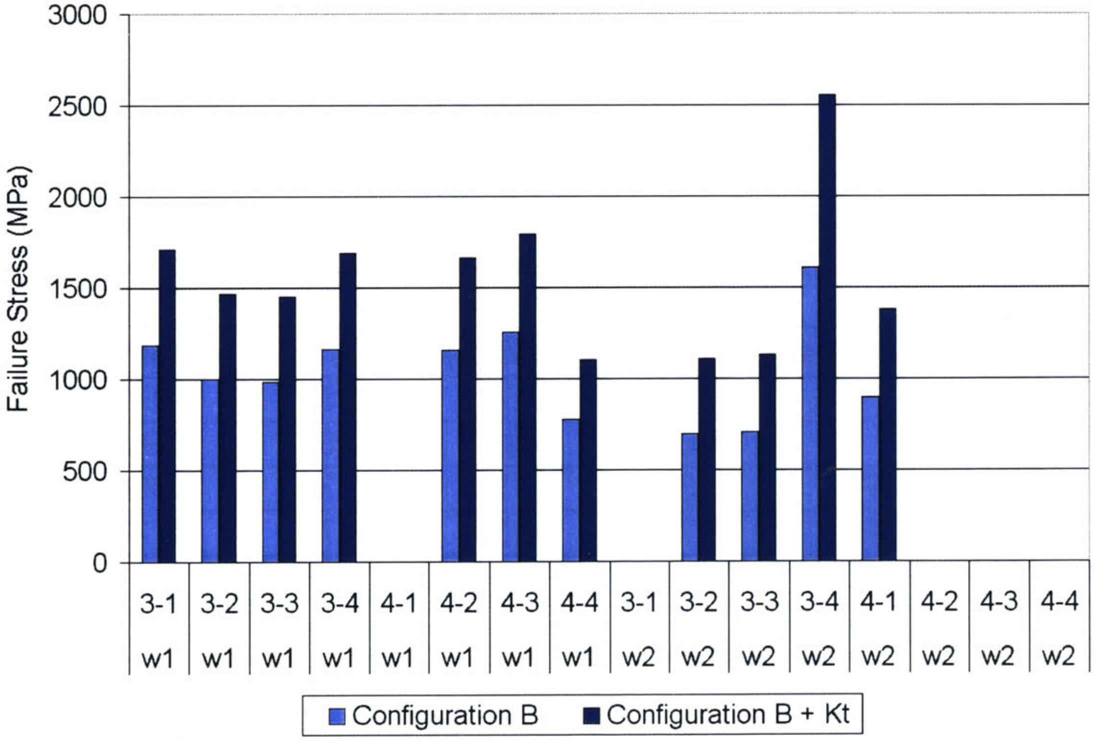

Figure 4-4: Configuration B: Pressure Test (Revisted) Failure Stress

4.2.3 Weibull Distribution

A two-parameter Weibull analysis was conducted with the data collected for Configurations A and B. The parameters are summarized in Table 4-2 with the Weibull parameters from the original tests (see Section 2.5.3). The difference in strength values between the data sets indicates the effect that an isotropic etch can have on the strength of an etched surface. This difference is presented graphically in Figure 4-5 with arrows indicating the shifts between the sets with and without the SF6 etch. Also included in the plot are the data lines for the radiused hub flexure specimens etched with ADAM06. While this plot cannot quantify or identify the source of the disparity between the radiused hub flexure specimens and the chamber specimens, it is plausible to assert that factors that influence that difference include differences specimen geometry and effective surface area/volume (see Section 1.3.5). This topic will be further addressed in Chapter 5. Figure 4-6 and Figure 4-7 present the effect of stress concentration factors on the Weibull distribution. The quantitative comparison can be made with the parameters summarized in Table 4-2.

Table 4-2: Weibull Parameters Chamber Tests (Original & Revisited)

			+ Kt	
Configuration	**m**	**σ_o (MPa)**	**m**	**σ_o (MPa)**
A	2.5	760	2.57	1070
B	6.86	410	9.67	590
A + SF6	1.38	4170	1.37	6360
B + SF6	3.75	1150	3.75	1720

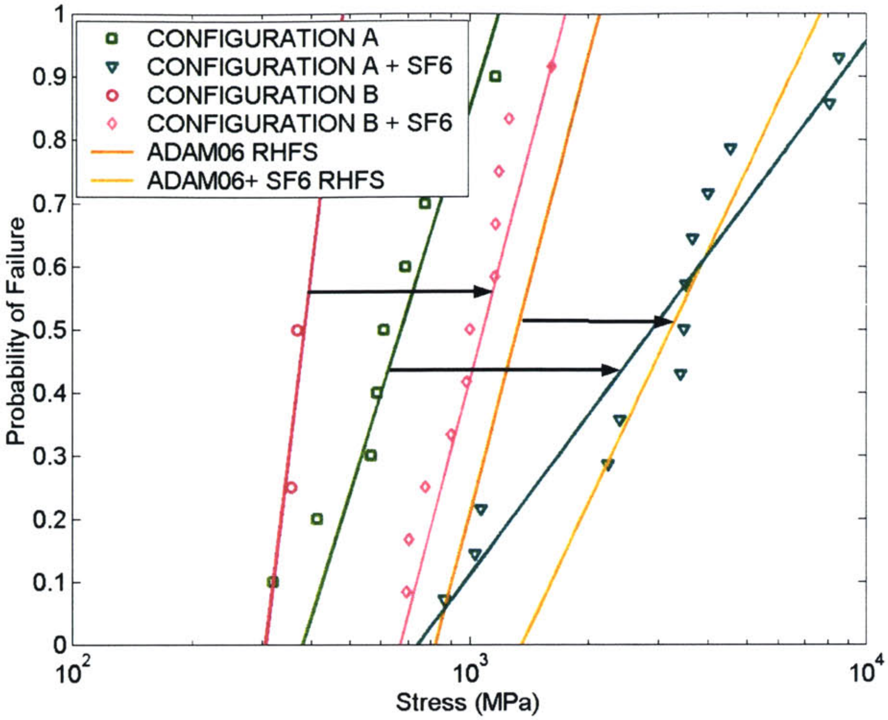

Figure 4-5: Weibull Distribution

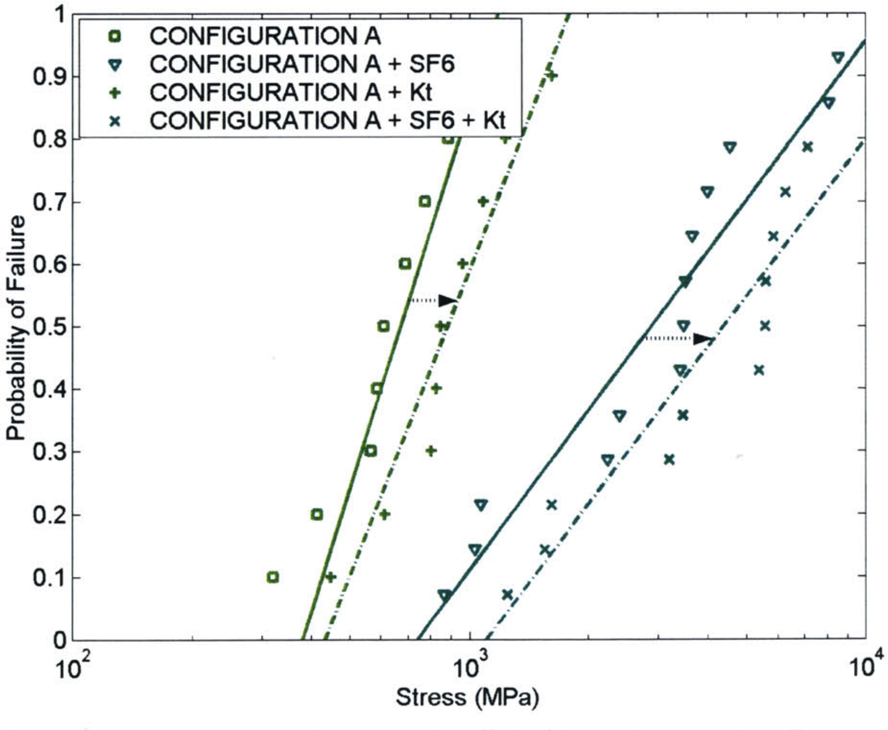

Figure 4-6: Pressure Chamber Configuration A: Effect of Stress Concentration Factor on Weibull Distribution

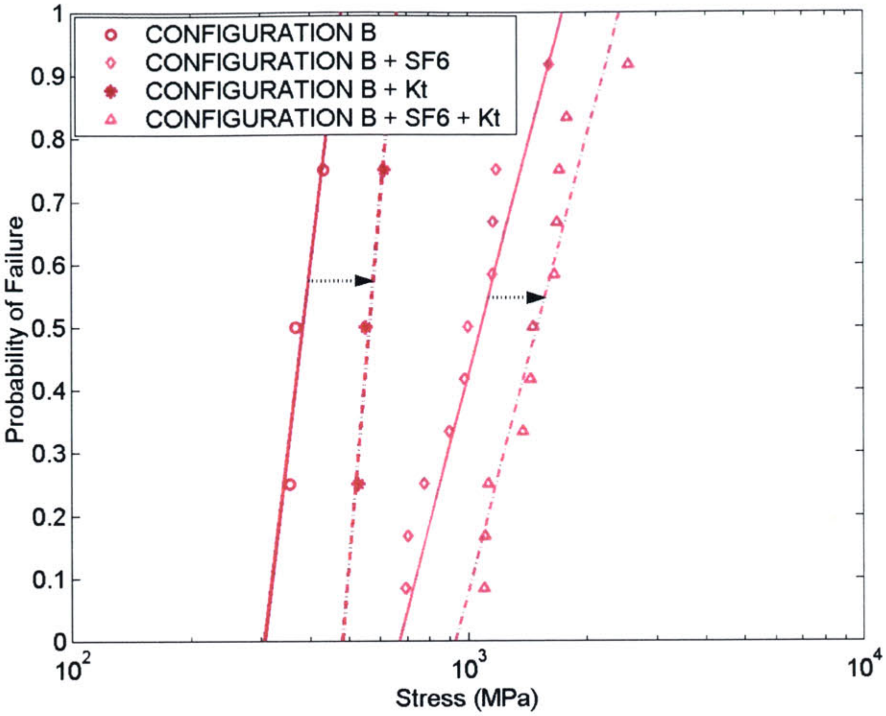

Figure 4-7: Pressure Chamber Configuration B: Effect of Stress Concentration Factor on Weibull Distribution

4.2.4 Surface Roughness

The surfaces of the walls in the pressure chambers etched with SF6 are quite different from the surfaces of the original chambers. While there is still extensive texture, the "stalagmitic" features present in the original images have been reduced to a porous looking structure. The reduction of visible sharp edges supports the data which indicates that the isotropic etch successfully removes the most significant stress concentrations introduced by the primary etch.

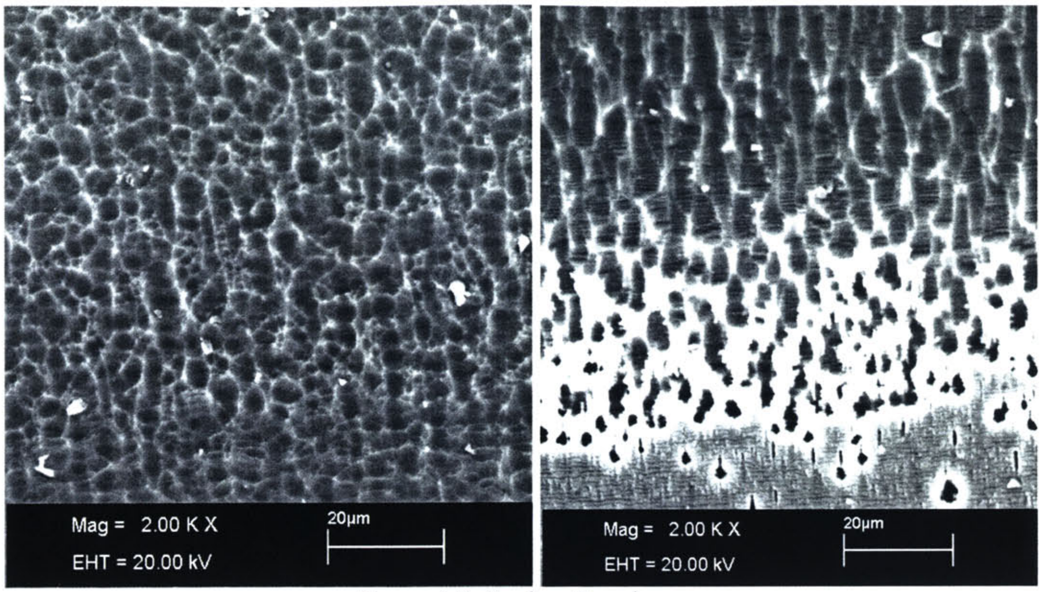

Figure 4-8: Surface Roughness

4.3 Summary

These tests have demonstrated the following:

1. Reaffirmed the effect of the isotropic etch on the material strength of etched silicon.
2. Verified the strength difference between Configuration A and Configuration B with larger data sets, thereby suggesting some influence of geometry, whether from the discontinuity of the chamber edge or from a side effect of the geometry on the processed surfaces
3. There is some difference between the radiused hub flexure specimens and the chambers, again introducing the question of geometry, specifically the loading condition and therefore the effective volume/surface area.

Chapter 5 Weibull Statistics and Predictive Modeling

5.1 Review of Weibull Statistics

Material strength of brittle materials, like silicon, is a stochastic variable. This variation means that the failure of the material is determined by both stress level and *local* strength in a structure. In accounting for local strength, the failure of a structure becomes less easily predicted because it does not necessarily occur at the location of highest stress. Instead, it is possible to determine the probability that a given material will have a certain strength, and therefore be able to withstand a particular load. For this reason, the probabilistic nature of the material strength must be incorporated into the structural design. Brittle materials, such as silicon, typically have a non-deterministic strength that is dictated by the population of flaws on the material surface and throughout the specimen volume. This type of strength is traditionally defined using a Weibull distribution (see Section 1.3.5). Using the Weibull distribution to design structures requires using a different approach from that required if strength is assumed to be a deterministic quantity. For all specimens, there exists a finite (non-zero) probability of failure. The stochastic nature of flaw size and distribution throughout the structure dictates that failure will not necessarily occur at the location of maximum stress and may occur at any location on the structure. These assumptions reaffirm the non-deterministic nature of brittle material strength and its extreme dependence on the flaw populations of a structure's volume and surface area.

As was discussed in Chapter 1, the probability of failure for a structure under uniaxial stress is

$$P_{\mathrm{fv}} = 1 - \exp\left(- \int_{vol} \left(\frac{\sigma}{\sigma_o} \right)^m dV \right) \tag{5-1}$$

For a multiaxial stress state, such as the pressurized chambers and the radiused hub flexure specimens, the probability must be calculated differently. One common method is the principle of independent action (PIA) [24]. The principle of independent action considers each principal stress to act independently and therefore the probability of failure is

$$P_{\mathrm{fV}} = 1 - \exp\left(\frac{V}{V_0 \sigma_0^m} \left(\sigma_1^m + \sigma_2^m + \sigma_3^m \right) \right) \tag{5-2}$$

where σ_1, σ_2, and σ_3 are the principal (tensile) stresses. Compressive principal stresses are not considered and therefore set to zero.

5.2 CARES

Ceramics Analysis and Reliability Evaluation of Structures Life Prediction (CARES/LIFE) software was developed by NASA for reliability prediction of ceramic materials. This reliability is determined by the presence of intrinsic surface and/or volume flaws. The program uses a finite element model of a component and experimental failure stress data to determine a two-parameter Weibull distribution for the component strength. It is possible to apply several different analytical methods depending on the nature of the problem being considered and discussions of the theory as well as specifics of application are available elsewhere [24]. This chapter will only cover approaches used for data collected in this study.

CARES software can be run with a graphical user interface, WinCARES, which does not require the user to master all required commands in order to process data. This interface depicts the flow of information through the program (Figure 5-2).

CARES consists of three separate modules: (1) finite element data interface, (2) material parameter estimation, and (3) component reliability evaluation. The finite element data interface translates the geometry and stress details of a finite element model from the FEA package, ANSYS for this study, to a neutral file (.neu or .nsg). The neutral specimen geometry (.nsg) file is one of the two input files required for the parameter estimation (Pest). The input file is created by the user (from a template) and provides information about the material properties, the type of probabilistic analysis, the loading conditions, flaw type, and experimental stress data. The input information for the analyses discussed below is included in Appendix E. Pest calculates the Weibull parameters based on the experimental data and also provides data about the quality of fit of the parameters. The parameters, material data, and fit analysis are output into several files, one of which generates Weibull curves in a data plot as well as a file that may be input into the reliability module (LIFE) with the .neu file.

The principle of independent action (PIA) is used for analysis and modeling of multiaxial stress states (see Section 5.1) and does not require specification of flaw geometry. The PIA model only considers tensile stresses as contributing to failure because in brittle materials the compressive strength is typically significantly higher than the tensile strength. A component fails when the equivalent stress at a flaw reaches a critical value.

The reliability of a structure is determined by integrating the stress over the entire device. This is done using the geometry of the finite element model and is depicted in Figure 5-1. The geometry is divided into elements. The software uses the element's Gaussian integration points to create subelements. The probability of failure is then calculated for each subelement using PIA and Weibull statistics. The subelement failure probabilities are summed to find the probability of failure for the entire structure:

$$P_f = 1 - \sum_{i=1}^{N} \sum_{j=1}^{M} \left(1 - P_{fij}\right) \tag{5-3}$$

where N is the number of elements and M is the number of subelements per element.

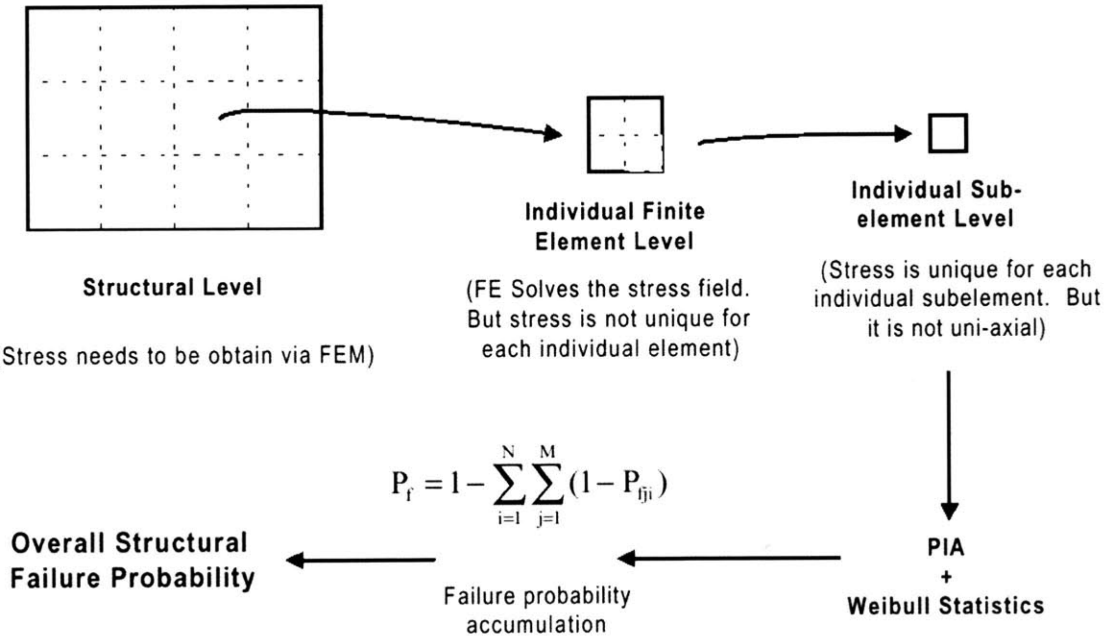

Figure 5-1: Schematic process flow of structural failure probability calculation [21]

The effective volume is the equivalent volume subject to a uniform uniaxial tensile stress, of magnitude σ_f, required to produce an identical failure probability of the specimen. It is calculated from the finite element model as

$$V_{eff} = \left(\frac{1}{\sigma_f}\right)^{m_v} \int_V \left(\sigma_1^{m_v} + \sigma_2^{m_v} + \sigma_3^{m_v}\right) dV \qquad (5\text{-}4)$$

where σ_f is the maximum principal (tensile) stress in the model. The effective area is calculated similarly, however, a special application must be used in the finite element program (ANSYS) for the correct data to be output to the neutral files. This application is discussed in more detail in Appendix E.

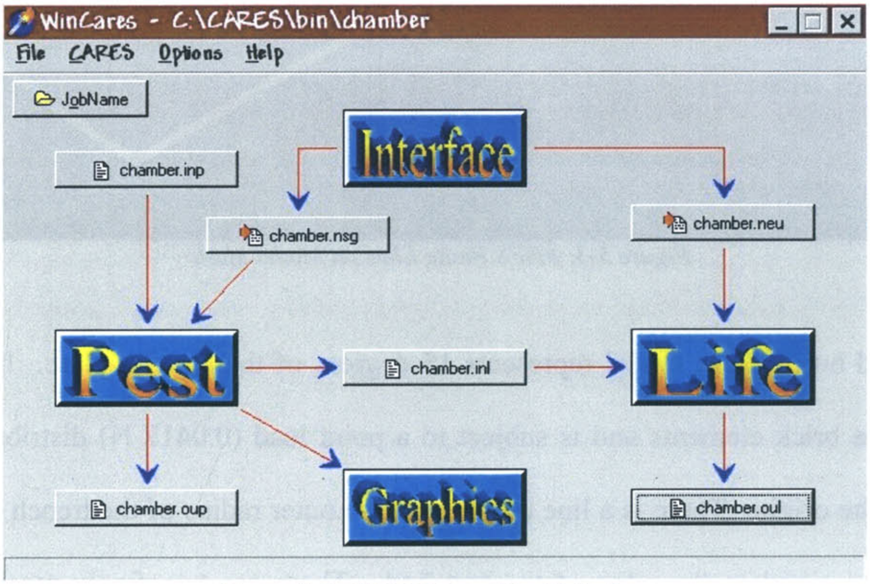

Figure 5-2: CARES Graphical Interface

5.3 Finite Element Modeling

All finite element models used for these analyses were created in ANSYS with 20 node brick elements (Solid 95). Symmetry of both specimens modeled required only partial modeling of each device. Material properties applied assume isotropic material behavior with a Young's Modulus of 165 GPa and a Poisson's Ratio of 0.2177 [21].

5.3.1 Radiused Hub Flexure Specimens

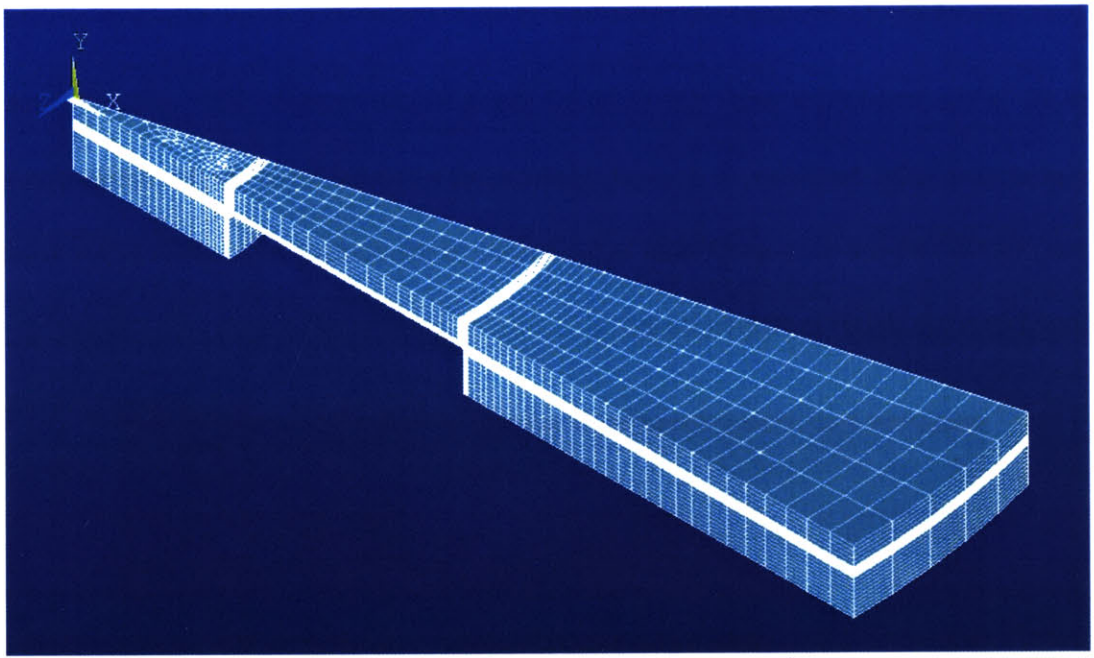

Figure 5-3: RHFS Finite Element Model Mesh

The radiused hub flexure model represents 15 degrees of the annular plate. It is meshed with 20-node brick elements and is subject to a point load (0.0417 N) distributed to two nodes near the origin. There is a line of nodes at the outer radius of the trench fixed in the z-direction to simulate the edge of the test bed. There are two finely meshed regions creating 8 μm fillet radii (Figure 5-4) at either end of the plate region. The length scale of this model is meters.

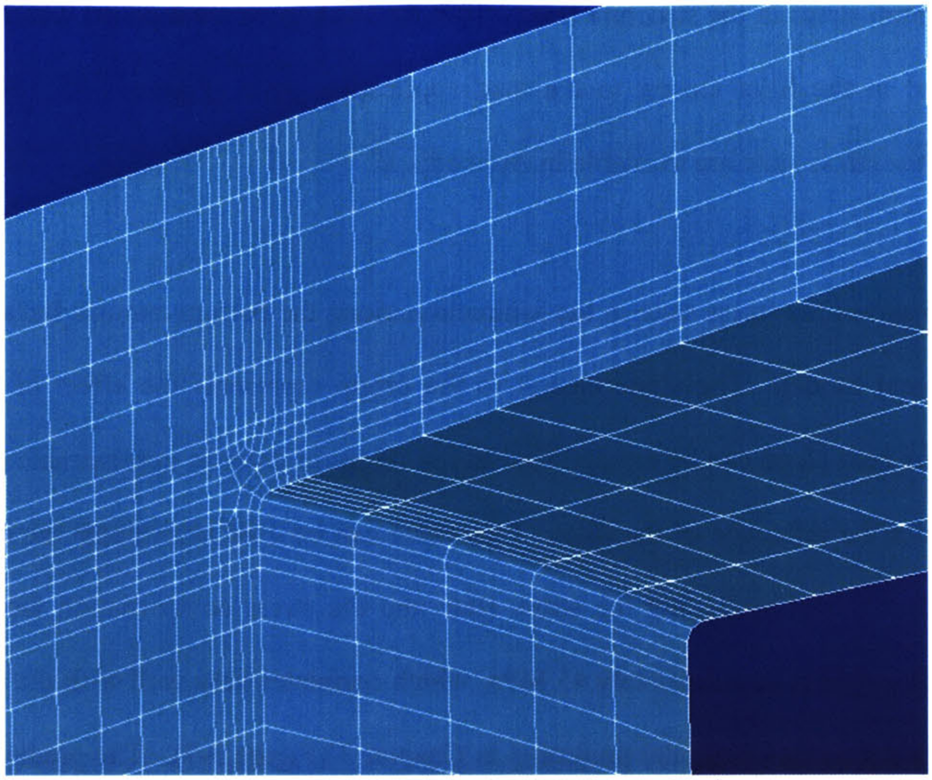

Figure 5-4: Fillet of RHFS Finite Element Mesh

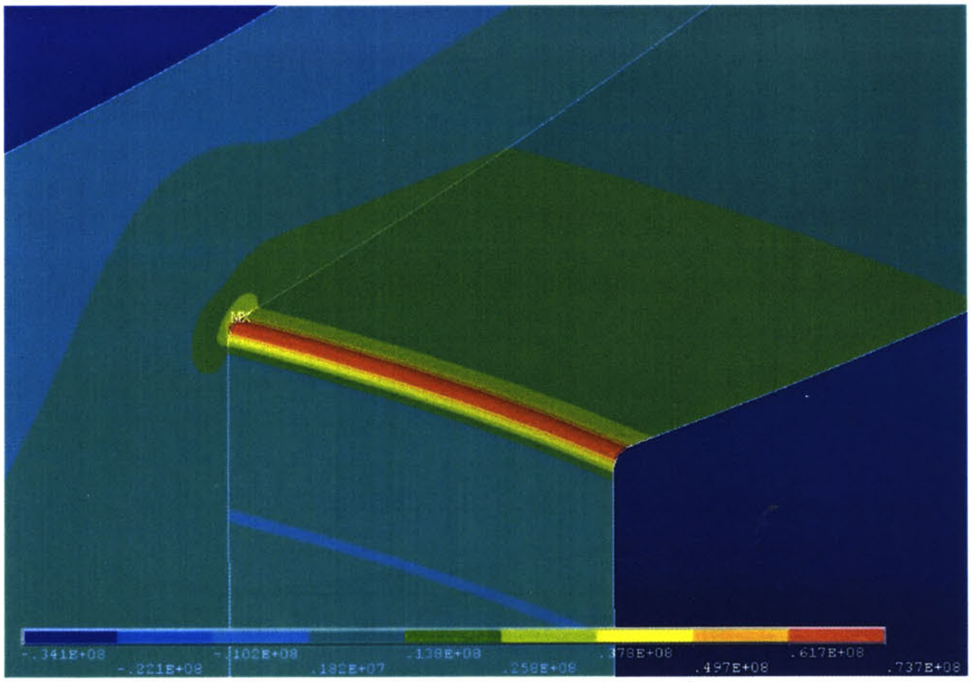

Figure 5-5: RHFS Fillet Principal Stress State

The maximum stress in the structure (away from the load application point) was 73.7 MPa and located in the fillet closest to the load application point (Figure 5-5). Additional images of the stress state are available in Appendix E.

Figure 5-6 shows the stress state in the x-direction along the bottom annular surface of the finite element model. The slope closest to the origin represents the effect of the fillet radius. The next slope can be extrapolated to the origin in order to approximate the stress state without the influence of the fillet. This value can be used to evaluate the quality of the analytical model predicting the stress state and the stress concentration factor. The value at the origin is approximately 45 MPa, which correlates very well with the predicted stress from the analytical model presented in Chapter 3 (Figure 5-7). The predicted value is 45.7 MPa.

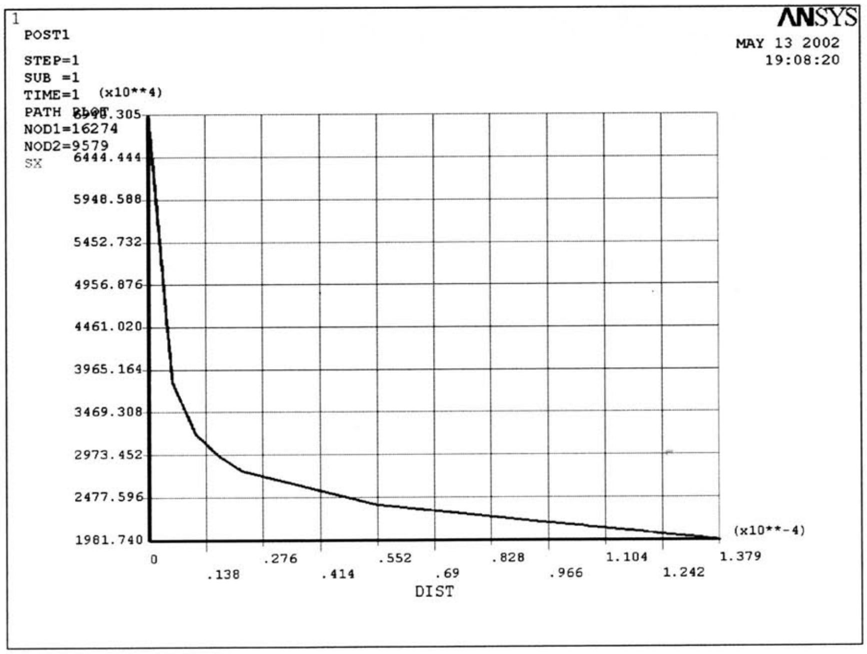

Figure 5-6: X-Direction Stress (Pa) Along Radial Trench Position (m) from FEA RHFS Model

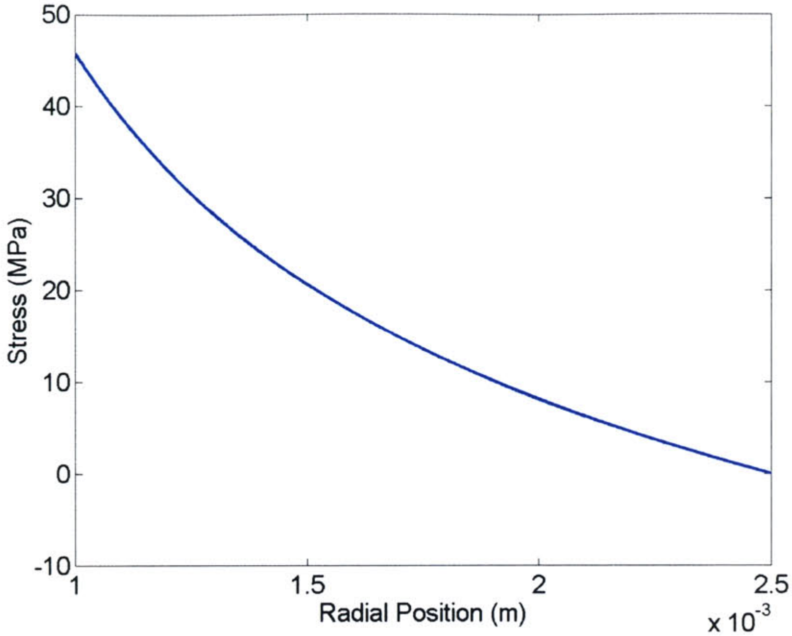

Figure 5-7: Analytical Prediction of X-Direction (Radial) Stress in RHFS Model

5.3.2 Pressurized Chamber Devices

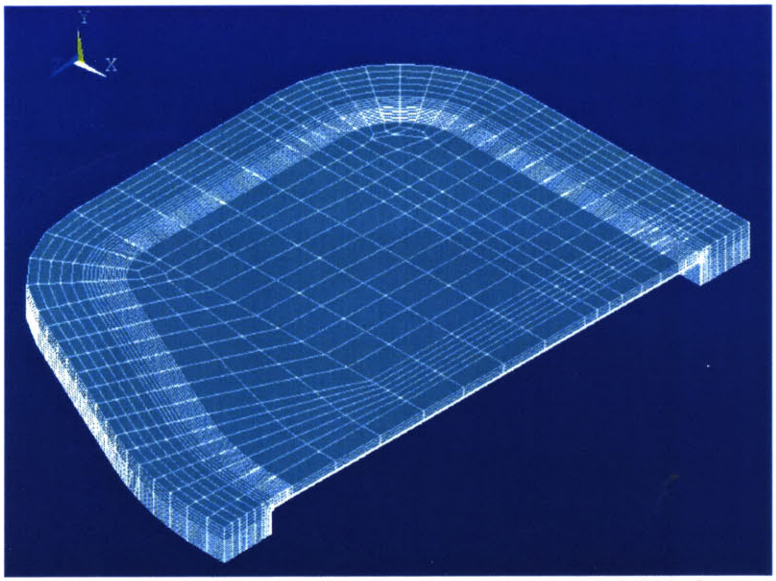

Figure 5-8: Pressure Chamber Finite Element Model Mesh

The pressurized chamber model represents one quarter of a full device. Symmetry boundary conditions are applied on the faces in the x- and y-directions along the planes of symmetry. One node, at the lower corner of the chamber, is fixed in the z-direction to prevent rotation of the structure. The model does not model either of the top plate configurations with the pressure ports; however, earlier analysis demonstrated that the presence of holes on the chamber wall does not change the location of maximum stress (Section 2.4.3). This model is meshed with 20–node brick elements and is subjected to a uniform pressure of 0.1013 Pa (1 atm) applied on all internal surfaces. The length scale of this model is millimeters.

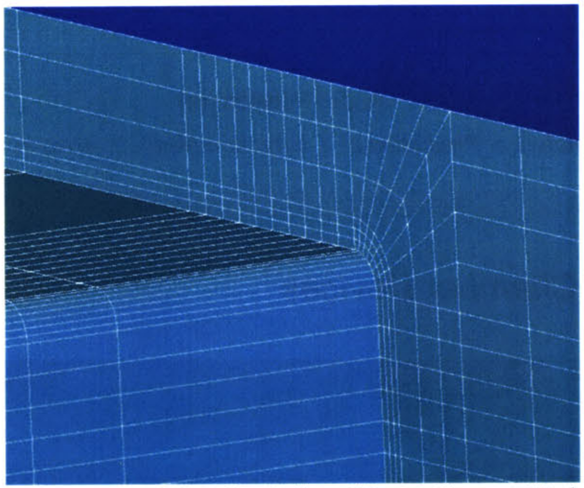

Figure 5-9: Pressure Chamber Fillet of Finite Element Model Mesh

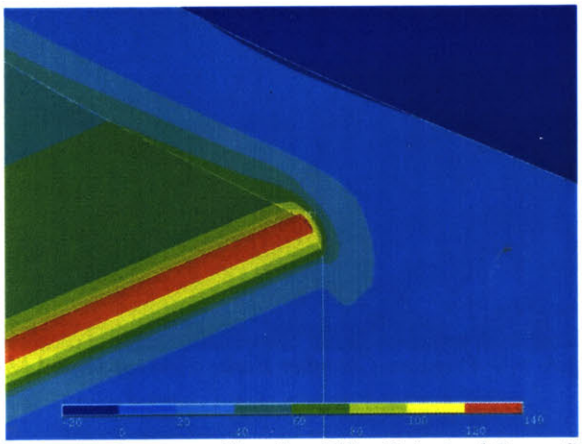

Figure 5-10: Pressure Chamber Fillet Principal Stress State

The maximum stress in the model was 138 MPa and was located in the fillet at the center of the upper chamber wall (Figure 5-11). Additional images of the stress state are available in Appendix E.

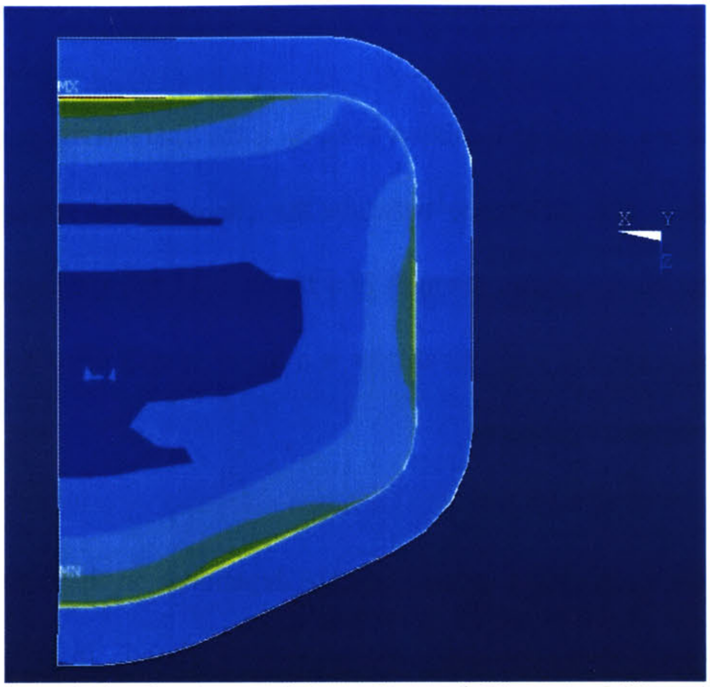

Figure 5-11: Pressurized Chamber Principal Stress State with Maximum & Miminum Stress Locations

5.4 Analysis

The maximum likelihood method was used to calculate the characteristic strength and shape parameter based on the failure data from each sample set. This method makes allowances for non-normal distributions, like Weibull. The maximum likelihood parameters are estimated from an equation with a unique solution and as the sample size increases, the solution converges to the true parameter values. The likelihood equation is

$$L = \prod_{i=1}^{n} \left(\frac{m}{\sigma_\theta} \right) \left(\frac{\sigma_{fi}}{\sigma_\theta} \right)^{m-1} \exp\left[-\left(\frac{\sigma_{fi}}{\sigma_\theta} \right)^{m} \right] \qquad (5\text{-}5)$$

The Weibull parameters are found by maximizing the likelihood function by taking the partial derivative of the logarithm of the likelihood function with respect to m and σ_θ. Using the Weibull parameters, the scale parameter is calculated as

$$\sigma_o = \sigma_\theta A_e^{\frac{1}{m}} \tag{5-6}$$

where A_e is the effective area (see Equation 5-4), σ_θ is the characteristics strength, and m is the shape parameter. The difference between the characteristic strength and the scale parameter is that the characteristic strength is a function of the specimen dimensions and stress distribution whereas the scale parameter is a function only of material properties and is therefore, itself a material property.

Because the maximum likelihood estimations are dependent on the number of specimens in the data set, the parameters calculated are considered biased. In order to minimize the deviation between parameters generated by the sample population and by a complete population, an unbiasing factor is calculated and multiplied by the biased parameters. The calculation of the unbiasing factor is documented elsewhere [25].

In addition to calculation of the Weibull parameters, CARES conducts several 'goodness of fit' tests. The data is provided in the Pest output file and can be used to evaluate the data set for outlying points that may need to be censored. The Stefansky outlier test can only be approximately applied to Weibull statistics as it assumes a normal distribution from a complete data set [24]. The CARES software calculates the outlier significance from 0% to 10% with 0.1% resolution. The Kolmogorov-Smirnov test is described as a member of the supremum class and effective for small samples [24]. It takes the largest vertical difference between the two distribution functions. The Anderson-Darling test is of the quadratic class and is a more powerful test. The Anderson-Darling test evaluates the discrepancy between the two distributions using squared differences and a weighting function. Using the goodness of fit measures, a level of significance is calculated for each data point, however the assumptions associated with the significance calculation are not valid for Weibull statistics and therefore, the significance levels cannot be the sole motivation for censoring a data set. Kanofsky-Srinivasan confidence bands are also calculated for the proposed distribution and included in the program generated plots. The confidence bands are calculated in a manner similar to the Kolmogorov-Smirnov parameters. [24]

5.5 Results

5.5.1 Volume versus Surface Area Flaw Populations

Surface flaws are typically due to handling and processing (etching). Volumetric flaws are most commonly caused by imperfections in the creation of the material, such as voids, lattice defects, and grain boundaries. Thus, because these structures are created from semiconductor grade silicon, it may be assumed that all flaws found in the structure are due to the handling and processing of the wafer following its creation, and therefore, are surface flaws. [21]

5.5.2 Radiused Hub Flexure Specimens

The results of the CARES parameter estimation for the radiused hub flexure specimens are summarized in Table 5-1 and Table 5-2. The parameters of note are the shape parameter (Weibull modulus, m), characteristic strength, the equivalent volumes/areas (for surface and volume flaws) and the scale parameters (for surface and volume flaws). It should be noted that the length scale of the finite element model used for this analysis was meters. However, the CARES software could not process the ten significant digits required for GPa stresses, etc. Thus, a scaling factor of 10^{-6} was applied to use stresses in units of MPa. This scaling factor must be unapplied to the scale parameters output from CARES. All strength values remain in MPa.

Table 5-1: CARES Output Summary for RHFS

	MIT69	**MIT69 + SF6**	**ADAM06**	**ADAM06 + SF6**
number of data points	30	30	30	30
biased shape parameter (m)	2.834	2.469	4.756	2.661
unbiased shape parameter (m)	2.706	2.358	4.542	2.541
characteristic strength	1963	3450	1493	3985
mean characteristic strength	1749	3060	1367	3542
standard deviation (char. strength)	669	1324	327.7	1433
specimen equivalent effective volume	7.02E-14	1.47E-13	2.16E-14	9.49E-14
scale parameter (volume)	4.48E+04	2.19E+04	2.00E+06	5.09E+04
specimen equivalent effective area	7.26E-07	1.07E-06	1.12E-07	8.73E-07
scale parameter (surface)	1.34E+07	1.32E+07	5.16E+07	2.11E+07

Table 5-2: CARES Output Summary for RHFS + Kt

	MIT69	MIT69 + SF6	ADAM06	ADAM06 + SF6
number of data points	30	30	30	30
biased shape parameter (m)	3.101	2.642	5.014	2.693
unbiased shape parameter (m)	2.961	2.524	4.788	2.572
characteristic strength	4691	8584	3402	8821
mean characteristic strength	4195	7628	3124	7488
standard deviation (char. strength)	1480	3106	713.7	3140
specimen equivalent effective volume	5.04E-14	9.86E-14	1.98E-14	8.91E-14
scale parameter (volume)	2.41E+05	1.03E+05	6.29E+06	1.26E+05
specimen equivalent effective area	5.48E-07	8.90E-07	9.07E-08	8.43E-07
scale parameter (surface)	4.49E+07	4.41E+07	1.34E+08	4.90E+07

On the following Weibull plots, and all other CARES generated plots, there are three sets of lines. The centermost line is the Weibull curve fit. The straight lines on either side of the data points represent the 90% Kanofsky-Srinivasan confidence bands. The tapered lines are the Kolmogorov-Smirnov bands. The points that are circled were flagged as Stefansky outliers with significance of 0.1%. The points with squares around them were flagged as having Kolmogorov-Smirnov test significances less than 99%. The Weibull plots below are for all four data sets without a stress concentration factor and are followed by plots for the same data sets with the stress concentration applied.

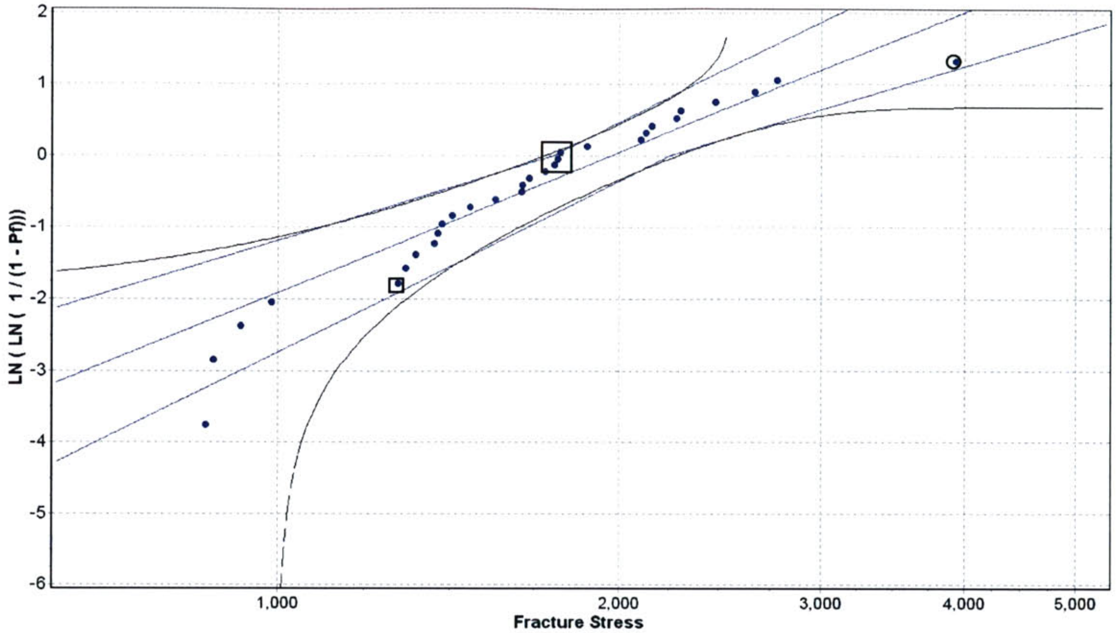

Figure 5-12: MIT69 RHFS Weibull Distribution

The MIT69 RHFS Weibull distribution had one outlier with a sigificance of 0.1%. In addition, there were four points with Kolmogorov-Smirnov test significances less than 99%.

The MIT69 + SF6 Weibull distribution had one outlier with a significance of 0.1%. There were no points with Kolmogorov-Smirnov test significances less than 99%.

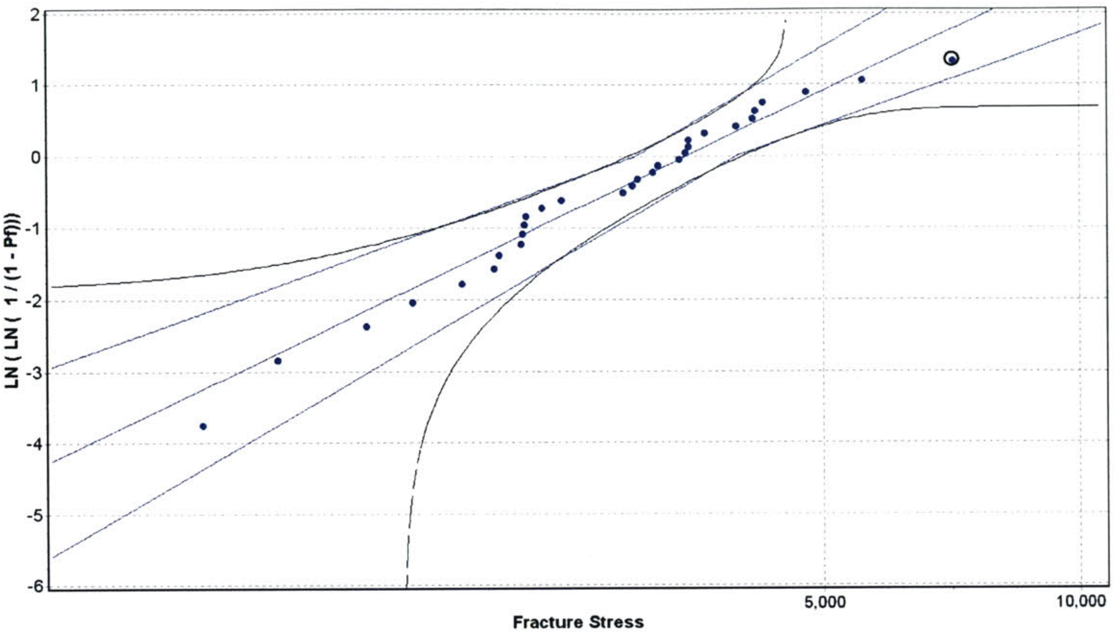

Figure 5-13: MIT69 + SF6 RHFS Weibull Distribution

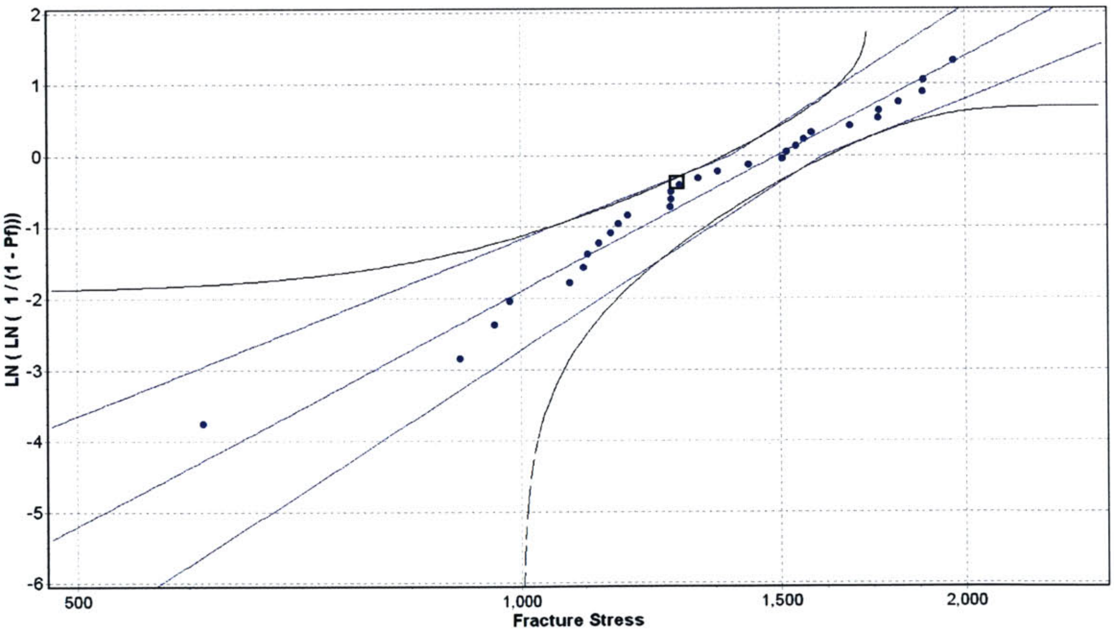

Figure 5-14: ADAM06 RHFS Weibull Distribution

The Weibull distribution for ADAM06 had no outliers but had one point with Kolmogorov-Smirnov test significance of 90.3 %.

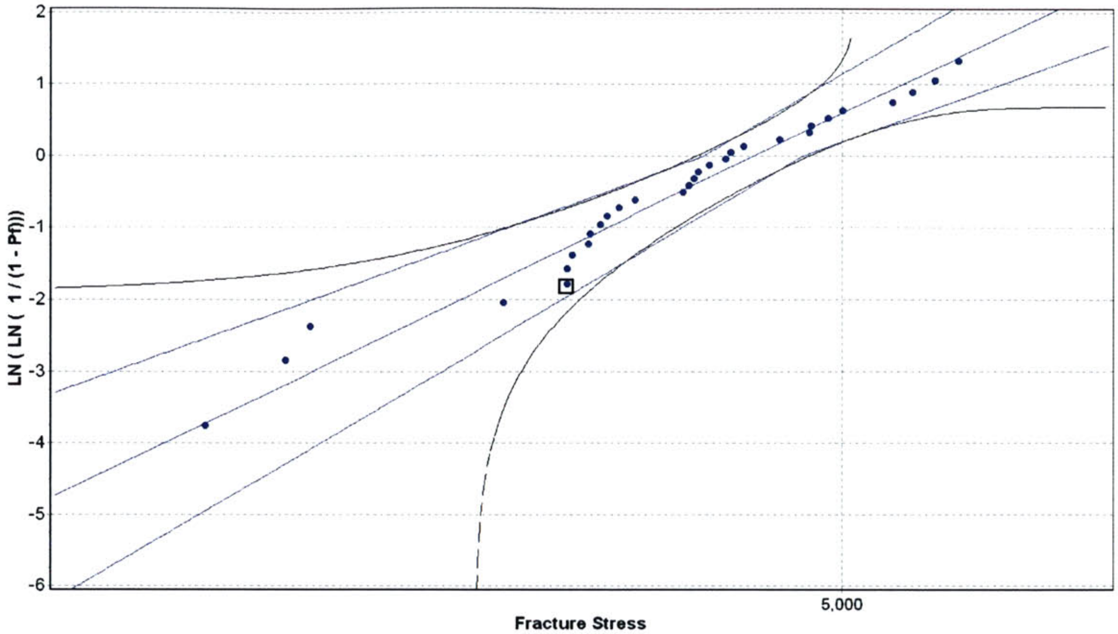

Figure 5-15: ADAM06 + SF6 RHFS Weibull Distribution

The ADAM06 + SF6 Weibull distribution had no outliers and one point with Kolmogorov-Smirnov test significance of 91 %.

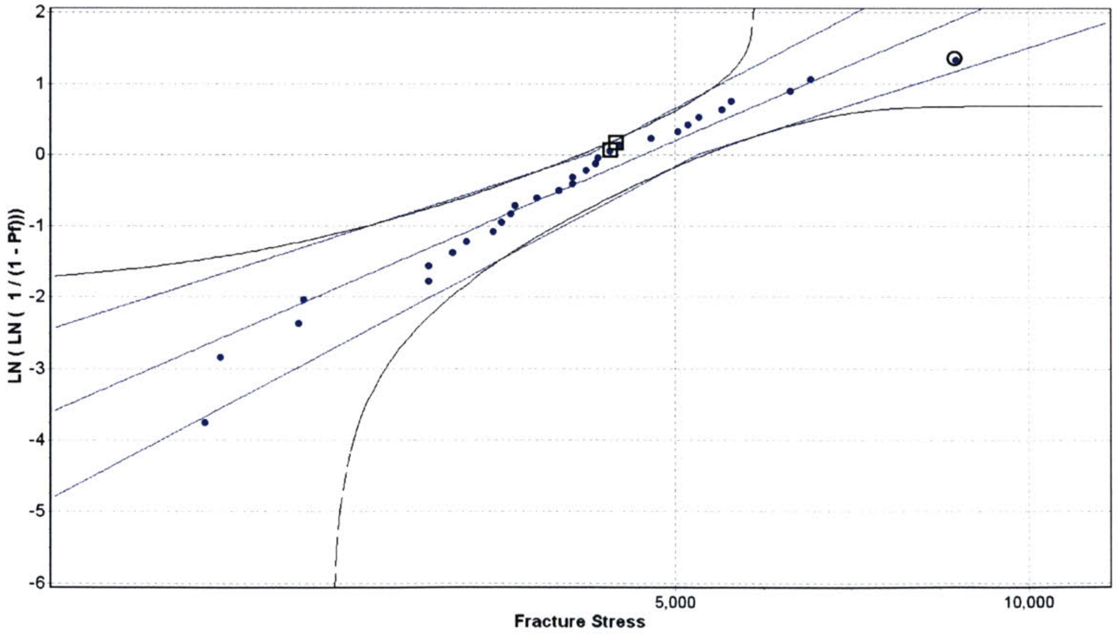

Figure 5-16: MIT69 + Kt Weibull Distribution

With the applied stress concentration factor, the MIT69 data had one outlier and two points with Kolmogorov-Smirnov test significance less than 99%.

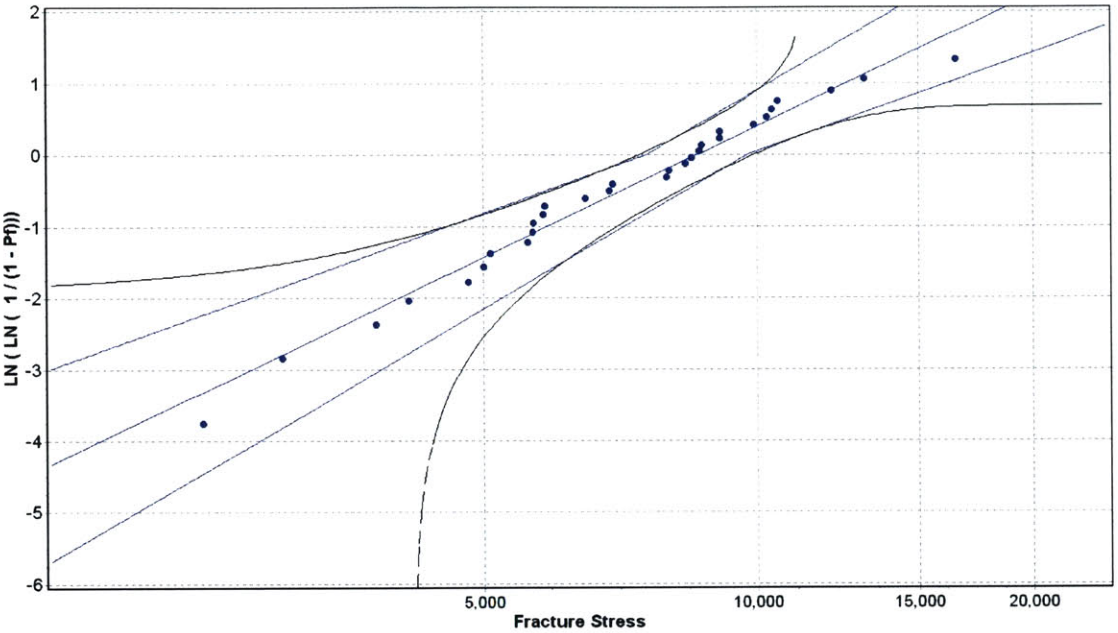

Figure 5-17: MIT69 + SF6 + Kt Weibull Distribution

The Weibull distribution for a stress concentration factor applied to MIT69 + SF6, ADAM06, and ADAM06 + SF6 had no outliers and no points with Kolmogorov-Smirnov test significance less than 99%.

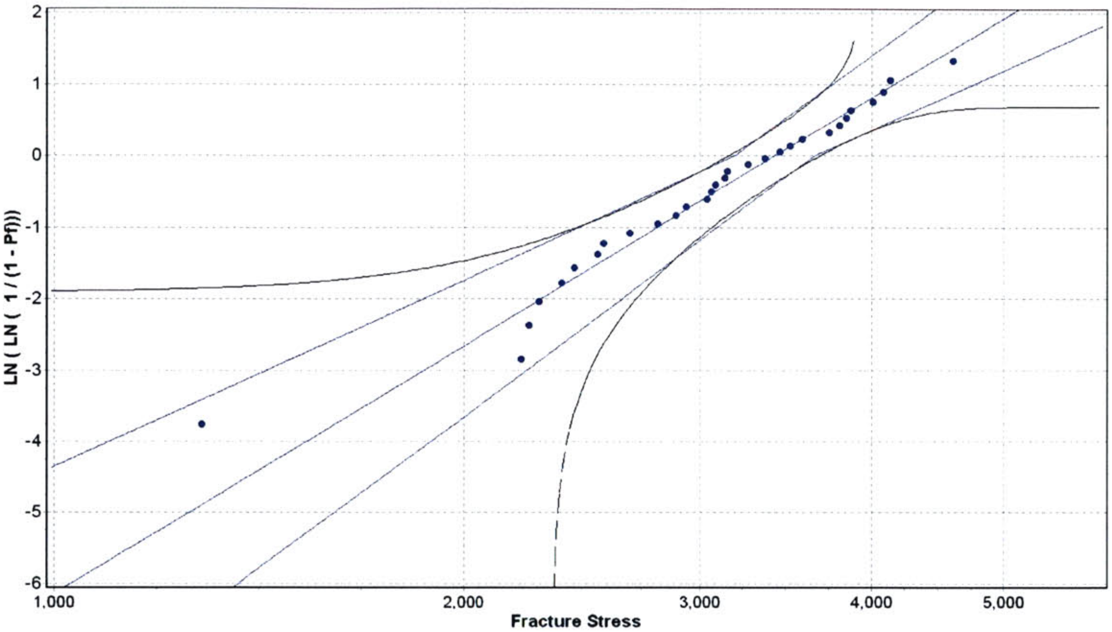

Figure 5-18: ADAM06 + Kt Weibull Distribution

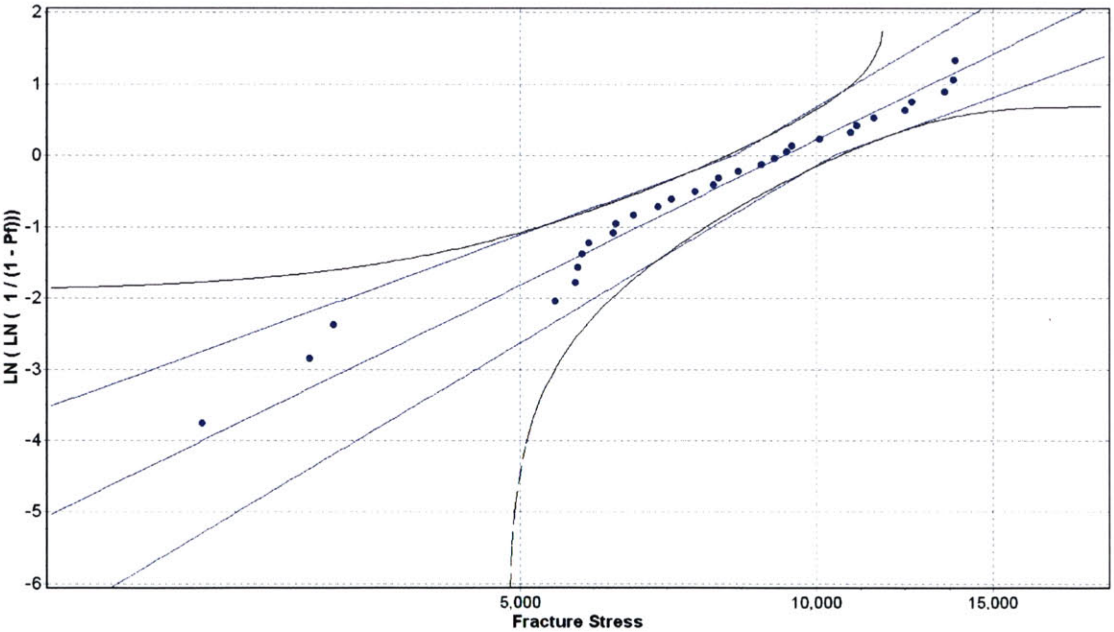

Figure 5-19: ADAM06 + SF6 + Kt Weibull Distribution

5.5.3 Pressurized Chamber Devices

The length scale of the finite element model used for the calculations in CARES was millimeters. In order to be able to compare values for RHFS and chambers, the effective volumes and areas as well as the scaling parameters have been scaled into meters. The strength values remain in MPa.

Table 5-3: CARES Output Summary for Pressure Chambers

	Config A	**Config B**	**Config A + SF6**	**Config B + SF6**
number of data points	9	3	13	11
m (biased)	2.996	11.8	1.643	4.201
m (unbiased)	2.523	0	1.467	3.664
characteristic strength	749.6	401.9	4046	1141
mean characteristic strength	669.4	384.9	3620	1037
standard deviation (char. Strength)	243.6	39.58	2261	278.4
specimen equivalent effective volume	9.711E-09	6.26E-12	4.137E-08	3.082E-09
scaling parameter (volume)	1.59E+06	4.51E+07	1.30E+05	1.08E+07
specimen equivalent effective area	1.10E-06	6.75E-08	4.22E-06	5.79E-07
scaling parameter (area)	7.68E+06	9.92E+07	2.22E+06	3.57E+07

Table 5-4: CARES Output Summary for Pressure Chambers + Kt

	Config A	**Config B**	**Config A + SF6**	**Config B + SF6**
number of data points	9	3	13	11
m (biased)	3.062	16.35	1.676	3.881
m (unbiased)	2.578	0	1.497	3.384
characteristic strength	1049	584.2	6158	1705
mean characteristic strength	938	565	5500	1543
standard deviation (char. Strength)	334.7	42.57	3374	444.9
specimen equivalent effective volume	9.11E-09	3.53E-13	3.97E-08	4.15E-09
scaling parameter (volume)	2.48E+06	1.01E+08	2.36E+05	1.18E+07
specimen equivalent effective area	1.10E-06	6.75E-08	4.40E-06	4.78E-07
scaling parameter (area)	1.17E+07	2.07E+08	3.82E+06	4.21E+07

Below are figures of the Weibull distributions for Configurations A & B, with and without the isotropic etch and with and without the applied stress concentration factor.

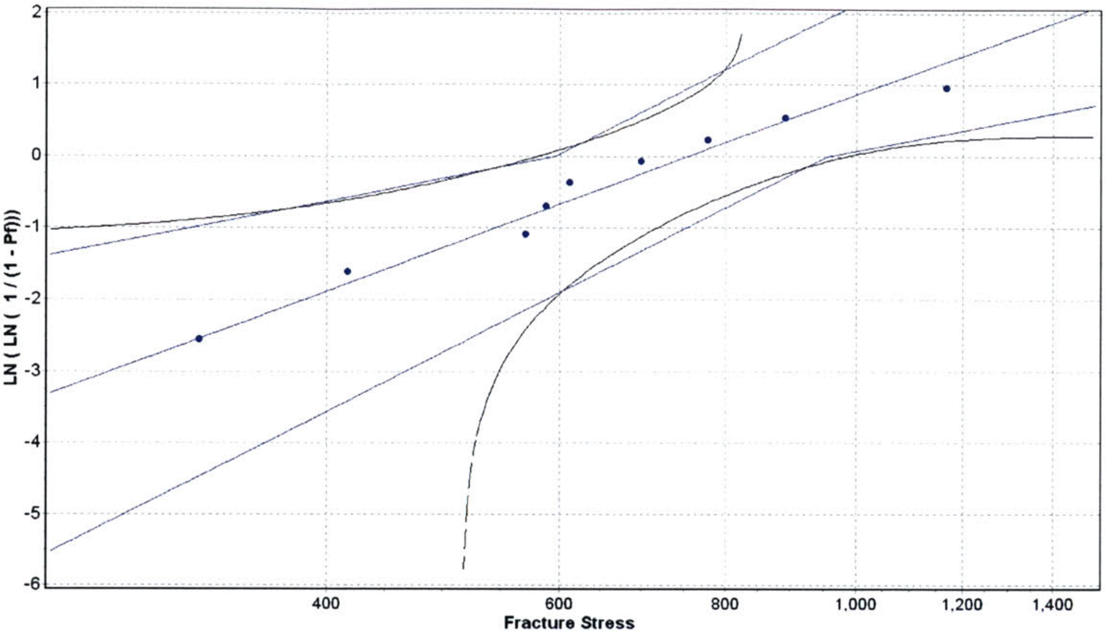

Figure 5-20: Chamber Tests Configuration A Weibull Distribution

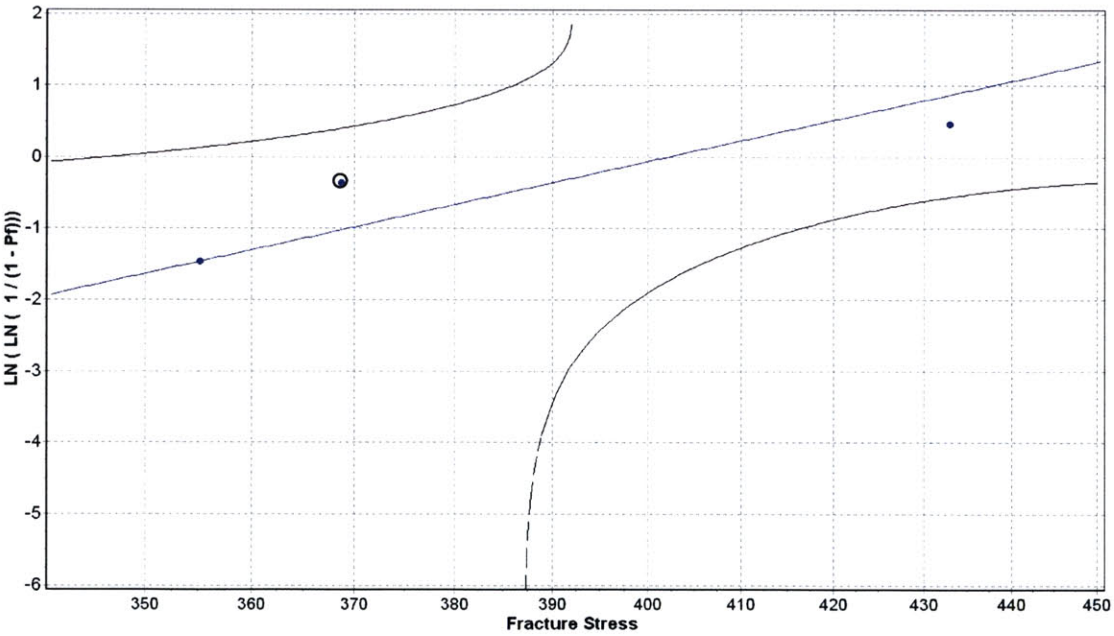

Figure 5-21: Chamber Tests Configuration B Weibull Distribution

The Configuration B Weibull distribution had one point with Kolmogorov-Smirnov test significance of 64%.

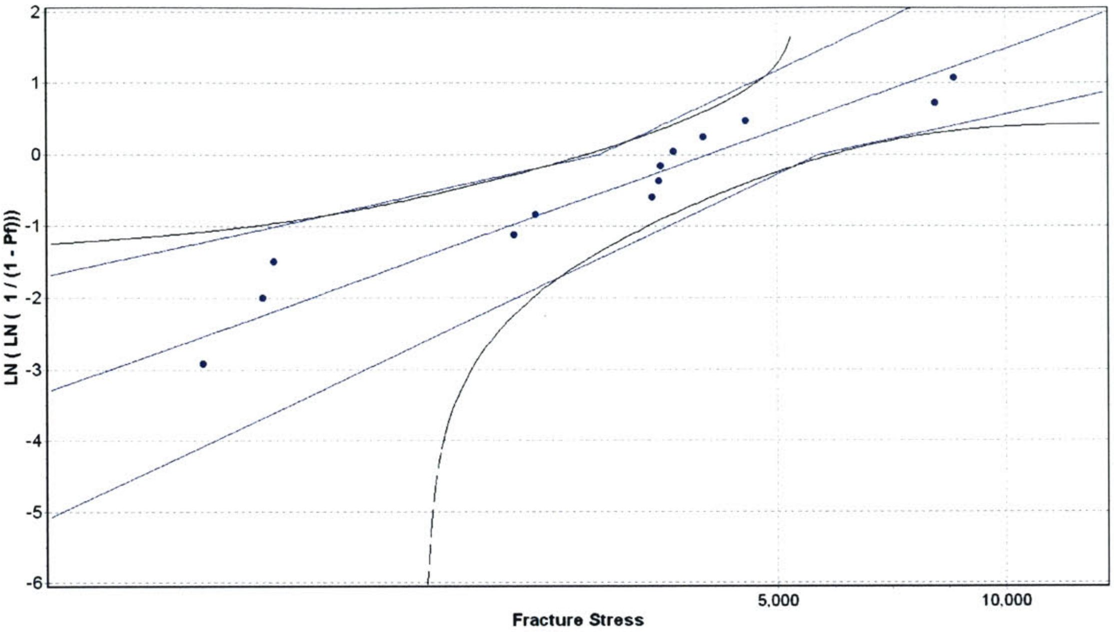

Figure 5-22: Chamber Tests Configuration A + SF6 Weibull Distribution

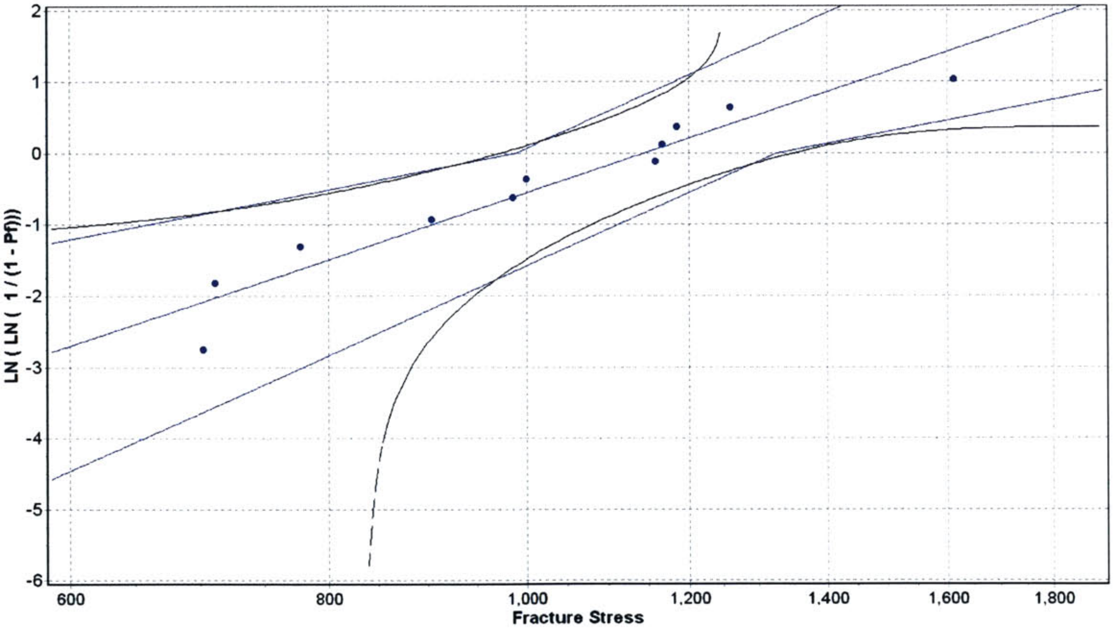

Figure 5-23: Chamber Tests Configuration B + SF6 Weibull Distribution

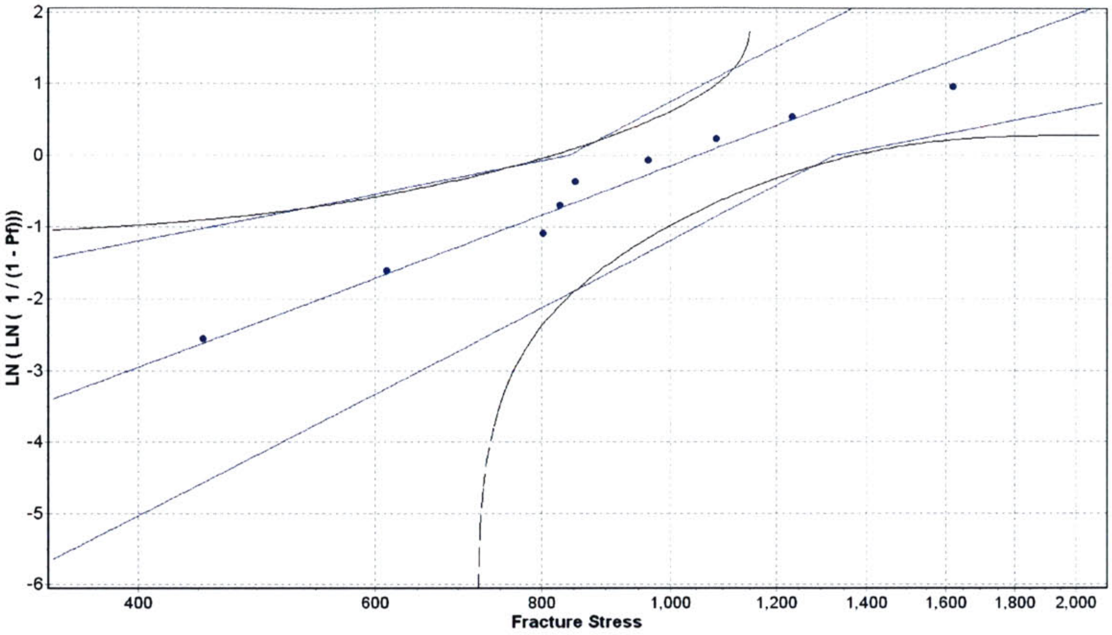

Figure 5-24: Chamber Tests Configuration A + Kt Weibull Distribution

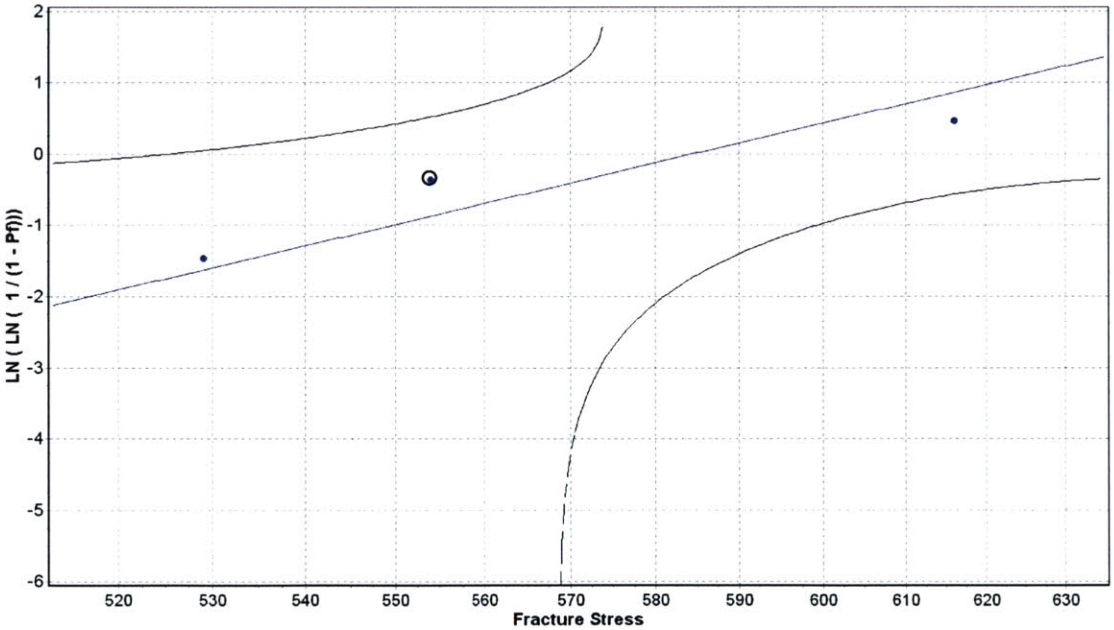

Figure 5-25: Chamber Tests Configuration B+ Kt Weibull Distribution

With the application of a stress concentration factor the Configuration B distribution has one point with Kolmogorov-Smirnov test significance of 81%.

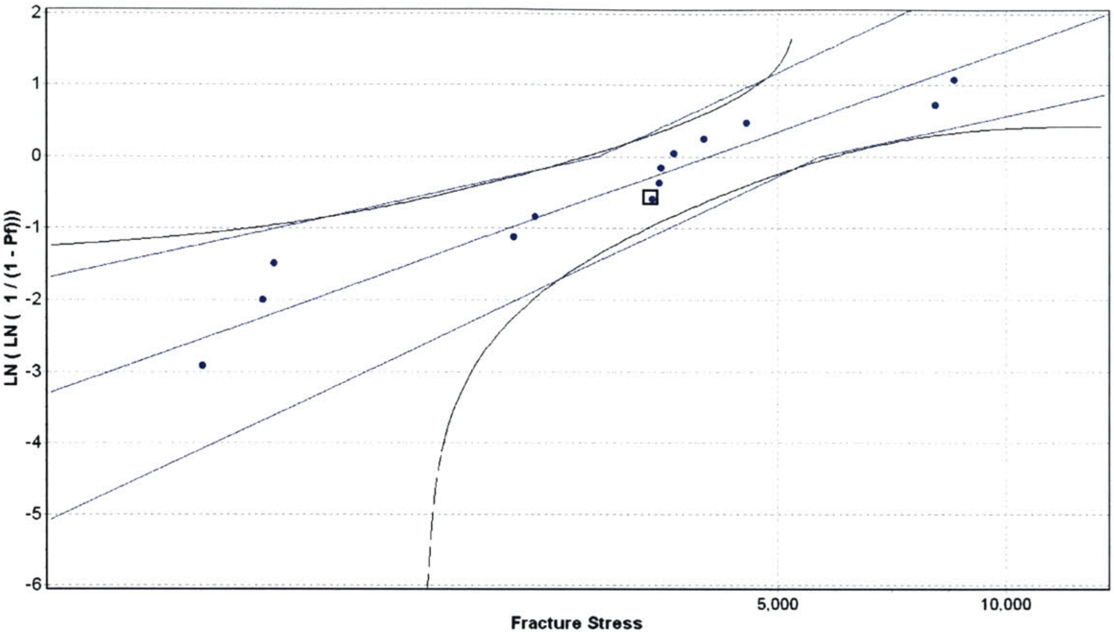

Figure 5-26: Chamber Tests Configuration A + SF6 + Kt Weibull Distribution

Configuration A + SF6 + Kt has one point with Kolmogorov-Smirnov test significance of 93%.

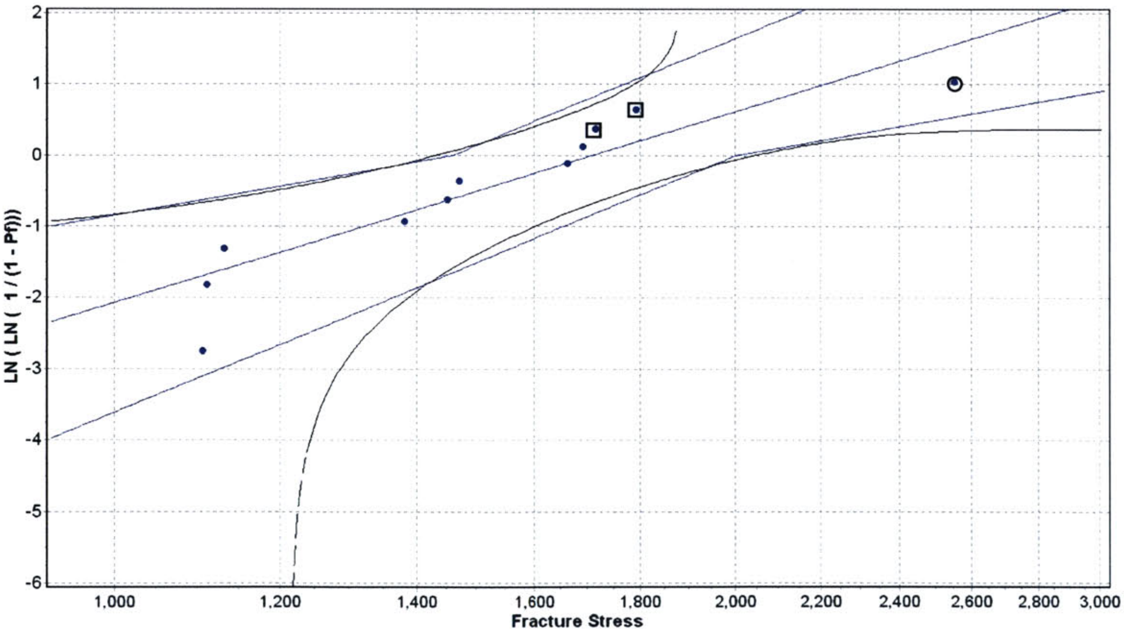

Figure 5-27: Chamber Tests Configuration B + SF6 + Kt Weibull Distribution

Configuration B + SF6 + Kt has one outlier with significance of 0.1%. In addition, two points have Kolmogorov-Smirnov test significance below 99%.

5.5.4 Correlation: Volumetric/Surface Area Scaling

The analysis conducted with CARES assumes that all flaws in a given data set are either surface flaws or volumetric flaws. It is not possible to determine definitively the nature of the failure-causing flaw much less the location of that flaw on the specimen.

One goal of this research is to evaluate the feasibility of using simple specimen geometries to predict the behavior of more complex geometries. Within the frame of the experiments conducted for this work, that would allow testing of radiused hub flexure specimens to predict the strength behavior of chambers fabricated using nominally the same processes. In order to quantify this correlation, it is necessary to find the effective area or volume of each specimen (see Equation (5-4)). The predicted characteristic strength for a pressure chamber, based on the Weibull parameters of a radiused hub flexure specimen, is calculated as:

$$\sigma_{chamber} = \sigma_{rhfs}\left(\frac{A_{rhfs-eff}}{A_{chamber-eff}}\right)^{\left(\frac{1}{m_{rhfs}}\right)} \qquad (5\text{-}7)$$

where σ_{rhfs} is the characteristic strength of the RHFS specimen sample, $A_{x\text{-eff}}$ is the effective area of the x specimen, and m_{rhfs} is the Weibull modulus of the RHFS sample. The same can be calculated using effective volumes. The difference in the effective areas between the RHFS geometry and the chamber geometry can be approximated calculating the area using the fillet radius and the circumference of the loaded geometry. For the chamber this value is approximately 0.81 mm^2 and for the RHFS this value is approximately 0.08 mm^2.

The prediction curves are generated using CARES without doing the explicit calculation presented above. Instead, the Weibull parameters (shape parameter and scaling parameter) from the RHFS data sets (for ADAM06) are applied to the finite element of the model. This is processed through the parameter estimation (PEST) module and produces a .inl file which is then processed with a .neu file generated from the finite element results in the LIFE module. The LIFE module calculates the probability of component failure, where the entire structure is the component, and provides the maximum effective stress. By repeating this process with neutral files for several loading conditions, a curve may be generated using the maximum effective stress and the failure probability values to create a predicted Weibull curve.

In order to keep the units consistent across the data sets (as the length scales and stress scaling for CARES are different for RHFS and the chamber), the radiused hub flexure specimen scaling parameter had to be modified. The scale parameters listed in Section 5.5.2 are in units of Pascal meter$^{(2/\text{shape parameter})}$ for surface calculations or Pascal meter$^{(3/\text{shape parameter})}$ for volume calculations. For use with the chamber models, where the length scale is millimeters,

$$SP_{chamber} = SP_{RHFS}(10^3)^{\frac{n}{m_{RHFS}}} \qquad (5\text{-}8)$$

where SP is the scale parameter (in units of MPa), m_{RHFS} is the shape parameter, and n is 2 for surface area and 3 for volume.

The data shown below is for failure stresses with an applied stress concentration factor (Kt). The same plots for the unmodified data sets are available in Appendix E.

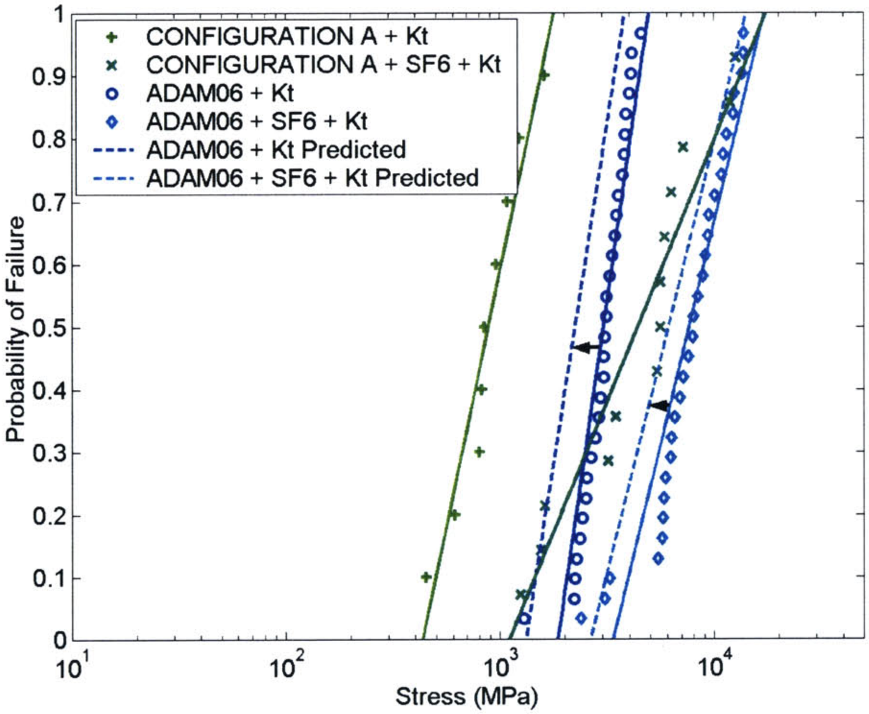

Figure 5-28: Configuration A + Kt Effective Area Scaling

Figure 5-28 shows the predicted strength based on effective area scaling for Configuration A. The Configuration A + SF6 curve falls in the vicinity of the RHFS line and the estimated scaling. With a larger sample size, the Configuration A + SF6 could correlate reasonably well with the prediction. The slope of the Configuration A line is not drastically different from the predicted line, however the characteristic strength is much lower.

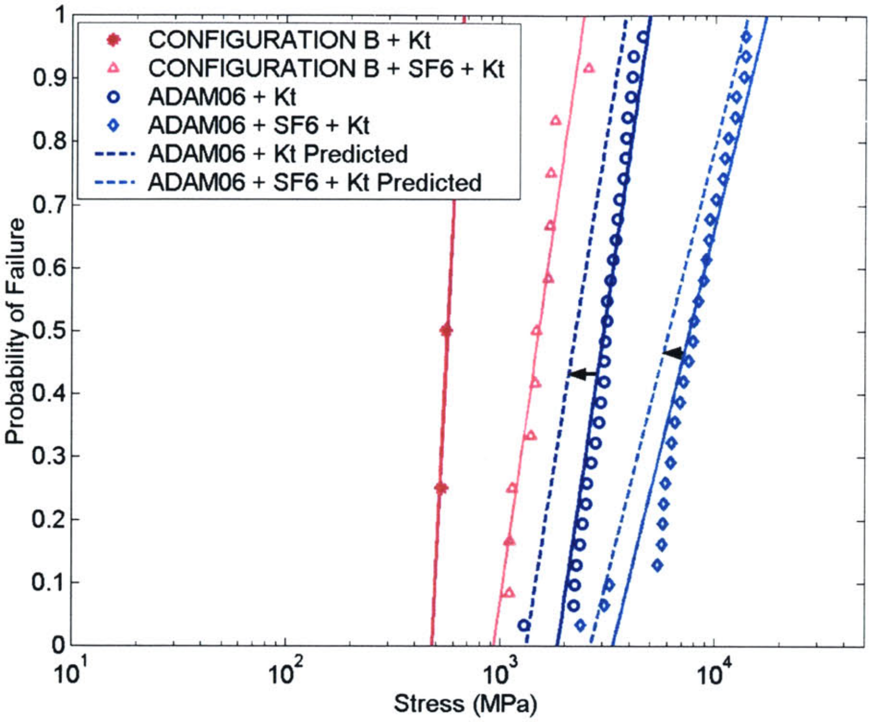

Figure 5-29: Configuration B + Kt Effective Area Scaling

Figure 5-29 shows the effective area scaling for Configuration B. The shift is rather small relative to the distance from the Configuration B data curves. As Configuration B consists of only three data points, it is difficult to evaluate the usefulness of the predicted curve. The ADAM06 prediction appears more consistent with the Configuration B + SF6 curve, indicating that the strength of the chambers is much less than the RHFS.

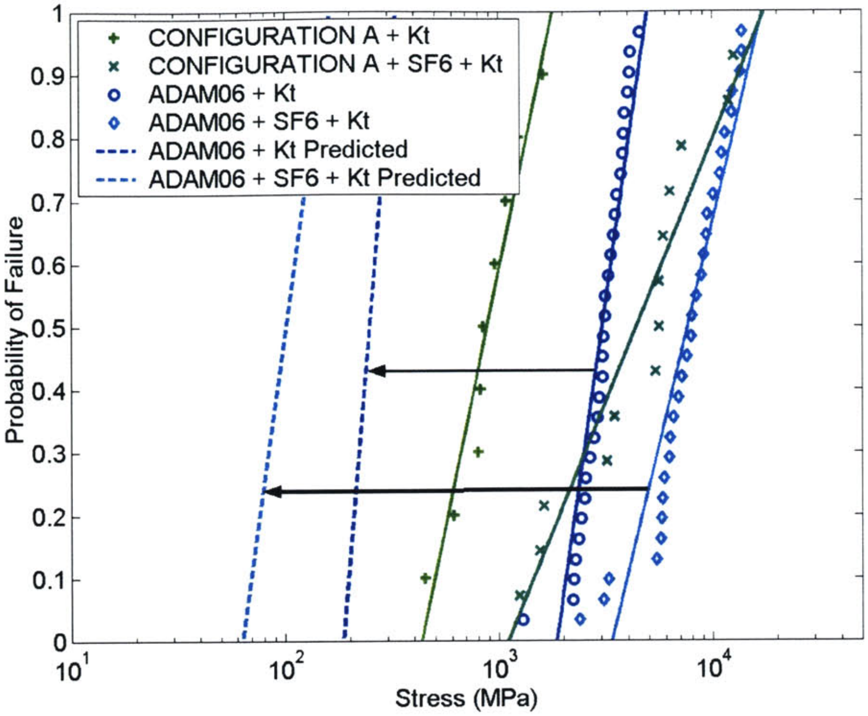

Figure 5-30: Configuration A + Kt Effective Volume Scaling

The volumetric scaling prediction shown in Figure 5-30 is very large and the pressure chamber data is closer to the actual radiused hub flexure values than to the predicted scaling.

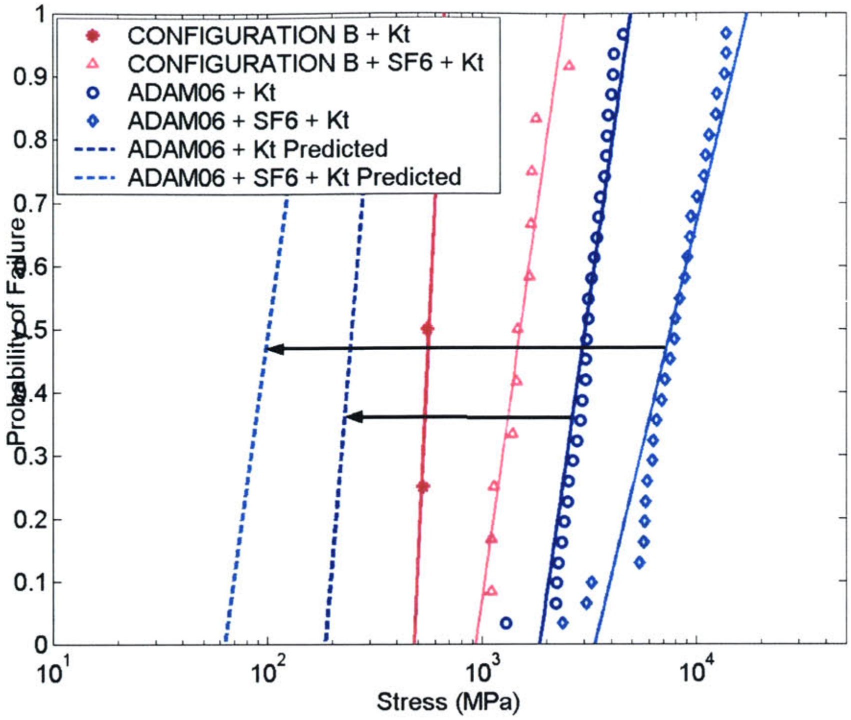

Figure 5-31: Configuration B + Kt Effective Volume Scaling

The volumetric scaling prediction for Configuration B is similar to the predictions for Configuration A. Again, the chamber data points correlate to curves much closer to the RHFS data itself than to the scaled prediction.

The scaled predictions of characteristic strength for correlation between radiused hub flexure specimens and pressure chambers have not been demonstrated to predict accurately the shift in strength due to changes in geometry. However, this should not eliminate the possibility of correlation between varied specimen geometries. What these results indicate is that a large number of specimens are required in all data sets in order to evaluate truly the potential for prediction capability. They also support the assumption that the flaw population resides on the surface of the material, and not throughout the volume. The disparity between the geometries may indicate that the influence of local geometry has a more significant effect on the surface roughness than previously accounted for. In order to properly relate two geometries, the models used would have to represent the fabricated geometry, not the designed geometry. The data sets included in the study are not large enough to validate any such theory, however, they may serve as evidence to justify further study.

5.6 Summary

The overview of Weibull statistics has been expanded to include the applications of the NASA CARES/LIFE software. The CARES software uses experimental data with a finite element model of the test specimen to calculate the Weibull parameters and to evaluate the goodness of fit of the data to the parameters. These parameters have been calculated for each set of test data discussed previously. Characteristic strengths for radiused hub flexure specimens range from 1500 to 4000 MPa (3400 – 9200 MPa for applied stress concentration factor). For pressure chambers the characteristic strengths vary by an order of magnitude across data sets – 400 to 4000 MPa without stress concentration factors and 600 to 6000 MPa with stress concentration factors applied. The RHFS data was used to try to predict characteristic strength values for the chambers by scaling with respect to surface area and volume. The correlation for the data was not very good. However, increasing the number of data points in both sets, and particularly in the chamber sets, could improve the correlation, as the overall scatter should decrease. The results of the attempted scaling are one of several indicators for this study that imply that the nature of the surface flaws are dictated by the influence of the geometry on the etching. Further investigation into the nature of etch induced flaws could improve the analysis of the failure data and ultimately improve the quality of a predictive scaling tool.

Chapter 6 Discussion

6.1 Strength Recovery in Fabrication

The application of an isotropic etch following the conclusion of a deep etch can improve the ability of the material to withstand loading. This is done by eliminating very sharp features, which behave as sharp cracks with very high stress concentrations. Careful examination of the etched surfaces has revealed that an isotropic etch leaves a very distinctive etch surface. This porous looking surface appears significantly more textured that the anisotropic etch surfaces, however, the test results reveal that the porous looking surface does not contain features with severe stress concentrations that reduce the strength of the structure significantly from the intrinsic strength of the material.

The benefits of the isotropic etch have been demonstrated for two distinct geometries. The increases in characteristic strength with the application of an isotropic etch range from a factor 1.75 to a factor of almost 6. As with any etch, the effect of the isotropic etch is determined, in part, by its duration. All isotropic etches used in this study were 2 minutes long. For very small features, or very tightly spaced features, a two minute isotropic etch could decimate the designed spacing and dimensions. This is the case with the micro rocket. Thus it is very important to understand the relationship between etch time and achievable strength.

6.2 Volume/Surface Area Effects

The nature of single crystal silicon, free of bulk material defects, suggests that the flaws of principal concern are those introduced by fabrication onto the surface of the material, principally on the etched surfaces. Images taken from failed chambers without isotropic etching show extreme roughness on the walls. This was initially assumed to be the surface left by the etch ADAM06. Examination of radiused hub flexure specimens etched with ADAM06 revealed a very different looking surface. The surfaces of the ADAM06 + SF6 radiused hub flexure specimens appear similar to those from the failed chambers. There are two possible explanations for the differences. First, the grass type defects might be created on all surfaces etched by ADAM06 and the SF6 etch removes the features because it etches evenly in all directions. These thin structures might also be removed from the surface of a pressure chamber wall when the chamber is pressurized, leaving the surfaces seen in the failed device. Another possibility is that the geometry of the device being etched has a significant influence on the condition of the etched surface. The radiused hub flexure specimens and chambers have such different trench geometries; the walls on the RHFS are only 1.5 mm apart whereas the walls on the chamber have at least 5 mm between them. Additional work would be required to verify either of these possibilities.

6.3 Predictive Capability

Before evaluating the potential to predict the strength of etched silicon, it is necessary to reiterate that the strength of silicon is stochastic and as such there is an inherent danger in designing to a specific stress value. There are statistics at work, whether they are definitively Weibull or governed by another probability density function. A minimum strength cannot be guaranteed. While significantly high characteristic strengths have been observed, it is necessary to remain conservatively optimistic about achievable strengths. Another issue to be considered is the effect of geometry, as the more complex a structure, whether consisting of many small features, several wafers or both, the more conservative a strength estimate must be. This is the reason that the micro rocket is designed to1 GPa strength when higher strengths have been demonstrated. If the geometry, and particularly features like fillet radii, is accurately characterized on a specimen, it is possible to obtain repeatable strength data. It is only through careful characterization of and rigorous adherence to fabrication processes that the quality of surfaces and structures might be readily reproducible. This attention to detail may be so demanding as to use the etcher at the same time of day, as the amount of continuous (or near continuous) operating time can have significant effects on the etch rate and surfaces.

6.4 Relating Varied Geometry

The ability to relate data from various specimens is highly desirable and linked to the desire for predictive capabilities. If one can characterize an etch process using basic specimen geometries, which require fewer fabrication steps, and apply that strength to a more complex geometry, there is a significant savings in manpower and processing time. Additionally, the testing of basic specimen geometries is often less complex, allowing for a greater number of tests within a given time. This study has attempted to correlate the radiused hub flexure geometry with the pressure chamber geometry using scaling factors based on effective geometry. The results presented here are not successful in accurate prediction of the characteristic strength of the chamber data sets from the RHFS data. However, these results are not discouraging either; there appears to be potential for such predictions. The key factor hindering a definitive evaluation of the scaling predictions is the small size of the samples. Sample sizes on the order to 30 specimens or more are recommended for good statistics. The chamber data sets were far less than that and the relatively large scatter in the existing data precludes the assertion that the characteristic strength values obtained are sufficiently accurate to evaluate the quality of the predicted characteristic strength. In addition, there was a discrepancy between the size of the fillet radii in the radiused hub flexure specimens and in the model of the RHFS geometry. A glitch in the software prevented the use of the corrected model for CARES input. As always, any predictions that would be made with this method should be considered carefully and applied in the most conservative manner.

6.5 Differences Between the Pressure Chamber and the Rocket Chamber

The failure pressures recorded for the pressure chamber experiments have exceeded all recorded micro rocket cold test pressure levels. As the pressure chamber walls are significantly thinner than those of the rocket, it is imperative to examine the possible reasons why these results can be achieved in this device but not in the rocket itself. In addition, comparison to hot tests may be made, but the fact that they are hot tests (with combustion occurring in the chamber) broadens the potential failure modes beyond the scope of this research to include the effects of raised temperatures on the material properties of silicon.

1. Different packaging

The pressure chamber is packaged between two stainless steel plates and held in place with O-rings. The micro rocket has several different packaging configurations. It has been packaged in an O-ring package; however, the O-rings were used to create interface seals but not as structural elements. The more traditional micro rocket packaging placed the rocket in one stainless steel plate where tubes are brazed to the plate and then joined to the surface of the rocket by melting glass beads around them and creating a sealed interface. The process of attaching the tubes to the micro rocket involves elevated temperatures which can introduce a variety of residual stresses due to thermal mismatch of the tube material, the glass, and the silicon. This configuration also does not constrain the rocket when it is pressurized and it is free to push against the tubes.

2. Temperature

As was mentioned previously, the micro rocket is designed to operate at temperatures well above room temperature. Thus, even if the pressures can be achieved at room temperature, there must be sufficient cooling to maintain the structural integrity of the device. Even with cooling, the temperature of the device will be significantly higher than room temperature and therefore there are still thermal considerations to be taken into account relative to material performance.

3. Detailed features

The micro rocket device consists of many small features, such as fuel injectors and cooling passages. The fabrication of these features requires a multiple etches for each processed wafer, which includes a considerable amount of additional handling. In addition, dimensional tolerances of these features are much more stringent than the pressure chamber because dimensions of the passages affect the mass flow through them and this in turn influences the ultimate performance of the device. These tolerances make the application of a secondary isotropic etch rather precarious, as the etch will systematically enlarge all cavities and reduce all walls as a function of the etch time. This detailed geometry not only limits the allowable etch time for isotropic material removal, but it creates a multitude of potential stress concentrations. Because these features can not be highly smoothed, they may remain rough enough to trigger failure with a stress concentration.

4. Different geometry

There are several characteristics of the micro rocket geometry that the pressure chamber does not include. While overall, the walls of the combustion chamber in the micro rocket are much thicker than the walls in the pressure chamber specimens, there are cooling passages etched just on the other side of every wall surface. If the coolant pressure and the chamber pressure are not equal, there is an induced stress in the thin wall between the passages and the chamber. The micro rocket combustion chamber opens into the nozzle, which changes the boundary conditions for the chamber wall subject to uniform pressure. The effect of this opening on the stress state of the chamber wall has not been quantified, but it is clear that it will be different. In addition there are many more external connections to the micro rocket, inlets and outlets for fuel, oxidizer, and coolant. These connections are made through holes in the outer walls of the rocket. These holes, in conjunction with the sealed connections discussed above, are yet another source of stress concentrations that threaten the structural integrity of the device.

This is simply an overview of configuration differences between the functional device and the experimental device. Several of these issues have been analyzed for their role in the micro rocket failures and modifications have been made which have improved the performance of the device. However, these items must be kept in mind when examining the data from these experiments, because the micro rocket is a significantly more complex structure and as the results of the radiused hub flexure specimens cannot be directly applied to the chambers, the results of the pressure chambers cannot be directly applied to the micro rocket combustion chamber.

Chapter 7 Conclusions

7.1 Summary of Experimental Results and Conclusions

Several experiments and analyses were conducted with the objective of identifying the key factors contributing to diminished structural strength of the micro rocket combustion chamber. Five overarching objectives were outlined for this thesis. They addressed the issues of failure modes, specimen geometry, effective material strength, etch recipes, and predictive tools and how these issues could be used to improve the structural performance of the micro rocket. The work conducted has laid the groundwork for several avenues of investigation that have demonstrated promise with their initial results. In order to capitalize on this potential, further work is necessary and these recommendations follow in Section 7.2.

Both specimen geometries demonstrated repeated failures at the predicted location of maximum stress, the top of the chamber for the pressure chamber and at the inner fillet for the radiused hub flexure specimens. The observed failure modes, in conjunction with finite element modeling, validate the analytical modeling used for data reduction and calculation of stress values. The testing of two different pressure chamber configurations revealed a significant difference in the characteristic strength of slightly different geometries. Modeling conditions that predicted this behavior were not found. It is suspected that the different geometry of Configuration B may produce unanticipated features during fabrication, which contribute to increased stress concentrations and therefore a lower characteristic strength.

The effective characteristic strength of etched single crystal silicon has been calculated for various etch conditions and specimen geometries. Calculated values were as low as 600 MPa and as high as 9 GPa for different geometries. The results demonstrate significant improvements in characteristic strength with the application of a secondary isotropic etch. The improvement to the surface etched with ADAM06 was so great that its characteristic strength was greater than that of the surface etched with MIT69 and the isotropic etch although for primary etches only, the MIT69 strength was better than that of ADAM06. The data sets used to obtain these values did not have sample sizes large enough to ensure rigorous statistical reliability. It cannot be definitively stated that the material properties of etched silicon are accurately represented by Weibull statistics; however, the available data does not discredit the working assumption that Weibull distributions apply. Nonetheless, these strength results have demonstrated that the achievable strength levels in etched single crystal silicon structures are acceptable—satisfying, if not exceeding the assumed design strength of 1 GPa.

Identification of failure initiation locations in specimen geometries has had limited success. While some possible initiation points were identified on failed specimens, the large majority of specimens failed catastrophically, leaving little material from the failure surfaces for post mortem analysis. Careful examination of the etched surfaces has offered additional insight into the nature of the flaws resulting from the etching process. While more questions have been raised than answered concerning the true effects of these features, further investigation could offer significant benefits in identifying the most critical features of an etched surface.

The use of simple specimens (RHFS) to predict the strength of more complex specimens (pressure chambers) was uncertain. The predictions did not demonstrate consistency across data sets. It appears that the small sample population of the chamber data sets heavily influenced the quality of the predictions. It is believed that larger samples could provide sufficient data to better evaluate the predictive potential. In addition, a technical difficulty with the finite element model input into CARES required the use of a model with larger fillet radii than was measured for radiused hub flexure specimens. Correction of this disparity could be significant in improving the quality of the prediction.

Recommendations for modifications to the micro rocket to improve effective material strength can only be summarized in the general terms of paths of further study to inquire along. The data from this study is not complete enough to offer detailed recommendations. The results of the experiments conducted have validated initial hypotheses that the greatest potential for improvement lies with the etch recipes and the surfaces they create. Thus it is recommended to reevaluate the micro rocket etch recipe, ADAM06, and to consider re-optimizing the recipe with more emphasis on the surface quality.

7.2 Recommendations for Future Work

The experiments and analyses conducted in pursuit of improved structural performance of the micro rocket combustion chamber have been most successful in identifying several key routes of investigation that may hold the key to achieving improved effective strength. The recommendations for further work in the pursuit of improving the structural performance of the micro rocket are:

1. Understanding the factors that create such a large disparity between the failure stresses of Configurations A and B. This would begin with detailed examination of the surfaces of specimens from a top pressure chamber wafer.
2. Characterization of the effect of DRIE isotropic etching as a function of time. This would allow designers to determine how much isotropic etching their structures can afford without endangering the integrity of the device functionality.
3. Investigating the effects of re-optimizing the micro rocket etch recipe with greater concern for the quality of the surface roughness. Perhaps partner this with the characterization of the isotropic etching, as the surfaces etched with ADAM06 demonstrated such dramatic improvement with the long (2 minute) secondary isotropic etch.
4. Characterization of the flaws introduced by the deep primary etches. Identifying how the features of the geometry being etched influences the nature of the surface roughness and understanding how that affects the statistical nature of the effective material strength.
5. Apply the predictive modeling to a larger sample size using accurate finite element models of the geometry.

Appendix A: Fabrication Details

A.1 Fabrication Step Definitions

HMDS: hexamethyldisilazane vapor prime over to improve adhesion of photo resist to oxide

Pre Bake: 90°C for 30 minutes

Post Bake: 120°C for 30 minutes (thin photo resist) / 90°C for 60 minutes (thick photo resist)

RCA Clean: Removal of contaminants from the surface of a silicon wafer through three sequential steps:

1. Removal of insoluable organic containinants with a 5:1:1 $H_2O:H_2O_2:NH_4$ solultion
2. Removal of a think silicon dioxide layer where metallic contaminants may have accumulated as a result of Step 1, using a diluted 50:1 $H_2O:HF$ solution
3. Removal of ionic and heavy metal atomic contaminants using a solution of 6:1:1 $H_2O:H_2O_2:HCL$

Buffered Oxide Etch (BOE): $HF + NH_4F$

Piranha Etch: 3:1 $H_2SO_4 : H_2O_2$ (Sulfuric Acid and Hydrogen Peroxide)

A.2 Etch Recipes

ALIGN Etch Recipe

	Etch
Time (s)	13
Platen Generator Power (W)	120
Coil Generator Power (W)	800
SF6 Flow (sccm)	105
C4F8 Flow (sccm)	0
APC Angle	65
Overrun	0

ADAM06 Etch Recipe

	Etch	**Passivate**
Time (s)	15	9.5
Platen Generator Power (W)	120	0
Coil Generator Power (W)	600	600
SF6 Flow (sccm)	140	0
C4F8 Flow (sccm)	0	95
APC Angle	62.5	62.5
Overrun	0.5	0

MIT69 Etch Recipe

	Etch	**Passivate**
Time (s)	14	11
Platen Generator Power (W)	100	60
Coil Generator Power (W)	750	600
SF6 Flow (sccm)	105	0
C4F8 Flow (sccm)	0	40
APC Angle	75	75
Overrun	0.5	0

MIT59 Etch Recipe

	Etch	**Passivate**
Time (s)	15	11
Platen Generator Power (W)	120	60
Coil Generator Power (W)	750	600
SF6 Flow (sccm)	105	0
C4F8 Flow (sccm)	0	40
APC Angle	65	65
Overrun	0.5	0

SF6-4 Etch Recipe

	Etch
Time (s)	variable
Platen Generator Power (W)	120
Coil Generator Power (W)	950
SF6 Flow (sccm)	30
C4F8 Flow (sccm)	0
APC Angle	75
Overrun	0

A.3 Fabrication Process Steps

Photo Resist Cycle

HMDS
Spin thin/thick photo resist
Pre bake
Develop
Coat back side
Post bake

Radiused Hub Flexure Specimen Fabrication Steps

RCA clean
0.5 μm thermal oxidation
Thin photo resist cycle
Expose mask: Fillet 1/2 (alignment marks)
Buffered Oxide Etch (BOE)
Etch STS 1: ALIGN
Pirhana strip photo resist
FLIP WAFER
Thick photo resist cycle
Expose mask Fillet 2/2 (hub feature)
Mount on handle wafer
Etch 250 μm STS 1: ADAM06 or MIT69
(Etch STS1: SF6-4 (20 s, 2 min))
Pirhana: dismount / strip photo resist
Measure etch depth on each device and wafer thickness

Pressure Chamber Fabrication Steps

Top & Bottom Wafer
RCA clean
0.5 mm thermal oxidation
Thin photo resist cycle for alignment marks
Buffered Oxide Etch (BOE)
~2 µm STS1 etch : ALIGN
Piranha strip photo resist
Bottom Wafer
Thick photo resist cycle for chamber features (mask presstest_ch_only…)
BOE
250 µm STS1 etch: ADAM06
Isotropic STS1 etch: SF6-4
Inspect and measure depth of each chamber and wafer thickness
Top Wafer
Thick photo resist cycle for chamber features (mask presstest_tube…)
BOE
Piranha strip photo resist
Thick photo resist cycle for chamber features (mask presstest_ch_only…)
Check (If there are holes on the top 8 devices then patch them)
BOE
240 µm STS1 etch: ADAM06
Piranha strip photo resist
10 µm STS1 etch: ADAM06
Isotropic STS1 etch: SF6-4
Inspect and measure depth of each chamber and wafer thickness
Flip wafer
Thick PR cycle for chamber features (mask presstest_text…)
BOE
Mount wafer to handle wafer
STS1 through etch: MIT59
Remove handle wafer
Bonding Steps
Piranha strip photo resist.
RCA
Bond
Anneal.

Appendix B: LabVIEW Files

B.1 Chamber Pressure Tests: chamber_pressure.vi

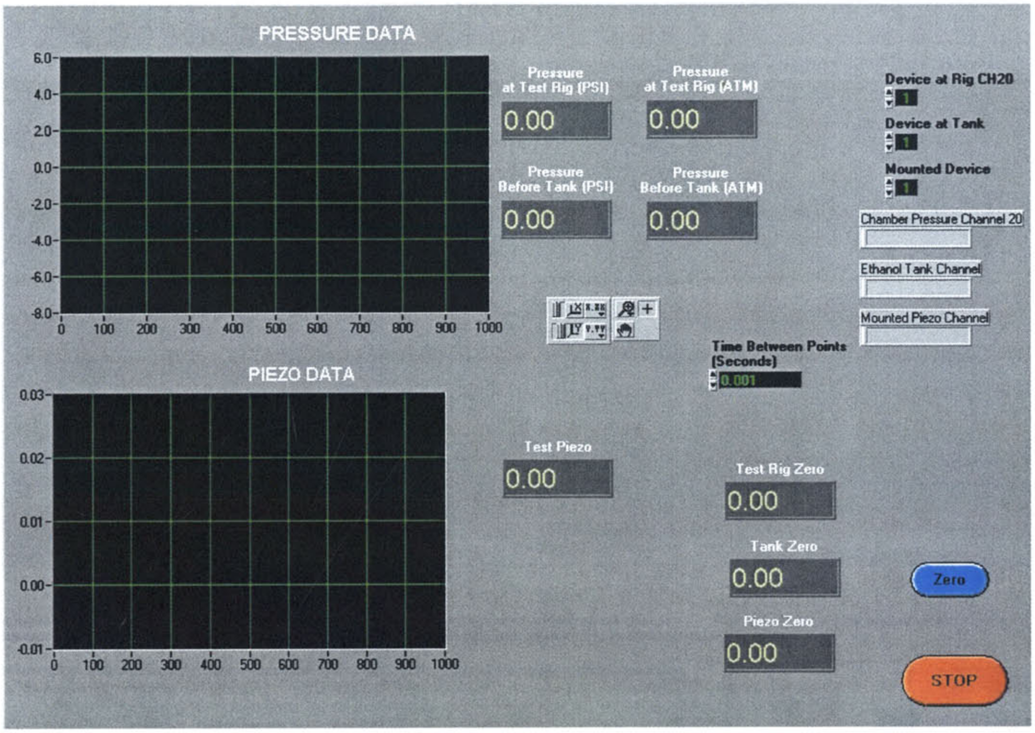

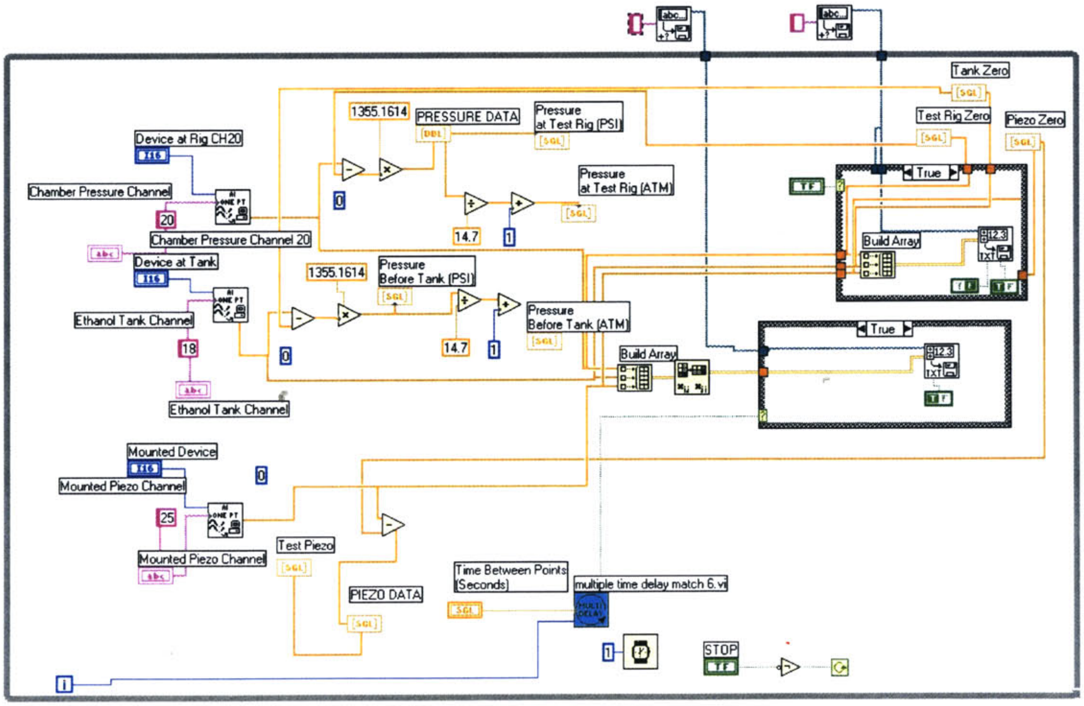

B.2 Radiused Hub Flexure Tests: statictest2.vi

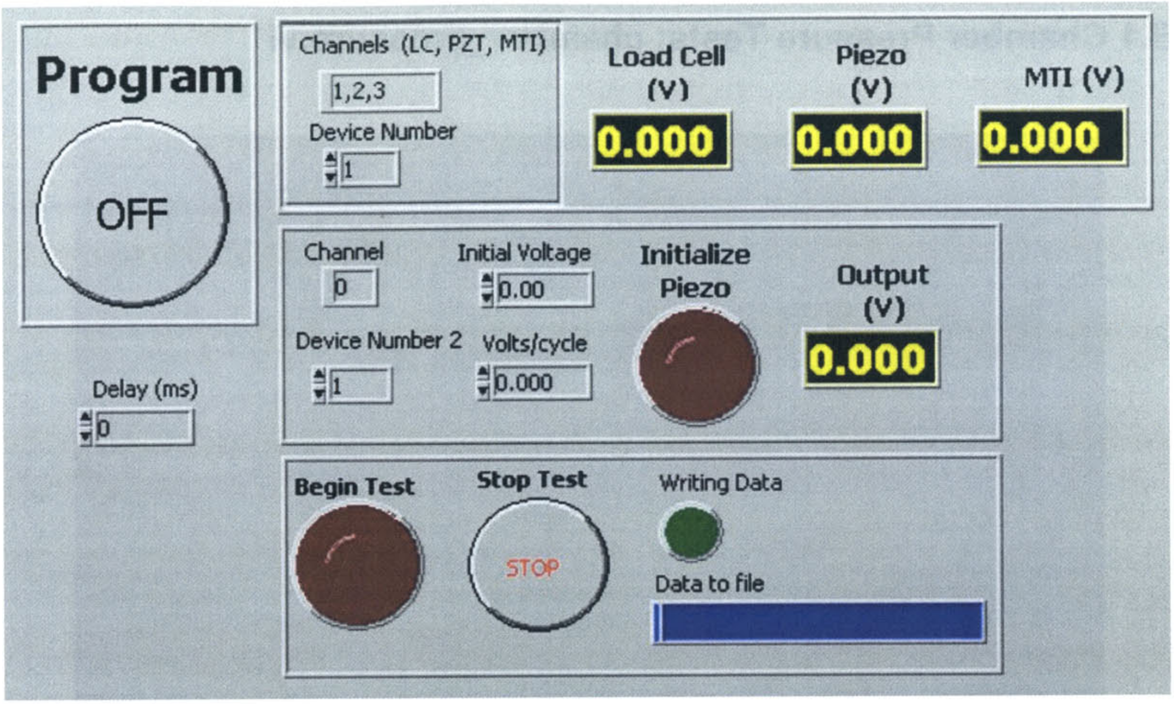

Channels (LC, PZT, MTI): 1,2,3
Device Number: 1
Load Cell (V): 0.000
Piezo (V): 0.000
MTI (V): 0.000
Channel: 0
Initial Voltage: 0.00
Device Number 2: 1
Volts/cycle: 0.000
Output (V): 0.000
Delay (ms): 0

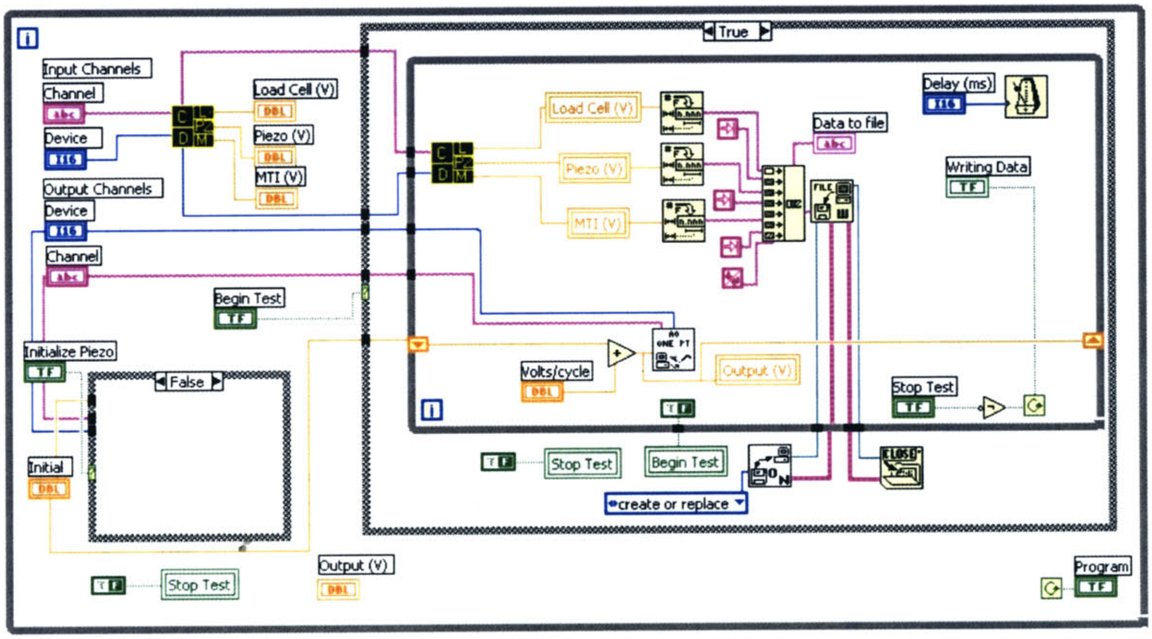

Appendix C: Test Procedures

C.1 Micro Rocket Chamber Pressure Experiment Procedure

1. Turn on transducers/board power
    a. Brown box:
        i. Brown switch to on
        ii. DC on (switch up)
    b. Gray box:
        i. Switch up (red light on)
        ii. Press main power start button (green light on)
2. Open coolant valve on table with wrench and c-clamp
3. Mount test rig on test stand with long screws, tighten with allen wrench
4. IF NECESSARY: take copper tube off of He T Swagelok fitting in control room and connect steel tube to it. Tighten with wrenches from test cell toolbox. Fitting is tightened when spacing matches other connects.
5. Start Labview
6. Open D:\ROCKETDAQ\chamber_pressure.vi
7. Start vi running (white arrow on menu bar)
8. Hit 'zero'button
9. At first prompt save zero values in file D:\Erin\zero_bx_x-x.xls
10. At second prompt save data file as D:\Erin\bx_x-x_mmddyy.xls
11. Wait for signals to stabilize (if necessary, resave zero file)
12. Values for pressure at ethanol tank and pressure at rig should be roughly equal
13. Check that connects are closed
    a. Methane (knob crosses perpendicular to tubing)
    b. Second pressure gauge (gold)
        i. Large number of threads are visible and handle turns easily/loosely
    c. He external vent (needle valve—tightened clockwise)
14. Open He tank all the way and then back ¼ turn
    a. First gauge should read ~3500 psi (if tank is full)
    b. Second gauge should read 0 (closed)
15. Turn gold knob CW on second gauge to increase pressure
    a. CW to open, CCW to close
    b. Can feel resistance in the knob when opening valve
16. Check and make sure pressures at both locations are ~ equal
17. Run test by increasing pressure
    a. Can hear increase in gas flow when device breaks
18. When device fails:
    a. Close second gauge
    b. Close bottle
    c. Vent test cell lines to outside (needle valve: all the way CW to close, CCW to open)
    d. Turn on exhaust fan in test cell (switch is gray box in hallway, says fan)

    e. Once lines are vented, open second gauge and vent He from line between tank and gauges

19. Stop Labview using STOP button on vi (not on menu bar)
20. Verify that piece has failed (if possible) using flashlight and hole in packaging
21. Remove test rig from test stand and remove failed device

C.2 RHFS Calibration Process

Load Cell Calibration

The load cell was calibrated using an Instron test machine and weights. The load cell was mounted between two aluminum plates with threaded holes in the center. The plates were then placed on a base with a load cell mounted in the Instron machine and the Instron test machine load cell was zeroed. Weights were manually placed on the top plate and the readings from the Instron machine and the voltmeter attached to the load cell were recorded. This process was repeated for loading and unloading up to 50 lbs.

Precision Stage Calibration

This calibration should be conducted periodically to ensure centered loading. The effect of minimal off centered loading has been analyzed and was determined not to be a major factor in the results of radiused hub flexure tests [22].

1. Fill test bed fixture hole (on bottom) with soft wax
2. Make wax flush with surface with razor blade
3. Place in test stand
4. Move precision x-stage to extreme right
5. Verify that the center of the test bed can be translated (using the precision stage) between the load application point and the microscope. If this is not the case, use the x-y stage to improve the position.
6. Reset x-stage to the right and zero the digital micrometer
7. Lower the load application point into the wax to make an indentation
8. Translate with the precision stage to the microscope and place cross hairs in center of the indentation
9. Record the distance displayed on the micrometer
10. Repeat this process a minimum of 10 times to get the average translation distance

C.3 RHFS Test Procedure

1. Load vi
    a. Open library: SILICON2.lib
    b. Open statictest2.vi
2. Check cable connections
    a. CH 1—Load Cell
    b. CH 2—Piezo
    c. OUT 0—From PC
    d. BNC T-connector should be mounted on Load Cell port (on box) to allow connection of voltmeter for monitoring load voltage while watching/conducting test
3. Turn box on
4. Load specimen
    a. RHFS device with etched features (hub) facing DOWN
5. Align specimen
    a. Turn on light
    b. Maximize translation to left with micrometer x-stage
    c. Place device roughly centered under eye piece using bottom x- & y-stages
    d. Verify necessary range of translation between eye piece and load cell using micrometer x-stage—if distance cannot be fully translated, compensate with bottom x-stage
    e. Center device on cross-hairs (using bottom stages)
    f. Zero micrometer and translate calibrated distance to loading point
    g. Turn off light
6. Turn program on (button on vi)
7. Select run arrow
8. Set piezo
    a. Initialize piezo to zero
        i. Set value, hit initialize
        ii. Verify that piezo value and output value match
    b. Initialize piezo to 1.0
    c. Bring load tip into contact using z-stage (voltage should change)
    d. Re-initialize piezo to zero to retract piezo
9. Settings
    a. Delay = 250 ms
    b. Rate = 0.01 to 0.05 Volts/cylce
        i. Rate can be modified during test if loading progression is too slow
10. Start test
    a. VOLTAGE SHOULD NOT EXCEED 10 VOLTS ON ANY CHANNEL (it will not stop itself)
11. Continue recording data after failure to record zero values
12. Reinitialize piezo to zero after each test

13. If piezo travel is not sufficient to break devices being tested in one expansion, use the automated loading to get compliance curve (for one or two devices) and then test by hand

Appendix D: Test Data Supplements

D.1 Chamber Pressure Tests

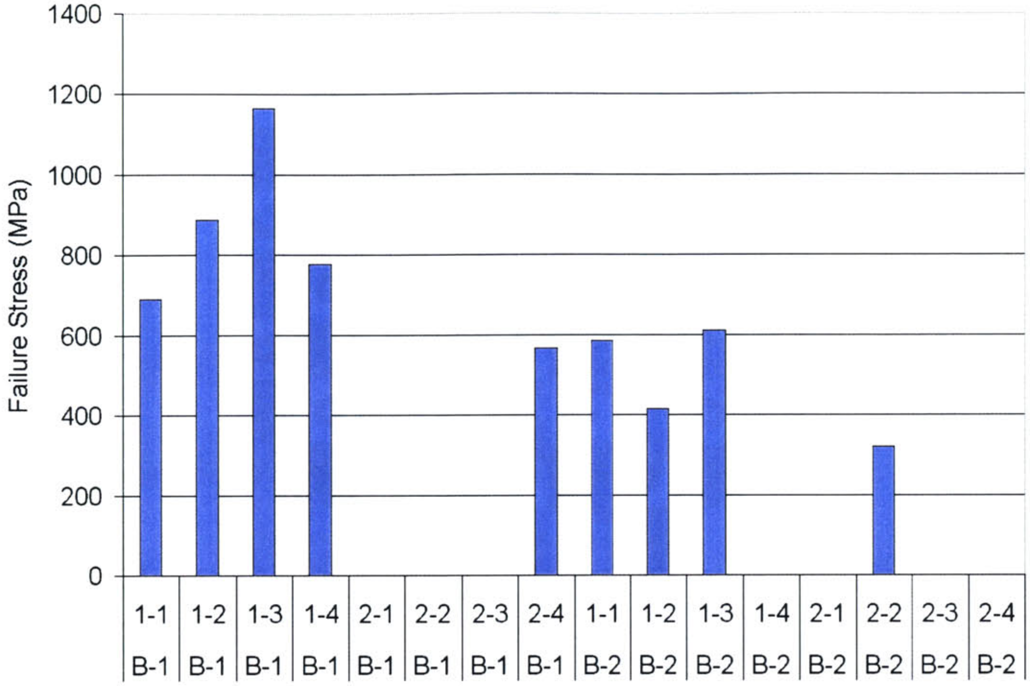

Configuration A: Pressure Test Failure Stress

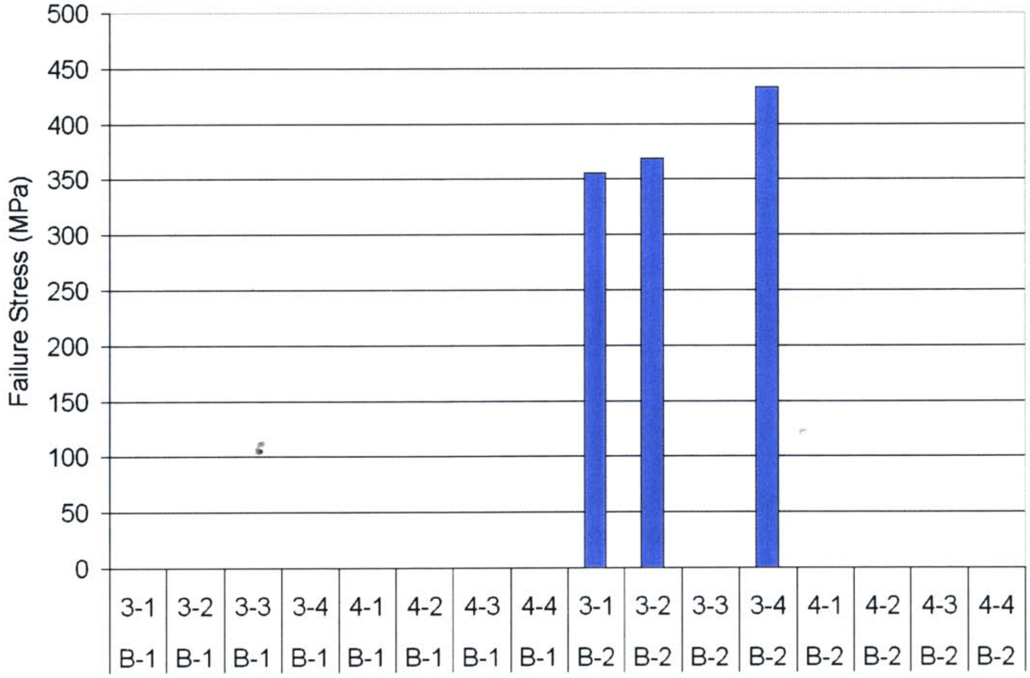

Configuration B: Pressure Test Failure Stress

D.2 Radiused Hub Flexure Tests

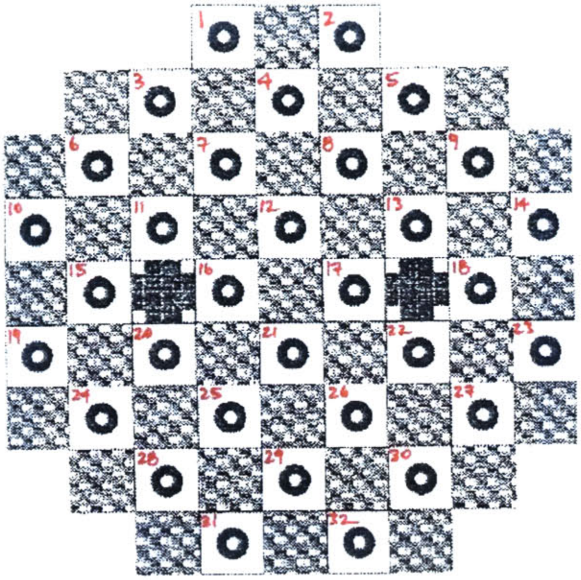

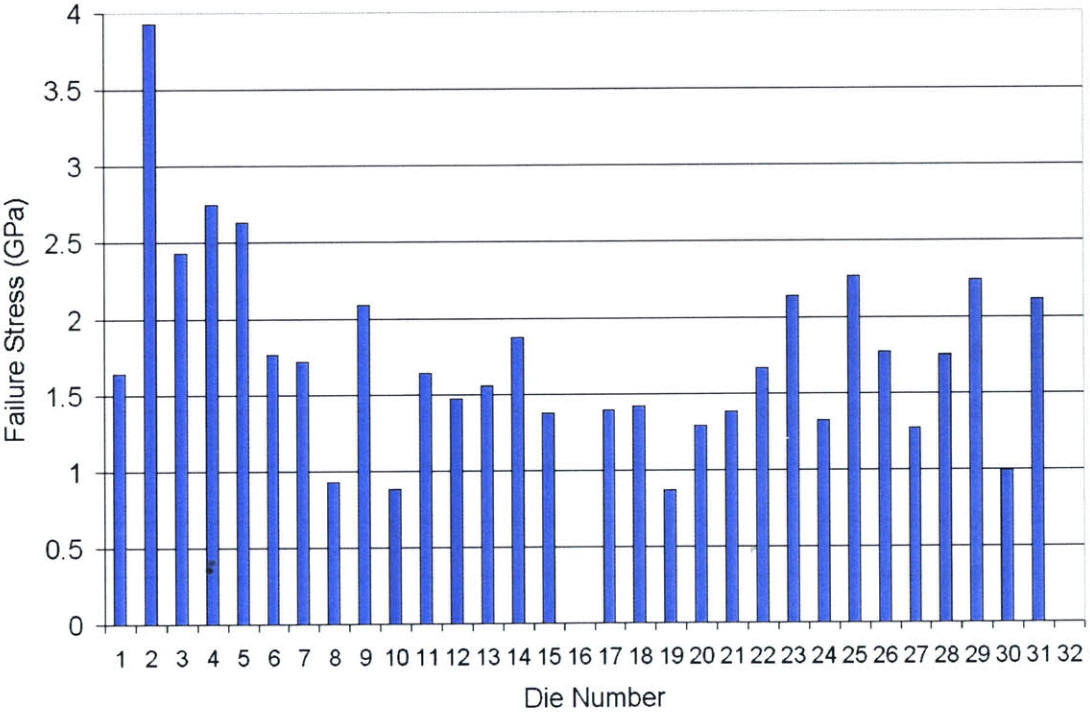

RHFS: MIT69 Failure Stress

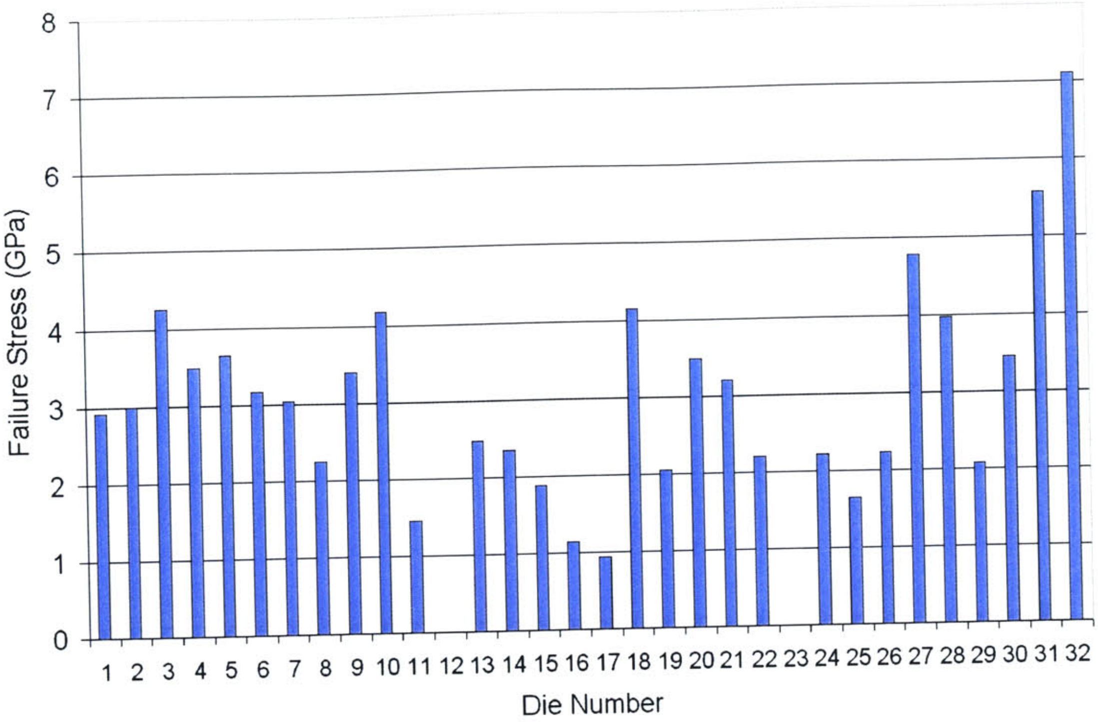

RHFS MIT69 + SF6 Failure Stress

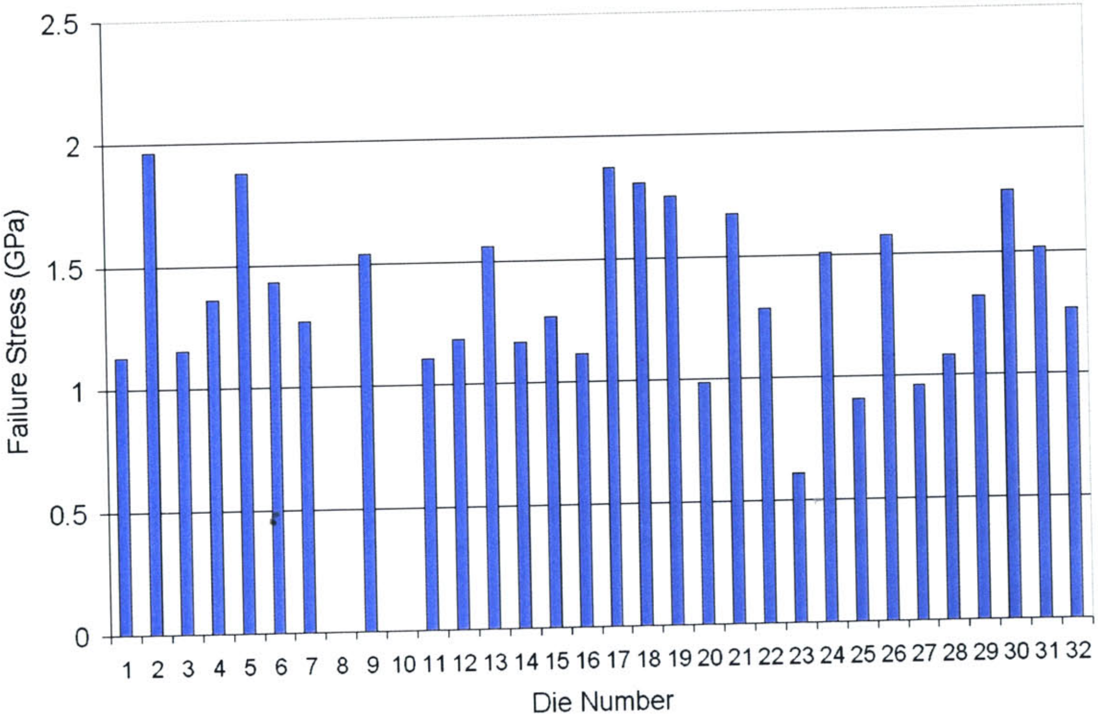

RHFS ADAM06 Failure Stress

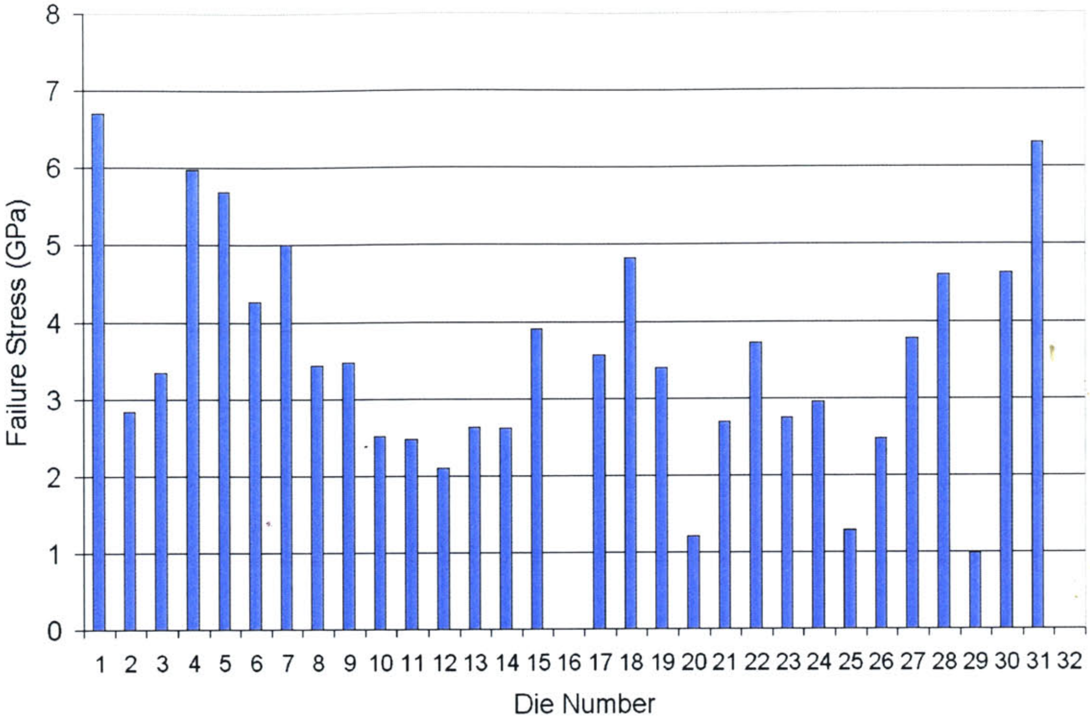

RHFS ADAM06 + SF6 Failure Stress

D.3 Matlab Codes

RHFS Model Plot Generation (rhfs1.m)

```
%rhfs1.m
%Calculates the deflection and corresponding stresses for an annular
plate with boundary conditions corresponding to a radiused hub flexure
specimen

clear all
close all

%P is the load applied at the center of the specimen

P=-1;

%Annular Dimensions
%b is the radius of the hub and the beginning point of the membrane
region a is the radius of the end of the membrane region

a=2.5e-3;
b=1.0e-3;

%Material Properties of Silicon
E=165e9;
v=0.2117;

%Thickness of Annular Membrane
h=150e-6;
```

```
%Plate Modulus
D=E*h^3/(12*(1-v^2));

%Moment applied at hub
M1=P/4/pi*((a^2/b^2-1)*(1-v)-2*a^2/b^2*(1+v)*log(b/a))/(a^2/b^2*(1+v)+1-
v);

%Constants for equation of deflection for shear loaded hole
C1=P/(4*pi*D)*((1-v)/(1+v)-2*b^2/(a^2-b^2)*log(b/a));

C2=-(1+v)/(1-v)*P/(4*pi*D)*a^2*b^2/(a^2-b^2)*log(b/a);

C3=P*a^2/(8*pi*D)*(1+1/2*(1-v)/(1+v)-b^2/(a^2-b^2)*log(b/a));

%Calculation of deflection and corresponding derivatives as a function of
radial position leading to the calculation of the bending moments in the
radial and tangential directions
c=0;

for r=b:1e-6:a
   c=c+1;

   w(c)=P*r^2/8/pi/D*(log(r/a)-1)-C1*r^2/4-C2*log(r/a)+C3-
b^2*M1/(2*(1+v)*D*(a^2-b^2))*(a^2-r^2)+a^2*b^2*M1/((1-v)*D*(a^2-
b^2))*log(r/a);

   R(c)=r;

   dw(c)=P*r/4/pi/D*(log(r/a)-1)+P*r/8/pi/D-C1*r/2-
C2/r+b^2*M1*r/((1+v)*D*(a^2-b^2))+1/r*a^2*b^2*M1/((1-v)*D*(a^2-b^2));

   d2w(c)=P/4/pi/D*(log(r/a)-1)+3*P/8/pi/D-
C1/2+C2/r^2+b^2*M1/((1+v)*D*(a^2-b^2))-a^2*b^2*M1/(r^2*(1-v)*D*(a^2-
b^2));

   d3w(c)=P/4/pi/D*1/r-2*C2/r^3+2*a^2*b^2*M1/(r^3*(1-v)*D*(a^2-b^2));

   Mr(c)=-D*(d2w(c)+v/r*dw(c));
   Mt(c)=-D*(1/r*dw(c)+v*d2w(c));

end

%Stress
Sr=-6*Mr/h^2;
St=-6*Mt/h^2;
Tau=3/h^2*(Mr-Mt);

figure
plot(R,Sr/10^6)
xlabel('Radial Position (m)')
ylabel('Stress (MPa)')
%legend('Radial','Tangential')

%figure
%plot(R,Tau)
%title('shear stress')
```

```
figure

plot(R,w)
title('deflection')
```

RHFS Data Reduction (datar.m)

```
%datar.m
%Using failure loads and device dimensions (wall thickness) for RHFS
%calculate the maximum stress, the stress concentration factor (Kt),
%and the maximum stress including the stress concentration factor
%for each specimen

clear all
close all

%Failure Loads
%MIT69
P690=[-21.804096  -49.653024  -38.6976 -52.392992  -51.570112  -34.07168
-44.41328   -27.969024  -43.310176  -14.6775104 -41.357504  -46.930848  -
46.766272   -33.64912   -28.418272  0  -46.299232  -33.18208   -13.375136
-32.577152  -42.527328  -51.24096   -43.65712   -22.364544  -48.2608 -
49.199328   -26.385536  -30.1352 -39.191328  -21.337056  -30.548864  0];
%MIT69 + SF6
P696=[-56.46736   -47.7048 -95.640896  -86.709312  -94.026272  -88.968896
-107.801728 -78.587264  -86.673728  -97.5433056 -51.365504  0  -87.621152
-49.893216  -57.236864  -41.12176   -34.3372256 -119.286464 -51.005216  -
119.931424  -109.016032 -82.483712  0  -60.942048  -44.05744   -65.58576
-132.843968 -103.740704 -43.096672  -93.603712  -101.6808352   -
118.543648];
%ADAM06
P060=[-8.13984 -12.525568  -14.576096  -22.053184  -16.106208  -21.390432
-26.625728  0  -20.81664   0  -22.604736  -28.725184  -30.966976  -
9.598784 -25.53152   -29.436864  -42.629632  -26.118656  -14.718432  -
22.960576   -40.107616  -25.8864704 -6.151584   -25.122304  -23.761216  -
36.31792 -15.283328  -18.334656  -24.828736  -27.417472  -19.486688  -
18.921792];
%ADAM06 + SF6
P066=[-51.57456   -22.30672   -48.331968  -92.278208  -69.330976  -
77.866688   -113.962208 -75.12672   -55.315328  -40.583552  -68.886176  -
67.022464   -65.434528  -31.945536  -84.1103456 0  -103.79408  -89.355872
-57.432576  -34.676608  -83.0437152 -98.5663456 -29.983968  -62.863584  -
35.610688   -67.160352  -65.78592   -89.046736  -21.270336  -80.780128  -
74.290496   0];

%RHFS dimensions
a=2.5e-3;
b=1.0e-3;

%Material Properties of Si
E=165e9;
v=0.2117;
```

```
%Wall thickness
%MIT69
h690=[0.000117 0.000114 0.000128 0.00014  0.000142 0.000141 0.000163
   0.000176 0.000146 0.000131 0.000161 0.000181 0.000176 0.000136
   0.000146 0.000176 0.000185 0.000155 0.000126 0.000161 0.000178
   0.000178 0.000145 0.000132 0.000148 0.000169 0.000146 0.000133
   0.000134 0.000149 0.000122 0.000115];
%MIT69 + SF6
h696=[0.000141 0.000128 0.000152 0.00016  0.000163 0.00017  0.000191
   0.00019  0.000162 0.000155 0.000191 0.000191 0.000191 0.000148
   0.000177 0.000193 0.000195 0.000172 0.00016  0.000188 0.000187
   0.000196 0.000162 0.000168 0.000166 0.000174 0.000169 0.000164
   0.000146 0.000167 0.000137 0.000131];
%ADAM06
h060=[0.000086 0.000081 0.000114 0.000129 0.000094 0.000124 0.000147
   0.000154 0.000118 0.000115 0.000145 0.000158 0.000143 0.000092
   0.000144 0.000165 0.000153 0.000122 0.000093 0.000155 0.000157
   0.000144 0.000102 0.000131 0.000164 0.000154 0.000128 0.000132
   0.000139 0.000127 0.000115 0.000124];
%ADAM06 + SF6
h066=[0.000089 0.00009  0.000122 0.000126 0.000112 0.000137 0.000153
   0.00015  0.000128 0.000129 0.000169 0.000181 0.00016  0.000112
   0.000149 0.000172 0.000173 0.000138 0.000132 0.000172 0.000178
   0.000165 0.000106 0.000148 0.000169 0.000167 0.000134 0.000141
   0.000149 0.000134 0.00011  0.000111];

%Wafer thickness
thick=[416 451 386 412]*10^(-6);

for i=1:1:4

   if i==1
      p=P690;
      H=h690;
   elseif i==2
      p=P696;
      H=h696;
   elseif i==3
      p=P060;
      H=h060;
   elseif i==4
      p=P066;
      H=h066;
   else
   end

   for j=1:1:32

      P=p(j);
      h=H(j);

      %Plate Modulus
      D=E*h^3/(12*(1-v^2));

      %Moment at hub
      M1=P/(4*pi*((1+v)*a^2/b^2+1-v))*((1-v)*(a^2/b^2-
1)+2*(1+v)*a^2/b^2*log(a/b));
```

```
        %Integration Constants
        C1=P/(4*pi*D)*((1-v)/(1+v)-2*b^2/(a^2-b^2)*log(b/a));

        C2=-(1+v)/(1-v)*P/(4*pi*D)*a^2*b^2/(a^2-b^2)*log(b/a);

        C3=P*a^2/(8*pi*D)*(1+1/2*(1-v)/(1+v)-b^2/(a^2-b^2)*log(b/a));

        %Offset calculation
        h1=thick(i);
        a1=3e-3;

        D1=E*h1^3/(12*(1-v^2));

        r1=a;

        w1=P/8/pi/D1*((3+v)/2/(1+v)*(a1^2-r1^2)+r1^2*log(r1/a1));

        shift=w1;

        %Set location for stress calculation (b is at the hub)
        r=b;

        %Deflection and associated dervivative wrt r
        w(j,i)=P*r^2/8/pi/D*(log(r/a)-1)-C1*r^2/4-C2*log(r/a)+C3-
b^2*M1/(2*(1+v)*D*(a^2-b^2))*(a^2-r^2)+a^2*b^2*M1/((1-v)*D*(a^2-
b^2))*log(r/a)+shift;

        dw=P*r/4/pi/D*(log(r/a)-1)+P*r/8/pi/D-C1*r/2-
C2/r+b^2*M1*r/((1+v)*D*(a^2-b^2))+1/r*a^2*b^2*M1/((1-v)*D*(a^2-b^2));

        d2w=P/4/pi/D*(log(r/a)-1)+3*P/8/pi/D-
C1/2+C2/r^2+b^2*M1/((1+v)*D*(a^2-b^2))-a^2*b^2*M1/(r^2*(1-v)*D*(a^2-
b^2));

        d3w=P/4/pi/D*1/r-2*C2/r^3+2*a^2*b^2*M1/(r^3*(1-v)*D*(a^2-b^2));

        %Moment in radial & tangential direction
        Mr=-D*(d2w+v/r*dw);
        Mt=-D*(1/r*dw+v*d2w);

        %Stress
        Sr(j,i)=6*Mr/h^2;
        St(j,i)=6*Mt/h^2;
        Tau(j,i)=3/h^2*(Mr-Mt);

       %Geometric ratios used for stress concentration estimation
        Dd(j,i)=thick(i)/h;
        rd(j,i)=8e-6/h;

        %Curve fit equation for the stress concentration factor curve for
D/d=3 from Peterson
        Kt(j,i)=702.11*(rd(j,i))^4-605.77*(rd(j,i))^3+199.89*(rd(j,i))^2-
31.95*(rd(j,i))+3.6539;

        %Stress with stress concentration factor applied
        SrKt(j,i)=Sr(j,i)*Kt(j,i);
```

```
   end
end
```

Weibull Plot Generation (plotw.m)

```
%plotw.m
%Weibull semilogxs - Chamber & RHFS

%Generation of Weibull plots for all data sets

clear all;
close all;

%MIT69

stress1=[3930.8   2750.2   2631.3   2430  2266.8   2245.5   2136.3
   2111.6   2090.4   1871.7   1772.3   1763.2   1752.7   1719.8   1663.9
1641.5   1638.7   1553.3   1473.8   1421  1391.8   1380.9   1371.6
   1320.5   1293  1273.5   988.8 929   879.9 866.8];
stress1k=[8663.09012 6532.55006  6281.17623  5590.701 5488.37616
   5251.99995  5136.51972  5037.864 4773.2718   4481.61501  4400.92821
   4299.15604  4275.55744  4198.53184  4088.52329  4087.0067   3977.53531
3806.23588  3646.92685  3617.9841   3548.36064  3494.239 3305.556
   3219.3114   3072.0112   3069.135 2399.61984  2378.8903   2041.368
   1982.805];
pfail1=[0.967741935  0.935483871 0.903225806 0.870967742 0.838709677
   0.806451613 0.774193548 0.741935484 0.709677419 0.677419355 0.64516129
0.612903226 0.580645161 0.548387097 0.516129032 0.483870968 0.451612903
   0.419354839 0.387096774 0.35483871  0.322580645 0.290322581
   0.258064516 0.225806452 0.193548387 0.161290323 0.129032258
   0.096774194 0.064516129 0.032258065];

%MIT69 + SF6
stress2=[7106.90  5573.70  4785.30  4258.90  4177.10  4148.40  3968.30
   3641.00  3491.10  3484.70  3453.00  3397.80  3207.40  3167.30  3040.20
2995.60  2922.10  2471.10  2343.50  2239.70  2228.70  2221.50  2209.00
   2080.10  2049.80  1879.60  1644.90  1448.60  1135.80  929.00];
stress2k=[16488.008  13139.44038 12100.58811 10547.72184 10404.91859
   10271.4889  9939.40101  9118.40409  9101.7718   8698.7976   8658.78256
8476.83144  8364.25772  8023.72109  7977.4848   6958.10452  6891.97692
   6484.1664   5868.014 5839.7124   5686.97379  5674.0822   5606.84385
   5093.34304  5013.041 4821.54992  4135.93656  3801.1264   2989.31202
   2452.2813];
pfail2=[0.967741935  0.935483871 0.903225806 0.870967742 0.838709677
   0.806451613 0.774193548 0.741935484 0.709677419 0.677419355 0.64516129
0.612903226 0.580645161 0.548387097 0.516129032 0.483870968 0.451612903
   0.419354839 0.387096774 0.35483871  0.322580645 0.290322581
   0.258064516 0.225806452 0.193548387 0.161290323 0.129032258
   0.096774194 0.064516129 0.032258065];

%ADAM06
```

```
stress3=[1964.10  1875.30  1873.60  1805.40  1750.80  1748.90  1674.10
   1575.50  1558.00  1538.10  1515.90  1506.10  1431.30  1363.40  1322.10
1284.40  1267.70  1266.80  1266.10  1183.80  1166.80  1153.90  1132.30
   1112.40  1106.10  1082.60  983.20   959.70   908.90   608.30];
stress3k=[4587.5096  4134.18995  4081.1067   4012.15149  3865.9619
   3836.8638   3793.46274  3728.1382   3567.255 3494.152 3433.96206
   3351.80649  3254.91933  3145.63648  3132.58374  3080.89028  3062.38289
3038.67316  2929.43148  2879.23801  2791.5678   2659.50684  2543.08021
   2518.56064  2417.6888   2367.32052  2276.52183  2237.99095  2207.98179
1284.66877];
pfail3=[0.967741935  0.935483871 0.903225806 0.870967742 0.838709677
   0.806451613 0.774193548 0.741935484 0.709677419 0.677419355 0.64516129
0.612903226 0.580645161 0.548387097 0.516129032 0.483870968 0.451612903
   0.419354839 0.387096774 0.35483871  0.322580645 0.290322581
   0.258064516 0.225806452 0.193548387 0.161290323 0.129032258
   0.096774194 0.064516129 0.032258065];

%ADAM06 + SF6
stress4=[6698.80  6316.70  5980.00  5686.30  5008.60  4827.30  4628.50
   4608.10  4268.30  3897.80  3769.30  3724.80  3568.00  3473.50  3435.20
3391.20  3340.90  2952.70  2833.30  2745.50  2696.60  2629.70  2620.10
   2509.10  2481.40  2477.50  2104.80  1282.80  1205.90  985.70];
stress4k=[13733.76914   13679.25 13417.02652 12447.87933 12263.5571
   11408.84082 10972.80772 10825.59865 10062.09042 9459.18104  9347.3856
9088.4096   8816.01577  8355.43696  7991.48145  7889.28768  7552.10445
   7149.07724  6929.18336  6534.27856  6274.71618  6241.318 5884.97925
   5788.99552  5735.66091  5699.74961  5435.85648  3243.81636  3066.12134
2392.09676];
pfail4=[0.967741935  0.935483871 0.903225806 0.870967742 0.838709677
   0.806451613 0.774193548 0.741935484 0.709677419 0.677419355 0.64516129
0.612903226 0.580645161 0.548387097 0.516129032 0.483870968 0.451612903
   0.419354839 0.387096774 0.35483871  0.322580645 0.290322581
   0.258064516 0.225806452 0.193548387 0.161290323 0.129032258
   0.096774194 0.064516129 0.032258065];

%CONFIG A

stress5=[1165.9   886.76   776.13   690.84   610.24   585.83   566.03
   415.06   321.07];
stress5k=[1620.519923   1233.94786   1083.992817 962.2828329 848.5456251
   825.6269034 801.68249   612.5973078 449.9593987];
pfail5=[0.9 0.8   0.7   0.6   0.5   0.4   0.3   0.2   0.1];

%CONFIG B

stress6=[432.91   368.66   355.23];
stress6k=[616.0357951   553.9862697 529.1263683];
pfail6=[0.75   0.5   0.25];

%CONFIG A + SF6

stress7=[8552.145864 8080.307404 4546.641618 3992.142046 3652.35388
   3511.232158 3486.44755  3418.802497 2395.996914 2238.677905
   1068.870568 1032.779978 862.3530125];
stress7k=[12562.85914   11812.87928 7154.545243 6281.990815 5845.166625
   5588.822758 5572.715236 5379.790007 3468.662193 3201.147957 1613.76341
1547.393866 1245.337715];
```

```
pfail7=[0.928571429  0.857142857 0.785714286 0.714285714 0.642857143
   0.571428571 0.5   0.428571429 0.357142857 0.285714286 0.214285714
   0.142857143 0.071428571];

%CONFIG B + SF6

stress8=[1611.081831 1257.046841 1184.014039 1164.994043 1155.800476
   1000.151845 984.8240745 898.7964174 775.3180574 704.3317639
   695.5276168];
stress8k=[2552.644368   1793.110476 1714.085987 1690.714141 1660.869031
   1469.194627 1450.113637 1381.194835 1129.05338  1107.590334
   1103.286309];
pfail8=[0.916666667  0.833333333 0.75  0.666666667 0.583333333 0.5
   0.416666667 0.333333333 0.25  0.166666667 0.083333333];

%Calculate values for curves representing the Weibull paramters
%Equations based on log curve fits to plot of stress (MPa) versus Pfail

c=0;

for x=200:100:2*10^4
   c=c+1;

   fit1(c)=0.7881*log(x)-5.3395;
   fit2(c)=0.6062*log(x)-4.3083;
   fit3(c)=1.0463*log(x)-7.0218;
   fit4(c)=0.5775*log(x)-4.1649;

   fit1k(c)=0.8149*log(x)-6.2558;
   fit2k(c)=0.6370*log(x)-5.1397;
   fit3k(c)=1.0222*log(x)-7.6952;
   fit4k(c)=0.6147*log(x)-4.9936;

   ks1(c)=1.5295*log(x)-10.569;
   ks2(c)=0.5758*log(x)-4.1602;

   fit5(c)=0.8802*log(x)-5.2319;
   fit6(c)=2.2372*log(x)-12.814;
   fit7(c)=0.3672*log(x)-2.4265;
   fit8(c)=1.0429*log(x)-6.7861;

   fit5k(c)=0.7041*log(x)-4.2755;
   fit6k(c)=3.1243*log(x)-19.299;
   fit7k(c)=0.3624*log(x)-2.5396;
   fit8k(c)=1.0429*log(x)-7.1303;


   s(c)=x;
end

%Weibull Distribution: RHFS
figure
semilogx(stress1,pfail1,'rs',stress2,pfail2,'mv',stress3,pfail3,'bo',
stress4,pfail4,'cd',s,ks1,'g-',s,ks2,'y-',s,fit1,'r-',s,fit2,'m-
',s,fit3,'b-',s,fit4,'c-')
title('')
xlabel('Stress (MPa)')
```

```
ylabel('Probability of Failure')
axis([10^2 10^4 0 1])
legend('MIT69','MIT69 + SF6','ADAM06','ADAM06 + SF6','MIT59 (Chen
1998)','MIT59 + SF6 (Chen 1998)')

%Weibull Distribution: RHFS + Kt
figure
semilogx(stress1k,pfail1,'r+',stress2k,pfail2,'mx',stress3k,pfail3,'b*',
stress4k,pfail4,'c^',s,ks1,'g-',s,ks2,'y-',s,fit1k,'r-',s,fit2k,'m-
',s,fit3k,'b-',s,fit4k,'c-')
title('')
xlabel('Stress (MPa)')
ylabel('Probability of Failure')
axis([10^3 10^5 0 1])
legend('MIT69 + Kt','MIT69 + SF6 + Kt','ADAM06 + Kt','ADAM06 + SF6 +
Kt','MIT59 (Chen 1998)','MIT59 + SF6 (Chen 1998)')

%Weibull Distribution: ADAM06 RHFS
figure
semilogx(stress3,pfail3,'bo',stress4,pfail4,'cd',stress3k,pfail3,'b*',
stress4k,pfail4,'c^', s,fit3,'b-',s,fit4,'c-',s,fit3k,'b-.',s,fit4k,'c-
.')
title('')
xlabel('Stress (MPa)')
ylabel('Probability of Failure')
axis([10^2 10^5 0 1])
legend('ADAM06','ADAM06 + SF6','ADAM06 + Kt','ADAM06 + SF6 + Kt')

%Weibull Distribution: MIT69 RHFS
figure
semilogx(stress1,pfail1,'rs',stress2,pfail2,'mv',stress1k,pfail1,'r+',
stress2k,pfail2,'mx',s,fit1,'r-',s,fit2,'m-',s,fit1k,'r-.',s,fit2k,'m-.')
title('')
xlabel('Stress (MPa)')
ylabel('Probability of Failure')
axis([10^2 10^5 0 1])
legend('MIT69','MIT69 + SF6','MIT69 + Kt','MIT69 + SF6 + Kt')

%Weibull Distribution: Configurations A & B orig + KS
figure
semilogx(stress5,pfail5,'rs',stress6,pfail6,'bo',s,ks1,'g-',s,ks2,'y-
',s,fit5,'r-',s,fit6,'b-')
title('')
xlabel('Stress (MPa)')
ylabel('Probability of Failure')
axis([10^2 10^4 0 1])
legend('CONFIGURATION A','CONFIGURATION B','MIT59 (Chen 1998)','MIT59 +
SF6 (Chen 1998)')

%Weibull Distribution: Configurations A & B orig + Kt & KS
figure
semilogx(stress5k,pfail5,'r+',stress6k,pfail6,'b*',s,ks1,'g-',s,ks2,'y-
',s,fit5k,'r-',s,fit6k,'b-')
title('')
xlabel('Stress (MPa)')
ylabel('Probability of Failure')
axis([10^2 10^4 0 1])
```

```
legend('CONFIGURATION A + Kt','CONFIGURATION B + Kt','MIT59 (Chen
1998)','MIT59 + SF6 (Chen 1998)')

%Weibull Distribution: Configurations A & B both
figure
semilogx(stress5,pfail5,'rs',stress7,pfail7,'mv',stress6,pfail6,'bo',
stress8,pfail8,'cd',s,fit3,'g-',s,fit4,'y-',s,fit5,'r-',s,fit7,'m-
',s,fit6,'b-',s,fit8,'c-')
title('')
xlabel('Stress (MPa)')
ylabel('Probability of Failure')
axis([10^2 10^4 0 1])
legend('CONFIGURATION A','CONFIGURATION A + SF6','CONFIGURATION
B','CONFIGURATION B + SF6','ADAM06 RHFS','ADAM06+ SF6 RHFS')

%Weibull Distribution: Configuration A
figure
semilogx(stress5,pfail5,'rs',stress7,pfail7,'mv',stress5k,pfail5,'r+',
stress7k,pfail7,'mx',s,fit5,'r-',s,fit7,'m-',s,fit5k,'r-',s,fit7k,'m-')
title('')
xlabel('Stress (MPa)')
ylabel('Probability of Failure')
axis([10^2 10^4 0 1])
legend('CONFIGURATION A','CONFIGURATION A + SF6','CONFIGURATION A +
Kt','CONFIGURATION A + SF6 + Kt')

%Weibull Distribution: Configuration B
figure
semilogx(stress6,pfail6,'bo',stress8,pfail8,'cd',stress6k,pfail6,'b*',
stress8k,pfail8,'c^',s,fit6,'b-',s,fit8,'c-',s,fit6k,'b-',s,fit8k,'c-')
title('')
xlabel('Stress (MPa)')
ylabel('Probability of Failure')
axis([10^2 10^4 0 1])
legend('CONFIGURATION B','CONFIGURATION B + SF6','CONFIGURATION B +
Kt','CONFIGURATION B + SF6 + Kt')

%Weibull Distribution: Configuration A & B Kt
figure
semilogx(stress5,pfail5,'bs',stress6,pfail6,'co',stress5k,pfail5,'b+',
stress6k,pfail6,'c*',s,fit5,'b-',s,fit6,'c-',s,fit5k,'b-',s,fit6k,'c-')
title('')
xlabel('Stress (MPa)')
ylabel('Probability of Failure')
axis([10^2 10^4 0 1])
legend('CONFIGURATION A','CONFIGURATION B','CONFIGURATION A +
Kt','CONFIGURATION B + Kt')
```

Plot Generation for Predictive Scaling (shift.m)

```
%shift.m
```

```
%Plot generation for predicted surface/volumetric scaling of chamber
values based on RHFS Weibull results
clear all;
close all;

%ADAM06
stress3=[1964.10  1875.30  1873.60  1805.40  1750.80  1748.90  1674.10
   1575.50  1558.00  1538.10  1515.90  1506.10  1431.30  1363.40  1322.10
1284.40  1267.70  1266.80  1266.10  1183.80  1166.80  1153.90  1132.30
   1112.40  1106.10  1082.60  983.20   959.70   908.90   608.30];
stress3k=[4587.5096  4134.18995  4081.1067   4012.15149  3865.9619
   3836.8638   3793.46274  3728.1382   3567.255 3494.152 3433.96206
   3351.80649  3254.91933  3145.63648  3132.58374  3080.89028  3062.38289
3038.67316  2929.43148  2879.23801  2791.5678   2659.50684  2543.08021
   2518.56064  2417.6888   2367.32052  2276.52183  2237.99095  2207.98179
1284.66877];
pfail3=[0.967741935  0.935483871 0.903225806 0.870967742 0.838709677
   0.806451613 0.774193548 0.741935484 0.709677419 0.677419355 0.64516129
0.612903226 0.580645161 0.548387097 0.516129032 0.483870968 0.451612903
   0.419354839 0.387096774 0.35483871  0.322580645 0.290322581
   0.258064516 0.225806452 0.193548387 0.161290323 0.129032258
   0.096774194 0.064516129 0.032258065];

%ADAM06 + SF6
stress4=[6698.80  6316.70  5980.00  5686.30  5008.60  4827.30  4628.50
   4608.10  4268.30  3897.80  3769.30  3724.80  3568.00  3473.50  3435.20
3391.20  3340.90  2952.70  2833.30  2745.50  2696.60  2629.70  2620.10
   2509.10  2481.40  2477.50  2104.80  1282.80  1205.90  985.70];
stress4k=[13733.76914   13679.25 13417.02652 12447.87933 12263.5571
   11408.84082 10972.80772 10825.59865 10062.09042 9459.18104  9347.3856
9088.4096   8816.01577  8355.43696  7991.48145  7889.28768  7552.10445
   7149.07724  6929.18336  6534.27856  6274.71618  6241.318 5884.97925
   5788.99552  5735.66091  5699.74961  5435.85648  3243.81636  3066.12134
2392.09676];
pfail4=[0.967741935  0.935483871 0.903225806 0.870967742 0.838709677
   0.806451613 0.774193548 0.741935484 0.709677419 0.677419355 0.64516129
0.612903226 0.580645161 0.548387097 0.516129032 0.483870968 0.451612903
   0.419354839 0.387096774 0.35483871  0.322580645 0.290322581
   0.258064516 0.225806452 0.193548387 0.161290323 0.129032258
   0.096774194 0.064516129 0.032258065];

%CONFIG A

stress5=[1165.9   886.76   776.13   690.84   610.24   585.83   566.03
   415.06   321.07];
stress5k=[1620.519923   1233.94786  1083.992817 962.2828329 848.5456251
   825.6269034 801.68249   612.5973078 449.9593987];
pfail5=[0.9 0.8   0.7   0.6   0.5   0.4   0.3   0.2   0.1];

%CONFIG B

stress6=[432.91   368.66   355.23];
stress6k=[616.0357951   553.9862697 529.1263683];
pfail6=[0.75   0.5   0.25];

%CONFIG A + SF6
```

```
stress7=[8552.145864 8080.307404 4546.641618 3992.142046 3652.35388
   3511.232158 3486.44755  3418.802497 2395.996914 2238.677905
   1068.870568 1032.779978 862.3530125];
stress7k=[12562.85914   11812.87928 7154.545243 6281.990815 5845.166625
   5588.822758 5572.715236 5379.790007 3468.662193 3201.147957 1613.76341
1547.393866 1245.337715];
pfail7=[0.928571429  0.857142857 0.785714286 0.714285714 0.642857143
   0.571428571 0.5   0.428571429 0.357142857 0.285714286 0.214285714
   0.142857143 0.071428571];

%CONFIG B + SF6

stress8=[1611.081831 1257.046841 1184.014039 1164.994043 1155.800476
   1000.151845 984.8240745 898.7964174 775.3180574 704.3317639
   695.5276168];
stress8k=[2552.644368   1793.110476 1714.085987 1690.714141 1660.869031
   1469.194627 1450.113637 1381.194835 1129.05338  1107.590334
   1103.286309];
pfail8=[0.916666667  0.833333333 0.75  0.666666667 0.583333333 0.5
   0.416666667 0.333333333 0.25  0.166666667 0.083333333];

%Calculate values for curves representing the Weibull paramters
%Equations based on log curve fits to plot of stress (MPa) versus Pfail

c=0;

for x=1:50:2*10^4
   c=c+1;

   fit3(c)=1.0463*log(x)-7.0218;
   fit4(c)=0.5775*log(x)-4.1649;

   fit3k(c)=1.0222*log(x)-7.6952;
   fit4k(c)=0.6147*log(x)-4.9936;

   ks1(c)=1.5295*log(x)-10.569;
   ks2(c)=0.5758*log(x)-4.1602;

   fit5(c)=0.8802*log(x)-5.2319;
   fit6(c)=2.2372*log(x)-12.814;
   fit7(c)=0.3672*log(x)-2.4265;
   fit8(c)=1.0429*log(x)-6.7861;

   fit5k(c)=0.7041*log(x)-4.2755;
   fit6k(c)=3.1243*log(x)-19.299;
   fit7k(c)=0.3624*log(x)-2.5396;
   fit8k(c)=1.0429*log(x)-7.1303;

   Aa06(c)=1.158*log(x)-7.5324;
   Aa066(c)=0.6601*log(x)-4.6968;
   Aa06k(c)=.9367*log(x)-6.7261;
   Aa066k(c)=0.5974*log(x)-4.7075;

   Av06(c)=1.5216*log(x)-6.8642;
   Av066(c)=0.8457*log(x)-2.9474;
   Av06k(c)=1.7666*log(x)-9.2398;
   Av066k(c)=1.0633*log(x)-4.4123;
```

```
   s(c)=x;
end

pick=input('1. Surface Area 2. Volume');

if pick ==1

figure
semilogx(stress5,pfail5,'rs',stress7,pfail7,'mv',stress3,pfail3,'bo',
stress4,pfail4,'cd',s, Aa06,'r--',s,Aa066,'m--',s,fit3,'b-',s,fit4,'c-
',s,fit5,'r-',s,fit7,'m-')
title('')
xlabel('Stress (MPa)')
ylabel('Probability of Failure')
axis([10^2 10^4 0 1])
legend('CONFIGURATION A','CONFIGURATION A + SF6','ADAM06','ADAM06 +
SF6','ADAM06 Predicted','ADAM06 + SF6 Predicted')

figure
semilogx(stress5k,pfail5,'rs',stress7k,pfail7,'mv',stress3k,pfail3,'bo',
stress4k,pfail4,'cd',s, Aa06k,'r--',s,Aa066k,'m--',s,fit3k,'b-
',s,fit4k,'c-',s,fit5k,'r-',s,fit7k,'m-')
title('')
xlabel('Stress (MPa)')
ylabel('Probability of Failure')
axis([10^2 10^5 0 1])
legend('CONFIGURATION A + Kt','CONFIGURATION A + SF6 + Kt','ADAM06 +
Kt','ADAM06 + SF6 + Kt','ADAM06 + Kt Predicted','ADAM06 + SF6 + Kt
Predicted')

figure
semilogx(stress6,pfail6,'bo',stress8,pfail8,'cd',stress3,pfail3,'bo',
stress4,pfail4,'cd',s, Aa06,'r--',s,Aa066,'m--',s,fit3,'b-',s,fit4,'c-
',s,fit6,'r-',s,fit8,'m-')
title('')
xlabel('Stress (MPa)')
ylabel('Probability of Failure')
axis([10^2 10^4 0 1])
legend('CONFIGURATION B','CONFIGURATION B + SF6','ADAM06','ADAM06 +
SF6','ADAM06 Predicted','ADAM06 + SF6 Predicted')

figure
semilogx(stress6k,pfail6,'bo',stress8k,pfail8,'cd',stress3k,pfail3,'bo',
stress4k,pfail4,'cd',s, Aa06k,'r--',s,Aa066k,'m--',s,fit3k,'b-
',s,fit4k,'c-',s,fit6k,'r-',s,fit8k,'m-')
title('')
xlabel('Stress (MPa)')
ylabel('Probability of Failure')
axis([10^2 10^5 0 1])
legend('CONFIGURATION B + Kt','CONFIGURATION B + SF6 + Kt','ADAM06 +
Kt','ADAM06 + SF6 + Kt','ADAM06 + Kt Predicted','ADAM06 + SF6 + Kt
Predicted')

elseif pick==2
```

```
figure
semilogx(stress5,pfail5,'rs',stress7,pfail7,'mv',stress3,pfail3,'bo',
stress4,pfail4,'cd',s, Av06,'r--',s,Av066,'m--',s,fit3,'b-',s,fit4,'c-
',s,fit5,'r-',s,fit7,'m-')
title('')
xlabel('Stress (MPa)')
ylabel('Probability of Failure')
axis([10^1 10^5 0 1])
legend('CONFIGURATION A','CONFIGURATION A + SF6','ADAM06','ADAM06 +
SF6','ADAM06 Predicted','ADAM06 + SF6 Predicted')

figure
semilogx(stress5k,pfail5,'rs',stress7k,pfail7,'mv',stress3k,pfail3,'bo',
stress4k,pfail4,'cd',s, Av06k,'r--',s,Av066k,'m--',s,fit3k,'b-
',s,fit4k,'c-',s,fit5k,'r-',s,fit7k,'m-')
title('')
xlabel('Stress (MPa)')
ylabel('Probability of Failure')
axis([10^1 10^5 0 1])
legend('CONFIGURATION A + Kt','CONFIGURATION A + SF6 + Kt','ADAM06 +
Kt','ADAM06 + SF6 + Kt','ADAM06 + Kt Predicted','ADAM06 + SF6 + Kt
Predicted')

figure
semilogx(stress6,pfail6,'bo',stress8,pfail8,'cd',stress3,pfail3,'bo',
stress4,pfail4,'cd',s, Av06,'r--',s,Av066,'m--',s,fit3,'b-',s,fit4,'c-
',s,fit6,'r-',s,fit8,'m-')
title('')
xlabel('Stress (MPa)')
ylabel('Probability of Failure')
axis([10^1 10^4 0 1])
legend('CONFIGURATION B','CONFIGURATION B + SF6','ADAM06','ADAM06 +
SF6','ADAM06 Predicted','ADAM06 + SF6 Predicted')

figure
semilogx(stress6k,pfail6,'bo',stress8k,pfail8,'cd',stress3k,pfail3,'bo',
stress4k,pfail4,'cd',s, Av06k,'r--',s,Av066k,'m--',s,fit3k,'b-
',s,fit4k,'c-',s,fit6k,'r-',s,fit8k,'m-')
title('')
xlabel('Stress (MPa)')
ylabel('Probability of Failure')
axis([10^1 10^5 0 1])
legend('CONFIGURATION B + Kt','CONFIGURATION B + SF6 + Kt','ADAM06 +
Kt','ADAM06 + SF6 + Kt','ADAM06 + Kt Predicted','ADAM06 + SF6 + Kt
Predicted')

else
end
```

D.4 RHFS Surface Roughness

MIT69

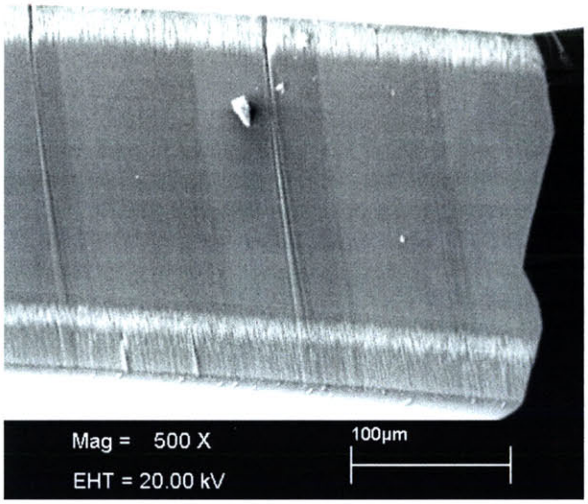

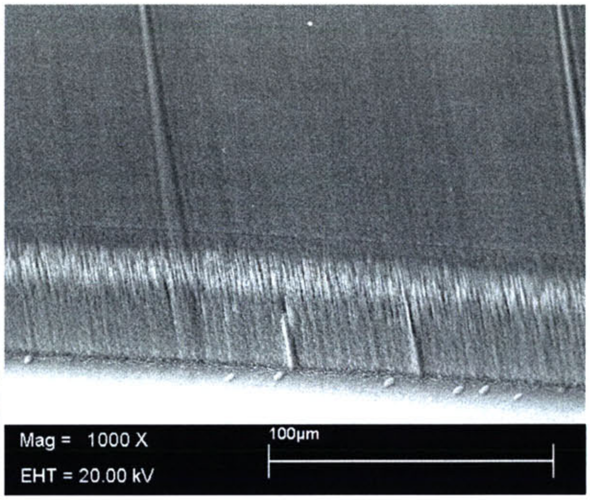

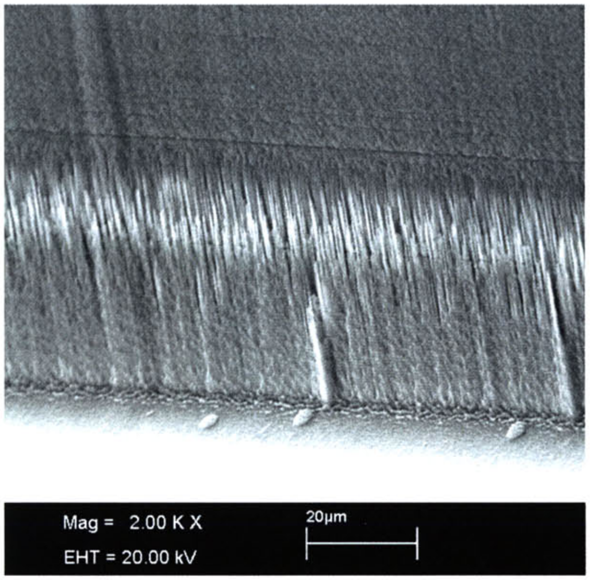

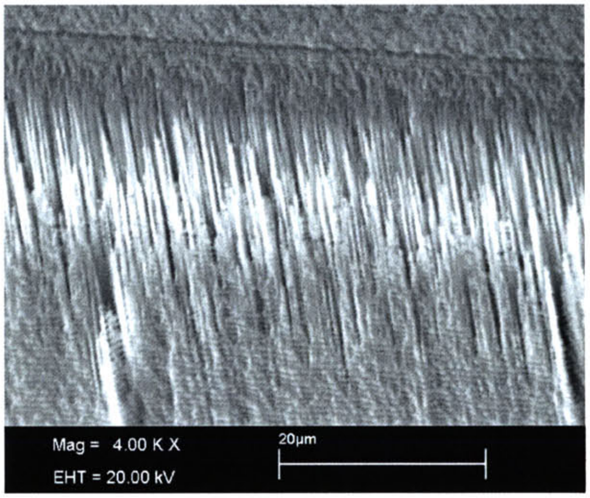

MIT69 + SF6

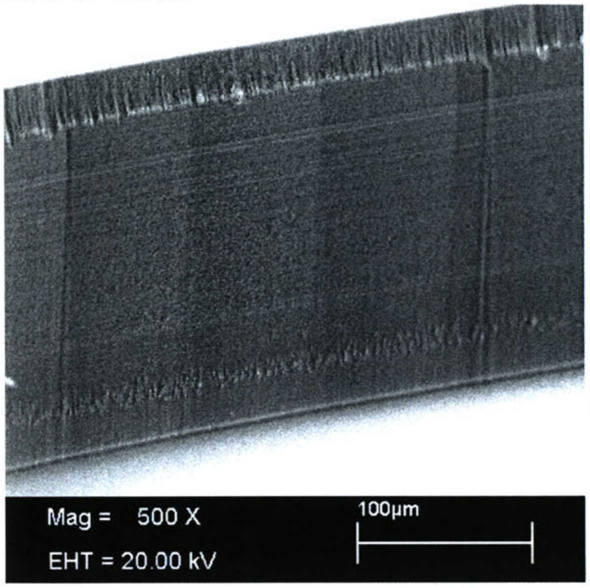
Mag = 500 X
EHT = 20.00 kV
100µm

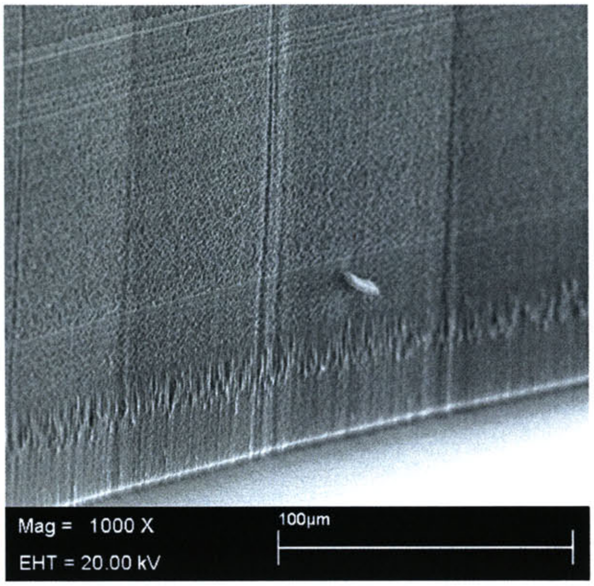
Mag = 1000 X
EHT = 20.00 kV
100µm

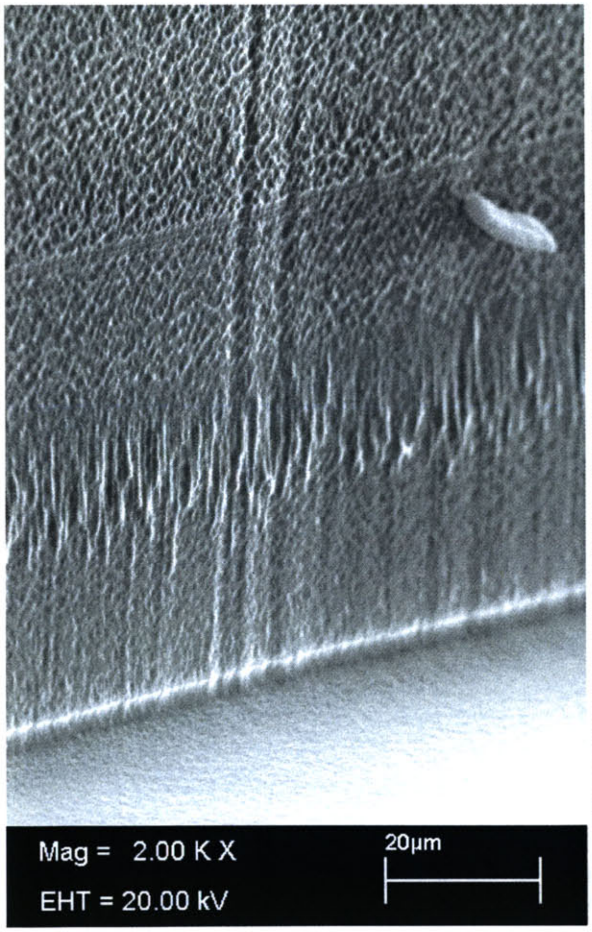
Mag = 2.00 K X
EHT = 20.00 kV
20µm


Mag = 2.00 K X
EHT = 20.00 kV
20µm

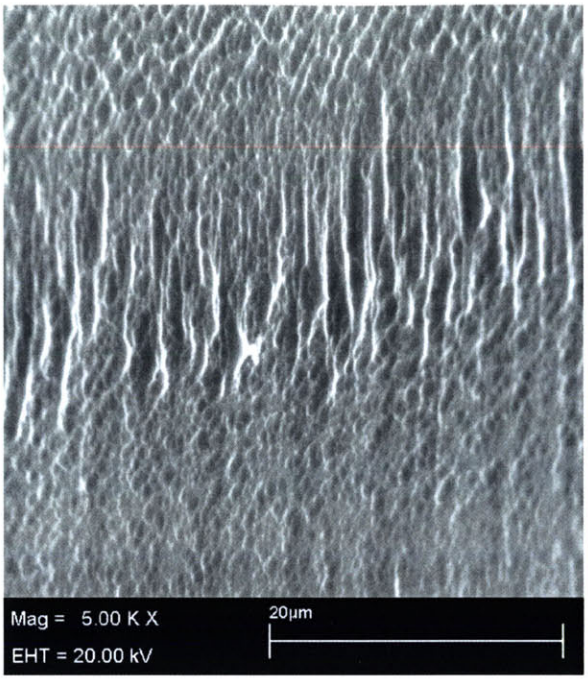
Mag = 5.00 K X
EHT = 20.00 kV
20µm

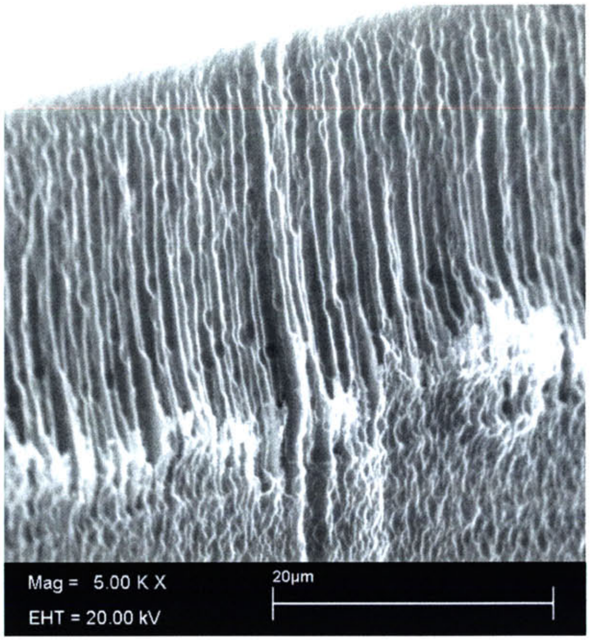
Mag = 5.00 K X
EHT = 20.00 kV
20µm

ADAM06

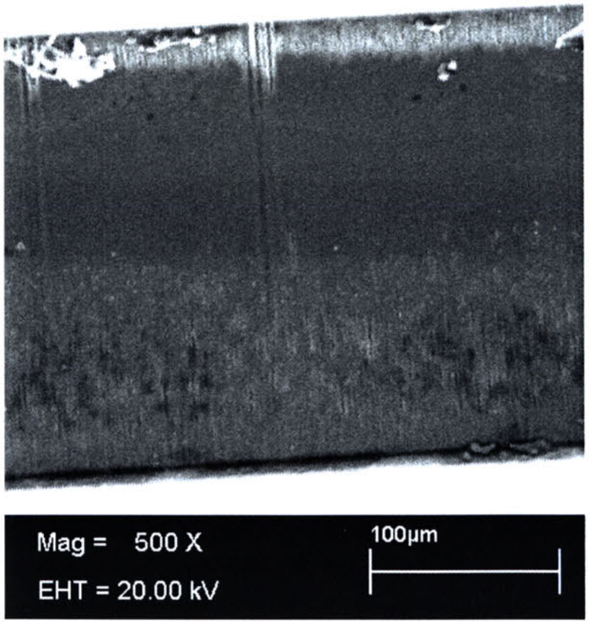
Mag = 500 X
EHT = 20.00 kV
100µm

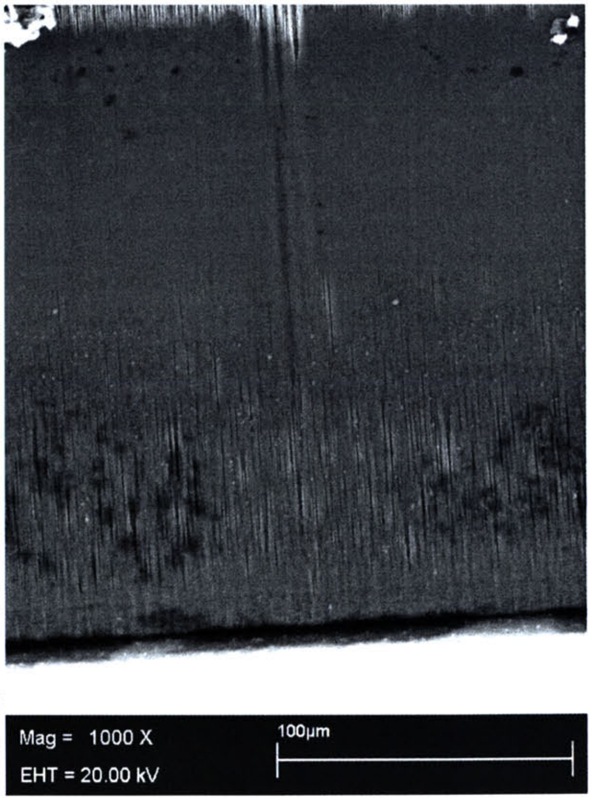
Mag = 1000 X
EHT = 20.00 kV
100µm

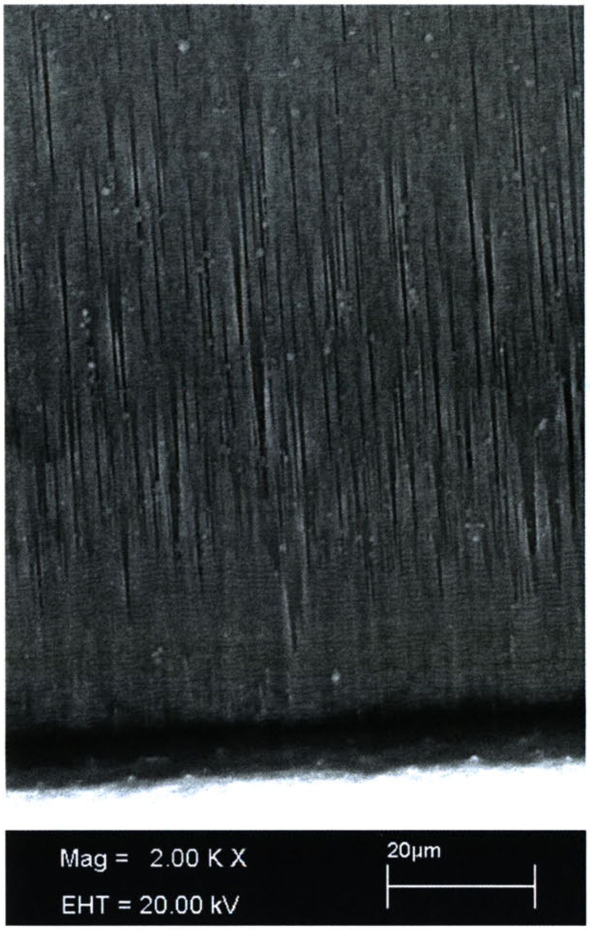
Mag = 2.00 K X
EHT = 20.00 kV
20µm

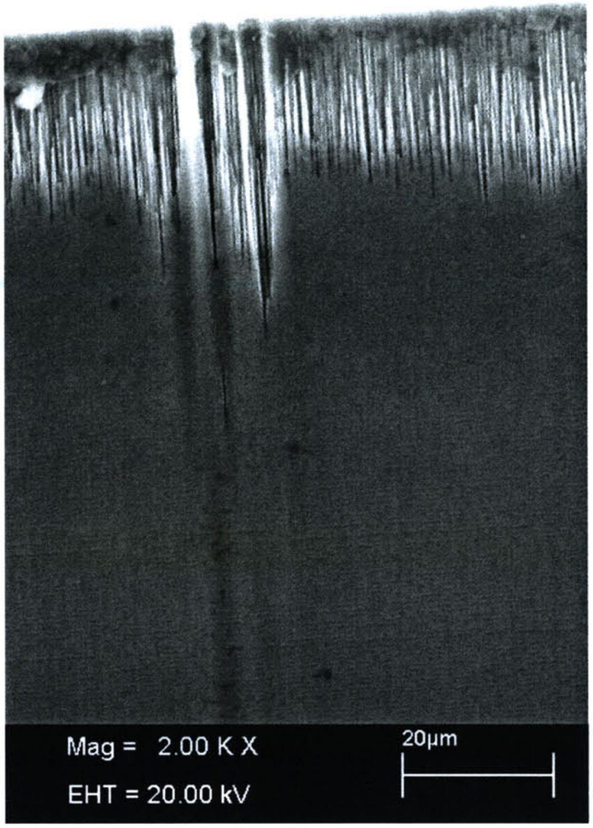
Mag = 2.00 K X
EHT = 20.00 kV
20µm

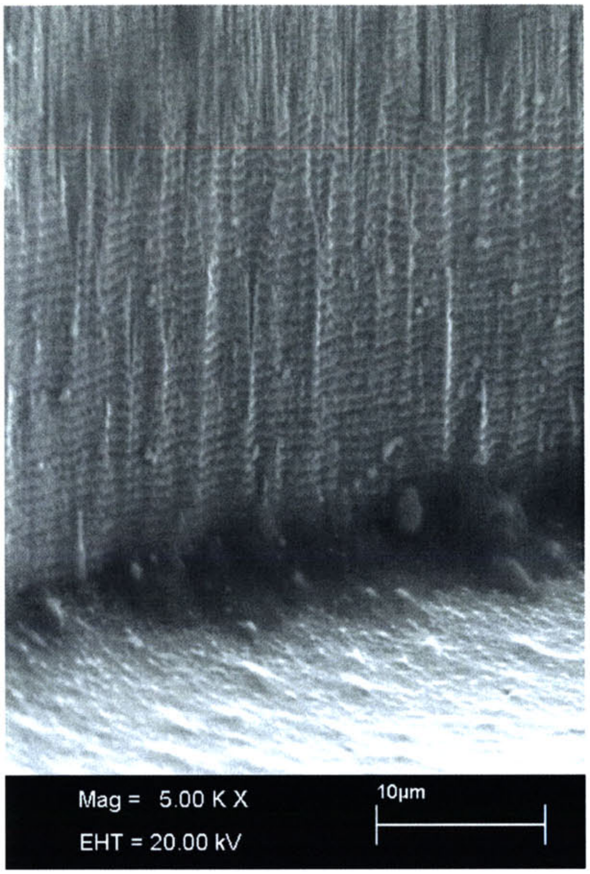
Mag = 5.00 K X
EHT = 20.00 kV
10μm

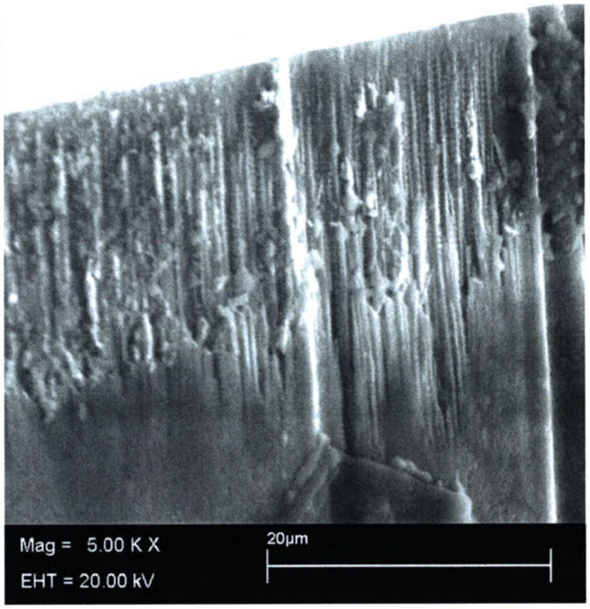
Mag = 5.00 K X
EHT = 20.00 kV
20μm

ADAM06 + SF6

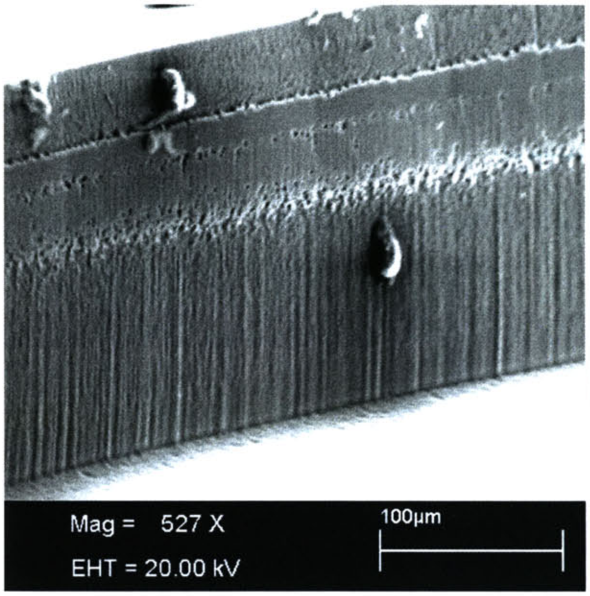
Mag = 527 X
EHT = 20.00 kV
100µm

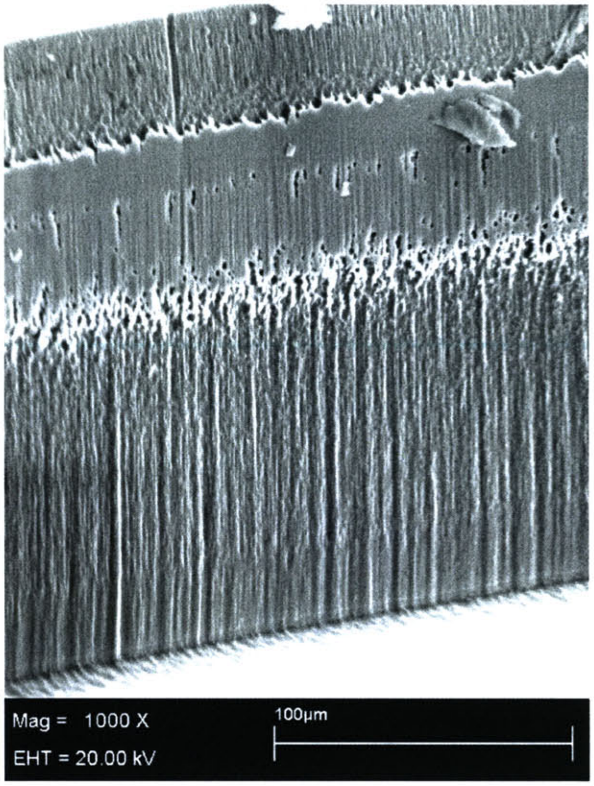
Mag = 1000 X
EHT = 20.00 kV
100µm

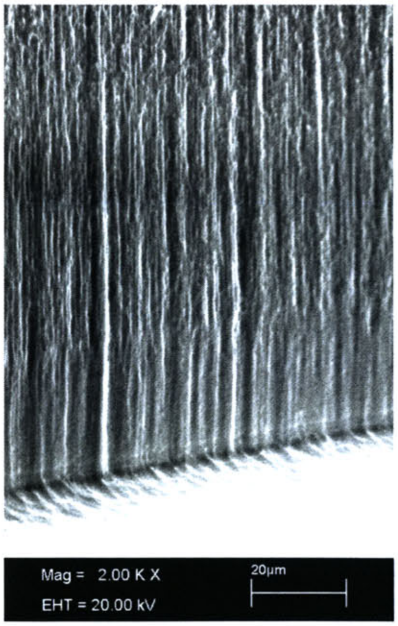
Mag = 2.00 K X
EHT = 20.00 kV
20µm

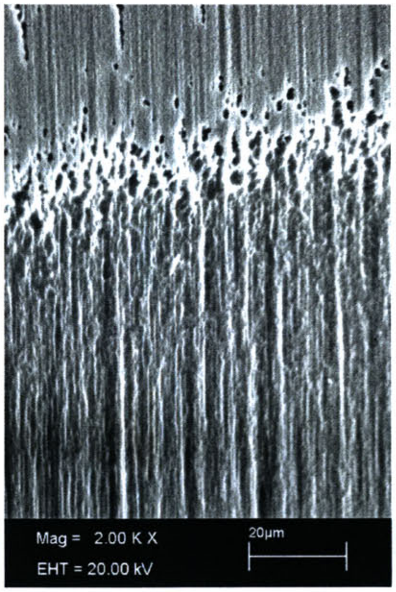
Mag = 2.00 K X
EHT = 20.00 kV
20µm

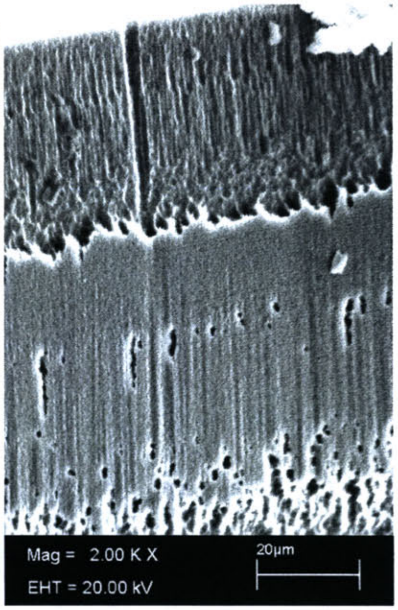
Mag = 2.00 K X
EHT = 20.00 kV
20µm

D.5 Pressure Chamber (Revisited) Failure Stress

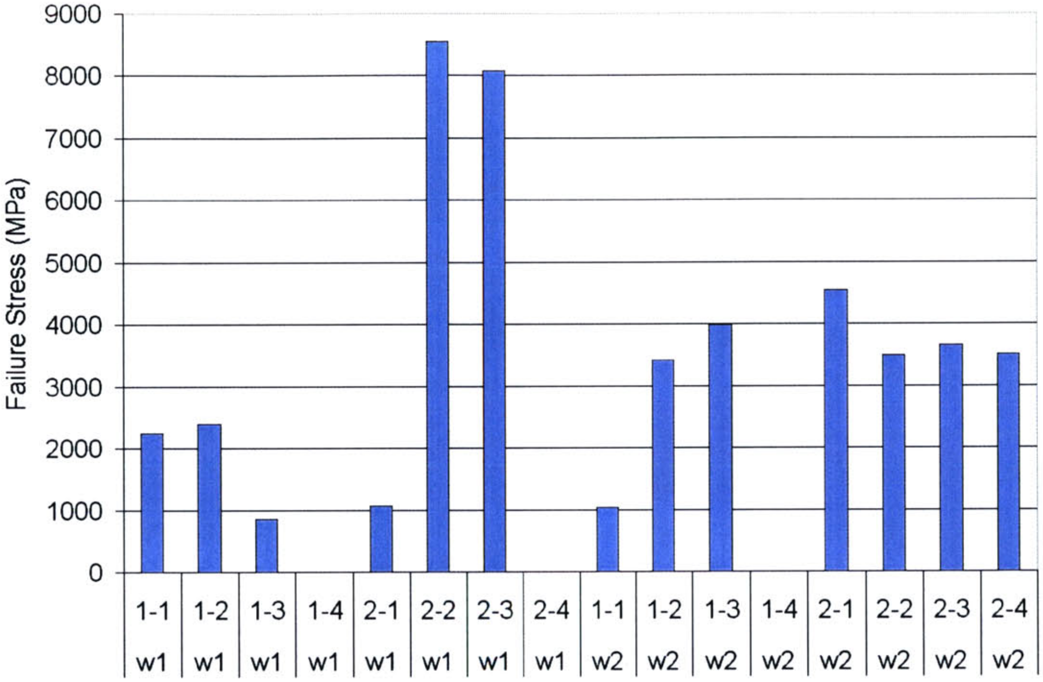

Configuration A: Pressure Test (Revisited) Failure Stress

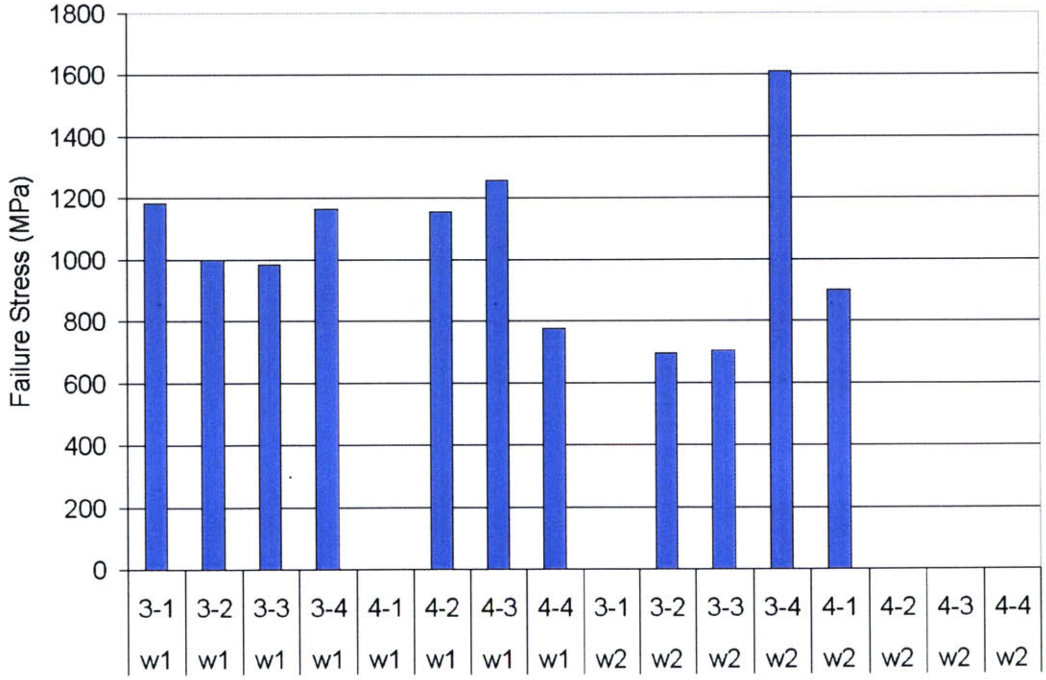

Configuration B: Pressure Test (Revisited) Failure Stress

Appendix E: CARES/LIFE

E.1 ANSCARES Surface Generation Macro

The surface generation macro is included with the ANSCARES software. The macro must be run in the ANSYS program, not in CARES. With a solid three dimensional model, the stresses on the element faces that mesh the selected component surfaces are used to calculate surface stresses and geometry for a surface flaw analysis.

1. Using 'Select Entities' command, select the areas that comprise the stressed surface where the flaw analysis should be conducted.
2. Create and name a component from the selected areas.
3. Run finite element analysis.
4. Load macro library anscares.lib with *ULIB command
5. Run macro SURF with *USE command

This function generates a file with the extension .sur. When the .sur file and the .rst file (the results file from the finite element model) are in the same directory and the Interface module of CARES is run, a neutral file is generated for a surface flaw analysis to be run through Pest.

E.2 Radiused Hub Flexure Specimens

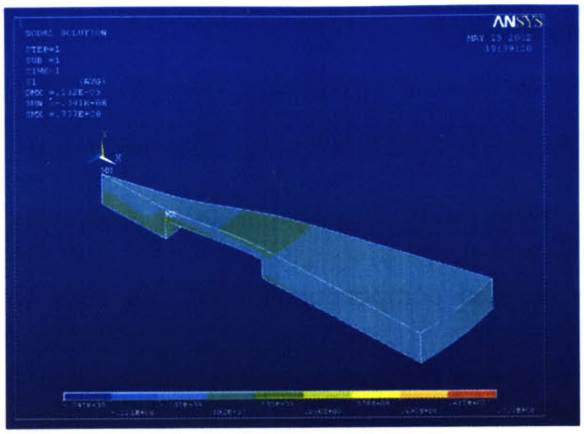

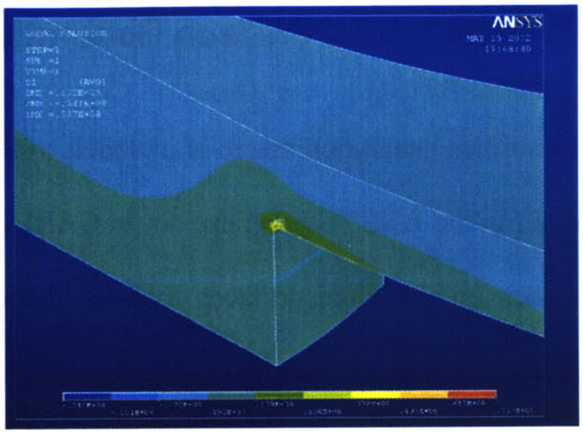

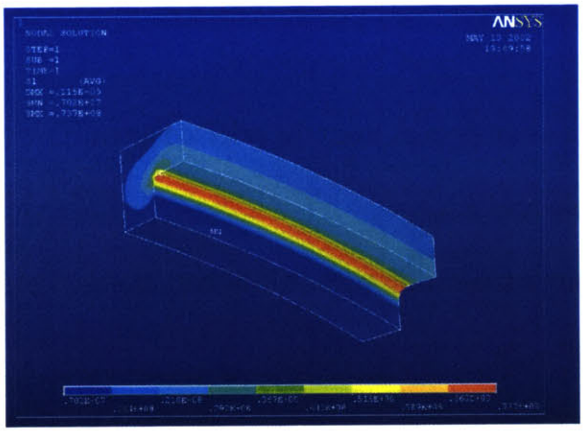

CARES Input File for RHFS (Surface Analysis)

```
------------------------------------------------------------------------------
FILTER
 1 1 0 2 0 0 1
------------------------------------------------------------------------------

*** WARNING ; DO NOT MAKE ANY CHANGES ABOVE THIS LINE **********************


 +-----------------------------------------------------------------+
 |                                                                 |
 |           --- INPUT TEMPLATE FOR CARES/LIFE ---                 |
 |                                                                 |
 |      CERAMICS ANALYSIS AND RELIABILITY EVALUATION               |
 |        OF STRUCTURES LIFE PREDICTION PROGRAM                    |
 |                                                                 |
 +-----------------------------------------------------------------+
```

```
            +----------------------+
            | MASTER CONTROL INPUT |
            +----------------------+

TITLE     rhfsgeo4
----------------------------------------------------------------------
Project Title: RHFS_1
----------------------------------------------------------------------

NE
 +-+      ---------------------------------------------
  3   =  CONTROL INDEX FOR FINITE ELEMENT POSTPROCESSING
 +-+      ---------------------------------------------

        0 : Experimental rupture data analysis only
        3 : Component reliability analysis with a NEUTRAL FILE
            DATA BASE


IPRINC
 +-+      ---------------------------------------
  1   =  CONTROL INDEX FOR ELEMENT STRESS OUTPUT
 +-+      ---------------------------------------

        0 : Use material coordinate system stresses
            (ANISOTROPIC MODEL)
        1 : Calculate and use principal stresses (ISOTROPIC MODEL)
        2 : Use element or material coordinate system stresses
            (ISOTROPIC MODEL). This option can be used with the
            Batdorf theory. It can not be used with the PIA theory.
            When two neutral files are read (proof testing option)
            then IPRINC should be set to this value.


NMATS
 +--+     -------------------------------------------
  1   =  NUMBER OF MATERIALS FOR SURFACE FLAW ANALYSIS
 +--+     -------------------------------------------
  |
  |
  |     +----------------------------------------------------------+
  |     | This keyword indicates how many different surface residing |
  |     | flaw types are required to predict a component's surface   |
  |     | reliability. Only one flaw population can be associated    |
  +------> | with a particular material identification (ID) number for |
        | the purpose of component reliability prediction. The ID    |
        | number is matched to the finite element ID number. If      |
        | specimen rupture data consists of multiple flaw            |
        | populations (competing failure modes), then only one of    |
        | the flaw populations can be associated with the particular |
        | material ID. This selection of the "active" flaw           |
        | population depends on the choice of the ID4 keyword.       |
        +----------------------------------------------------------+
```

```
NMATV
 +--+     ------------------------------------------
  0   = NUMBER OF MATERIALS FOR VOLUME FLAW ANALYSIS
 +--+     ------------------------------------------
  |
  |
  |     +--------------------------------------------------------+
  |     | This keyword indicates how many different volume residing |
  |     | flaw types are required to predict a component's volume   |
  |     | reliability.  Only one flaw population can be associated  |
  +------> | with a particular material identification (ID) number for |
        | the purpose of component reliability prediction.  The ID  |
        | number is matched to the finite element ID number. If     |
        | specimen rupture data consists of multiple flaw           |
        | populations (competing failure modes), then only one of   |
        | the flaw populations can be associated with the particular |
        | material ID.  This selection of the "active" flaw         |
        | population depends on the choice of the ID4 keyword.      |
        +--------------------------------------------------------+


NGP
 +--+     -------------------------------------------------
  15  = NUMBER OF GAUSSIAN QUADRATURE POINTS (15, 30, or 50)
 +--+     -------------------------------------------------
  |
  |
  |      +-------------------------------------------------------+
  |      | Number of Gaussian quadrature points for unit sphere    |
  +-------> | (volume flaw orientation space) and unit circle (surface |
         | flaw orientation space) integration (Batdorf and Weibull |
         | normal stress averaging methods only).                   |
         +-------------------------------------------------------+


NS
----------  ------------------------------------
   24   = NUMBER OF SEGMENTS IN SYMMETRY PROBLEM
----------  ------------------------------------
  |
  |     +---------------------------------------------------------+
  |     | Multiplication factor for finite element volumes and areas |
  |     | necessary to reproduce the whole component.  This option   |
  +------> | is useful for finite element models that take advantage of |
        | geometrical and loading symmetries (MODEL REDUCTION        |
        | VIA SYMMETRY).  The total volume and surface area of the   |
        | component under load effects reliability (the so-called    |
        | Weibull size effect).                                      |
        +---------------------------------------------------------+


FACTOR
----------  ------------------------------------------------
1.0000e-06 = LOAD FACTOR FOR WHICH TO MULTIPLY ELEMENT STRESSES
----------  ------------------------------------------------
```

```
*******************************************************************************
$ENDX     : END OF MASTER CONTROL INPUT
*******************************************************************************


          +------------------------+
          |                        |
          | MATERIAL CONTROL INPUT |
          |                        |
          +------------------------+

TITLE     : MATERIAL TITLE (ECHOED IN CARES OUTPUT)
----------------------------------------------------------------------
Material Title:  Silicon
----------------------------------------------------------------------


MATID
+-------+    ------------------------------
     1  =  MATERIAL IDENTIFICATION NUMBER
+-------+    ------------------------------
   |
   |
   |      +-----------------------------------------------------+
   |      | Material identification number from the finite element  |
   +------> | material property card (If finite element postprocessing |
          | is not being performed this entry should be some unique  |
          | number.  This input must be in the form of an integer.   |
          +-----------------------------------------------------+


ID1
  +-+       --------------------------------------------------
   7    =  CONTROL INDEX FOR EXPERIMENTAL (SPECIMEN RUPTURE) DATA
  +-+       --------------------------------------------------

          1 : TENSILE SPECIMEN (single failure mode - unimodal)
          2 : THREE-POINT or FOUR-POINT bend bar (unimodal)
          3 : Direct input of the required parameters
          4 : TENSILE SPECIMEN (multiple failure modes - multimodal)
          5 : THREE-POINT or FOUR-POINT bend bar (multimodal)
          6 : UNIAXIAL loaded FINITE ELEMENT MODEL of the specimen,
              such as bend bar,TENSILE SPECIMEN, C- or O-RING, etc...
          7 : MULTIAXIALLY loaded FINITE ELEMENT MODEL of the specimen,
              such as RING-ON-RING, BALL-ON-RING, PRESSURE-ON-DISK


ID2
  +-+       ---------------------------------------------
   4    =  CONTROL INDEX FOR MICROCRACK FRACTURE CRITERION
  +-+       ---------------------------------------------

          1 : Weibull Normal Stress Averaging
          2 : Maximum Tensile Stress criterion (for volume flaw only)
          3 : Coplanar Strain Energy Release Rate criterion (G sub T)
```

```
          4 : Weibull PIA model
          5 : Shetty's semi-empirical criterion (recommended option)
              (noncoplanar Strain Energy Release Rate (SERR) criterion)
              (KI/KIc) + (KII/(C*KIc))**2 = 1   (Note: KII or KIII)
          6 : Weibull compression criterion (function of shear only)
              (KII/KIIc) = 1

               ***(IF ID2 > 5, IPRINC = 0 IS REQUIRED)***


ID3
 +-+     -------------------------------
  1   =  CONTROL INDEX FOR CRACK GEOMETRY
 +-+     -------------------------------

          1 : Griffith crack (volume flaw or surface flaw)
          2 : Penny-Shaped crack (volume flaw only)
          3 : Griffith Notch (surface flaw only)
              (ID2 = 3 or 5 is required)
          4 : Semicircular crack (surface flaw only)
              (ID2 = 5 is required)


ID4
 +-+     ----------------------------------------------------------
  2   =  CONTROL INDEX FOR VOLUME OR SURFACE FLAW RELIABILITY ANALYSIS
 +-+     ----------------------------------------------------------
  |
  |       1 : VOLUME (flaws reside throughout the material volume)
  |       2 : SURFACE (flaws reside exclusively on the material surface)
  |
  |    +--------------------------------------------------------------+
  |    | If specimen rupture data contains multiple flaw populations,  |
  +---->| this keyword designates the one flaw population to be made    |
       | "active" for subsequent component reliability analysis.       |
       | If only one flaw population is present, the choice must match |
       | with the failure mode of the specimen data.  The selected flaw |
       | category will have a complete set of parameters calculated and |
       | written to the output template file by the CARES/Life program. |
       | The parameters are associated with the material ID keyword.   |
       +--------------------------------------------------------------+


C
----------   --------------------------------------------------------
  1.0000 =  CONSTANT FOR SEMI-EMPIRICAL MIXED-MODE FRACTURE CRITERIA
----------   --------------------------------------------------------
  |
  |
  |       +--------------------------------------------------------+
  |       | Constant for semi-empirical mixed-mode fracture criteria |
  +---------> | (KI/KIc)+(KII/(C*KIc))**2 = 1      ref. D.K.Shetty      |
          | Observed values range from 0.8 to 2. (ref. D.K. Shetty)  |
          | NOTE: As C approaches infinity, predicted failure        |
          | probabilityes approach normal stress criterion values    |
          +--------------------------------------------------------+
```

```
PR
----------   ---------------------------------------------------------
   0.2177 =  Poisson's ratio (used only in failure criterion calculations)
----------   ---------------------------------------------------------


MLORLE
  +-+        ---------------------------------------------
   0     =  CONTROL INDEX FOR METHOD OF CALCULATING WEIBULL
  +-+        PARAMETERS FROM THE EXPERIMENTAL FRACTURE DATA
           ---------------------------------------------

           0 : Maximum likelihood
           1 : Least-Squares linear regression with
              rank increment adjustment
           2 : Least-Squares linear regression for the
              truncated Weibull distribution.  This option
              uses the ZSTRES keyword (you must activate
              the three-parameter analysis option)
           3 : Maximum likelihood (Pool temperature data)
           4 : Least-Squares (Pool temperature data)


OUTLIE
----------   ------------------------------------
   2.0000 =  SIGNIFICANCE LEVEL TO DETECT OUTLIERS
----------   ------------------------------------
  |
  |
  |        +----------------------------------------------------+
  |        | Significance level for which OUTLIERS are to       |
  +--------->| be detected. Input is in percent and must be between |
           | the range of 0.1 percent to 10.0 percent           |
           | (OUTLIE = 2.0 percent is recommended)              |
           +----------------------------------------------------+


***********************************************************************
$ENDM     : END OF TEMPERATURE-INDEPENDENT MATERIAL CONTROL INPUT
***********************************************************************

MIT69

DTABLE    : DATA TABLE (FAST-FRACTURE, STATIC OR DYNAMIC FATIGUE)
-TEST-I-FLAW-I-----FIELD1------I-----FIELD2------I-----FIELD3------I
TEMP       0.2200000000E+02
RSTRES      0.0000000000E+00  0.0000000000E+00  0.0000000000E+00
+STRES      0.0000000000E+00  0.0000000000E+00  0.0000000000E+00
FAST    S   0.1639000000E+04
FAST    S   0.3931000000E+04
FAST    S   0.2430000000E+04
FAST    S   0.2750000000E+04
FAST    S   0.2631000000E+04
FAST    S   0.1763000000E+04
```

```
FAST     S   0.1720000000E+04
FAST     S   0.0929000000E+04
FAST     S   0.2090000000E+04
FAST     S   0.0880000000E+04
FAST     S   0.1642000000E+04
FAST     S   0.1474000000E+04
FAST     S   0.1553000000E+04
FAST     S   0.1872000000E+04
FAST     S   0.1372000000E+04
FAST     S   0.1392000000E+04
FAST     S   0.1421000000E+04
FAST     S   0.0867000000E+04
FAST     S   0.1293000000E+04
FAST     S   0.1381000000E+04
FAST     S   0.1664000000E+04
FAST     S   0.2136000000E+04
FAST     S   0.1321000000E+04
FAST     S   0.2267000000E+04
FAST     S   0.1772000000E+04
FAST     S   0.1274000000E+04
FAST     S   0.1753000000E+04
FAST     S   0.2246000000E+04
FAST     S   0.0989000000E+04
FAST     S   0.2112000000E+04
ZSTRES       0.0000000000E+00  0.0000000000E+00
$ENDD
-TEST-I-FLAW-I-----FIELD1------I-----FIELD2------I-----FIELD3------I
         END OF DATA FOR THE ABOVE TEMPERATURE
```

MIT69 + SF6

```
DTABLE     : DATA TABLE (FAST-FRACTURE, STATIC OR DYNAMIC FATIGUE)
-TEST-I-FLAW-I-----FIELD1------I-----FIELD2------I-----FIELD3------I
TEMP         0.2300000000E+02
RSTRES       0.0000000000E+00  0.0000000000E+00  0.0000000000E+00
+STRES       0.0000000000E+00  0.0000000000E+00  0.0000000000E+00
FAST     S   0.2922000000E+04
FAST     S   0.2996000000E+04
FAST     S   0.4259000000E+04
FAST     S   0.3485000000E+04
FAST     S   0.3641000000E+04
FAST     S   0.3167000000E+04
FAST     S   0.3040000000E+04
FAST     S   0.2240000000E+04
FAST     S   0.3398000000E+04
FAST     S   0.4177000000E+04
FAST     S   0.1449000000E+04
FAST     S   0.2471000000E+04
FAST     S   0.2344000000E+04
FAST     S   0.1880000000E+04
FAST     S   0.1136000000E+04
FAST     S   0.0929000000E+04
FAST     S   0.4148000000E+04
```

```
FAST     S   0.2050000000E+04
FAST     S   0.34910000000E+04
FAST     S   0.3207000000E+04
FAST     S   0.2209000000E+04
FAST     S   0.2222000000E+04
FAST     S   0.1645000000E+04
FAST     S   0.2229000000E+04
FAST     S   0.4785000000E+04
FAST     S   0.3968000000E+04
FAST     S   0.2080000000E+04
FAST     S   0.3453000000E+04
FAST     S   0.5574000000E+04
FAST     S   0.7107000000E+04
ZSTRES        0.0000000000E+00  0.0000000000E+00
$ENDD
-TEST-I-FLAW-I-----FIELD1------I-----FIELD2------I-----FIELD3------I
         END OF DATA FOR THE ABOVE TEMPERATURE
```

```
ADAM06

DTABLE      : DATA TABLE (FAST-FRACTURE, STATIC OR DYNAMIC FATIGUE)
-TEST-I-FLAW-I-----FIELD1------I-----FIELD2------I-----FIELD3------I
TEMP          0.2400000000E+02
RSTRES         0.0000000000E+00  0.0000000000E+00  0.0000000000E+00
+STRES        0.0000000000E+00  0.0000000000E+00  0.0000000000E+00
FAST     S   0.11320000000E+04
FAST     S   0.1964000000E+04
FAST     S   0.1154000000E+04
FAST     S   0.1363000000E+04
FAST     S   0.1875000000E+04
FAST     S   0.1431000000E+04
FAST     S   0.1268000000E+04
FAST     S   0.1538000000E+04
FAST     S   0.1106000000E+04
FAST     S   0.1184000000E+04
FAST     S   0.1558000000E+04
FAST     S   0.1167000000E+04
FAST     S   0.1267000000E+04
FAST     S   0.1112000000E+04
FAST     S   0.1874000000E+04
FAST     S   0.1805000000E+04
FAST     S   0.1751000000E+04
FAST     S   0.0983000000E+04
FAST     S   0.1674000000E+04
FAST     S   0.1284000000E+04
FAST     S   0.0608000000E+04
FAST     S   0.15061000000E+04
FAST     S   0.0909000000E+04
FAST     S   0.1576000000E+04
FAST     S   0.0960000000E+04
FAST     S   0.1083000000E+04
FAST     S   0.1322000000E+04
```

```
FAST     S   0.1749000000E+04
FAST     S   0.1516000000E+04
FAST     S   0.1266000000E+04
ZSTRES        0.0000000000E+00  0.0000000000E+00
$ENDD
-TEST-I-FLAW-I-----FIELD1------I-----FIELD2------I-----FIELD3------I
          END OF DATA FOR THE ABOVE TEMPERATURE
```

```
ADAM06 + SF6

DTABLE      : DATA TABLE (FAST-FRACTURE, STATIC OR DYNAMIC FATIGUE)
-TEST-I-FLAW-I-----FIELD1------I-----FIELD2------I-----FIELD3------I
TEMP         0.2500000000E+02
RSTRES        0.0000000000E+00  0.0000000000E+00  0.0000000000E+00
+STRES        0.0000000000E+00  0.0000000000E+00  0.0000000000E+00
FAST     S   0.6699000000E+04
FAST     S   0.2833000000E+04
FAST     S   0.3341000000E+04
FAST     S   0.5980000000E+04
FAST     S   0.5686000000E+04
FAST     S   0.4268000000E+04
FAST     S   0.5009000000E+04
FAST     S   0.3435000000E+04
FAST     S   0.3474000000E+04
FAST     S   0.2509000000E+04
FAST     S   0.2481000000E+04
FAST     S   0.2105000000E+04
FAST     S   0.2630000000E+04
FAST     S   0.2620000000E+04
FAST     S   0.3898000000E+04
FAST     S   0.3568000000E+04
FAST     S   0.4827000000E+04
FAST     S   0.3391000000E+04
FAST     S   0.1206000000E+04
FAST     S   0.2697000000E+04
FAST     S   0.3725000000E+04
FAST     S   0.2746000000E+04
FAST     S   0.2953000000E+04
FAST     S   0.1283000000E+04
FAST     S   0.2478000000E+04
FAST     S   0.3769000000E+04
FAST     S   0.4608000000E+04
FAST     S   0.0986000000E+04
FAST     S   0.4629000000E+04
FAST     S   0.6317000000E+04
ZSTRES        0.0000000000E+00  0.0000000000E+00
$ENDD
-TEST-I-FLAW-I-----FIELD1------I-----FIELD2------I-----FIELD3------I
          END OF DATA FOR THE ABOVE TEMPERATURE
```

MIT69 KT

```
DTABLE     : DATA TABLE (FAST-FRACTURE, STATIC OR DYNAMIC FATIGUE)
-TEST-I-FLAW-I-----FIELD1------I-----FIELD2------I-----FIELD3------I
TEMP        0.2700000000E+02
RSTRES       0.0000000000E+00  0.0000000000E+00  0.0000000000E+00
+STRES       0.0000000000E+00  0.0000000000E+00  0.0000000000E+00
FAST     S   0.3647000000E+04
FAST     S   0.8663000000E+04
FAST     S   0.5591000000E+04
FAST     S   0.6533000000E+04
FAST     S   0.6281000000E+04
FAST     S   0.4199000000E+04
FAST     S   0.4299000000E+04
FAST     S   0.2379000000E+04
FAST     S   0.5038000000E+04
FAST     S   0.2041000000E+04
FAST     S   0.4087000000E+04
FAST     S   0.3806000000E+04
FAST     S   0.3978000000E+04
FAST     S   0.4401000000E+04
FAST     S   0.3306000000E+04
FAST     S   0.3618000000E+04
FAST     S   0.3494000000E+04
FAST     S   0.1983000000E+04
FAST     S   0.3219000000E+04
FAST     S   0.3548000000E+04
FAST     S   0.4276000000E+04
FAST     S   0.5137000000E+04
FAST     S   0.3072000000E+04
FAST     S   0.5488000000E+04
FAST     S   0.4482000000E+04
FAST     S   0.3069000000E+04
FAST     S   0.4089000000E+04
FAST     S   0.5252000000E+04
FAST     S   0.2400000000E+04
FAST     S   0.4773000000E+04
ZSTRES       0.0000000000E+00  0.0000000000E+00
$ENDD
-TEST-I-FLAW-I-----FIELD1------I-----FIELD2------I-----FIELD3------I
          END OF DATA FOR THE ABOVE TEMPERATURE
```

MIT69 + SF6 KT

```
DTABLE     : DATA TABLE (FAST-FRACTURE, STATIC OR DYNAMIC FATIGUE)
-TEST-I-FLAW-I-----FIELD1------I-----FIELD2------I-----FIELD3------I
TEMP        0.2800000000E+02
RSTRES       0.0000000000E+00  0.0000000000E+00  0.0000000000E+00
+STRES       0.0000000000E+00  0.0000000000E+00  0.0000000000E+00
FAST     S   0.6958000000E+04
FAST     S   0.6892000000E+04
FAST     S   1.0400000000E+04
FAST     S   0.8659000000E+04
```

```
FAST    S  0.9102000000E+04
FAST    S  0.8024000000E+04
FAST    S  0.7977000000E+04
FAST    S  0.5868000000E+04
FAST    S  0.8477000000E+04
FAST    S  1.0270000000E+04
FAST    S  0.3801000000E+04
FAST    S  0.6484000000E+04
FAST    S  0.5674000000E+04
FAST    S  0.4822000000E+04
FAST    S  0.2989000000E+04
FAST    S  0.2452000000E+04
FAST    S  1.0550000000E+04
FAST    S  0.5093000000E+04
FAST    S  0.9118000000E+04
FAST    S  0.8364000000E+04
FAST    S  0.5840000000E+04
FAST    S  0.5607000000E+04
FAST    S  0.4136000000E+04
FAST    S  0.5687000000E+04
FAST    S  1.2100000000E+04
FAST    S  0.9939000000E+04
FAST    S  0.5013000000E+04
FAST    S  0.8699000000E+04
FAST    S  1.3140000000E+04
FAST    S  1.6490000000E+04
ZSTRES      0.0000000000E+00  0.0000000000E+00
$ENDD
-TEST-I-FLAW-I-----FIELD1------I-----FIELD2------I-----FIELD3------I
         END OF DATA FOR THE ABOVE TEMPERATURE
```

ADAM06 + KT

```
DTABLE     : DATA TABLE (FAST-FRACTURE, STATIC OR DYNAMIC FATIGUE)
-TEST-I-FLAW-I-----FIELD1------I-----FIELD2------I-----FIELD3------I
TEMP       0.2900000000E+02
RSTRES      0.0000000000E+00  0.0000000000E+00  0.0000000000E+00
+STRES      0.0000000000E+00  0.0000000000E+00  0.0000000000E+00
FAST    S  0.2238000000E+04
FAST    S  0.3793000000E+04
FAST    S  0.2543000000E+04
FAST    S  0.3146000000E+04
FAST    S  0.3837000000E+04
FAST    S  0.3255000000E+04
FAST    S  0.3062000000E+04
FAST    S  0.3434000000E+04
FAST    S  0.2660000000E+04
FAST    S  0.2929000000E+04
FAST    S  0.3728000000E+04
FAST    S  0.2367000000E+04
FAST    S  0.3039000000E+04
FAST    S  0.2792000000E+04
FAST    S  0.4588000000E+04
```

```
FAST     S   0.4081000000E+04
FAST     S   0.3567000000E+04
FAST     S   0.2418000000E+04
FAST     S   0.4134000000E+04
FAST     S   0.3081000000E+04
FAST     S   0.1285000000E+04
FAST     S   0.3494000000E+04
FAST     S   0.2277000000E+04
FAST     S   0.3866000000E+04
FAST     S   0.2208000000E+04
FAST     S   0.2519000000E+04
FAST     S   0.3133000000E+04
FAST     S   0.4012000000E+04
FAST     S   0.3352000000E+04
FAST     S   0.2879000000E+04
ZSTRES        0.0000000000E+00  0.0000000000E+00
$ENDD
-TEST-I-FLAW-I-----FIELD1------I-----FIELD2------I-----FIELD3------I
          END OF DATA FOR THE ABOVE TEMPERATURE
```

ADAM06 + SF6 + KT

```
DTABLE     : DATA TABLE (FAST-FRACTURE, STATIC OR DYNAMIC FATIGUE)
-TEST-I-FLAW-I-----FIELD1------I-----FIELD2------I-----FIELD3------I
TEMP         0.3000000000E+02
RSTRES        0.0000000000E+00  0.0000000000E+00  0.0000000000E+00
+STRES        0.0000000000E+00  0.0000000000E+00  0.0000000000E+00
FAST     S   0.1342000000E+04
FAST     S   0.5700000000E+04
FAST     S   0.7552000000E+04
FAST     S   1.3680000000E+04
FAST     S   1.2450000000E+04
FAST     S   1.0060000000E+04
FAST     S   1.2260000000E+04
FAST     S   0.8355000000E+04
FAST     S   0.7991000000E+04
FAST     S   0.5789000000E+04
FAST     S   0.6275000000E+04
FAST     S   0.5436000000E+04
FAST     S   0.6534000000E+04
FAST     S   0.5736000000E+04
FAST     S   0.9459000000E+04
FAST     S   0.9088000000E+04
FAST     S   1.1410000000E+04
FAST     S   0.7889000000E+04
FAST     S   0.3066000000E+04
FAST     S   0.6929000000E+04
FAST     S   0.9347000000E+04
FAST     S   0.5885000000E+04
FAST     S   0.7149000000E+04
FAST     S   0.3244000000E+04
FAST     S   0.6241000000E+04
FAST     S   0.8816000000E+04
```

```
FAST     S   1.0970000000E+04
FAST     S   0.2392000000E+04
FAST     S   1.0830000000E+04
FAST     S   1.3730000000E+04
ZSTRES       0.0000000000E+00  0.0000000000E+00
$ENDD
-TEST-I-FLAW-I-----FIELD1------I-----FIELD2------I-----FIELD3------I
         END OF DATA FOR THE ABOVE TEMPERATURE


************************************************************************
$ENDT      : END OF DATA FOR THE ABOVE MATERIAL
************************************************************************
```

E.3 Pressure Chamber

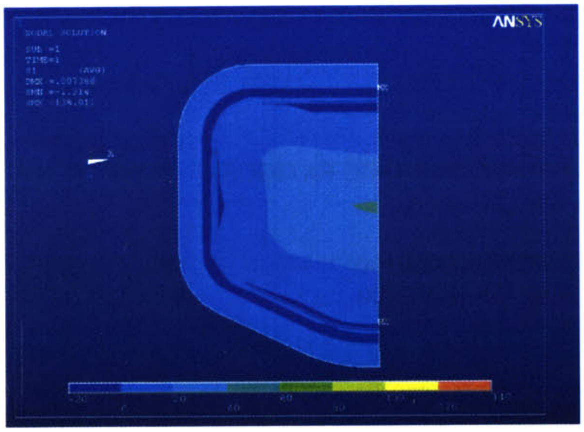

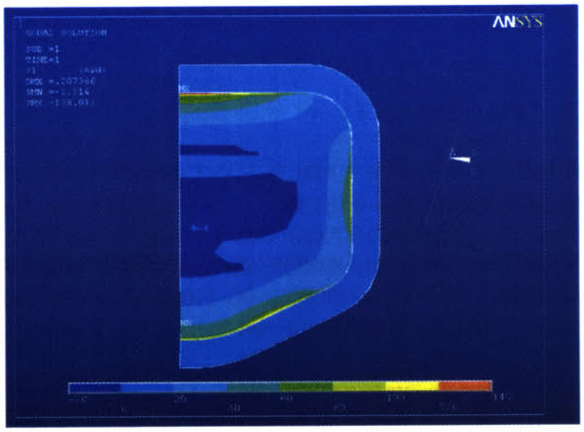

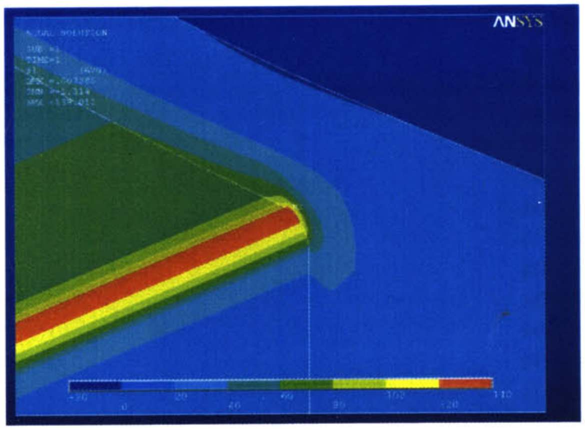

CARES Input File for Chamber (Surface Analysis)

```
------------------------------------------------------------------------
FILTER
 1  1  0  2  0  0  1
------------------------------------------------------------------------

*** WARNING ; DO NOT MAKE ANY CHANGES ABOVE THIS LINE **********************



 +-----------------------------------------------------------------+
 |                                                 |
 |          --- INPUT TEMPLATE FOR CARES/LIFE ---          |
 |                                                 |
 |       CERAMICS ANALYSIS AND RELIABILITY EVALUATION         |
 |          OF STRUCTURES LIFE PREDICTION PROGRAM        |
 |                                                 |
 +-----------------------------------------------------------------+

                 +-----------------------+
                 | MASTER CONTROL INPUT |
                 +-----------------------+

TITLE      ch_1La
-----------------------------------------------------------------------
Project Title: Chamber_1
-----------------------------------------------------------------------

NE
  +-+      ---------------------------------------------
   3   = CONTROL INDEX FOR FINITE ELEMENT POSTPROCESSING
  +-+      ---------------------------------------------

          0 : Experimental rupture data analysis only
          3 : Component reliability analysis with a NEUTRAL FILE
             DATA BASE


IPRINC
  +-+      --------------------------------------
   1   = CONTROL INDEX FOR ELEMENT STRESS OUTPUT
  +-+      --------------------------------------

          0 : Use material coordinate system stresses
             (ANISOTROPIC MODEL)
          1 : Calculate and use principal stresses (ISOTROPIC MODEL)
          2 : Use element or material coordinate system stresses
             (ISOTROPIC MODEL).  This option can be used with the
             Batdorf theory.  It can not be used with the PIA theory.
             When two neutral files are read (proof testing option)
             then IPRINC should be set to this value.
```

```
NMATS
 +--+     ------------------------------------------
  1   = NUMBER OF MATERIALS FOR SURFACE FLAW ANALYSIS
 +--+     ------------------------------------------
   |
   |
   |       +--------------------------------------------------------+
   |       | This keyword indicates how many different surface residing |
   |       | flaw types are required to predict a component's surface   |
   |       | reliability.  Only one flaw population can be associated   |
   +------> | with a particular material identification (ID) number for  |
           | the purpose of component reliability prediction.  The ID   |
           | number is matched to the finite element ID number. If      |
           | specimen rupture data consists of multiple flaw            |
           | populations (competing failure modes), then only one of    |
           | the flaw populations can be associated with the particular |
           | material ID.  This selection of the "active" flaw          |
           | population depends on the choice of the ID4 keyword.       |
           +--------------------------------------------------------+


NMATV
 +--+     ------------------------------------------
  0   = NUMBER OF MATERIALS FOR VOLUME FLAW ANALYSIS
 +--+     ------------------------------------------
   |
   |
   |       +--------------------------------------------------------+
   |       | This keyword indicates how many different volume residing  |
   |       | flaw types are required to predict a component's volume    |
   |       | reliability.  Only one flaw population can be associated   |
   +------> | with a particular material identification (ID) number for  |
           | the purpose of component reliability prediction.  The ID   |
           | number is matched to the finite element ID number. If      |
           | specimen rupture data consists of multiple flaw            |
           | populations (competing failure modes), then only one of    |
           | the flaw populations can be associated with the particular |
           | material ID.  This selection of the "active" flaw          |
           | population depends on the choice of the ID4 keyword.       |
           +--------------------------------------------------------+


NGP
 +--+     -------------------------------------------------
  15  = NUMBER OF GAUSSIAN QUADRATURE POINTS (15, 30, or 50)
 +--+     -------------------------------------------------
   |
   |
   |       +-------------------------------------------------------+
   |       | Number of Gaussian quadrature points for unit sphere     |
   +-------> | (volume flaw orientation space) and unit circle (surface |
           | flaw orientation space) integration (Batdorf and Weibull |
           | normal stress averaging methods only).                   |
           +-------------------------------------------------------+
```

```
NS
----------   -------------------------------------
   4    = NUMBER OF SEGMENTS IN SYMMETRY PROBLEM
----------   -------------------------------------
   |
   |      +-----------------------------------------------------------+
   |      | Multiplication factor for finite element volumes and areas |
   |      | necessary to reproduce the whole component.  This option   |
   +------> | is useful for finite element models that take advantage of |
          | geometrical and loading symmetries (MODEL REDUCTION        |
          | VIA SYMMETRY).  The total volume and surface area of the   |
          | component under load effects reliability (the so-called    |
          | Weibull size effect).                                      |
          +-----------------------------------------------------------+


FACTOR
----------   -------------------------------------------------
0.1000E+01 =  LOAD FACTOR FOR WHICH TO MULTIPLY ELEMENT STRESSES
----------   -------------------------------------------------


*************************************************************************
$ENDX      : END OF MASTER CONTROL INPUT
*************************************************************************


               +-------------------------+
               |                         |
               | MATERIAL CONTROL INPUT  |
               |                         |
               +-------------------------+

TITLE      : MATERIAL TITLE (ECHOED IN CARES OUTPUT)
----------------------------------------------------------------------
Material Title:  Silicon
----------------------------------------------------------------------


MATID
+-------+    -----------------------------
     1   =  MATERIAL IDENTIFICATION NUMBER
+-------+    -----------------------------
   |
   |
   |      +---------------------------------------------------------+
   |      | Material identification number from the finite element   |
   +-------> | material property card (If finite element postprocessing |
          | is not being performed this entry should be some unique   |
          | number.  This input must be in the form of an integer.    |
          +---------------------------------------------------------+


ID1
 +-+         -----------------------------------------------------
  7     =  CONTROL INDEX FOR EXPERIMENTAL (SPECIMEN RUPTURE) DATA
```

```
 +-+      ---------------------------------------------------

         1 : TENSILE SPECIMEN (single failure mode - unimodal)
         2 : THREE-POINT or FOUR-POINT bend bar (unimodal)
         3 : Direct input of the required parameters
         4 : TENSILE SPECIMEN (multiple failure modes - multimodal)
         5 : THREE-POINT or FOUR-POINT bend bar (multimodal)
         6 : UNIAXIAL loaded FINITE ELEMENT MODEL of the specimen,
             such as bend bar,TENSILE SPECIMEN, C- or O-RING, etc...
         7 : MULTIAXIALLY loaded FINITE ELEMENT MODEL of the specimen,
             such as RING-ON-RING, BALL-ON-RING, PRESSURE-ON-DISK


ID2
 +-+      ---------------------------------------------
  4   =  CONTROL INDEX FOR MICROCRACK FRACTURE CRITERION
 +-+      ---------------------------------------------

         1 : Weibull Normal Stress Averaging
         2 : Maximum Tensile Stress criterion (for volume flaw only)
         3 : Coplanar Strain Energy Release Rate criterion (G sub T)
         4 : Weibull PIA model
         5 : Shetty's semi-empirical criterion (recommended option)
             (noncoplanar Strain Energy Release Rate (SERR) criterion)
             (KI/KIc) + (KII/(C*KIc))**2 = 1   (Note: KII or KIII)
         6 : Weibull compression criterion (function of shear only)
             (KII/KIIc) = 1

              ***(IF ID2 > 5, IPRINC = 0 IS REQUIRED)***


ID3
 +-+      -------------------------------
  1   =  CONTROL INDEX FOR CRACK GEOMETRY
 +-+      -------------------------------

         1 : Griffith crack (volume flaw or surface flaw)
         2 : Penny-Shaped crack (volume flaw only)
         3 : Griffith Notch (surface flaw only)
             (ID2 = 3 or 5 is required)
         4 : Semicircular crack (surface flaw only)
             (ID2 = 5 is required)


ID4
 +-+      ---------------------------------------------------------
  2   =  CONTROL INDEX FOR VOLUME OR SURFACE FLAW RELIABILITY ANALYSIS
 +-+      ---------------------------------------------------------
  |
  |      1 : VOLUME (flaws reside throughout the material volume)
  |      2 : SURFACE (flaws reside exclusively on the material surface)
  |
  |   +----------------------------------------------------------------+
  |   | If specimen rupture data contains multiple flaw populations,   |
  +---->| this keyword designates the one flaw population to be made   |
      | "active" for subsequent component reliability analysis.        |
```

```
        | If only one flaw population is present, the choice must match  |
        | with the failure mode of the specimen data.  The selected flaw |
        | category will have a complete set of parameters calculated and |
        | written to the output template file by the CARES/Life program. |
        | The parameters are associated with the material ID keyword.    |
        +----------------------------------------------------------------+


C
----------   ------------------------------------------------------
   1.0000 =  CONSTANT FOR SEMI-EMPIRICAL MIXED-MODE FRACTURE CRITERIA
----------   ------------------------------------------------------
   |
   |
   |         +------------------------------------------------------+
   |         | Constant for semi-empirical mixed-mode fracture criteria |
   +---------> | (KI/KIc)+(KII/(C*KIc))**2 = 1       ref. D.K.Shetty      |
             | Observed values range from 0.8 to 2. (ref. D.K. Shetty)  |
             | NOTE: As C approaches infinity, predicted failure        |
             | probabilityes approach normal stress criterion values    |
             +------------------------------------------------------+


PR
----------   ------------------------------------------------------------
   0.2177 =  Poisson's ratio (used only in failure criterion calculations)
----------   ------------------------------------------------------------


MLORLE
  +-+        ---------------------------------------------
   0    =  CONTROL INDEX FOR METHOD OF CALCULATING WEIBULL
  +-+      PARAMETERS FROM THE EXPERIMENTAL FRACTURE DATA
           ---------------------------------------------

           0 : Maximum likelihood
           1 : Least-Squares linear regression with
               rank increment adjustment
           2 : Least-Squares linear regression for the
               truncated Weibull distribution.  This option
               uses the ZSTRES keyword (you must activate
               the three-parameter analysis option)
           3 : Maximum likelihood (Pool temperature data)
           4 : Least-Squares (Pool temperature data)


OUTLIE
----------   ------------------------------------
   2.0000 =  SIGNIFICANCE LEVEL TO DETECT OUTLIERS
----------   ------------------------------------
   |
   |
   |         +----------------------------------------------------+
   |         | Significance level for which OUTLIERS are to        |
   +---------> | be detected. Input is in percent and must be between |
             | the range of 0.1 percent to 10.0 percent            |
```

```
          | (OUTLIE = 2.0 percent is recommended)              |
          +----------------------------------------------------+


************************************************************************
$ENDM     : END OF TEMPERATURE-INDEPENDENT MATERIAL CONTROL INPUT
************************************************************************

CONFIG A
DTABLE    : DATA TABLE (FAST-FRACTURE, STATIC OR DYNAMIC FATIGUE)
-TEST-I-FLAW-I-----FIELD1------I-----FIELD2------I-----FIELD3------I
TEMP       0.2200000000E+02
RSTRES       0.0000000000E+00  0.0000000000E+00  0.0000000000E+00
+STRES       0.0000000000E+00  0.0000000000E+00  0.0000000000E+00
FAST     S   0.1165900000E+04
FAST     S   0.0886800000E+04
FAST     S   0.0776100000E+04
FAST     S   0.0690800000E+04
FAST     S   0.0610200000E+04
FAST     S   0.0585800000E+04
FAST     S   0.0566000000E+04
FAST     S   0.0415100000E+04
FAST     S   0.0321100000E+04
ZSTRES       0.0000000000E+00  0.0000000000E+00
$ENDD
-TEST-I-FLAW-I-----FIELD1------I-----FIELD2------I-----FIELD3------I
          END OF DATA FOR THE ABOVE TEMPERATURE

CONFIG A + SF6

DTABLE    : DATA TABLE (FAST-FRACTURE, STATIC OR DYNAMIC FATIGUE)
-TEST-I-FLAW-I-----FIELD1------I-----FIELD2------I-----FIELD3------I
TEMP       0.2300000000E+02
RSTRES       0.0000000000E+00  0.0000000000E+00  0.0000000000E+00
+STRES       0.0000000000E+00  0.0000000000E+00  0.0000000000E+00
FAST     S   0.8552200000E+04
FAST     S   0.8080300000E+04
FAST     S   0.4546600000E+04
FAST     S   0.3992100000E+04
FAST     S   0.3652400000E+04
FAST     S   0.3511200000E+04
FAST     S   0.3486400000E+04
FAST     S   0.3418800000E+04
FAST     S   0.2396000000E+04
FAST     S   0.2238700000E+04
FAST     S   0.1068900000E+04
FAST     S   0.1032800000E+04
FAST     S   0.0862400000E+04
ZSTRES       0.0000000000E+00  0.0000000000E+00
$ENDD
-TEST-I-FLAW-I-----FIELD1------I-----FIELD2------I-----FIELD3------I
          END OF DATA FOR THE ABOVE TEMPERATURE


CONFIG B
```

```
DTABLE     : DATA TABLE (FAST-FRACTURE, STATIC OR DYNAMIC FATIGUE)
-TEST-I-FLAW-I-----FIELD1------I-----FIELD2------I-----FIELD3------I
TEMP        0.2400000000E+02
RSTRES        0.0000000000E+00  0.0000000000E+00  0.0000000000E+00
+STRES        0.0000000000E+00  0.0000000000E+00  0.0000000000E+00
FAST     S   0.0432900000E+04
FAST     S   0.0368700000E+04
FAST     S   0.0355200000E+04
ZSTRES       0.0000000000E+00  0.0000000000E+00
$ENDD
-TEST-I-FLAW-I-----FIELD1------I-----FIELD2------I-----FIELD3------I
         END OF DATA FOR THE ABOVE TEMPERATURE
```

CONFIG B + SF6

```
DTABLE     : DATA TABLE (FAST-FRACTURE, STATIC OR DYNAMIC FATIGUE)
-TEST-I-FLAW-I-----FIELD1------I-----FIELD2------I-----FIELD3------I
TEMP        0.2500000000E+02
RSTRES        0.0000000000E+00  0.0000000000E+00  0.0000000000E+00
+STRES        0.0000000000E+00  0.0000000000E+00  0.0000000000E+00
FAST     S   0.1611100000E+04
FAST     S   0.1257000000E+04
FAST     S   0.1184000000E+04
FAST     S   0.1165000000E+04
FAST     S   0.1155800000E+04
FAST     S   0.1000200000E+04
FAST     S   0.0984800000E+04
FAST     S   0.0898800000E+04
FAST     S   0.0775300000E+04
FAST     S   0.0704300000E+04
FAST     S   0.0695500000E+04
ZSTRES       0.0000000000E+00  0.0000000000E+00
$ENDD
-TEST-I-FLAW-I-----FIELD1------I-----FIELD2------I-----FIELD3------I
         END OF DATA FOR THE ABOVE TEMPERATURE
```

CONFIG A + Kt

```
DTABLE     : DATA TABLE (FAST-FRACTURE, STATIC OR DYNAMIC FATIGUE)
-TEST-I-FLAW-I-----FIELD1------I-----FIELD2------I-----FIELD3------I
TEMP        0.2600000000E+02
RSTRES        0.0000000000E+00  0.0000000000E+00  0.0000000000E+00
+STRES        0.0000000000E+00  0.0000000000E+00  0.0000000000E+00
FAST     S   0.1620500000E+04
FAST     S   0.1234000000E+04
FAST     S   0.1084000000E+04
FAST     S   0.0962300000E+04
FAST     S   0.0848500000E+04
FAST     S   0.0825600000E+04
FAST     S   0.0801700000E+04
FAST     S   0.0612600000E+04
FAST     S   0.0447000000E+04
ZSTRES       0.0000000000E+00  0.0000000000E+00
$ENDD
-TEST-I-FLAW-I-----FIELD1------I-----FIELD2------I-----FIELD3------I
         END OF DATA FOR THE ABOVE TEMPERATURE
```

CONFIG A + SF6 + Kt

```
DTABLE     : DATA TABLE (FAST-FRACTURE, STATIC OR DYNAMIC FATIGUE)
-TEST-I-FLAW-I-----FIELD1------I-----FIELD2------I-----FIELD3------I
TEMP        0.2700000000E+02
RSTRES       0.0000000000E+00  0.0000000000E+00  0.0000000000E+00
+STRES       0.0000000000E+00  0.0000000000E+00  0.0000000000E+00
FAST     S  1.2562900000E+04
FAST     S  1.1812900000E+04
FAST     S  0.7154600000E+04
FAST     S  0.6282000000E+04
FAST     S  0.5845200000E+04
FAST     S  0.5588800000E+04
FAST     S  0.5572700000E+04
FAST     S  0.5379800000E+04
FAST     S  0.3468700000E+04
FAST     S  0.3201200000E+04
FAST     S  0.1613800000E+04
FAST     S  0.1547400000E+04
FAST     S  0.1245300000E+04
ZSTRES       0.0000000000E+00  0.0000000000E+00
$ENDD
-TEST-I-FLAW-I-----FIELD1------I-----FIELD2------I-----FIELD3------I
          END OF DATA FOR THE ABOVE TEMPERATURE
```

CONFIG B + Kt

```
DTABLE     : DATA TABLE (FAST-FRACTURE, STATIC OR DYNAMIC FATIGUE)
-TEST-I-FLAW-I-----FIELD1------I-----FIELD2------I-----FIELD3------I
TEMP        0.2800000000E+02
RSTRES       0.0000000000E+00  0.0000000000E+00  0.0000000000E+00
+STRES       0.0000000000E+00  0.0000000000E+00  0.0000000000E+00
FAST     S  0.0616000000E+04
FAST     S  0.0554000000E+04
FAST     S  0.0529100000E+04
ZSTRES       0.0000000000E+00  0.0000000000E+00
$ENDD
-TEST-I-FLAW-I-----FIELD1------I-----FIELD2------I-----FIELD3------I
          END OF DATA FOR THE ABOVE TEMPERATURE
```

CONFIG B + SF6 + Kt

```
DTABLE     : DATA TABLE (FAST-FRACTURE, STATIC OR DYNAMIC FATIGUE)
-TEST-I-FLAW-I-----FIELD1------I-----FIELD2------I-----FIELD3------I
TEMP        0.2900000000E+02
RSTRES       0.0000000000E+00  0.0000000000E+00  0.0000000000E+00
+STRES       0.0000000000E+00  0.0000000000E+00  0.0000000000E+00
FAST     S  0.25526000000E+04
FAST     S  0.1793100000E+04
FAST     S  0.1714100000E+04
FAST     S  0.1690700000E+04
FAST     S  0.1660900000E+04
FAST     S  0.1469200000E+04
```

```
FAST    S  0.1450100000E+04
FAST    S  0.1381200000E+04
FAST    S  0.1129100000E+04
FAST    S  0.1107600000E+04
FAST    S  0.1103300000E+04
ZSTRES      0.0000000000E+00  0.0000000000E+00
$ENDD
-TEST-I-FLAW-I-----FIELD1------I-----FIELD2------I-----FIELD3------I
          END OF DATA FOR THE ABOVE TEMPERATURE


**********************************************************************
$ENDT     : END OF DATA FOR THE ABOVE MATERIAL
**********************************************************************
```

E.4 Surface Area / Volume Scaling of Strength

CARES Input for Predictive Scaling of Chamber using RHFS Parameters (Surface)

```
--------------------------------------------------------------------------
FILTER
 1 1 0 2 0 0 1
--------------------------------------------------------------------------

*** WARNING ; DO NOT MAKE ANY CHANGES ABOVE THIS LINE *********************



 +---------------------------------------------------------------+
 |                                                               |
 |           --- INPUT TEMPLATE FOR CARES/LIFE ---               |
 |                                                               |
 |       CERAMICS ANALYSIS AND RELIABILITY EVALUATION            |
 |         OF STRUCTURES LIFE PREDICTION PROGRAM                 |
 |                                                               |
 +---------------------------------------------------------------+

                +---------------------+
                | MASTER CONTROL INPUT |
                +---------------------+

TITLE      ch_1La
-----------------------------------------------------------------------
Project Title: Chamber_1
-----------------------------------------------------------------------

NE
  +-+      ---------------------------------------------
   3    =  CONTROL INDEX FOR FINITE ELEMENT POSTPROCESSING
  +-+      ---------------------------------------------

          0 : Experimental rupture data analysis only
          3 : Component reliability analysis with a NEUTRAL FILE
```

```
          DATA BASE


IPRINC
 +-+      -------------------------------------
  1   =  CONTROL INDEX FOR ELEMENT STRESS OUTPUT
 +-+      -------------------------------------

         0 : Use material coordinate system stresses
             (ANISOTROPIC MODEL)
         1 : Calculate and use principal stresses (ISOTROPIC MODEL)
         2 : Use element or material coordinate system stresses
             (ISOTROPIC MODEL).  This option can be used with the
             Batdorf theory.  It can not be used with the PIA theory.
             When two neutral files are read (proof testing option)
             then IPRINC should be set to this value.


NMATS
 +--+     ------------------------------------------
  0   =  NUMBER OF MATERIALS FOR SURFACE FLAW ANALYSIS
 +--+     ------------------------------------------
  |
  |
  |     +---------------------------------------------------------+
  |     | This keyword indicates how many different surface residing |
  |     | flaw types are required to predict a component's surface   |
  |     | reliability.  Only one flaw population can be associated   |
  +------> | with a particular material identification (ID) number for |
        | the purpose of component reliability prediction.  The ID   |
        | number is matched to the finite element ID number.  If     |
        | specimen rupture data consists of multiple flaw           |
        | populations (competing failure modes), then only one of   |
        | the flaw populations can be associated with the particular |
        | material ID.  This selection of the "active" flaw          |
        | population depends on the choice of the ID4 keyword.      |
        +---------------------------------------------------------+


NMATV
 +--+     ------------------------------------------
  1   =  NUMBER OF MATERIALS FOR VOLUME FLAW ANALYSIS
 +--+     ------------------------------------------
  |
  |
  |     +---------------------------------------------------------+
  |     | This keyword indicates how many different volume residing  |
  |     | flaw types are required to predict a component's volume    |
  |     | reliability.  Only one flaw population can be associated   |
  +------> | with a particular material identification (ID) number for |
        | the purpose of component reliability prediction.  The ID   |
        | number is matched to the finite element ID number.  If     |
        | specimen rupture data consists of multiple flaw           |
        | populations (competing failure modes), then only one of   |
        | the flaw populations can be associated with the particular |
        | material ID.  This selection of the "active" flaw          |
```

```
        | population depends on the choice of the ID4 keyword.      |
        +-----------------------------------------------------------+


NGP
 +--+    ----------------------------------------------------
  15   = NUMBER OF GAUSSIAN QUADRATURE POINTS (15, 30, or 50)
 +--+    ----------------------------------------------------
  |
  |
  |     +--------------------------------------------------------+
  |     | Number of Gaussian quadrature points for unit sphere   |
  +-------> | (volume flaw orientation space) and unit circle (surface |
        | flaw orientation space) integration (Batdorf and Weibull |
        | normal stress averaging methods only).                 |
        +--------------------------------------------------------+


NS
----------   --------------------------------------
   4    = NUMBER OF SEGMENTS IN SYMMETRY PROBLEM
----------   --------------------------------------
  |
  |     +-----------------------------------------------------------+
  |     | Multiplication factor for finite element volumes and areas |
  |     | necessary to reproduce the whole component.  This option   |
  +------> | is useful for finite element models that take advantage of |
        | geometrical and loading symmetries (MODEL REDUCTION        |
        | VIA SYMMETRY).  The total volume and surface area of the   |
        | component under load effects reliability (the so-called    |
        | Weibull size effect).                                      |
        +-----------------------------------------------------------+


FACTOR
----------   --------------------------------------------------
0.1000E+01 = LOAD FACTOR FOR WHICH TO MULTIPLY ELEMENT STRESSES
----------   --------------------------------------------------


**************************************************************************
$ENDX      : END OF MASTER CONTROL INPUT
**************************************************************************


              +-------------------------+
              |                         |
              | MATERIAL CONTROL INPUT  |
              |                         |
              +-------------------------+

TITLE      : MATERIAL TITLE (ECHOED IN CARES OUTPUT)
----------------------------------------------------------------------
Material Title:  Silicon
----------------------------------------------------------------------
```

```
MATID
+-------+   -----------------------------
    1  = MATERIAL IDENTIFICATION NUMBER
+-------+   -----------------------------
   |
   |
   |      +---------------------------------------------------------+
   |      | Material identification number from the finite element   |
   +-------> | material property card (If finite element postprocessing |
          | is not being performed this entry should be some unique   |
          | number.  This input must be in the form of an integer.    |
          +---------------------------------------------------------+
```

```
ID1
  +-+      -----------------------------------------------------
  7    = CONTROL INDEX FOR EXPERIMENTAL (SPECIMEN RUPTURE) DATA
  +-+      -----------------------------------------------------
```

1 : TENSILE SPECIMEN (single failure mode - unimodal)
2 : THREE-POINT or FOUR-POINT bend bar (unimodal)
3 : Direct input of the required parameters
4 : TENSILE SPECIMEN (multiple failure modes - multimodal)
5 : THREE-POINT or FOUR-POINT bend bar (multimodal)
6 : UNIAXIAL loaded FINITE ELEMENT MODEL of the specimen,
   such as bend bar,TENSILE SPECIMEN, C- or O-RING, etc...
7 : MULTIAXIALLY loaded FINITE ELEMENT MODEL of the specimen,
   such as RING-ON-RING, BALL-ON-RING, PRESSURE-ON-DISK

```
ID2
  +-+      ----------------------------------------------
  4    = CONTROL INDEX FOR MICROCRACK FRACTURE CRITERION
  +-+      ----------------------------------------------
```

1 : Weibull Normal Stress Averaging
2 : Maximum Tensile Stress criterion (for volume flaw only)
3 : Coplanar Strain Energy Release Rate criterion (G sub T)
4 : Weibull PIA model
5 : Shetty's semi-empirical criterion (recommended option)
   (noncoplanar Strain Energy Release Rate (SERR) criterion)
   (KI/KIc) + (KII/(C*KIc))**2 = 1   (Note: KII or KIII)
6 : Weibull compression criterion (function of shear only)
   (KII/KIIc) = 1

(IF ID2 > 5, IPRINC = 0 IS REQUIRED)

```
ID3
  +-+      --------------------------------
  1    = CONTROL INDEX FOR CRACK GEOMETRY
  +-+      --------------------------------
```

1 : Griffith crack (volume flaw or surface flaw)
2 : Penny-Shaped crack (volume flaw only)

```
        3 : Griffith Notch (surface flaw only)
            (ID2 = 3 or 5 is required)
        4 : Semicircular crack (surface flaw only)
            (ID2 = 5 is required)


ID4
 +-+    ----------------------------------------------------------
  1   = CONTROL INDEX FOR VOLUME OR SURFACE FLAW RELIABILITY ANALYSIS
 +-+    ----------------------------------------------------------
  |
  |      1 : VOLUME (flaws reside throughout the material volume)
  |      2 : SURFACE (flaws reside exclusively on the material surface)
  |
  |   +--------------------------------------------------------------+
  |   | If specimen rupture data contains multiple flaw populations,   |
  +---->| this keyword designates the one flaw population to be made    |
      | "active" for subsequent component reliability analysis.        |
      | If only one flaw population is present, the choice must match |
      | with the failure mode of the specimen data.  The selected flaw |
      | category will have a complete set of parameters calculated and |
      | written to the output template file by the CARES/Life program. |
      | The parameters are associated with the material ID keyword.    |
      +--------------------------------------------------------------+


C
----------  --------------------------------------------------------
  1.0000 =  CONSTANT FOR SEMI-EMPIRICAL MIXED-MODE FRACTURE CRITERIA
----------  --------------------------------------------------------
  |
  |
  |       +--------------------------------------------------------+
  |       | Constant for semi-empirical mixed-mode fracture criteria |
  +---------> | (KI/KIc)+(KII/(C*KIc))**2 = 1      ref. D.K.Shetty        |
          | Observed values range from 0.8 to 2. (ref. D.K. Shetty)  |
          | NOTE: As C approaches infinity, predicted failure          |
          | probabilityes approach normal stress criterion values      |
          +--------------------------------------------------------+


PR
----------  ------------------------------------------------------------
  0.2177 =  Poisson's ratio (used only in failure criterion calculations)
----------  ------------------------------------------------------------


MLORLE
 +-+    ---------------------------------------------
  0   = CONTROL INDEX FOR METHOD OF CALCULATING WEIBULL
 +-+    PARAMETERS FROM THE EXPERIMENTAL FRACTURE DATA
       ---------------------------------------------

        0 : Maximum likelihood
        1 : Least-Squares linear regression with
            rank increment adjustment
```

```
        2 : Least-Squares linear regression for the
            truncated Weibull distribution.  This option
            uses the ZSTRES keyword (you must activate
            the three-parameter analysis option)
        3 : Maximum likelihood (Pool temperature data)
        4 : Least-Squares (Pool temperature data)


OUTLIE
----------   ------------------------------------
   2.0000 =  SIGNIFICANCE LEVEL TO DETECT OUTLIERS
----------   ------------------------------------
  |
  |
  |         +----------------------------------------------------+
  |         | Significance level for which OUTLIERS are to        |
  +---------> | be detected. Input is in percent and must be between |
            | the range of 0.1 percent to 10.0 percent            |
            | (OUTLIE = 2.0 percent is recommended)                |
            +----------------------------------------------------+


************************************************************************
$ENDM     : END OF TEMPERATURE-INDEPENDENT MATERIAL CONTROL INPUT
************************************************************************


TEMP
----------
  25.0000
----------

PARAM
*--------M--------*-------SP--------*
 0.501400000E+01  0.392200000E+03
*-----------------*-----------------*


************************************************************************
$ENDT     : END OF DATA FOR THE ABOVE MATERIAL
************************************************************************
```

Additional Parameters for Scaling

SURFACE

```
ADAM06

PARAM
*--------M--------*-------SP--------*
 0.475600000E+01  0.942500000E+03
*-----------------*-----------------*

ADAM06 + SF6
```

```
PARAM
*--------M--------*-------SP--------*
 0.266100000E+01  0.37848000E+04
*-----------------*-----------------*
```

ADAM06 + Kt

```
PARAM
*--------M--------*-------SP--------*
 0.501400000E+01  0.210740000E+04
*-----------------*-----------------*
```

ADAM06 + SF6 + Kt

```
PARAM
*--------M--------*-------SP--------*
 0.269300000E+01  0.8284800000E+04
*-----------------*-----------------*
```

VOLUME

ADAM06

```
PARAM
*--------M--------*-------SP--------*
 0.475600000E+01  0.156000000E+03
*-----------------*-----------------*
```

ADAM06 + SF6

```
PARAM
*--------M--------*-------SP--------*
 0.266100000E+01  0.12260000E+03
*-----------------*-----------------*
```

ADAM06 + Kt

```
PARAM
*--------M--------*-------SP--------*
 0.501400000E+01  0.392200000E+03
*-----------------*-----------------*
```

ADAM06 + SF6 + Kt

```
PARAM
*--------M--------*-------SP--------*
 0.269300000E+01  0.2769000000E+03
*-----------------*-----------------*
```

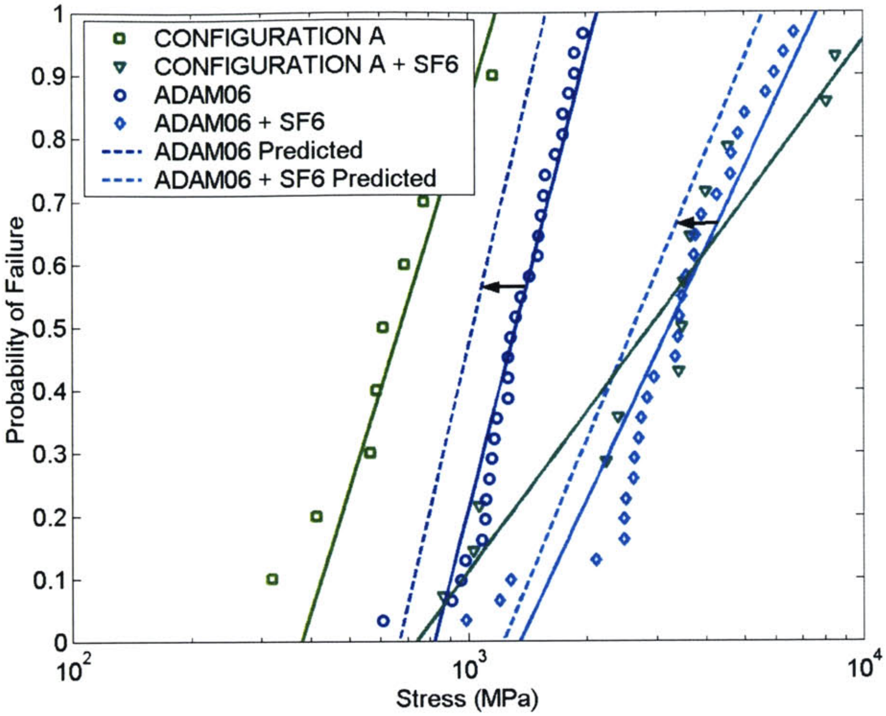

Configuration A Surface Area Scaling Prediction

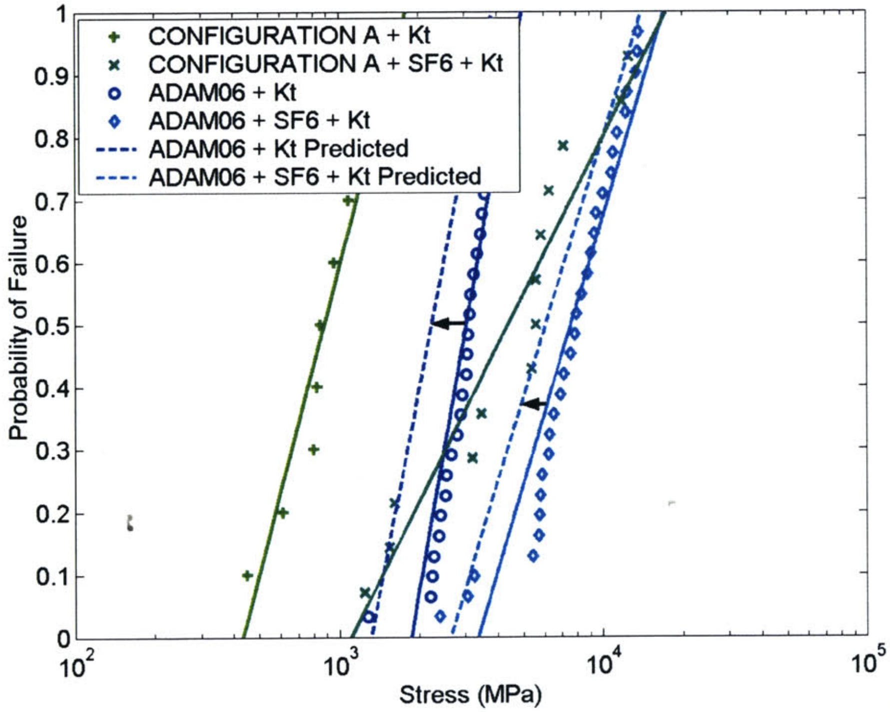

Configuration A + Kt Surface Area Scaling Prediction

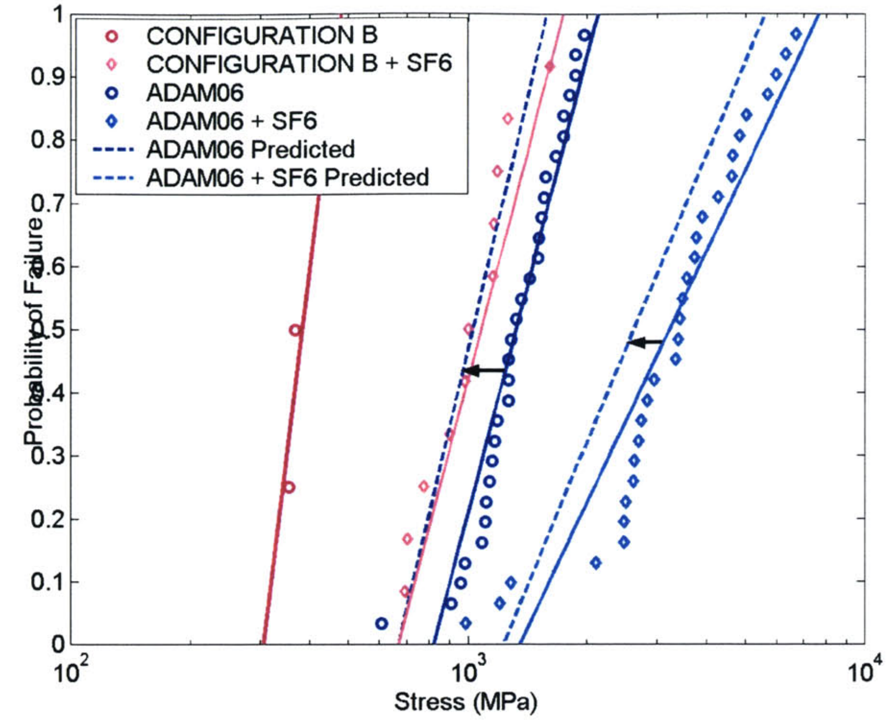

Configuration B Surface Area Scaling Prediction

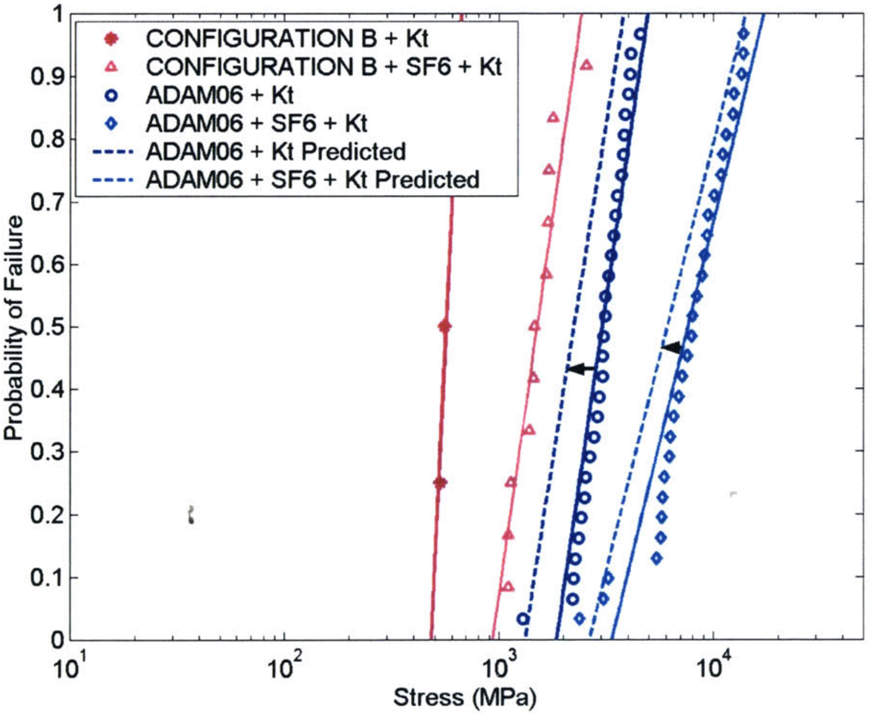

Configuration B + Kt Surface Area Scaling Prediction

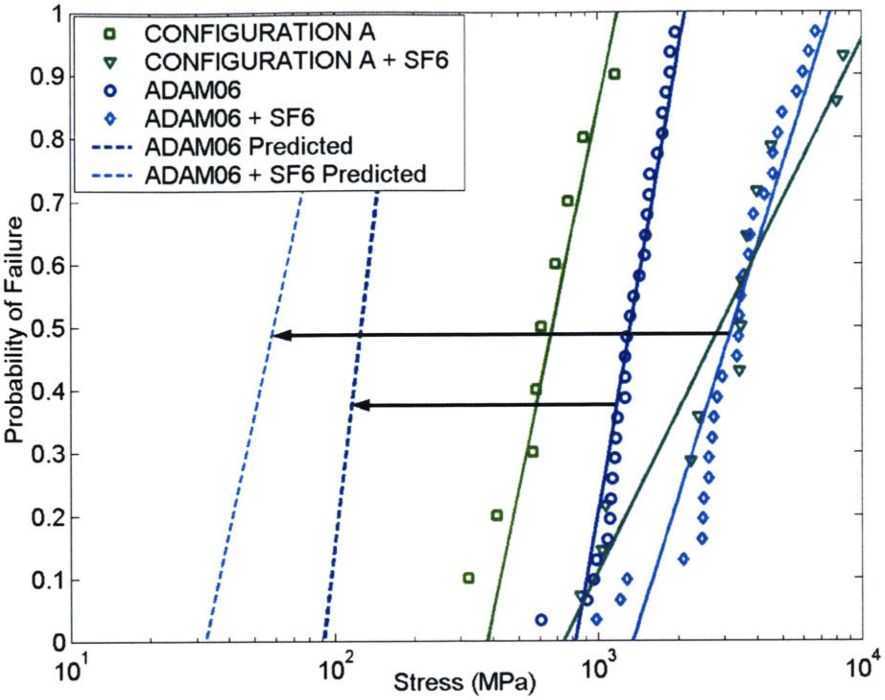

Configuration A Volume Scaling Prediction

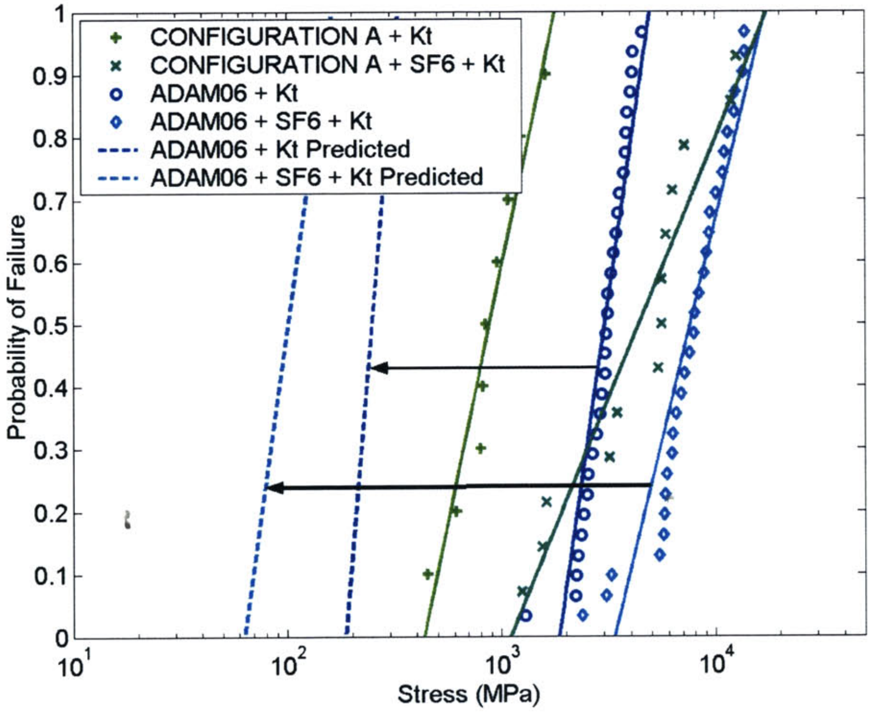

Configuration A + Kt Volume Scaling Prediction

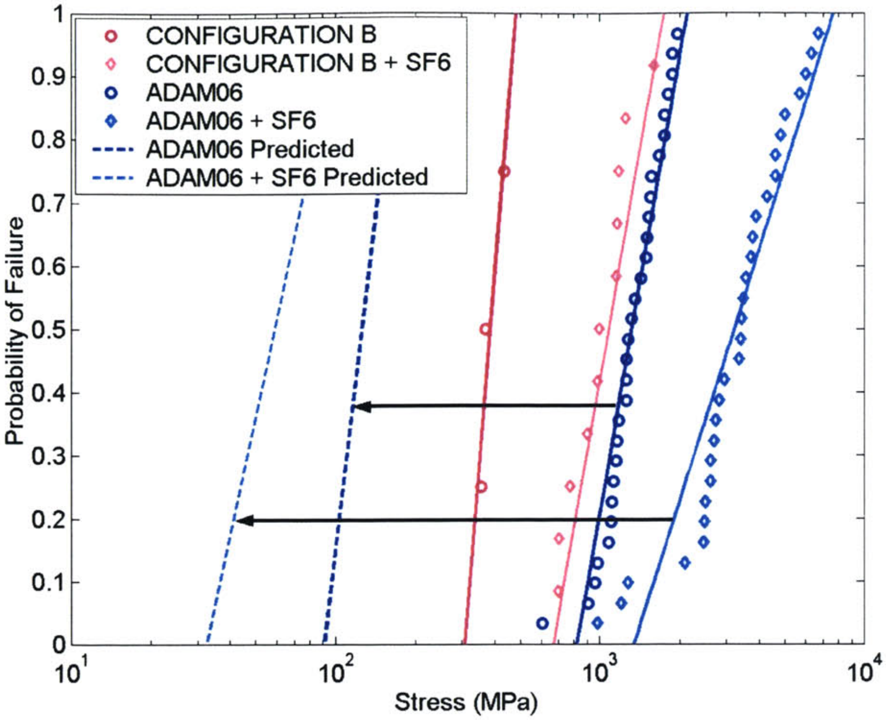

Configuration B Volume Scaling Prediction

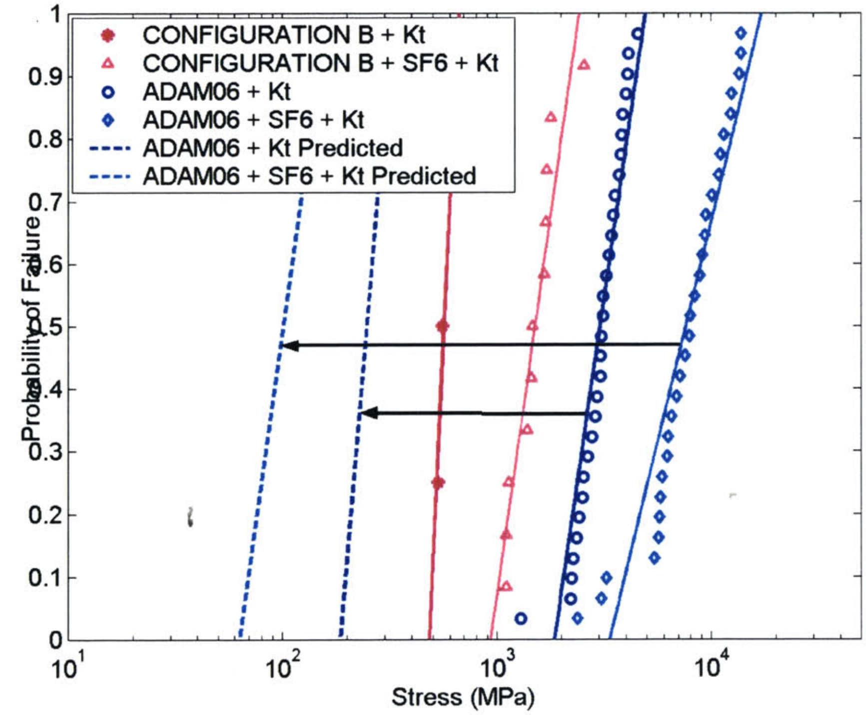

Configuration B + Kt Volume Scaling Prediction

References

---

1 A.H. Epstein, S.D Senturia, G. Anathasuresh, A. Ayon, K. Breuer, K.-S. Chen, F.E. Ehrich, G. Gauba, R. Ghodssi, C. Grosherny, S. Jacobson, J.H. Lang, C.-C. Lin, A. Merha, J.M. Miranda, S. Nagle, D.J. Orr, E. Piekos, M.A. Schmidt, G. Shirley, S.M. Spearing, C.S. Tan, Y.-S. Tzeng, I.A. Waitz, "Power MEMS and Microengines" in *The Proceedings of the IEEE Transducers '97 Conference*, Chicago, IL, June 1997, 753-756. New York: Institute of Electrical and Electronics Engineers, 1997.

2 A.H. Epstein, S.D. Senturia, O. Al-Midani, G. Anathasuresh, A. Ayon, K. Breuer, K.-S. Chen, F.E. Ehrich, E. Esteve, L. Frechette, G. Gauba, R. Ghodssi, C. Groshenry, S.A. Jacobson, J.L. Kerrebrock, J.H. Lang, C-C Lin, A. London, J. Lopata, A. Mehra, J.O. Mur Miranda, S. Nagle, D.J. Orr, E. Piekos, M.A. Schmidt, G. Shirley, S.M. Spearing, C.S. Tan, Y-S Tzeng, I.A. Waitz, "Micro-heat engines, gas turbines, and rocket engines: The MIT microengine project", AIAA Paper 97-1773, 1997.

3 "Boeing: Rocketdyne: Space Shuttle Main Engine" Online: http://www.boeing.com/defense-space/space/propul/SSME.html, April 2002.

4 R. Francis, "A systems study of very small launch vehicles", M.S. thesis, Department of Aeronautics and Astronautics, Massachusetts Institute of Technology, Cambridge, MA, 1999.

5 MIT Microengine Project, *MIT Gas Turbine Project Annual Program Review*, MIT Proprietary, Cambridge, MA, May 2001.

6 A.P. London, "Development and test of a microfabricated bipropellant rocket engine", Ph.D. dissertation, Department of Aeronautics and Astronautics, Massachusetts Institute of Technology, Cambridge, MA, 2000.

7 A.P. London, A.H. Epstein, and J.L. Kerrebrock, "High-Pressure Bipropellant Microrocket Engine", *Journal of Propulsion and Power* 17 (4), (2001): 780-787.

8 A.A. Ayon, R.L. Bayt, K.S. Breuer, "Deep reactive ion etching: a promising technology for micro- and nanosatellites", *Smart Materials and Structures* 10, (2001): 1135-1144.

9 A.A. Ayon, R.A. Braff, R. Bayt, H.H. Sawin, and M.A. Schmidt, "Influence of Coil Power on the Etching Characteristics in a High Density Plasma Etcher", *Journal of the Electrochemical Society* 146 (7), (1999): 2730-2736.

10 A.A. Ayon, R. Braff, C.C. Lin, H.H. Sawin, and M.A. Schmidt, "Characterization of a Time Multiplexed Inductively Coupled Plasma Etcher", *Journal of the Electrochemical Society* 146 (1), (1999): 339-349.

11 C.S. Protz, "Micro-Rocket Thrust Chamber Update", MIT Microengine Meeting, Massachusetts Institute of Technology, Cambridge, MA, April 2, 2002.

12 K.-S. Chen, A. Ayon, and S.M. Spearing, "Controlling and Testing the Fracture Strength of Silicon on the Mesoscale", *Journal of the American Ceramic Society* 20, (2000): 1476-84.

13 A.M. Fitzgerald, R.H. Dauskardt, and T.W. Kenny, "Fracture toughness and crack growth phenomena of plasma-etched single crystal silicon", *Sensors and Actuators* 83, (2000): 194-199.

14 T. Yi, L. Li, and C.-J. Kim, "Microscale material testing of single crystalline silicon: process effects on surface morphology and tensile strength", *Sensors and Actuators* 83, (2000): 172-178.

15 M.F. Ashby and D.R.H. Jones, *Engineering Materials 2*, New York: Pergamon Press, 1992, 169-173.

16 R.J. Roark and W.C. Young, *Roark's Formulas for Stress and Strain*, 6th ed., New York: McGraw-Hill, 1989, 464.

17 R.E. Peterson, *Stress Concentration Factors*, New York: Wiley, 1974, 98.

18 N.N. Nemeth,O. Jadaan, J.P. Palko, J. Mitchell, and C.A. Zorman, "Structural Modeling and Probabilitistic Characterization of MEMS Pressure Sensor Membranes" in *Proceedings of the MEMS: Mechanics and Measurements Symposium*, Portland Oregon, 2001, 46-51.

19 R.W. Rice, in *Fractography of Ceramic and Metal Failures*, ASTM STP 827, edited by J. J. Mecholsky, Jr., and S. R. Powell, Jr., American Society for Testing Materials, 1984, 5-103.

20 A.Ayon, X. Zhang, and R. Khanna, "Ultra Deep Anisotropic Silicon Trenches Using Deep Reactive Ion Etching (DRIE)", in *Technical Digest: Solid-State Sensor and Actuator Workshop*, Hilton Head Island, SC, 2000, 339-342.

21 K-S Chen, "Materials Characterization and Structural Design of Ceramic Micro Turbomachinery", PhD Dissertation, Dept of Mechanical Engineering, Massachusetts Institute of Technology, Cambridge, MA , 1998.

---

22 K.T. Turner, "An Evaluation of Critical Issues for Microhydraulic Transducers: Silicon Wafer Bonding, Strength of Silicon on Insulator Membranes and Gold-Tin Solder Bonding", M.S. thesis, Department of Mechanical Engineering, Massachusetts Institute of Technology, Cambridge, MA, 2001.

23 S. Timoshenko and S. Woinowsky-Krieger, *Theory of Plates and Shells,* 2nd Edition, New York: McGraw-Hill, 1959, 51-78.

24 N.N. Nemeth, L.M. Powers, L.A. Janosik, and J.P. Gyekenyesi, *Preliminary Draft of CARES/LIFE (Ceramics Analysis and Reliability Evaluation of Structures Life Prediction Program) Users and Programmers Manual,* NASA - Lewis Research Center, March 30, 1993.

25 D.R. Thoman, L.J. Bain, and C.E. Antle, "Inferences on the Parameters of the Weibull Distribution," *Technometrics* 11 (3), (1969): 445-460.